Aus dem Biomedizinischen Centrum

Lehrstuhl für Molekularbiologie

Ludwig-Maximilians-Universität München

Lehrstuhl für Molekularbiologie

Vorstand: Prof. Dr. rer. nat. Peter B. Becker

Remodeling of higher order chromatin structures

Dissertation

zum Erwerb des Doktorgrades der Naturwissenschaften

an der Medizinischen Fakultät der

Ludwig-Maximilians-Universität München

vorgelegt von

Petra Vizjak

aus

Varaždin, Kroatien

Jahr

2023

Mit Genehmigung der Medizinischen Fakultät
der Universität München

Betreuer:	Prof. Dr. rer. nat. Peter B. Becker
Zweitgutachter(in):	Prof. Dr. rer. nat. Andreas Ladurner
Dekan:	Prof. Dr. med. Thomas Gudermann
Tag der mündlichen Prüfung:	20. Juli 2023

Table of content

Zusammenfassung

In fast allen Eukaryoten ist die DNA in einem dynamischen Polymer namens Chromatin organisiert. Das Nukleosom, der elementare Baustein des Chromatins, besteht aus einem Histonoktamer, um das 146 Basenpaare der DNA gewickelt werden. Zwischen den Nukleosomen befindet sich ein Stück freie DNA, die sogenannte Linker-DNA. Die Nukleosomen sind meist auf der DNA in sehr regelmäßigen Abstand angeordnet. Dieser regelmäßige Abstand ist wichtig, um kryptische Transkription zu verhindern und das Genom vor Doppelstrangbrüchen zu schützen. Die Position der Nukleosomen auf der DNA wird durch ATP-abhängige Nukleosomen-*Remodeling*-Enzyme beeinflusst. Diese Enzyme können die Nukleosomen von der DNA entfernen, sie auf der DNA zusammenbauen, umstrukturieren und entlang der DNA verschieben.

Chromatin faltet sich sowohl *in vitro* als auch *in vivo* zu Strukturen höherer Ordnung. Nukleosomen-Arrays unterliegen auch einer Phasentrennung und bilden dadurch dichte Chromatinkondensate. Die Chromatinfaltung und die Phasentrennung stellen eine Herausforderung für Nukleosomen-*Remodeling*-Enzyme dar, da sie das Chromatin binden und darauf einwirken können müssen. In dieser Arbeit habe ich die Nukleosom *Verschiebereaktion* von *Remodeling*-Enzymen in unterschiedlich gefalteten Chromatinsubstraten charakterisiert.

Im ersten Kapitel verwendete ich die Spalthefe als Modellsystem, um das *nucleosome sliding* im Euchromatin und im kompakteren Heterochromatin zu vergleichen. Dafür überexprimierte ich Nukleosomen-*Remodeling*-Enzyme, deren Targeting zu Heterochromatin durch die Fusion mit einer Heterochromatin-bindenden Domäne erreicht wurde. Allerdings stellte sich heraus, dass die Überexpression des *Remodelers* Hrp3 für *S. pombe* toxisch war, unabhängig vom Targeting. Hrp3 Überexpression unterdrückte die Expression eines in Heterochromatin platzierten Reportergens und verursachte Defekte bei der Positionierung von Nukleosomen an den Genkörpern.

Obwohl die Informationen, die durch *Short-Read*-Sequenzierung für Heterochromatin-Regionen erhalten wurden, spärlich waren, ließ sich eine ATP –Hydrolyse-abhängige Zunahme der Regelmäßigkeit der Nukleosomenpositionierung über subtelomerischen Regionen feststellen. Darüber hinaus führten wir erfolgreich eine *gene-by-gene* Analyse durch, um die Regelmäßigkeit und Wiederholungslängen, die sog. *Nucleosome Repeat Length* (NRL) von Nukleosomen-*Arrays* in Wildtyp- und *Remodeler*-Deletionsstämmen zu messen. Die häufigste NRL beträgt 150 bp; sie ist damit um ein paar Basenpaare noch geringer als bislang angenommen.

Im zweiten Kapitel testete ich *in vitro*, ob die Chromatinfaltung und die Phasentrennung das *nucleosome sliding* behindern. Diese Studie wurde mit der *D. melanogaster* ATPase ISWI durchgeführt, die Nukleosomen verschieben kann. Nach der Rekonstitution von Nukleosomen-*Arrays* induzierte ich die intramolekulare Faltung und Phasentrennung durch Zugabe unterschiedlicher Salzmengen. Die gebildeten Chromatinkondensate enthielten Nukleosomenkonzentrationen wie sie auch im Zellkern zu finden sind. Erstaunlicherweise blieben die Kondensate für sehr voluminöse Komplexe zugänglich, was sie zu einem nützlichen Modellsubstrat macht, um die Herausforderungen zu untersuchen, denen *Remodeler* in einer dichten Chromatinumgebung begegnen. ISWI reicherte sich in Chromatinkondensaten an und verlangsamte die Fusion der Kondensate in einer konzentrationsabhängigen Weise. Mit Hilfe eines neuartigen, bildgebenden *nucleosome sliding Assays* konnten wir die *Remodeling*-Raten innerhalb und außerhalb von Chromatinkondensaten vergleichen. Wir konnten bestätigen, dass das *nucleosome sliding* innerhalb von Chromatinkondensaten stattfindet. Die Anfangsgeschwindigkeit für das *nucleosome sliding* innerhalb der Kondensate war nur um das Zweifache niedriger als in Lösung. Zusammenfassend stellen die Kondensate keine starke Barriere für *nucleosome sliding* dar. Um die viskoelastischen

Eigenschaften von Chromatinkondensaten zu charakterisieren, setzten wir optische Pinzetten ein, um die Kondensate kontrolliert fusionieren zu lassen. Der Verlust der ATP-Hydrolyse führte zu einer Verhärtung der Chromatinkondensate und einer verringerten Dynamik von ISWI. Wir erklären unsere Ergebnisse mit Hilfe eines *monkey-bar* Modells, in dem die beiden DNA-Bindungsdomänen von ISWI zwischen starken und schwachen Bindungsmodi wechseln. So stellt ISWI sicher, dass es auch im Zellkern, wo die hohe Nukleosomenkonzentration die Dissoziationskonstanten deutlich übersteigt, mobil bleibt. Unsere Ergebnisse deuten darauf hin, dass Pathologie-assoziierte Phänotypen auch zum Teil durch Veränderungen der Chromatindynamik und nicht ausschließlich durch eine Störung der kanonischen *Remodeling*-Funktionen verursacht werden könnten.

Im dritten Kapitel untersuchte ich die Wechselwirkung zwischen ISWI und dem *acidic patch*, der für seine Aktivierung wichtig ist. ISWI durchläuft während der Katalyse globale Konformationsänderungen, was die Strukturanalyse schwierig macht. Ich verwendete Mononukleosomen mit einem UV-aktivierten Crosslinker, der in *acidic patch* Nähe angebracht war, mit dem Ziel ISWI in einer seltenen Konformation anzureichern. In dieser vorläufigen Studie zeigen wir, dass die Affinität von ISWI zum *acidic patch* mit der Länge der Linker-DNA und im ADPBeF_x-gebundenen Zustand zunimmt. Die im Rahmen dieser Dissertation entwickelten Assays und diskutierten Konzepte könnten in Zukunft dazu dienen, neue Wege für Therapeutika eröffnen.

Abstract

In almost all eukaryotes, the DNA is organized in a dynamic polymer called chromatin. The nucleosome, the smallest unit a building monomer of chromatin, is formed by wrapping 146 bp of DNA around an octamer composed of histone proteins. Nucleosomes are interspaced with a piece of free DNA, called linker DNA. Nucleosomes tend to be evenly spaced, and this regular spacing is important for preventing cryptic transcription and protecting the genome from double-strand breaks. Nucleosome positions on DNA are influenced by ATP-dependent chromatin remodeling complexes. These remodelers can evict or assemble nucleosomes, incorporate histone variants and slide nucleosomes along DNA.

Chromatin can fold into higher order structures, both *in vitro* and *in vivo*. Nucleosome arrays also undergo phase separation and form chromatin condensates. Chromatin folding and phase separation put challenges on nucleosome remodelers that must act on it. In this thesis, I characterized nucleosome sliding in differently folded chromatin substrates.

In the first chapter, I used fission yeast as a model system to compare nucleosome sliding in euchromatin and the generally more compact heterochromatin using overexpression and heterochromatin targeting approaches. Targeting was achieved by fusion of chromatin remodelers with a heterochromatin-binding domain. Overexpression of the remodeler Hrp3 was toxic to fission yeast, independent of targeting. Hrp3 overexpression derepressed expression of a reporter gene placed into heterochromatin and caused defects in nucleosome positioning over gene bodies. Although the information obtained by short read sequencing for heterochromatin regions was sparse, we have identified an ATP-dependent increase in a regularity over subtelomeric regions. Moreover, we have successfully performed a gene-by-gene analysis to measure the regularity and repeat lengths of nucleosome arrays in wild type and remodeler-deletion strains. The most prevalent NRL turned out to be 150 bp, even tighter than published before.

In the second chapter, I tested if nucleosome array folding and phase separation impede nucleosome sliding *in vitro*. This study was performed with *D. melanogaster* ATPase ISWI, that slides nucleosomes on its own. I have reconstituted nucleosome arrays and induced intramolecular folding and phase separation by addition of varying amounts of salt. The chromatin condensates that formed contained nucleosome concentrations in the same range as the nucleus and were accessible to large complexes, making them a useful model substrate to study challenges encountered by remodelers in a crowded chromatin environment. ISWI was enriched inside chromatin condensates and it slowed down condensate fusion in a concentration-dependent manner. We have developed a novel, imaging-based nucleosome sliding assay, which allowed us to compare remodeling rates in- and outside of chromatin condensates. We confirmed that nucleosome sliding takes place inside chromatin condensates. The initial velocity for nucleosome sliding inside the condensates was only two-fold lower than in solution. Taken together, ISWI slides nucleosomes inside chromatin condensates and condensates do not pose a strong barrier for sliding. To characterize viscoelastic properties of chromatin condensates, we employed optical tweezers to fuse them in a controlled manner. Loss of ATP hydrolysis led to hardening of chromatin condensates and decreased dynamics of the remodeler. We rationalize our results with the help of a ‘monkey-bar’ model in which ISWI’s two DNA binding domains cycle between strong and weak binding modes, thereby ensuring mobility through the nucleus, where the high nucleosomes concentration well exceeds the dissociation constants. Our findings suggest that pathologies-associated phenotypes might be caused in part by changes in chromatin dynamics, and not exclusively by disruption of canonical remodeler functions.

In the third chapter, I investigated the interaction of ISWI and the acidic patch, which is important for its activation. Nucleosome remodelers are going through global conformational changes during nucleosome sliding, making structural analysis challenging. I used mononuclesomes with a UV-activating crosslinker close to the acidic patch that will covalently bind molecules nearby. In this preliminary study, we show that the affinity of ISWI towards the acidic patch increases with linker DNA length and in ADPBeF$_x$ bound state. Developed assays and discussed concepts in this dissertation might open new avenues for therapeutics.

List of abbreviations

4-MBP	4-(*N*-maleinimido)-benzophenon
5-FOA	5-Fluoroorotic acid
A	Absorbance
ADP	Adenosine diphosphate
ATP	Adenosine triphosphate
ATPase	Adenosine 5'-triphosphatase
Bp	Base pairs
CD	Chromodomain
cDNA	Complementary DNA
C_t	Cycle threshold
CV	Column volume
DNA	Deoxyribonucleic acid
DNase	Deoxyribonuclease
DTT	Dithiothreitol
EDTA	Ethylenediaminetetraacetic acid
EM	Electron microscopy
EMM	Edinburgh minimal medium
EtBr	Ethidium bromide
Fft3	Fission yeast Fun30
FLIM	Fluorescence lifetime imaging
FRAP	Fluorescence recovery after photobleaching
FRET	Förster resonance energy transfer/ Fluorescence resonance energy transfer
HEPES	4-(2-hydroxyethyl)-1-piperazineethanesulfonic acid
IDR	Intrinsically disordered regions
Kb	Kilobase
kDa	Kilodalton
LB	Lysogeny broth
Leu	Leucine
LLPS	Liquid-liquid phase separation
MNase	Micrococcal nuclease
MOPS	3-(N-morpholino)propanesulfonic acid

NCP	Nucleosome core particle
NFR	Nucleosome free region
NRL	Nucleosome repeat length
OD	Optical density
PAGE	Polyacrylamide gel electrophoresis
PEG	Polyethylene glycol
PSB	Phase separation buffer
RT	Room temperature
SD	Standard deviation
SDS	Sodium dodecyl sulfate
SEM	Standard error of the mean
SHL	Superhelical location
RI	Refractive index
RNase	Ribonuclease
RT	Room temperature
RT-qPCR	Real-time quantitative PCR
TBE	Tris-borate-EDTA
TCA	Trichloroacetic acid
ThT	Thioflavin T
TSS	Transcription start site
Tris	Tris(hydroxymethyl)aminomethane
Ura	Uracil
UV	Ultraviolet
Wt	Wild type
YE	Yeast extract
YES	Yeast extract with supplements

1. Introduction

1.1 Chromatin

The DNA of all eukaryotic organisms, with the exception of dinoflagellates, is organized in a dynamic polymer called chromatin. Building units of chromatin are nucleosome core particles, 146 bp of DNA wrapped around an octamer core. Octamer is a protein complex that consists of two copies of each histone: H2A, H2B, H3 and H4. H3 and H4 form a central tetramer. On each side of a tetramer there is a H2A-H2B dimer (Figure 1.1.). Positively charged residues in the histones contact the phosphate backbone of the DNA every ~10.4 bp. These points of contact are called superhelical locations. NCPs are connected by a short piece of a naked DNA called linker DNA. NCP and its linker DNA together form a nucleosome. Linker DNA typically has a length from ~18 to ~60 bp, depending on an organism and a cell type (Perišić et al., 2010). Some linker DNAs are bound by linker histone H1 (H5 in birds). H1 binds the entry and the exit point of DNA from NCP (Syed et al., 2010; Zhou et al., 1998). Nucleosome with a linker histone is called a chromatosome. Besides these canonical histone forms, there are numerous sequence variants for H3, H2A, H2B and H1 (Franklin & Zweidler, 1977), but only two for the H4, one in wheat with only one amino acid change (Tabata & Iwabuchi, 1984) and another one discovered recently exclusively in hominids (Long et al., 2019). The incorporation of histone variants into nucleosomes can affect the stability of NCP, interaction partners, posttranslational modifications (PTMs) and higher order chromatin structures (McGinty & Tan, 2014).

Histones, especially their N-terminal tails that protrude out of nucleosome, are subjected to different kinds of PTMs such as methylation, acetylation, phosphorylation, ubiquitination, and sumoylation (McGinty & Tan, 2014). PTMs can modulate chromatin folding and recruit a variety of proteins thereby impacting cell differentiation, gene regulation and other key cellular processes. The comprehensive genome-wide analysis of chromatin landscape for *Drosophila melanogaster* based on 18 histone modifications revealed nine prevalent combinatorial patterns (Kharchenko et al., 2011). Around the same time, the Bas van Steensel group produced genome-wide binding maps of 53 chromatin proteins in *Drosophila* cells and showed that the genome is segmented into five principal chromatin types (Filion et al., 2010).

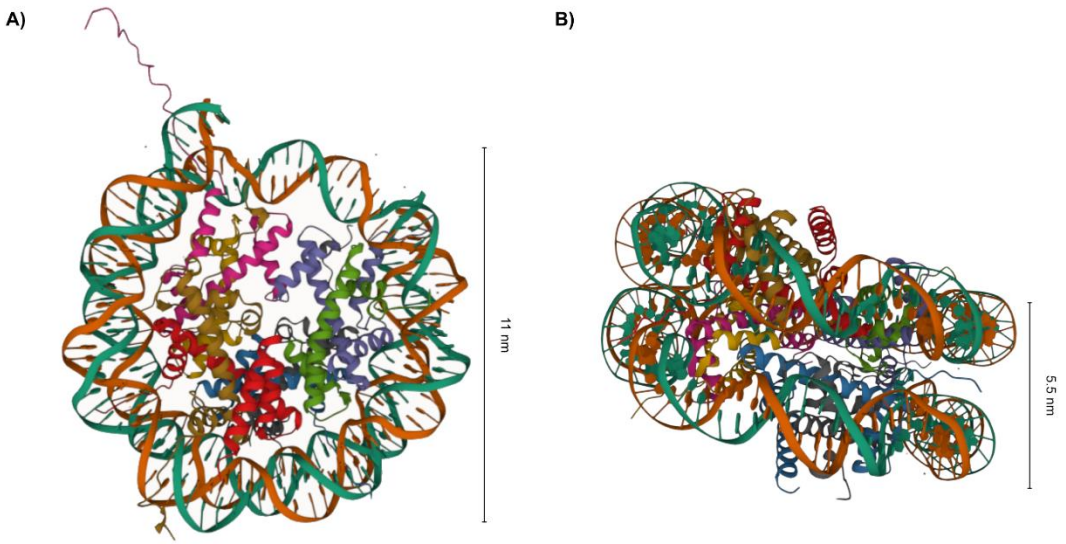

Figure 1.1. Nucleosome core particle. *(H2A brown and grey, H2B red and blue, H3 purple and magenta, H4 green and ochre, 146 bp DNA strands are in orange and dark blue). A) Front view; B) Side view, obtained by rotation of A) for 90° upwards. PDB ID: 1AOI (Luger et al., 1997). The image is created with Mol*Viewer (Berman et al., 2000; Sehnal et al., 2021).*

1.1.1 Chromatin folding

The biggest challenge in a packing of a long DNA molecule in a small nucleus is a neutralization of its extensive negative charge carried by phosphate groups. This negative charge is partially neutralized by wrapping around positively charged histone octamers. Resulting extended chromatin fiber was first described in 1974 and named 10 nm fiber or beads on string (Figure 1.2.A) (Olins & Olins, 1974; Woodcock, 1973).

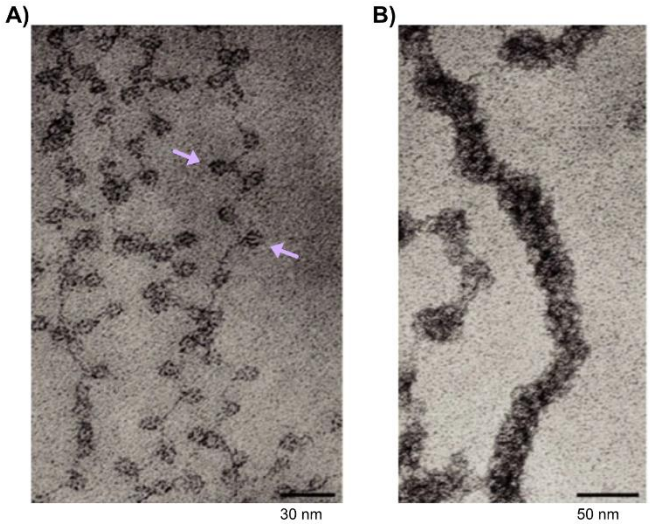

Figure 1.2. Chromatin spreads under different ionic strengths. *A) Low ionic-strength chromatin spread. Arrows indicate individual nucleosomes. B) Chromatin spread at a moderate ionic strength. Reprinted with permission from Olins and Olins, 2003.*

Further neutralization of DNA charge by cations, metabolites and proteins promotes higher order folding of chromatin. Applying light and electron microscopy to study chromatin higher order structures in a nucleus lead to very little information. Structural flexibility of histone tails, plethora of

histone modification and histone variants, absence or presence of linker histone and non-histone chromatin architectural proteins, differences in nucleosome repeat length (NRL) and nucleosome occupancy and positioning, DNA sequence heterogeneity – all those variations are likely to impact chromatin folding (Routh et al., 2008). For that reason, the efforts to decipher higher order chromatin structures were focused on isolated chromatin. The dependence of folding on ionic conditions was quickly established. Electron microscopy of isolated polynucleosomes revealed a 10 nm fiber in low salt that progressively compacts as the ionic strength is raised (Figure 1.2.B). A breakthrough in chromatin structure analysis was made when fully defined artificial polynucleosomes reconstituted onto DNA containing regularly spaced high nucleosome affinity sequences were being employed (Simpson, Thoma and Brubaker, 1985; Schalch, Duda, Sargent, et al., 2005). Low cation concentration (~<50 mM Na^+ and ~<1 mM Mg^{2+}, depending on the length of a chromatin fiber used) promoted folding into compact structure of roughly 30 nm diameter (Finch & Klug, 1976; Robinson et al., 2006; Schalch et al., 2005; Song et al., 2014; Woodcock et al., 1984) *in vitro*. These results led to the proposal of an elegant model for hierarchical chromatin folding (Figure 1.3.).

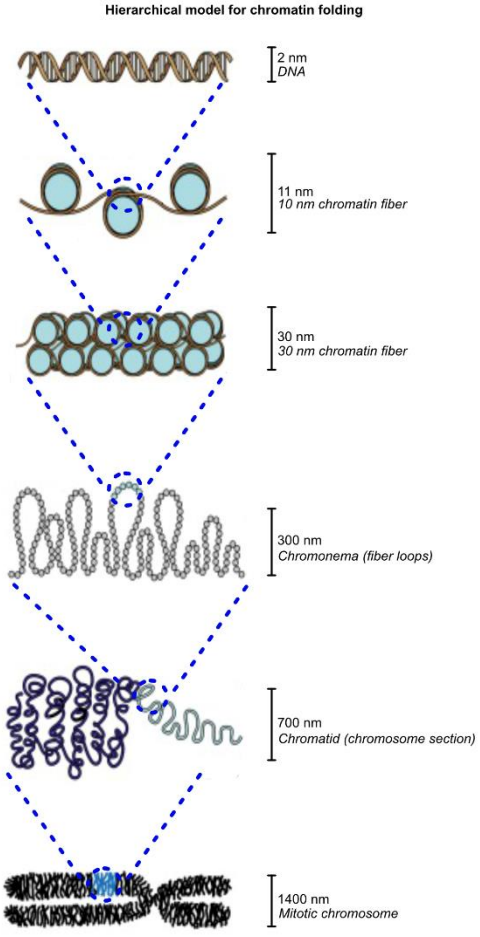

Figure 1.3. The hierarchical model of chromatin folding. *Reprinted under Creative Commons license and modified from Moraru and Schalch, 2019.*

This model suggests that the 30 nm fiber is the main building unit of chromatin (Finch & Klug, 1976). The 30 nm fiber is thought to gradually assemble into helically folded 120-nm chromonema, 300- and 700-nm chromatids, and eventually mitotic chromosomes (Belmont et al., 1987; Kireeva et al., 2004; Rattner & Lin, 1985). The arrangement of nucleosomes and linker DNA within the 30 nm fiber remains controversial to this day, with solenoid and zigzag fiber models being the

best supported (Robinson et al., 2006; Schalch et al., 2005). Incorporation of a linker histone increased a compaction of a nucleosome array further (Routh et al., 2008). *In situ,* in nuclei, evidence for the 30 nM fiber was found only in two special cases, echinoderm sperm nuclei and transcriptionally inert chicken erythrocyte nuclei (Horowitz et al., 1994), but it was rarely seen in a more typical nuclei (reviewed in Woodcock and Horowitz, 1995). The evidence of 30 nm fiber folding into hierarchical higher order chromatin structures is lacking (Müller et al., 2004). Higher order chromatin structures beyond 30 nm fiber (~120 nm) were observed with both light and electron microscopy, but if they indeed form via hierarchical folding of 30 nm fiber, was not possible to deduce in any of the studies (Belmont et al., 1989; Belmont & Bruce, 1994; Kireev et al., 2008). Cryo-EM (Eltsov, MacLellan, et al., 2008; McDowall et al., 1986), x-ray scattering (Nishino et al., 2012), and electron spectroscopy imaging (ESI) studies (Ahmed et al., 2010; Fussner et al., 2012) of the nucleus also do not support the hierarchical chromatin folding model. Ou et al. showed that chromatin assembles into irregular and variable structures, namely disordered flexible chains from 5 nm to 24 nm in diameter. They determined a chromatin volume concentration in an interphase nucleus and a mitotic chromosome to be 12-52% (with distinct spatial distribution patterns) and >40%, respectively. These data suggest that chromatin organization is achieved with different chromatin concentrations and not higher order folding (Ou et al., 2017). Recent *in vitro* study showed that nucleosomal arrays self-associate into large globular oligomers and the biophysical analysis suggested that inside the oligomers, the array monomers are packaged as extended 10 nm fibers, not as folded 30 nm fibers (Maeshima et al., 2016, also see chapter 1.4).

What is, then, the higher order chromatin structure in a cell? Chromosome conformation capture methods identified topologically associated domains (TADs), hundreds of kilobases in size (Dixon et al., 2012; Ge et al., 2012; Sexton et al., 2012). Experiments with higher resolution together with modeling suggested existence of much smaller compact chromatin domains around 0.2 Mbp in size (~200 nm) (Bascom et al., 2016; Bintu et al., 2018; Rao et al., 2014). Unlike TADs that are present only in the interphase, compact chromatin domains might persist through the cell cycle (Xu et al., 2018). Apart from nucleosome-nucleosome interactions, to fold the chromatin into domains, chromatin looping via cohesion is necessary (Rao et al., 2017; Sofueva et al., 2013; Wutz et al., 2017; Zuin et al., 2014) (Figure 1.4.). Current most widely accepted hypothesis for chromatin loop and TAD formation is a “loop extrusion model”. In this model, a ring-shaped SMC complexes (cohesin in interphase) engage chromatin and begin extruding a DNA loop in an ATP-dependent process. Loop extrusion continues until SMC complex spontaneously falls of or encounters a barrier – mostly CTCF, but RNA Pol II and other architectural factors can play a barrier role.

On a bigger scale, chromatin is organized into two compartments – A and B, composed of largely active and inactive chromatin, respectively – probably formed by a mechanism distinct from TAD formation (Hansen et al., 2018). Indeed, phase separation was suggested to play a role (Falk et al., 2019). At the largest scale, chromosomes are organized into chromosome territories, where each chromosome occupies its own position in the nucleus (Hansen et al., 2018) (Figure 1.4.). In mitosis, condensin I and II, another class of SMC complex, are the major proteins responsible for chromatin folding, together with topoisomerase II and others. Few models have been put forward to explain folding of a mitotic chromosome (Beseda et al., 2020). Regions with high gene density are associated with decondensed chromatin (Gilbert et al., 2004; Gilbert & Bickmore, 2006) and upon transcription induction chromatin fiber unfolds (Hu et al., 2009; Tumbar et al., 1999). Moreover, as the chromatin structure is dynamic, local ordered structures might not persist over long timescales.

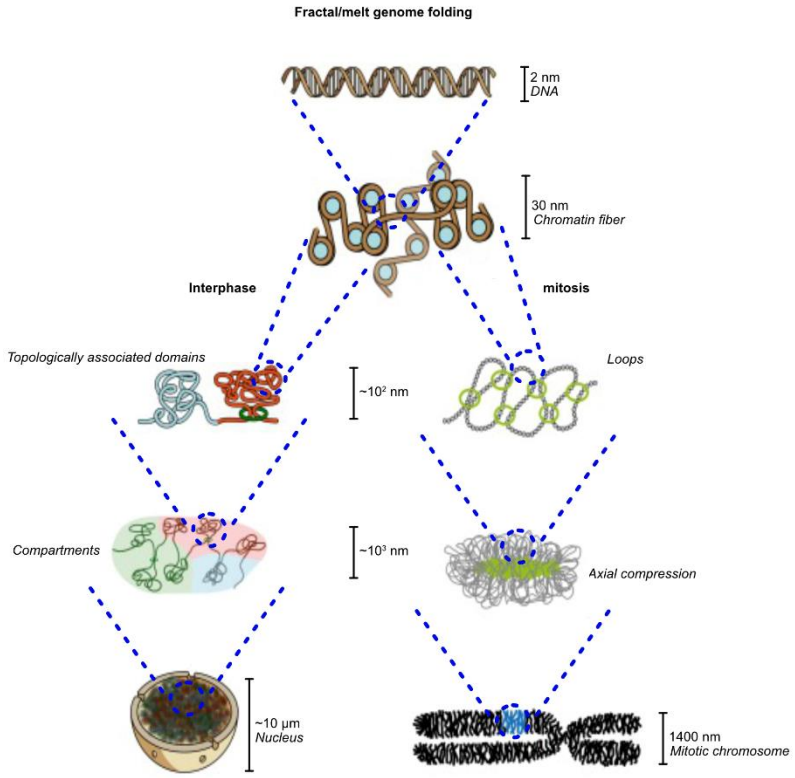

Figure 1.4. The emerging dynamic and fractal chromatin folding model. *Reprinted under Creative Commons license and modified from Moraru and Schalch, 2019.*

1.1.2 Chromatin dynamics

Whereas a static chromatin structure has been extensively researched, much less is known about its dynamics. In interphase, chromatin moves coherently (in the same direction) across micron-scale regions for a few seconds (Nozaki et al., 2017; Shaban et al., 2018; Xiang et al., 2018; Zidovska et al., 2013a). Activity of nuclear enzymes acting on the chromatin fiber is required to generate coherent chromatin motion, as predicted by several models and corroborated by experiments (Saintillan et al., 2018). This coherent motion constantly stirs the genome and could contribute to gene regulation by changing fiber conformation, accessibility, intragenomic interactions and distribution of nuclear enzymes (Zidovska, 2020). A chromatin locus displays constrained motion for short periods of time (on seconds timescale). This motion is similar in both mitosis and interphase, suggesting that the condensation does not necessary affect local diffusion dynamics of chromatin (Oliveira et al., 2021). However, different genomic loci may have characteristic local diffusion properties due to their specific cell or chromatin context. In yeast, chromatin mobility is reduced in centromeric and telomeric regions (Heun et al., 2001). There is significant dynamics also on a level of a nucleosome (reviewed in Fierz and Poirier, 2019). Accessible thermal energy is enough for a nucleosome for continuous partial DNA unwrapping and rewrapping. Histone octamer itself undergoes conformational dynamics, especially histone tails, although dimers and tetramers can even transiently disengage. Histone octamers continuously undergo structural fluctuations.

1.1.3 Nucleosome landscape

Nucleosome position along DNA has often been analyzed with micrococcal nuclease (MNase) digestion of isolated chromatin. Under the conditions of partial digestion, achieved by limiting

amount of nuclease and/or digestion time, only linker DNA is digested away while DNA wrapped around an octamer is protected. The product of digestion appears as a ladder on gel electrophoresis, consistent with regular and repetitive nature of nucleosome positioning (Figure 1.5.A). DNA band corresponding to mononucleosome is cut out from gel, sequenced and nucleosome position deduced (Baldi et al., 2020; Singh & Mueller-Planitz, 2021). A nucleosome is well positioned if it occupies the same translational position across an ensemble of cells (Figure 1.5.B). The central base pair is referred to as a nucleosome dyad position. A particular base pair in a certain cell is either occupied by a nucleosome or free. A fraction of cells that possess a nucleosome on this position is called a nucleosome occupancy. As nucleosomes are not perfectly positioned, it is commonly described as the probability for a given base pair to be occupied by any nucleosome in the cell population (Figure 1.5.C). Averaged nucleosome occupancy in *S. cerevisiae* is ~75% (Oberbeckmann et al., 2019). The nucleosome array is regular if linker DNA lengths in the array are similar, making nucleosomes evenly spaced. Nucleosome repeat length (NRL) can be determined for the array and it corresponds to the average dyad-to-dyad distance in this array. Lastly, when all nucleosomes within a certain nucleosome array assume similar positions in the cell population, they are phased. Phased arrays can be either regular or irregular (Singh & Mueller-Planitz, 2021) (Figure 1.5.D-F).

Nucleosome position on DNA is influenced by multiple factors. First, it depends on how easily DNA bends around the octamer, which is determined by underlying DNA sequence. Easily bendable sequences (AA, TT, AT and TA dinucleotides) are enriched every 10 bp on DNA-histone contacts (so called rotational positioning), whereas intrinsically stiff sequences (homopolymeric sequences poly(dA:dT) and poly(dG:dC)) stay solvent-exposed (Struhl & Segal, 2013). Poly(dA:dT) sequences are responsible for nucleosome depletion at most promoter sequences. Actively transcribed genes show a distinct nucleosome organization: nucleosome free region (NFR) at the promoter, well-positioned first nucleosome after the NFR (+1 nucleosome) and phased regular arrays over gene body (Yuan et al., 2005). NFR is enhanced and +1 nucleosome positioned by action of chromatin remodeling complexes guided by general regulatory factors (GRFs) (Krietenstein et al., 2016). In yeast, transcription start site (TSS) overlaps with the position of +1 nucleosome (Lee et al., 2007). Finally, the remodelers will generate regular nucleosome array aligned to the +1 nucleosome (Gkikopoulos et al., 2011; Kubik et al., 2019).

However, deciphering nucleosome positioning is not straightforward in all parts of genome. Specifically, heterochromatin prevalently contains repeats making mapping of short fragments after sequencing impossible. Therefore, nucleosome mapping techniques based on short read sequencing gave only very limited information on nucleosome architecture in heterochromatin. This challenge was recently partially circumvented by employment of long-read sequencing (Baldi et al., 2018), sometimes preceded with methylation footprinting of chromatin (Abdulhay et al., 2020; Lee et al., 2020; Shipony et al., 2020; Stergachis et al., 2020; Wang et al., 2019).

Proper nucleosome positioning and spacing might be important for chromatin folding and long-range interactions, preventing cryptic transcription, protecting the genome from double-strand breaks and regulating activity of certain chromatin enzymes (reviewed in Singh and Mueller-Planitz, 2021).

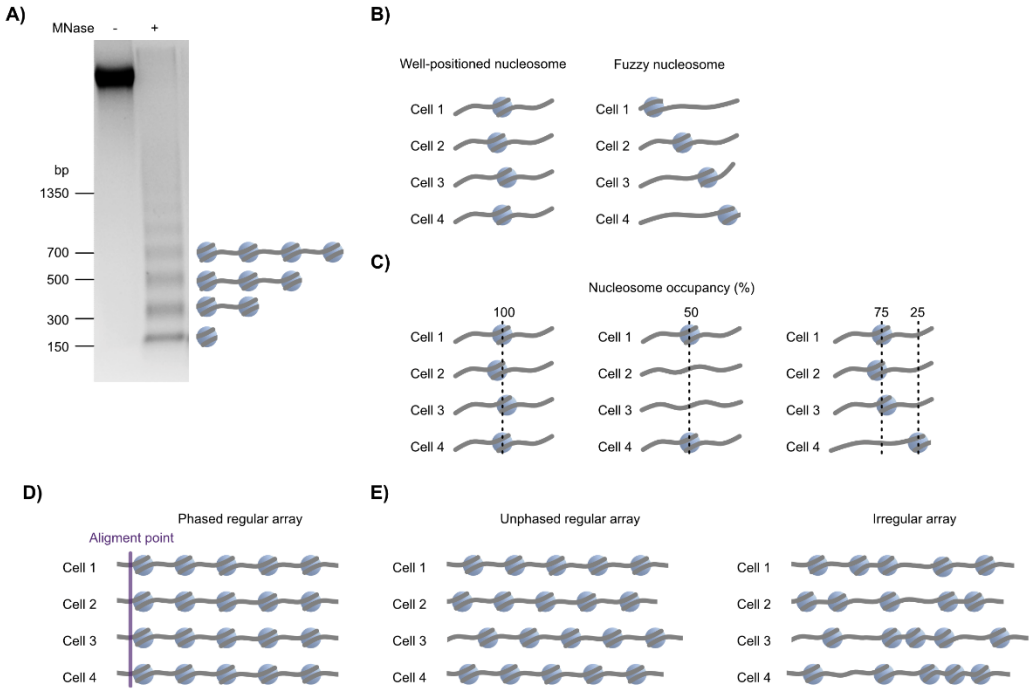

Figure 1.5. Descriptors of a nucleosome landscape. *A) MNase digestion of S. pombe chromatin. B) Left: nucleosomes with the same translational position (well positioned) across a cell population. Right: nucleosomes with a different translational position (fuzzy) in a cell population. C) Examples of different nucleosome occupancies across a cell population. D) Phased regular array. Across the cell population, nucleosomes are equally spaced over the gene and the nucleosome array is aligned with respect to a particular DNA sequence. E) Unphased regular array. Across the cell population, nucleosomes are equally spaced over the gene but the nucleosome array is not aligned with respect to a particular DNA sequence. F) Irregular array. Nucleosomes are not regularly spaced over the gene across the cell population.*

1.2 Chromatin remodelers – overview, function and mechanism

ATP-dependent chromatin remodeling complexes (remodelers) use energy derived from ATP-hydrolysis to evict or assemble nucleosomes, incorporate histone variants and slide nucleosomes along DNA (Clapier et al., 2017) (Figure 1.6.A). Thereby, they ensure proper nucleosome density, spacing, composition and DNA accessibility (Singh & Mueller-Planitz, 2021). They consist of a catalytical ATPase subunit accompanied by auxiliary subunits that have a role in regulation, specialization and targeting. All remodelers have similar ATPase subunit belonging to RNA/DNA helicase superfamily 2. Although ATPase domain in catalytical subunit is conserved, flanking domains are unique and provide basis for classification into four subfamilies, conserved from yeast to human: imitation switch (ISWI), chromodomain helicase DNA-binding (CHD), switch/sucrose non-fermentable (SWI/SNF) and INO80 (Flaus et al., 2006) (Figure 1.6.B). There is additional class of orphan remodelers, which lack identifiable accessory domains, but have important specialized functions: ALC1 (CHD1-like), scFun30/spFft3/dEtl1/hSMARCAD1, ATRX and CSB (McGinty & Tan, 2014). Remodelers function in many chromosomal processes including modulation of higher order chromatin structures (Corona et al., 1999; Fasulo et al., 2012), DNA replication (Biswas et al., 2008; Collins et al., 2002; Flanagan & Peterson, 1999; Li et al., 2005; Papamichos-Chronakis & Peterson, 2008; Poot et al., 2004; Shimada et al., 2008; Vincent et al., 2008; Zhou et al., 2005), repair and recombination (Kandasamy et al., 2009; Van Attikum et al.,

2004, 2007), chromosome cohesion and segregation (De La Fuente et al., 2004; Huang et al., 2004; Yokoyama et al., 2009), gene regulation (Armstrong et al., 2002; Kwon et al., 2008; Parnell et al., 2008; Whitehouse et al., 2007), transcription (Alén et al., 2002; Brown et al., 1996; Simic et al., 2003) and might affect higher-order chromatin architecture. They were also shown to enhance a locus movement inside the nucleus (Neumann et al., 2012) and to distort structural conformation of histone octamer (Sinha et al., 2017). It is then not surprising that they are required for a plethora of biological processes and involved in numerous pathologies (reviewed in Workman and Abmayr, 2014).

Remodelers act through diverse mechanisms (Clapier et al., 2017). ISWI and CHD subfamily are assembly remodelers (Lusser et al., 2005; Torigoe et al., 2013; Varga-Weisz et al., 1997). Following deposition, they are involved in nucleosome maturation and assembly from an initial histone-DNA complex (pre-nucleosomes). After that they create equal spacing throughout nucleosome arrays (Barisic et al., 2019; Fyodorov et al., 2004; Gkikopoulos et al., 2011; Ito et al., 1997; Ocampo et al., 2016; Tsukiyama et al., 1999; Wiechens et al., 2016). This process takes place after replication and during transcription (Yadav & Whitehouse, 2016). Members of SWI/SNF subfamily can slide or evict a nucleosome or its components (Asturias et al., 2002; Chaban et al., 2008; Dechassa et al., 2010; Logie & Peterson, 1997; Lorch et al., 2006). Thereby they can render chromatin more accessible to transcription activators or repressors. In *Drosophila*, ISWI promotes the association of the linker histone H1 with chromatin and regulates higher-order chromatin structure (Corona et al., 2007; Siriaco et al., 2009). While ISWI and CHD family remodelers space nucleosome arrays, SWI/SNF remodelers act to randomize initially spaced arrays. SWI/SNF lack additional DNA binding domain that is supposed to bind and “measure” linker DNA and it is necessary for a spacing activity (McKnight et al., 2011). Remodelers of INO80 subfamily can exchange histone variants (Brahma et al., 2017; Mizuguchi et al., 2004) which can affect factor recruitment. More recently it has been shown that INO80 can also slide (Udugama et al., 2011) and space (Singh et al., 2021) nucleosomes. Linker histone suppresses mobility of NCP along a DNA (Pennings et al., 1994). All subclasses of remodelers were inhibited by chromatosome arrays, an effect mainly independent of the array folding and relieved by linker histone phosphorylation (Horn et al., 2002). H1 altered the remodeling outcome by hSWI/SNF on mononucleosomes promoting more central position of an octamer (Ramachandran et al., 2003). Conversely, linker histones inhibited linear array remodeling by CHD1, but not ACF (Maier et al., 2008). In another study, linker histones did not preclude remodeling of minichromosomes by SWI/SNF or NURF (Clausell et al., 2009).

Extensive conformational changes during ATPase cycle ratchet the enzyme along DNA through what has been termed an inchworm mechanism (Gu & Rice, 2009; Lee & Yang, 2006; Velankar et al., 1999). How is ATP hydrolysis mechanistically coupled to nucleosome sliding? Two main models, not mutually exclusive, have been proposed (reviewed in Längst and Becker, 2004).

A twist defect diffusion model (Brandani et al., 2018; van Holde & Yager, 1985) was initially proposed to explain a spontaneous nucleosomes repositioning driven by thermal motion (Flaus & Richmond, 1998; Meersseman et al., 1992; Pennings et al., 1991) and later extended to ATP-driven unidirectional motion (van Holde & Yager, 2003). A twist defect arises when two adjacent segments of the same DNA duplex do not undergo a corkscrew motion in unison, and it comprises a gain or a loss of a base pair. The twist defect is then propagated around the nucleosomes, restoring DNA to its canonical conformation and repositioning the nucleosome 1 bp at the time (Bowman & Deindl, 2019). Indeed, remodeler´s action generates torsional stress (Havas et al., 2000) and when DNA topology is constrained in small circular nucleosomal arrays, ySWI/SNF

remodeling is nearly inhibited (Gavin et al., 2001). However, introduction of nicks to relieve torsional stress or steric blocks to impede twist diffusion within the nucleosomal DNA have little or no effect on remodeling (Aoyagi & Hayes, 2002; Längst & Becker, 2001), arguing against this simple twist diffusion model. Importantly, although some histone-DNA contacts must transiently shift, during twist defect diffusion DNA does not detach from the histone surface.

The second model, a loop diffusion model, proposes that DNA partially unwraps at the entry site, rebinds octamer with ten bp mismatch, thereby forming a loop or a bulge. The loop rapidly travels around the nucleosome and emerges on the exit site, repositioning the nucleosome in discrete steps that equal the length of the loop (increment of ten bp) (Kulić & Schiessel, 2003; Schiessel et al., 2001). Indeed, SWI/SNF remodelers were shown to create loops on nucleosomal DNA (Bazett-Jones et al., 1999; Lia et al., 2006; Zhang et al., 2006). Consistent with the predicted loop size, ISWI and SWI/SNF remodelers shift nucleosomes in steps of ~10 bp and ~50 bp, respectively (Kassabov et al., 2003; Schwanbeck et al., 2004). The model was further corroborated by the evidence that ACF detaches DNA at the borders of the nucleosome, indicative of DNA loop formation (Strohner et al., 2005).

Lastly, in the third model to explain sliding remodelers perturb DNA-histone interactions and shift entire segment of DNA in concert, equivalent to a rotation of the histone core with respect to the DNA (Bowman & Jenkins, 2010; Lorch et al., 2010).

Recently single molecule FRET experiments showed that ISWI slides nucleosomes in elementary steps of one bp (Deindl et al., 2013).

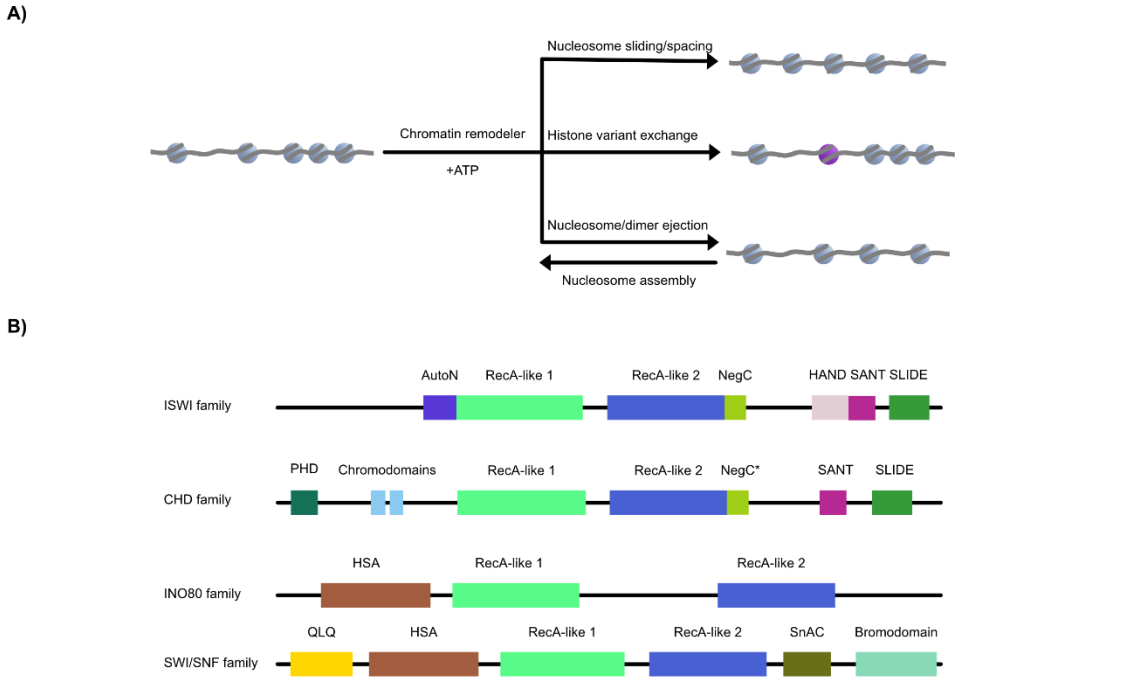

Figure 1.6. ATP-dependent chromatin remodelers. *A) Diverse functions exerted by remodelers. B) ATPase subunit contains two RecA-like lobes (DExx and HELICc) flanked by auxiliary domains (Clapier et al., 2017). In CHD NegC* is also referred to as brace-bridge.*

1.2.1 ISWI chromatin remodeler

In vitro part of this study was performed with *D. melanogaster* ATPase ISWI. This ATPase slides nucleosomes on its own (Corona et al., 1999; Längst et al., 1999; Abdulhay et al., 2021). The

activity of its ATPase domain is regulated by flanking domains, AutoN (autoinhibitory N terminal) and NegC (negative regulator of coupling). These autoinhibitory motifs keep the ATPase in an inactive state (Clapier & Cairns, 2012). Once when a substrate is encountered, the activity is positively regulated via nucleosome cues: N-terminal H4 tail (Clapier et al., 2001, 2002; Hamiche et al., 2001), linker DNA (Dang et al., 2006; Yang et al., 2006; Zofall et al., 2004) and a nucleosomal acidic patch formed by histones H2A and H2B (Dann et al., 2017; Gamarra et al., 2018). Nucleosomes containing the H2A.Z variant stimulate ISWI activity as well, due to an extended acidic patch (Goldman et al., 2010). AutoN inhibition is relieved by binding of H4 N-terminal tail to a motif adjacent to it, termed AcidicN (Ludwigsen et al., 2017; Yan et al., 2016). Upon deletion of an H4-tail, both ATPase activity and nucleosome sliding are compromised. The AutoN motif consists of only four amino acids (RHRK) and the same motif is present in a basic patch of the H4 tail. Mutation of the two arginines to alanines (ISWI2RA) increases DNA-stimulated ATPase activity, enhances the sliding activity and partially relieves dependence of ISWI on the H4 tail. The acidic patch relieves the autoinhibition imposed both by the AutoN and the NegC regions of the human ISWI remodeler SNF2h (Armache et al., 2019; Gamarra et al., 2018).

Binding of a carboxy-terminal HAND-SANT-SLIDE (HSS) domain to a linker DNA was proposed to counteract a NegC autoinhibition (Clapier & Cairns, 2012). When the linker DNA is absent or shorter than 20 bp, ISWI´s affinity for nucleosome drops and so does its ATP turnover and sliding capacity (Gangaraju & Bartholomew, 2007; Yang et al., 2006; Zofall et al., 2004). The HSS domain is a rigid entity that can bind histones, linker and nucleosomal DNA (Dang & Bartholomew, 2007; Grüne et al., 2003). Via its binding to a linker DNA, the HSS might have a role in spacing and act as a (part of a) molecular ruler that measures the distance between nucleosomes (Yamada et al., 2011; Yang et al., 2006). Therefore, ISWI preferentially slides nucleosomes towards the longer linker and as a result, nucleosomal arrays are evenly spaced (Ocampo et al., 2016; Singh et al., 2021; Tsukiyama et al., 1999) and mononucleosomes are centered (Kagalwala et al., 2004). It has been suggested that the HSS may pull the linker DNA into the nucleosome, but deletion and mutation analysis show that a power stroke between the HSS domain and the ATPase domain is unlikely (Ludwigsen et al., 2013; Mueller-Planitz et al., 2013).

The ATPase domain entails seven conserved helicase-related motifs, which play a key role in ATP hydrolysis (Dürr et al., 2006). Motifs I (Walker A) and II (Walker B) are located on ATPase lobe 1 and assist in binding of ATP and Mg^{2+}. They cooperate with motif VI on ATPase lobe 2, whose conserved arginine residue interacts with the γ-phosphate of the bound ATP, and it is as well necessary for ATP hydrolysis. Therefore, two ATPase lobes must spatially align for enzyme to be competent to hydrolyze ATP. In the apo state, NegC and AutoN keep ATPase domain in catalytically incompetent, globular conformation, where motifs are not oriented towards each other, preventing productive ATP hydrolysis (Harrer et al., 2018; Yan et al., 2016). In this resting state, HSS packs against the ATPase module and is not capable of binding DNA without prior conformational changes (Harrer et al., 2018). Upon binding to a nucleosome, the ATPase undergoes a global conformational change leading to the alignment of motifs I, II and VI by a rotation of the ATPase lobes (Chittori et al., 2019; Harrer et al., 2018; Yan & Wu, 2019). Lobe 2 rotates ~148° and AutoN shows coordinated adjustment. The ATPase is now catalytically competent and primed to bind and hydrolyze ATP. Lobe 2 itself undergoes some local conformational adjustments following the nucleosome binding. NegC becomes completely disordered in an activated state and the HSS domain was undetectable in the cryoEM structure, which could be attributed to its dynamic interaction with the linker DNA or the nucleosome (Yan & Wu, 2019). ISWI engages a nucleosome at the SHL2 position, two helical turns away from the dyad axis (Dang & Bartholomew, 2007; Kagalwala et al., 2004). It is possible for two enzyme molecules to bind one

nucleosome symmetrically at both sites (SHL±2). Indeed, Snf2h and ACF were suggested to act as dimers on a nucleosome substrate (Armache et al., 2019; Blosser et al., 2009; Johnson & Narlikar, 2022; Leonard & Narlikar, 2015; Racki et al., 2009). In addition to epitopes described above, ISWI also engages H3 through the residues that are highly conserved in ISWI proteins (Yan & Wu, 2019).

Several studies have shown that a conformation of domains depends on the nucleotide state, indicating structural dynamics and flexibility during the catalytical cycle. HSS domain moves away from the flanking DNA in a nucleotide dependent manner (Leonard & Narlikar, 2015) and it binds acidic patch region of the nucleosome in the presence of ADP-BeFx (Gamarra et al., 2018), accompanied by conformational change in HSS itself. Therefore, the HSS domain interaction interface is probably not static during the catalytic reaction. It has been suggested that the domain is released from linker DNA prior to the DNA translocation and may bind to the nucleosomes core (Gamarra et al., 2018; Leonard & Narlikar, 2015).

1.3 Heterochromatin

The term heterochromatin was first coined by Emil Heitz in 1928, depicting a part of a nucleus that stains all the way through the cell cycle with a boiling carmin acetate procedure he had devised (Heitz, 1928). Shortly after that, a position-effect variegation was described (Muller, 1930), a phenotype caused by a gene inactivation due to its relocation into a heterochromatin region (Elgin & Reuter, 2013; Schultz & Dobzhansky, 1934; Wakimoto & Hearn, 1990). Relatively early it was discovered that the heterochromatin forms over a repetitive DNA, termed satellite DNA, which is transcriptionally silenced, based on an inability to detect a corresponding RNA (a historical aspect is extensively reviewed in Allshire and Madhani, 2017).

Heterochromatin is generally more compact than euchromatin (Boettiger et al., 2016; Ou et al., 2017; Ricci et al., 2015) and inaccessible to enzyme probes (Spracklin & Pradhan, 2020). It is decorated with H3K9 methylation (Monika Lachner & Jenuwein, 2002) and hypoacetylated (Jeppesen & Turner, 1993). Hypoacetylation should contribute to a compaction of a chromatin fiber (Bascom & Schlick, 2018; Garcia-Ramirez et al., 1995; Wang et al., 2001). Methylated lysins are bound by a heterochromatin protein HP1 through its chromodomain (Lachner et al., 2001). H3K9me is deposited by Suv39 histone methyl transferases containing evolutionary strongly conserved catalytical SET domain (Rea et al., 2000). The methyl transferase itself has a chromodomain and can bind its own modification, thereby coupling modification writer and reader modules in the same protein (Müller et al., 2016). Moreover, HP1 directly interacts with the methyltransferase (Yamamoto & Sonoda, 2003) and recruits it to chromatin (Hathaway et al., 2012). This positive feedback loop enhances the spreading of the methylation mark. Further, the HP1 protein can bind two nucleosomes simultaneously and dimerizes on chromatin via chromoshadow domain, effectively bridging nucleosomes and condensing chromatin (Verschure et al., 2005). To avoid potentially deleterious gene silencing, heterochromatin spreading is antagonized by multiple mechanisms: generation of nucleosome free regions, promoting nucleosome turnover, binding of heterochromatin marks by antisilencing factors, tethering silencing machinery to their primary site of action by having writer and corresponding reader module present in the same enzyme, recruitment of euchromatic factors and deposition of euchromatin marks aided by low levels of transcription (reviewed in Allshire and Madhani, 2017). Sequences that restrain heterochromatin spreading by aforementioned mechanisms are known as barriers, for example tRNA genes (Partridge et al., 2000).

Heterochromatin prevents repetitive sequences from destabilizing a genome by suppressing their integration and recombination (Peng & Karpen, 2007). It is important in centromere function and kinetochore assembly. In yet unknown way, pericentromeric heterochromatin directs a proper incorporation of CENP-A histone variant and a functional kinetochore establishment (Ekwall et al., 1997; Folco et al., 2008; Lima de Faria, 1949; Nakano et al., 2008; Ohzeki et al., 2012). Heterochromatin is required for sister centromere cohesion and proper chromosome segregation (Bernard et al., 2001; Ekwall et al., 1995; Gregan et al., 2007). In mammals, heterochromatin can form in a specific manner to create a barrier to cell type reprogramming (it prevents binding of transcription factors) therefore preserving cell type identity of differentiated cells (Soufi et al., 2012). It is not then surprising that heterochromatin function is involved in various aspects of a human health, namely viral dormancy, premature ageing, metabolism and obesity (reviewed in Allshire and Madhani, 2017).

Once heterochromatin domains are established by nucleation and spreading, they are stably maintained through cell divisions (Wang & Moazed, 2017). However, mitotic and meiotic transmission of ectopically induced H3K9me mark is restricted (Audergon et al., 2015; Hathaway et al., 2012; Ragunathan et al., 2015). Transgenerational epigenetic inheritance, especially common in plants but examples exist in mammals (e.g., imprinted genes), is mediated via DNA methylation (Heard & Martienssen, 2014).

1.3.1 *Schizosaccharomyces pombe* as a model to study heterochromatin

Schizosaccharomyces pombe (fission yeast) shares many heterochromatin hallmarks with higher eukaryotes making it a good model organism for epigenetic research (reviewed in Allshire and Ekwall, 2015). Fission yeast heterochromatin is hypoacetylated (Ekwall et al., 1997). Silencing is mediated by H3K9 methylation (Noma, Allis and Grewal, 2001) that is recognized by Swi6, HP1 homologue (Bannister et al., 2001) which oligomerizes and spreads on chromatin (Canzio et al., 2011). Fission yeast has RNA interference (RNAi) machinery, whose role in heterochromatin assembly is conserved in protists, plants and some animals (e.g., *Drosophila*) (reviewed in Martienssen and Moazed, 2015). It lacks detectable DNA methylation (Wilkinson et al., 1995) and H3K27 methylation (Freitag, 2017). It has only one histone methyltransferase that is responsible for all H3K9 methylation, Clr4 (Nakayama et al., 2001). Clr4 binds and is stimulated by its own mark (Al-Sady et al., 2013; Zhang et al., 2008). H3K9 methylation will also recruit a SHREC complex, an equivalent of a mammalian NuRD, composed from chromodomain protein Chp2, an ATP-dependent chromatin remodeler from CHD family Mit1, histone deacetylase Clr3 and the poorly understood Clr1 and Clr2 proteins (Job et al., 2016; Motamedi et al., 2008; Sugiyama et al., 2007).

S. pombe genome is organized in three chromosomes. Heterochromatin is found at centromeres, telomeres, ribosomal DNA (rDNA) loci, and the mating-type region (Allshire & Ekwall, 2015). These regions contain *cenH* DNA elements (or *cenH* like repeats), made of *dg* and *dh* repeats (or their homologous). They are actively transcribed at low levels both in sense and antisense direction (Reinhart & Bartel, 2002). These transcripts pair up and double-stranded RNA (dsRNA) forms that subsequently induces heterochromatin formation. Briefly, dsRNA is trimmed by RNA endonuclease Dicer to form siRNA (short interfering RNAs) that are ~21-25 nucleotides long (Moazed, 2009; Provost et al., 2002). siRNA is loaded onto Argonaute (Ago1) protein. siRNA-loaded Ago1 is incorporated into RITS (RNA-induced transcriptional silencing) complex and one of the siRNA strands is released (Buker et al., 2007). The RITS complex is then targeted to nascent transcripts by an siRNA-RNA base-pairing (Bühler et al., 2006) and it recruits the methytransferase Clr4 (in CLRC complex) to nucleate heterochromatin (Verdel et al., 2004). Besides Ago1, RITS contains

Tas3 and chromodomain protein Chp1 that recognizes H3K9me mark, establishing and maintaining heterochromatin in yet another positive feedback loop (Schalch et al., 2009). On top of that, RITS recruits an RNA-directed RNA polymerase complex (RDRC) that will synthetize more of a dsRNA used by Dicer (Colmenares et al., 2007; Motamedi et al., 2004).

The centromeres occupy ~40, ~60 and ~120 kb on chromosomes I, II and III, respectively. They have two main regions: inner core containing kinetochore attachment site and the inner most repeats (*imr*) repeats; the outer repeats (*otr*) composed of multiple copies of *dh* and *dg* repeats (Wood et al., 2002) (Figure 1.7.). Metazoan centromeres also have a repetitive nature. Pericentromeric heterochromatin forms over *otr* and to a lesser extent over *imr* (Partridge et al., 2000). A reporter gene inserted into outer repeats will be silenced, but if placed into *imr* region, its expression will be variegated indicating unstable silencing. Just 1 kb distal to the outer repeats, no silencing occurs (Allshire et al., 1994, 1995).

The mating type region has three loci: *mat1* that is expressed and determines the mating type (P or M); *mat2-P* and *mat3-M* that contain *cenH* repeats and are silenced by heterochromatin (Figure 1.7.). Every second cell division (Holmes et al., 2005), in a homothallic strain (*h90*), a recombination happened between *mat1* and *mat2-P* or *mat3-M*, in a preferential fashion to switch a mating type (Grewal & Klar, 1997). Heterochromatin that assembles at telomeres and 40 kb subtelomeric region (Cam et al., 2005) suppresses their recombination and it is very important for genome stability (Bisht et al., 2008; Schoeftner & Blasco, 2009). Both in the mating type and a sub-telomeric regions, RNAi mediated heterochromatin formation is partially redundant with other pathways that act in parallel (Jia et al., 2004; Kanoh et al., 2005).

Lastly, facultative heterochromatin assembles at meiotic genes during vegetative growth (Hiriart et al., 2012; Zofall et al., 2012).

Pericentromeric heterochromatin is important for a normal chromosome segregation (Allshire et al., 1995; Ekwall et al., 1995), heterochromatin at the mating-type loci regulates mating type switching and at subtelomeric regions, adjacent to telomers, plays a role in meiotic chromosome segregation (Nimmo et al., 1998). The role of heterochromatin at rDNA locus is not known yet, but it could be involved in preventing recombination between rDNA repeats (Cam et al., 2005).

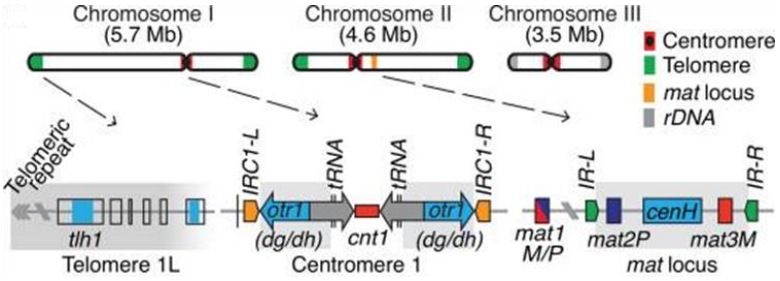

Figure 1.7. Overview of main heterochromatin regions in *S. pombe* genome. *Heterochromatin domains are highlighted in gray. tRNA genes and inverted repeats (IR) serve as heterochromatin boundaries. Tlh1 and its paralogs contain a cenH like element within the coding region. Reprinted with permission from Mizuguchi, Barrowman and Grewal, 2015.*

The relatively simple genetic manipulation coupled with the small genome allows for convenient genomic analyses in fission yeast. To infer if a protein of interest plays a role in a heterochromatin function, a reporter gene is placed within a heterochromatic region and silencing assays are performed. An auxotrophic marker, often used as a reporter gene, is a wild type allele of a gene coding for a necessary metabolic enzyme in a certain amino acid synthesis pathway. Two commonly used markers are *ura4* and *ade6*. When they become silenced, the cell growth will be

inhibited if uracil or adenine are not present, respectively. Therefore, their silencing can be assessed by plating serial dilutions of cells onto minimal agar or by a qPCR. Silencing of *ura4* will also render cells resistant to 5-fluoroorotic acid (5-FOA) and *ade6* silencing will cause a red colony colour on adenine-limiting agar (Cam & Whitehall, 2016).

1.3.2 Chromatin remodelers and heterochromatin

There is increasing evidence supporting a role of ATP-dependent chromatin remodelers in a heterochromatin establishment and maintenance (reviewed in Bi, 2012). Fft3 suppresses a nucleosome turnover to promote an epigenetic inheritance and its loss causes a variegated expression of a marker inserted into mating type loci (Taneja et al., 2017). It is localized to insulator elements and inhibits euchromatin assembly in silent chromatin domains. In its absence, a nucleosome occupancy is reduced over insulator elements and a chromosome segregation is defective (Steglich et al., 2015; Strålfors et al., 2011). Its human ortholog SMARCAD1 is important for a proper establishment of pericentromeric heterochromatin and to ensure a mitotic fidelity (Rowbotham et al., 2011). It is required to silence endogenous retroviruses in embryonic stem cells in an ATP-dependent manner (Sachs et al., 2019). Another orphan remodeler, ATRX, was found to interact with HP1 and H3K9me2/3 (Dhayalan et al., 2011; McDowell et al., 1999). Several ISWI remodelers have been implicated in heterochromatin and gene silencing (Deuring et al., 2000). WICH (WTSF-Snf2h chromatin remodeling complex) and ACF (Acf1-Snf2h) accumulate in a pericentric heterochromatin and are required for a replication through heterochromatin in mammalian cells (Bozhenok et al., 2002; Collins et al., 2002; Fyodorov et al., 2004). *S. pombe* lacks ISWI remodelers but has an expanded CHD family (Clapier & Cairns, 2009): Hrp1, Hrp3 and Mit1. Mit1, a part of a SHREC complex, is enriched on main heterochromatin regions, where it influences nucleosome positioning. It is essential for their silencing (Creamer et al., 2014; Garcia et al., 2010; Job et al., 2016; Sugiyama et al., 2007). Its human equivalent NuRD is required for assembly of a pericentromeric heterochromatin and progression through S phase (Helbling Chadwick et al., 2009; Sims & Wade, 2011). A mutant yeast carrying Hrp1 deletion displays a disrupted silencing of *otr* regions and chromosome segregation defects (Walfridsson et al., 2005). Its paralog Hrp3 is required for a transcriptional repression at mating type loci (Jae Yoo et al., 2002) and at *dg*/*dh* repeats (Shim et al., 2012). Brg1, the ATPase of a human SWI/SNF was found to interact with HP1 and its deletion leads to a dissolution of pericentromeric heterochromatin (Bourgo et al., 2009; Lavigne et al., 2009).

1.4 Phase separation in biology and chromatin organization

Phase separation is a property of multivalent polymers (proteins, nucleic acids) to demix from a concentrated solution into polymer-rich condensates and polymer-depleted solution. It happens when molecules reach their solubility limit, the threshold concentration at which they phase separate, and it depends on environmental conditions like temperature, pH, ionic strength and molecular crowders. Two phases that form may differ in component concentrations, chemical environment and material properties. Phase separation is emerging as a general mechanism by which membranelles organelles, recently termed biomolecular condensates (Banani et al., 2017), form.

Biomolecular condensates are ubiquitous in cell biology and involved in diverse processes (Figure 1.8.). A growing number of proteins shown to phase separate *in vitro* is curated in LLPSDB database together with corresponding experimental conditions, freely available at: http://bio-comp.org.cn/llpsdbv2 (Wang et al., 2022). Multi-domain proteins phase separate through multiple

specific interactions of folded domains (Li et al., 2012; Banani et al., 2016). Higher valency and affinity promote phase separation and decrease dynamics of phase separated condensates (Banjade & Rosen, 2014; Li et al., 2012).

One class of proteins that often undergo phase separation are proteins that contain intrinsically disordered regions (IDRs). IDRs lack a defined 3D structure and exhibit significant conformational heterogeneity. Often, they have low sequence complexity. They are enriched, when compared to the cellular proteome, in a limited number of amino acid types. This gives rise to repeated sequence motifs, termed “stickers” (Wang et al., 2018), that form multiple weak short lived intermolecular interactions (Brangwynne et al., 2015; García Quiroz & Chilkoti, 2015). For example, patterning of aromatic residues determines the phase behavior of prion-like domains (Martin et al., 2020; Wang et al., 2018).

IDR containing proteins are enriched in many biomolecular condensates, like in P granules in germ cells of *Caenorhabditis elegans*, the first membranelles organelles characterized as liquid forming by liquid-liquid phase separation (LLPS). They fuse with one another and subsequently relax into a spherical shape, wet the nuclear membrane, drip under applied shear stress and its constitutive protein component PGL-1 diffuses rapidly inside the granules and exchanges with surrounding cytoplasm (Brangwynne et al., 2009). Soon after, the same properties were attributed to other condensates such as nucleolus (Brangwynne et al., 2011), stress granules (Patel et al., 2015) and sites of DNA breaks (Altmeyer et al., 2015; Patel et al., 2015).

A possibility was then raised, for LLPS as a general concept for cytoplasmic organization (Hyman & Brangwynne, 2011). The phase boundary permits molecules to be concentrated in condensates, but still rapidly exchange with a surrounding solution and are often mobile within a dense phase (Banani et al., 2017). However, not all condensates will have liquid-like properties and assemblies of varied material states can emerge from phase separation (Weber, 2017).

Many biomolecular condensates have liquid-like properties, while others behave more gel-like or solid-like (Kroschwald et al., 2015). Moreover, molecular organization and biophysical properties of biomolecular condensates can change over time (Lin et al., 2015; Patel et al., 2015). In a process of maturation (hardening), intermolecular interactions rearrange and/or strengthen, and condensates go from liquid-like to solid-like. ATP-consuming processes can tune and regulate biophysical properties of biomolecular condensates as well (Brangwynne et al., 2011; Jain et al., 2016), possibly through a control of a degree of crosslink formation (Banani et al., 2017). Through its amphiphilic chemical nature, ATP itself acts as a hydrotrope solubilizing hydrophobic proteins in millimolar concentrations, a property shared with other nucleotides (Patel et al., 2017).

Liquid biomolecular condensates will grow if the amount of biomolecule rises above threshold concentration therefore buffering cellular noise arising from variable expression (Klosin et al., 2020), to keep biomolecule concentration constant in both phases. Phase separation is very sensitive to even minor changes in environmental conditions (Nott et al., 2015) such as concentration, temperature and salt. In addition, biomolecular condensates can form and dissolve very fast, making it an ideal regulation strategy. Indeed, it is used in an adaptive response to pH and heat stress (Kroschwald et al., 2018; Riback et al., 2017). Phase separation happens when molecules reach a threshold concentration, therefore it is regulated by intracellular concentration via changes in expression (Nott et al., 2015), localization (Berry et al., 2015; Chung et al., 2011; Kaiser et al., 2008; Mao et al., 2010; Shevtsov & Dundr, 2011) and cell volume (Weber & Brangwynne, 2015). Threshold concentration depends on valency and intrinsic solubility of condensate components and might be regulated via posttranslational modifications (Das et al., 2016; Nott et al., 2015) or interaction partners (Saha et al., 2016). The molecule that is essential for a

condensate formation is referred to as a scaffold, whereas clients are molecules that can localize to condensates and modulate their properties but are dispensable for their assembly (Banani et al., 2016). Clients often localize to condensates by directly specifically binding to scaffolds (Hanazawa et al., 2011) or due to general electrostatic properties (Su et al., 2016).

Many proteins have been shown to phase separate *in vitro*. It seems this might be a universal property of proteins and nucleic acids just the right set of conditions has to be found. However, it is not straightforward to prove phase separation and its functional relevance in a cell (reviewed in Alberti, Gladfelter and Mittag, 2019).

Aberrant condensed states of proteins can be involved in pathological processes (reviewed in Vendruscolo and Fuxreiter, 2022). Mutations can shift the phase boundary either towards the formation of condensates or their disassembly; or shift liquid-like properties of condensates towards the amyloid state (or vice versa). For example, mutations of protein FUS found in patients with amyotrophic lateral sclerosis (ALS), accelerate an aberrant phase transition of FUS from liquid to aggregated state (Patel et al., 2015). Importantly, maturation of condensates from liquid to solid-like can be important for physiological function. Several solid-like condensates are implicated in important physiological processes (Fowler et al., 2007), particularly in immunological signalling (Hou et al., 2011; Lu et al., 2014). Up to a third of human diseases is associated with mutations in phase separation promoting regions of corresponding proteins that form condensates *in vitro* (Vendruscolo & Fuxreiter, 2022). A connection is emerging between aberrant condensates and age-related diseases (Alberti & Carra, 2018). Understanding of condensate function is revealing novel therapeutic opportunities (Mitrea et al., 2022).

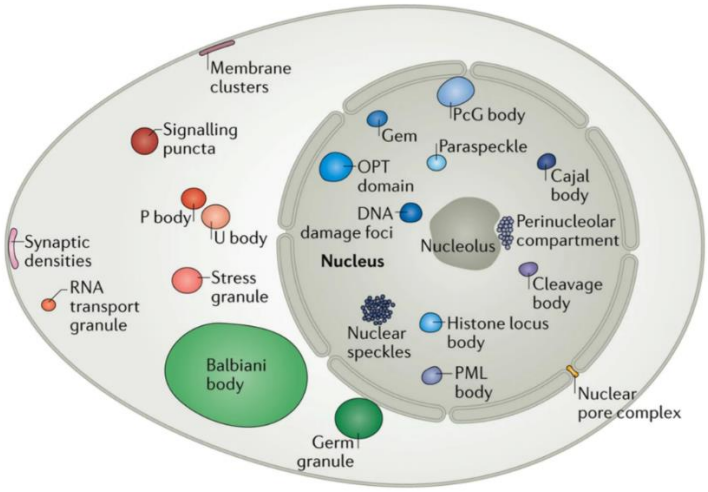

Figure 1.8. Biomolecular condensates in eukaryotic cells. *Reprinted with permission from Banani et al., 2017*

1.4.1 Intrinsic phase separation of chromatin

Chromatin reconstituted from purified components undergoes LLPS under physiological conditions both *in vitro* and when microinjected into cell nucleus (Gibson et al., 2019). Nucleosome concentration in formed condensates (~340 µM) was similar to those estimated for cells (~80-520 µM) (Hihara et al., 2012). The phase separation is modulated by a length of a nucleosome array, linker DNA length, linker histone and acetylation. It was promoted by increased length of nucleosome chain (12mer, 6mer and 4mer were tested), incorporation of a linker histone and the histone tails. FRAP experiments showed fast dynamics of arrays inside the formed condensates,

corroborating liquid-like properties together with condensate fusion. The linker histone, particularly its C-terminal domain, lead to condensate hardening inferred from a slower FRAP. The exact nature of formed condensates is shown to be sensitive to a sample preparation and it has been described both as liquid-like and solid-like (Gibson et al., 2021; Muzzopappa et al., 2021; Strickfaden et al., 2020b). Interestingly, 12mer nucleosome arrays with 10n + 5 (e.g., 5, 15, 25) bp nucleosome spacing had higher propensity to phase separate than 12mers with 10n (e.g., 10, 20, 30) bp spacing. In eukaryotes, distances between nucleosomes are biased toward 10n + 5 bp spacing and depleted for 10n bp spacing (Lohr & van Holde, 1979). Histone acetylation dissolved chromatin condensates *in vitro*. Addition of a multi-bromodomain protein (bromodomain binds acetylated lysines) induced phase separation of acetylated nucleosome arrays forming condensates of distinct physical properties.

After microinjection of the restriction enzyme *AluI* into a mitotic nucleus, chromosomes lost their elongated shape and formed round condensates that fused to each other (Schneider et al., 2022). The condensates had the same chromatin density as intact chromosomes, indicating that the integrity of chromatin fiber is not required for a full compaction of the mitotic chromatin, consistent with a phase separation mechanism of compaction. Therefore, when the long-range constraints are eliminated, the short-range chromatin dynamics manifest in a liquid like behaviour. The resulting condensates were pushed by polymerizing microtubules against the chromatin phase boundary. If *AluI* was injected into a G2 nucleus, homogeneously distributed chromatin formed instead of spherical condensates.

The authors propose that deacetylation during interphase to mitosis transition induces global chromatin phase separation. It endows chromatin with the material properties of mitotic chromosomes, without a need of condensin or any other chromatin associated factors. When the mitotic chromosomes were hyperacetylated, they had no defined surface boundary and were frequently perforated by microtubules and missegregated. Mitotic chromatin and nucleosome array condensates on the other hand excluded soluble tubulin, and polymerizing microtubules never perforated chromatin condensates *in vitro*.

By using fluorescent proteins and dextrans of different sizes and charges, they showed that electrical charge and molecular size are key determinants of macromolecular access to both mitotic chromatin and nucleosome array condensates. Positively charged moieties were enriched and negatively charged partially excluded from negatively charged chromatin.

Computational modelling approaches showed that nucleosome thermal fluctuations (nucleosome breathing) become significant at physiological salt concentrations. This intrinsic plasticity of nucleosome destabilizes 30 nm fiber and promotes LLPS (Farr et al., 2021). In a seminal experimental study, HP1 binding was shown to reshape the octamer core exposing hydrophobic residues, thereby promoting phase separation of the nucleosome array (Sanulli et al., 2019).

Consistent with a polymer behaviour, naked DNA forms condensates itself from a concentrated solution (Post and Zimm, 1982). Resulting condensates have a range of material properties depending on properties of DNA and condensing agents. Rod-like assemblies (Bloomfield, 1991), DNA gels (Carmen Morán et al., 2007), liquid crystals (Sikorav et al., 1994) and LLPS (Martin et al., 2019) have so far been described. The fact that DNA length decreases solubility has been long used in practice for separation of DNA fragments of different sizes via PEG precipitation (Lis & Schleif, 1975). A recent systematic study has found that shorter DNA molecules (<1 kb) formed round shaped liquid-like condensates and longer DNA (>10 kb) molecules formed irregularly shaped solid-like aggregates that were more resistant toward mechanical forces (Muzzopappa et al., 2021). DNA length and fluidity of obtained condensates anticorrelated regardless of how

phase separation was induced: via crowding polymers (PEG) and salts (Mg^{2+}), binding of H1 or chromatinization. Practically, that would mean that larger chromosomal domains or entire chromosomes tend to condense into solid-like structures, but smaller genomic regions (1-10 kb) might be able to form liquid-like condensates. Similar length-fluidity anticorrelation was also shown for RNA (Jain & Vale, 2017) and proteins (Peskett et al., 2018). DNA phase separation is promoted by its flexibility, encoded in the sequence (Shakya & King, 2018). ssDNA was more prone to phase separation than dsDNA, presumably due to rigidity of dsDNA acquired through base pairing. Furthermore, free nucleotides promoted LLPS of rigid DNA structures that would otherwise precipitate (Shakya & King, 2018). Under molecular crowding conditions and large range of monovalent salt concentrations, nucleosome core particles formed liquid crystals with estimated nucleosome concentration (~410 mg/mL) in the range of values measured in cell nuclei (Leforestier & Livolant, 1997).

Maeshima was the first to try and structurally characterized self-associated 12mer nucleosomal arrays (Maeshima et al., 2016). They suggested a polymer molten globule like structure, where 10 nm fibres interdigitate, and 30 nm fibre is absent. When they treated isolated human nuclei with EDTA, chromatin decondensed extensively. A related study corroborated the results and reported swelling of chromosomes and stretching chromosomal fibres into 10 nm like fibres in absence of $MgCl_2$ (Eltsov, Maclellan, et al., 2008). Mg^{2+}-dependent chromatin condensation is reversible and it protects genomic DNA from radiation damage (Takata et al., 2013). A transient rise in free Mg^{2+} released from Mg-ATP hydrolysis was suggested to contribute to mitotic chromosome condensation (Maeshima et al., 2018).

Zhang, Díaz-Celis and colleagues reconstituted phase separation of tetranucleosomes and analyzed it with cryo-electron tomography at different incubation times (Zhang et al., 2022). They found that the LLPS is a two-step process (Figure 1.9.). First, irregular elongated condensates form through a spinodal decomposition and continue to grow after ten minutes of reaction. Spinodal decomposition involves negative diffusion of soluble NCPs against a concentration gradient. Indeed, during the formation and growth, concentration of free NCPs decreased from 25.0 ± 3.5 μM (t=0), to 8.9 ± 2.3 μM (t=2 min), and to 3.9 ± 0.7 μM (t=10 min). After ten minutes of incubation, small globular condensates appeared and continue to grow via fusion among themselves and/or from accretion of surrounding spinodal structures. H1 catalysed the spinodal to spherical condensate transition, large micron sized spherical condensates appeared much faster (two minutes, compared to 60 min in its absence). The NCP concentration in spherical condensates (~470 μM) was ~1.3 to 3.6-fold higher than that in the spinodal condensates (~360 μM) and it increased significantly in the presence of H1. This concentration is in the same range as determined for mitotic chromosome (Hihara et al., 2012) and *in silico* model of nucleosome array oligomer (Maeshima et al., 2016). The highest concentration was determined for small initial nuclei (~740 μM), but they rearrange as they grow decreasing the concentration. Interestingly, NCP concentration in spinodal condensates decreased towards the periphery, whereas spherical condensates displayed a slight increase. Whereas NCPs in the interior were randomly oriented, NCPs at the surface showed a slight tendency to align perpendicular to the condensate surface, in all types of condensates analyzed. Isotropic orientation of NCPs supports liquid-like state. Condensates however have cavities that can still fit small and to an extend larger complexes like RNA Pol II, which will be progressively excluded as NCP concentration increases. Arrays were arranged in both stacked and extended conformations. However, cryo-ET is suitable to study only small condensates (<200 nm in diameter). The phase separation kinetics for 12mer was in good agreement except that the spherical condensates formed ~10-fold faster.

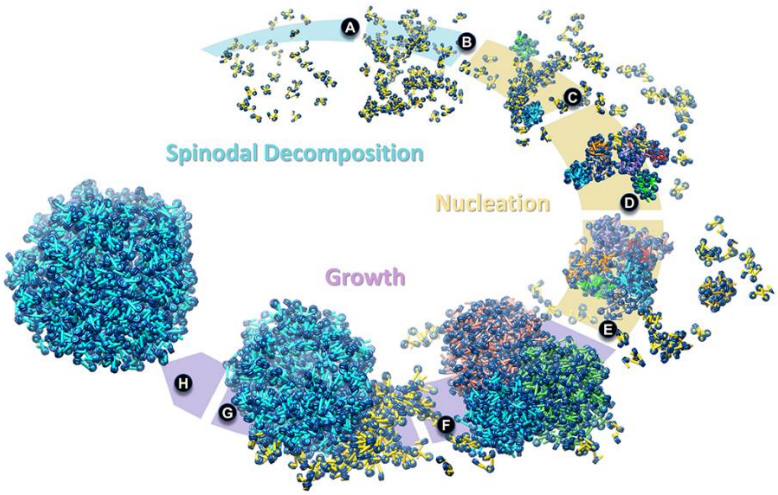

Figure 1.9. Mechanism of a phase separation of nucleosome arrays. *A)-B) Formation of irregular elongated condensates (B) from individual tetranucleosomes (A) through a spinodal decomposition. C)-E) Growth into spherical nuclei. Condensates grow asymmetrically along the long axes that changes from 89.0 ± 10.1 nm to 126.9 ± 19.6 nm, while the short axis stayed around 30 nm. During that time, average number of NCPs per condensate increases from 37 ± 6 to 89 ± 26. F)-H) After ten minutes of incubation, small globular condensates appeared (~35-40 nm in diameter) and increased in number and size (>100 nm) at longer incubation times. The structures grow via fusion among themselves (F) and/or from accretion of surrounding spinodal structures (G). Finally, distinctive spherical condensates appeared with variable size from ~40 nm to ~400 nm in diameter (H). Reprinted under Creative Commons license from Zhang et al., 2022.*

Several types of phase separation might be at play in chromatin: liquid–liquid phase separation (LLPS), intramolecular polymer–polymer phase separation (PPPS), viscoelastic phase separation (VPS), and combinations thereof (reviewed in Erdel, 2020 and Erdel and Rippe, 2018). The most important difference between these mechanisms is the nature of the formed phases. After LLPS, two liquid phases form, one dense and one diluted, each of a different viscosity and molecular composition, with a phase boundary between them acting as a diffusion barrier leading to a partial insulation (Taylor et al., 2019). Concentrations of molecules will stay constant and if their amounts change, it will be compensated with change of the compartment size. This effect was named concentration buffering (Banani et al., 2017). In case of other phase separation mechanisms, compartments are soaked in a common liquid and not isolated from each other.

Chromatin harbours properties of both liquid and solids. Mobility of small inert particles is fast and unconfined (Erdel et al., 2015), whereas movement of chromatin locus is slow and confined (see section 1.1.2). It has been suggested that the nucleus should be considered a two-component system, reminiscent of a hydrogel (Xing et al., 2018; Strickfaden, Tolsma, et al., 2020). A solid-like chromatin would act as a gel matrix soaked in a nucleoplasmic liquid. The hydrogel state would be consistent with a role that chromatin and its folding have in a mechanical rigidity of nucleus (Shimamoto et al., 2017). In his review, Erdel suggests that both phenomena are the two sides of the same coin, and that chromatin length and molecular environment direct which type of phase separation occurs, *in vivo* chromosomes undergo PPPS whereas short nucleosome arrays *in vitro* undergo LLPS (Erdel, 2020). Indeed, recent experimental data show that chromatin exists *in vivo* in solid-like (gel) state, but it serves as a platform to support LLPS of chromatin binding proteins, like a hydrogel (Strickfaden, Tolsma, et al., 2020). However, a genomic locus responds to a force of physiological magnitude in a fluid-like viscoelastic manner, challenging the view that interphase chromatin is a gel-like material (Keizer et al., 2022).

1.4.2 Phase separation of chromatin binding proteins

In addition to chromatin intrinsic phase separation, many chromatin binding proteins undergo phase separation (reviewed and listed in Sabari, Dall'agnese and Young, 2020). Transcription factors together with coactivators and RNA Pol II promote formation of transcription condensates at specific genomic loci, promoters and enhancers, thought to be important for gene activation (Boija et al., 2018; Cho et al., 2018; Han et al., 2020; Ma et al., 2021; Shrinivas et al., 2019; Zhang, Brown, et al., 2021). Another notable chromatin binding protein undergoing LLPS is HP1, both *in vitro* and *in vivo* in early Drosophila embryos (Larson et al., 2017; Strom et al., 2017). The direct role of phase separation in biological processes is still debated and alternative mechanisms have been proposed, particularly HP1-driven LLPS in heterochromatin (Erdel et al., 2020) and transcription (McSwiggen et al., 2019; Trojanowski et al., 2021). Assessing biophysical properties of pericentric heterochromatin in mouse fibroblasts found that HP1 has only a weak capacity to form liquid droplets in cells and size of heterochromatin foci was independent of total HP1 concentration, but its concentration in foci changed. Heterochromatin phase separation would explain a spatial compartmentalization of the genome (Falk et al., 2019). In a tumor cell nucleus, chemotherapeutics concentrate in specific protein condensates, through physicochemical properties that exist independently of their molecular targets. This selective partitioning influences drug activity and might lead to drug resistance (Klein et al., 2020). Mutations in another heterochromatin protein MeCP2 (methyl CpG binding protein 2) cause Rett syndrome. Mutations in MECP2 that lead to Rett syndrome disrupt the ability of MeCP2 to form condensates (Li et al., 2020). Phase separation of chimeric oncoprotein drives aberrant chromatin looping and cancer development of haematological malignancies (Ahn et al., 2021).

Hexane-1,6-diol interferes with weak hydrophobic interactions, that often mediate phase separation (Kroschwald et al., 2017). Purely electrostatic interactions should not be affected. It facilitates chromatin compaction *in vitro* (Itoh et al., 2021). Several studies have examined its effect on 3D chromatin architecture, but gave incoherent results, presumably due to serious side effects of the chemical on cell viability (Itoh et al., 2021; Liu et al., 2021; Shi et al., 2021; Ulianov et al., 2021). A short-term exposure to low concentration of hexane-1,6-diol reversibly dissolved biomolecular condensates of several chromatin binding proteins without affecting cell viability and resulted in a global reorganization of chromatin interactions and TADs (Liu et al., 2021). Optogenetically induced liquid condensates of proteins rich in IDR regions within the nucleus mechanically excluded chromatin and preferentially formed in low-density chromatin regions (Shin et al., 2018). Growing condensates deformed and push out surrounding chromatin network, but they were able to include loci they were targeted to, leading authors to propose a chromatin filter model for condensate induced genome restructuring, in which transcriptionally active condensates filter out non-specific elements of the genome, while pulling together targeted regions to which they are bound.

1.4.3 Consequences of phase separation on enzymatic reactions

Biomolecular condensates have a potential to affect reactions that occur within them, but the direction of a change of rate coefficient is not straightforward to predict (reviewed in Zhang, Narlikar and Kutateladze, 2021). They might render different solvent properties such as dielectric constant and viscosity, concentrated or excluded (depleted) enzyme, substrate, cofactor and/or product compared to surrounding solution, molecular crowding, different diffusion coefficients. These parameters may alter dissociation constant of enzyme-substrate complex and the kinetics of substrate binding and conversion rates (Peeples & Rosen, 2021). In biomolecular condensates, both enzyme and substrate might experience hydrophobic and electrostatic environment more

like organic solvent than water (Küffner et al., 2020; Nott et al., 2016). Increased concentrations of reactants can increase binding rate thereby speeding up the reaction, but the diffusion might slow down (Brady et al., 2017; Drobot et al., 2018; Taylor et al., 2019) due to crowding and high viscosity (Caragine et al., 2018). In addition, intermolecular interaction will decrease permeability (Wei et al., 2017) of a condensate. Concentrating an enzyme and its substrate together in a same compartment can accelerate the reaction from four to six-fold (Drobot et al., 2018; Küffner et al., 2020; Sokolova et al., 2013) and up to 20 to 70-fold (Drobot et al., 2018; Strulson et al., 2012) in some systems. However, some reactions were not affected by presence of condensates despite higher concentrations (Davis et al., 2015; Deryusheva & Gall, 2009). Molecular crowding itself can affect protein conformation, interactions and activity (reviewed in Kuznetsova et al., 2015). When a product is less prone to phase separate, it will get excluded from condensates and its removal will drive chemical equilibrium towards product formation, like in nucleolus (Riback et al., 2020). Enzymes that are taking part in subsequent reactions can be concentrated in the same condensate thereby speeding up the entire process (Castellana et al., 2014; Liu et al., 2020; Zhao et al., 2019; Zhao et al., 2015) and excluding enzymes of a competitive pathway (Su et al., 2016). Enzymes can be inactivated by phase separation in response to nutrient starvation (Prouteau et al., 2017) or substrate can be separated from enzyme by sequestration, for example mRNAs accumulated in stress granules is protected from translation and degradation (Wilbertz et al., 2019). Some enzymes will undergo phase separation only in an ATP-bound state, thereby coupling enzyme activation with phase separation (Hondele et al., 2019; Zhang et al., 2019). In chromatin, phase separation directs H2B ubiquitination specifically over nucleosomes in a gene body (Gallego et al., 2020). Cas12a (RNA-guided endonuclease/helicase) cleavage of linker DNA in phase separated nucleosome arrays was minimally affected when compared with a nucleosome-free DNA of the same length (Strohkendl et al., 2021). The three-fold inhibition was probably due to the presence of nucleosomes adjacent to the cleavage site, and not phase separation *per se*. In molten globule *in vitro*, linker DNA was also accessible to MNase, although oligomers remained partially intact after digestion (Maeshima et al., 2016). Similarly, Tet repressor was strongly recruited into chromatin condensates onto its operator (Gibson et al., 2019).

Moreover, enzyme reactions might change physical properties of biomolecular condensates. ATP depletion caused drastic decrease in an apparent viscosity of nucleoli (Brangwynne et al., 2011). ATP is required for stress granule assembly and dynamics (Jain et al., 2016).

Normally, enzyme activity is measured in test tube in diluted aqueous solutions, but the intracellular environment is very crowded and contains 300-400 ng/µL macromolecules, a fact that is often neglected (reviewed in Ellis, 2001). *In vitro*, biomolecular condensates could mimic similar level of crowding, viscosity and polarity and thus may serve as a convenient model system to challenges and emerging properties that high concentrations can entail.

1.5 Aims

Folding and phase separation of chromatin pose challenges for nucleosome remodelers that must act on individual nucleosomes inside the folded structure. Some nucleosomes might be buried and inaccessible. Even if the enzyme reaches the nucleosome, binding sites for the remodelers might be occluded and involved in internucleosome interactions.

Another potential challenge for remodelers is the different chemical environment inside and outside chromatin condensates that might lead to an exclusion of enzymes and cofactors. The high concentrations of nucleosomes in condensates, which far exceed typical K_M values, would require enzymes to constantly be bound to nucleosomes. Diffusion of enzymes through the condensate could be impaired.

The overarching aim of this thesis was to characterize nucleosome sliding on differently folded chromatin substrates.

The results are presented in three parts:

In Chapter 2.1, I used fission yeast as a model system and established the tools to ask if heterochromatin impedes remodeling. In this preliminary study, I have revisited a role of chromatin remodelers in nucleosome positioning and spacing in fission yeast with an improved technology.

In Chapter 2.2, I compared the kinetics of nucleosome sliding by ISWI in unfolded, folded and phase separated nucleosome arrays *in vitro*. I also explored the effect of ISWI´s motor activity on physical properties of nucleosome condensates *in vitro*. Large parts of this study are currently submitted for publication.

Nucleosome remodelers are going through global conformational changes during nucleosome sliding. These dynamic changes are difficult to capture with classical structural methods. In Chapter 2.3, I used mononuclesomes with a UV-activated crosslinker close to the acidic patch that will covalently bind molecules nearby. In this preliminary study, I quantified the extent of crosslinking in different nucleotide states of the remodeler and in presence of different nucleosome linker DNA lengths.

2. Results

2.1 Chapter 1: Nucleosome organization in euchromatin and heterochromatin in fission yeast

2.1.1 Contributions

All contributions were mine except:

Tatiana Abigailova performed western blots in 2.1.1.

Monica della Rosa performed experiments in 2.1.6. and 2.1.7., for which I purified the remodeler and coordinated sequencing and analysis. Dr. Ashish Singh prepared sequencing libraries.

Dr. Tamas Schauer performed the bioinformatic analysis (composite plots and Ocampo analysis).

2.1.2 Background

Heterochromatin is essential for genome stability, chromosome segregation and cell differentiation (Allshire & Madhani, 2017). Whether nucleosome spacing and positioning have a role in a heterochromatin establishment, maintenance and spreading is still not clear. Sequencing of micrococcal nuclease-digested chromatin (MNase–seq) from human cells revealed longer nucleosome repeat lengths in heterochromatin on average (Snyder et al., 2016; Valouev et al., 2011). This is confirmed in *Drosophila melanogaster* cells by array-sequencing which in addition unveiled higher regularity of nucleosome arrays in heterochromatin (Baldi et al., 2018). Nucleosomes in heterochromatin regions show large variation in positioning across different cells but are highly uniformly spaced along the nucleosome array (Lai et al., 2018). However, recent single molecule, long read sequencing applied on K-562 human cell line has suggested that the nucleosome arrays in heterochromatin and elsewhere can be highly diverse, harboring both irregular oligonucleosome patterns in addition to regular arrays (Abdulhay et al., 2020).

In *Schizosaccharomyces pombe*, MNase-seq studies hint towards elimination of nucleosome free regions (NFRs) in heterochromatin (Garcia et al., 2010) while chemical mapping argues in favor of a low nucleosome occupancy (Moyle-Heyrman et al., 2013). Garcia et al. report that the nucleosomes are arranged in a less periodic manner in heterochromatin than in euchromatin (Garcia et al., 2010). Lantermann et al. showed wider spacing in heterochromatin by spectral analysis (Lantermann et al., 2010).

Further hint for importance of nucleosome positioning for heterochromatin function comes from its transcriptional derepression in strains with remodeler deletion. Transcriptional changes were in few cases correlated with changes in nucleosome positioning (Ehrensberger & Kornberg, 2011; Straka & Horz, 1991). In an *hrp3Δ* strain, the nucleosome periodicity around transcription start site of highly expressed genes was perturbed to a higher degree than those of lower expressed genes, suggesting an involvement of Hrp3 in RNAPII-associated transcription (Shim et al., 2012). Garcia et al. identified Mit1 as responsible for occluding some NFRs in heterochromatin (Garcia et al., 2010). Mit1, an ATPase subunit of SHREC complex, prominently associates with major heterochromatin domains. Strains lacking Mit1 had upregulated transcription of heterochromatin loci that was not rescued by introducing an ATPase dead mutant of Mit1. SHREC activity is critical for proper positioning of nucleosomes at the silent *mat* locus (Sugiyama et al., 2007). It is still

unclear if Mit1 has a role in nucleosome positioning and spacing of nucleosomes in genic arrays in euchromatin (Lantermann et al., 2010; Pointner et al., 2012).

Hrp3, another nucleosome remodeling enzyme of the CHD1 class, as well as its paralog Hrp1, are required for heterochromatin silencing in fission yeast (Jae Yoo et al., 2002; Jin et al., 1998; Shim et al., 2012). Hrp3 physically interacts with Swi6, the HP1 orthologue in *S. pombe*, and Δ*hrp3* strain shows higher nucleosome occupancy in pericentromeric region (Shim et al., 2012). Hrp1 and Hrp3 have nucleosome positioning activity *in vivo* (Hennig et al., 2012; Pointner et al., 2012; Shim et al., 2012) and nucleosome spacing activity *in vitro* (Pointner et al., 2012).

Fft3 inhibits euchromatin assembly in silent chromatin domains and it is required for silencing of subtelomeric genes and a proper incorporation of histone variants in a centromere region (Strålfors et al., 2011). *Fft3* deletion did not change nucleosome positioning pattern over genic regions (Lantermann et al., 2010), but it led to a decrease in a nucleosome occupancy in Pol III transcribed genes (Steglich et al., 2015).

These remodelers must access and work on heterochromatin which is considered tightly packed and inaccessible (Boettiger et al., 2016; Ou et al., 2017; Ricci et al., 2015; Spracklin & Pradhan, 2020). In this chapter, I decided to challenge this paradigm and asked if heterochromatin impedes nucleosome remodeling. We have performed preliminary experiments towards answering this question. We have established fission yeast as a model organism in our group and characterized nucleosome arrays architecture in several different strains. We have tested the effect of a remodeler fusion with a heterochromatin binding domain on transcription and nucleosome positioning.

2.1.3 Overexpression of chromatin remodelers Hrp3 and Fft3 is toxic

To check if heterochromatin impedes chromatin remodeling, we have designed *in vivo* biochemistry approach to compare nucleosome sliding in euchromatin versus heterochromatin in *S. pombe*. For our experiments, we used remodelers that were already known to be implicated in heterochromatin and act as a single subunit: Hrp1, Hrp3 and Fft3. We overexpressed them on their own or as a fusion protein with a heterochromatin-binding domain.

I used genomic DNA from *S. pombe* to amplify *hrp1*, *hrp3* and *fft3* genes. All genes were successfully PCR-amplified, but cloning of the *hrp1* gene was not successful, presumably because AT-rich DNA sequence is unstable in bacteria (Inagaki et al., 2005; Mukai et al., 2016). The linear DNA cloning system might be considered in the future (Godiska et al., 2010; Pfander et al., 2011). Fft3 and Hrp3 were then fused to the chromodomain (CD) and the 3xFLAG tag. The purpose of a chromodomain was to direct chromatin remodeler to heterochromatin. I used the chromodomain from Chp1 protein because it has the highest affinity for H3K9me among four chromodomain proteins present in fission yeast (Isaac et al., 2017; Schalch et al., 2009).

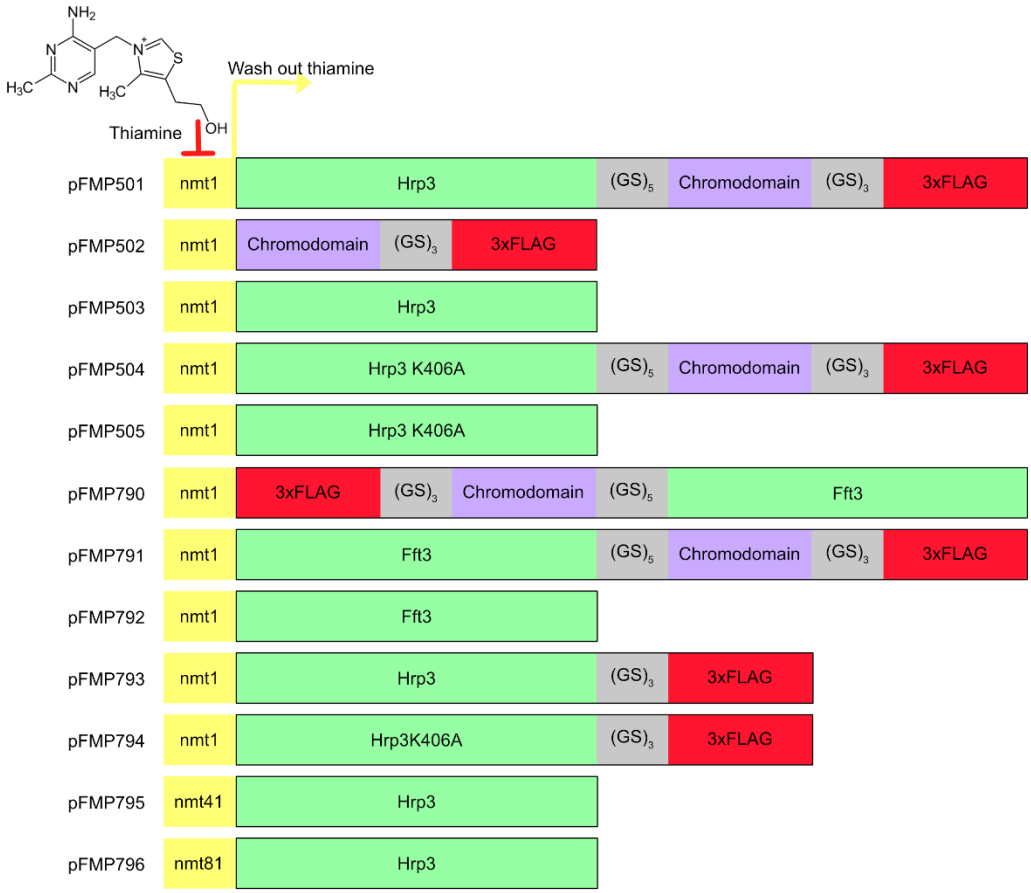

Figure 2.1. Plasmids cloned in this study. *Remodeler constructs were cloned under a control of a derepressible promotor. Nmt (no message in thiamine) promotor is repressed by thiamine, that is present in a yeast extract, a component of a full growth media. Expression is achieved by growing the strains in a synthetic media with limited or without added thiamine (Moreno et al., 2000). The strength of the promotors decreases nmt1>nmt41>nmt81. All transgenes were partially sequenced.*

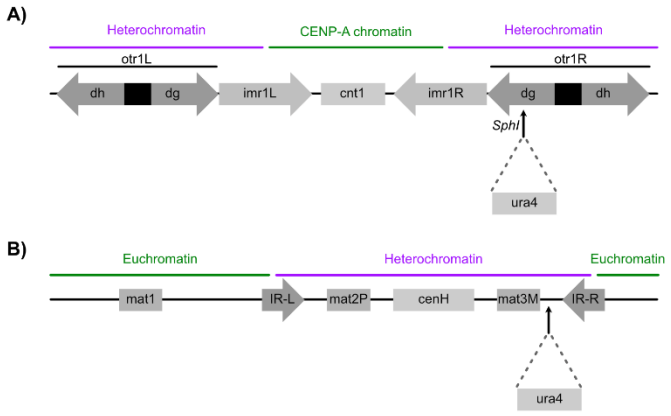

Figure 2.2. Heterochromatin reporter strains. *A) Pericentromeric reporter strain. Ura4 reporter gene was inserted into otr1R region of chromosome 1 with the help of SphI restriction enzyme (Allshire et al., 1995). B) Mating type reporter strain. Mating type locus is located on the right arm of chromosome 2. Ura4 reporter gene is placed just after mat3M gene. The mating type is determined by sequence integrated at mat1 (plus (P) for h^+ and minus (M) for h^-). Additionally, sequences for P and M are encoded at mat2P and mat3M, respectively, normally silenced and used for switching the mating type via transposition to mat1.*

These constructs were cloned into pJR1 plasmid under control of derepressible nmt1 promotor (Figure 2.1.; vector maps in the Appendix) and transformed into heterochromatin reporter strains (Figure 2.2.). These strains have an auxotrophic marker cloned in a heterochromatin region. Normally, the markers are silenced. In case of a disruption of heterochromatin silencing, the marker gene is transcribed and it can be detected by growth assays on a selective media and further confirmed via RT-qPCR.

Overexpression of Hrp3K406A-containing constructs upon thiamine removal was so strong that the induced proteins were detectable by a Coomassie staining (Figure 2.3.A). The expression of CD-FLAG and Hrp3-CD-FLAG was confirmed by western blot (Figure 2.3.B). The western blot of Hrp3-CD-FLAG revealed additional bands of lower molecular weight, likely due to protein degradation.

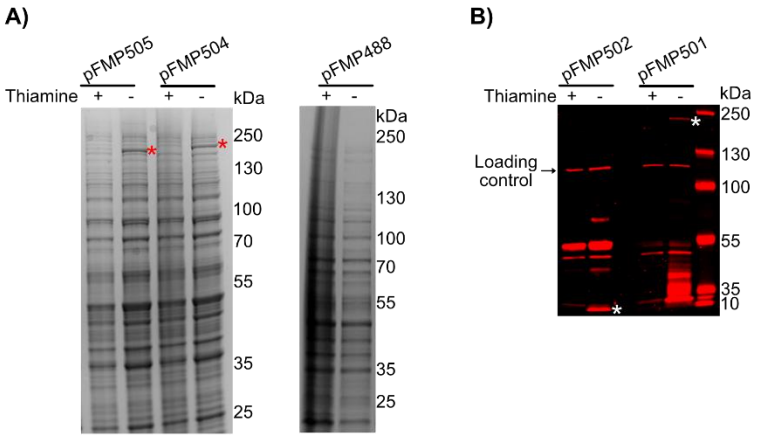

Figure 2.3. Proteins of interest are expressed after removal of thiamine. *Cells were grown without thiamine for ~24 hours. A) Expressions of Hrp3K406A (159 kDa) from pFMP505 and Hrp3K406ACDFLAG (170 kDa) from pFMP504 are detectable on the Coomassie stained SDS-PAGE and labelled with red asterisks. The corresponding band is absent from a protein extract of a strain containing the empty vector pFMP488. B) Western blots of the fusion proteins CDFLAG (11 kDa) expressed from pFMP502 and Hrp3CDFLAG (170 kDa) expressed from pFMP501. Proteins run at the expected sizes. On the blot, they are marked with white asterisks. An unspecific band that anti-FLAG antibody detects was utilized as a loading control.*

To test for yeast fitness upon overexpression of remodelers, I grew liquid precultures of pericentromeric heterochromatin reporter strains carrying constructed plasmids in the presence of thiamine and plated them in serial dilutions on plates without thiamine. The plates did not contain leucine allowing for plasmid selection. As positive controls, I spotted wild type fission yeast strain ($972h^-$) and the reporter strain with empty vector pJR1. Compared to the positive controls, the overexpression of Hrp3 strongly inhibited growth on the EMM-Leu plate (Figure 2.4). Despite higher expression levels, the CDFLAG fusion protein did not cause such a severe growth phenotype. I conclude that toxicity is caused by the Hrp3 region of the fusion protein. This conclusion is supported by the observation that expression of Hrp3 without CD also led to growth defects as severe as that of Hrp3CD. Toxicity is therefore not caused by targeting Hrp3 to heterochromatin.

To test for defects in heterochromatin silencing, I spotted cells on EMM-Leu-Ura plates and on plates containing 5-FOA (Figure 2.4). The wild type strain grew well on EMM-Leu-Ura plates and poorly on plates containing 5-FOA. If expressed, a product of a *ura4* gene will convert 5-FOA into 5-fluorouracil, a toxic metabolite. The reporter strain grew well on 5-FOA containing plates, but

poorly without uridine. The addition of 5-FOA did not inhibit the growth of strains overexpressing the Hrp3 variants, and they were not growing without uridine. Therefore, the silencing of the reporter gene in heterochromatin is not affected. However, the severe growth defect limits the interpretation of a reporter gene silencing assay.

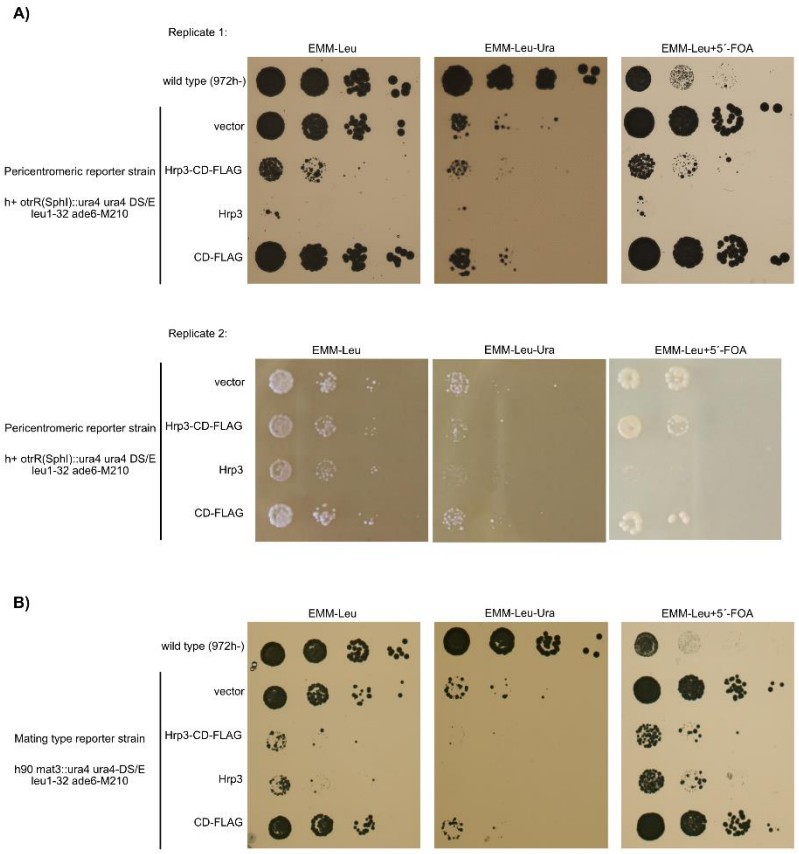

Figure 2.4. Spot assay for a silencing of a reporter gene *ura4* in strains overexpressing Hrp3 constructs. *Cells were washed twice to remove thiamine and plated in serial dilutions. The plates were incubated for several days at 30°C before taking an image. A) Reporter gene is inserted in a pericentromeric region. Two independent replicates are shown. The different colours originate from using different imaging systems. B) Reporter gene is inserted in a mating type region. Preliminary data pending replication are shown (N=1).*

For Fft3 constructs, a mild growth defect was detectable for N-terminally tagged Fft3, but none for Fft3 and Fft3-CDFLAG overexpression (Figure 2.5., 2.6.). Therefore, the N-terminal fusion may interfere with remodeler function. None of the constructs influenced heterochromatin silencing of a pericentromeric region (Figure 2.5.) nor mating type locus region (Figure 2.6.). However, these strains were not tested for a protein expression with western blot. Once again it was corroborated that CD-FLAG expression has no effect on the growth and silencing.

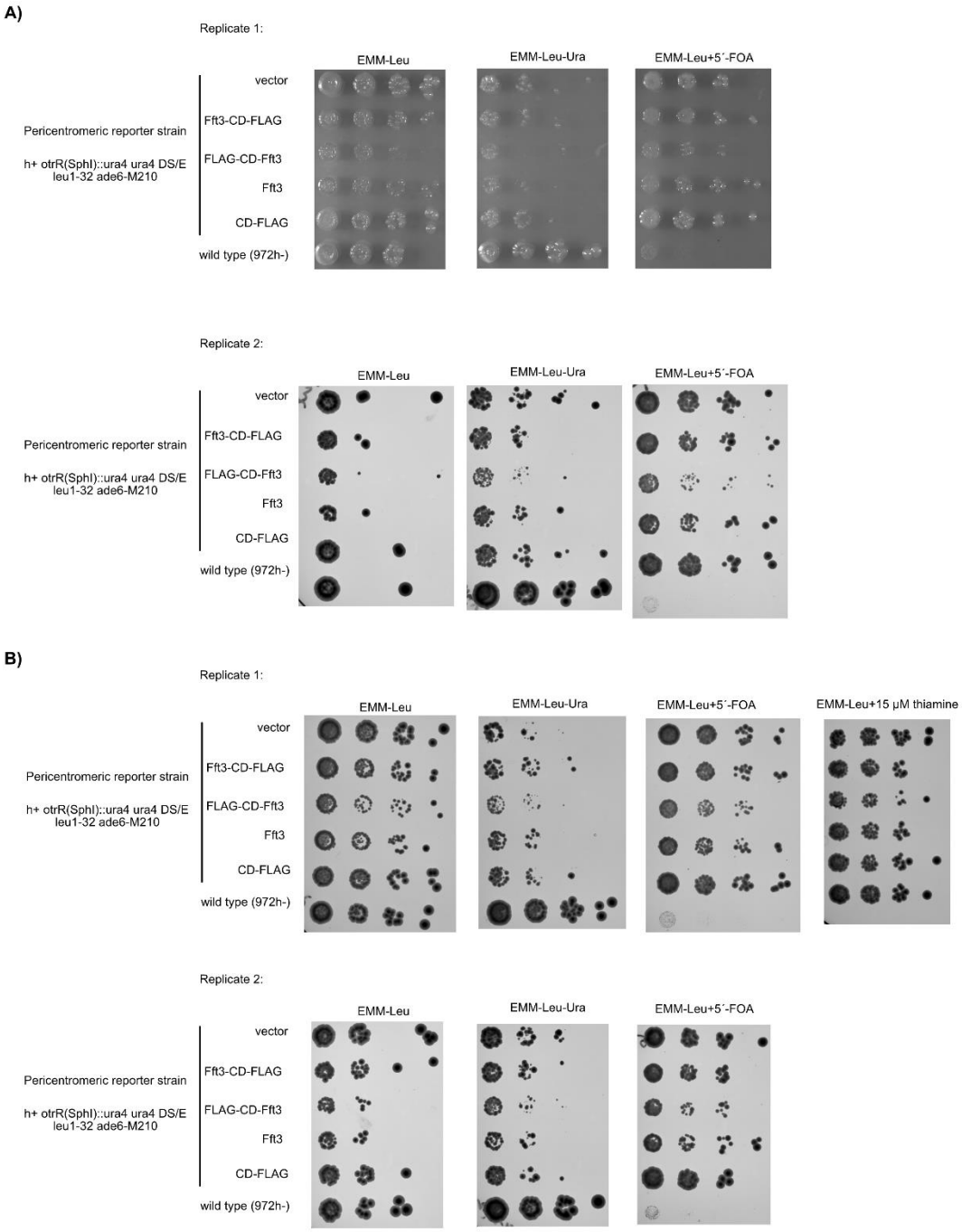

Figure 2.5. Spot assay for silencing of reporter gene *ura4* in pericentromeric reporter strains overexpressing Fft3 constructs. *Cells were washed twice to remove thiamine and plated in serial dilutions. The plates were incubated for several days before taking an image. Reporter gene is inserted in a pericentromeric region. In every experiment, two colonies were analysed for each strain and considered to represent independent replicates. The assays were performed at A) 30°C and B) 32°C. The different colours in A) originate from using different imaging systems.*

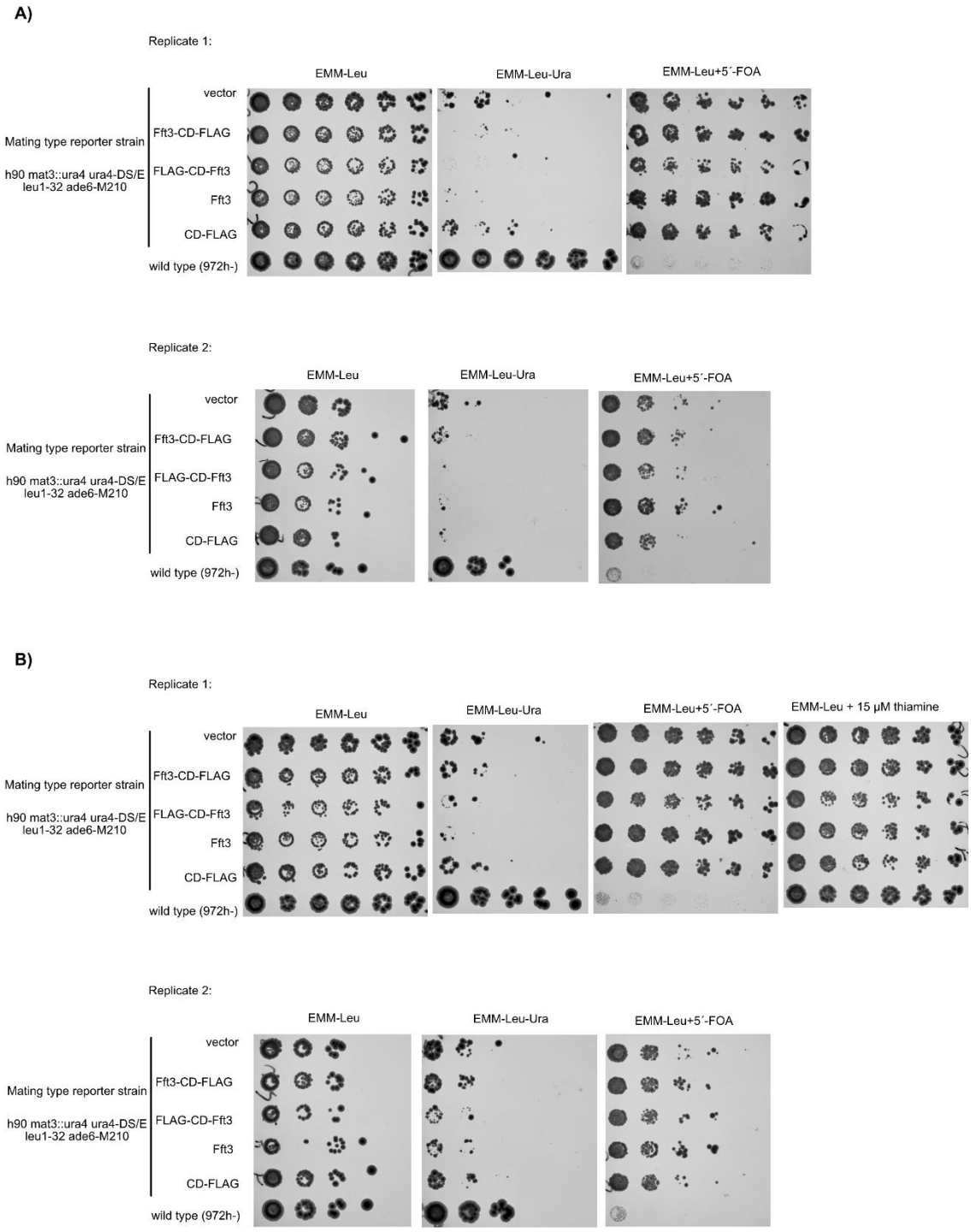

Figure 2.6. Spot assay for silencing of reporter gene *ura4* in mating type locus reporter strains overexpressing Fft3 constructs. *Cells were washed twice to remove thiamine and plated in serial dilutions. The plates were incubated for several days before taking an image. Reporter gene is inserted in a mating type region. In every experiment, two colonies were analysed for each strain and considered to be independent replicates. The assays were performed at A) 30°C and B) 32°C.*

2.1.4 Hrp3 overexpression derepresses heterochromatin in a non-monotonous manner

The strong toxicity of the Hrp3 overexpression is limiting the interpretation of reporter gene silencing assays. Therefore, I assayed for a heterochromatic transcription by RT-qPRC. The

heterochromatic transcripts were normalized to actin, which had the most stable transcript level from three eukaryotic genes tested (less than 1.8-fold change relative to wild type in any condition, compared to 2.8- and 2.4-fold change for alcohol dehydrogenase and glyceraldehyde-3-phosphate dehydrogenase, respectively).

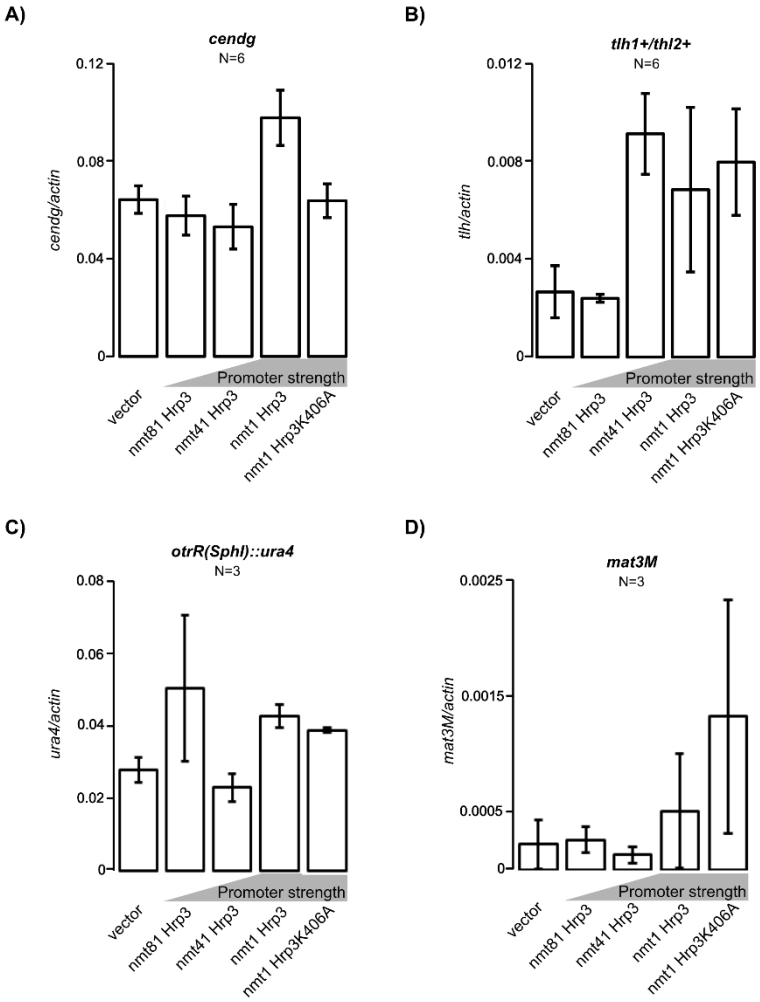

Figure 2.7. Hrp3 overexpression derepresses heterochromatin silencing in an ATP-independent manner in three out of four heterochromatin regions tested. *Quantification of heterochromatin transcripts by RT-qPCR in pericentromeric reporter strains expressing Hrp3 from promotors of different strengths. Promotor strength increases in the following order: nmt81<nmt41<nmt1. RNA was isolated after overnight growth without thiamine. Plotted is an average of all biological replicates and a standard error of the mean. A) Transcripts from cendg repeat normalized to actin mRNA. N=6. B) Transcripts from tlh gene in subtelomeric regions normalized to actin mRNA. The qPCR primers do not distinguish between tlh transcripts originating from chromosome 1 and 2. N=6. C) Transcripts from ura4 reporter gene inserted in otrR pericentromeric region normalized to actin mRNA. N=3. D) Transcripts from mat3M in mating type locus normalized to actin mRNA. N=3.*

To test if Hrp3 overexpression impairs heterochromatin silencing, I measured the amount of heterochromatic transcripts in strains expressing Hrp3 from three related promotors of different strengths (Figure 2.7.). The highest expression level of Hrp3 upregulated transcripts from four heterochromatin regions between 1.5- and 2.3-fold. To test if this effect is dependent on the ATPase activity of the remodeler, I cloned and expressed an ATPase-dead mutant of Hrp3 (K406A) (Shim et al., 2012). Surprisingly, this had the same effect as wt Hrp3 on transcript levels from subtelomeric, pericentromeric and mating type locus heterochromatin regions. Only cendg

transcripts reacted differently and derepression was absent upon overexpression of Hrp3K406A. Lower expression levels of Hrp3 had varying effects on different transcripts. The results are pointing towards a complex, non-monotonous role of Hrp3 in regulating heterochromatin silencing. For three out of four heterochromatin regions tested, ATPase activity of the overexpressed Hrp3 was not necessary for derepression. Only the cendg region showed an ATP-hydrolysis dependence of the derepression. To ascertain this effect, more replicates would be required, however.

To test if heterochromatin silencing is more affected if we target Hrp3 to heterochromatic regions, we overexpressed Hrp3CDFLAG and measured transcript levels by RT-qPCR. Contrary to overexpression of Hrp3, overexpression of Hrp3CDFLAG did not further derepress transcription from heterochromatin (Figure 2.8.). The *mat3M* locus had expression levels hundred times higher than usual (Figure 2.8.). Further experiments are needed to confirm that the strong derepression of the mating type locus is a direct consequence of Hrp3 targeting and not cell starvation during culturing for RNA isolation (Kelly *et al.*, 1988) or mating type switching (Beach and Klar, 1984). Overexpression of chromodomain itself led to a mild derepression of heterochromatic transcripts (Figure 2.9.), possibly due to competition for a H3K9me binding site with silencing factors.

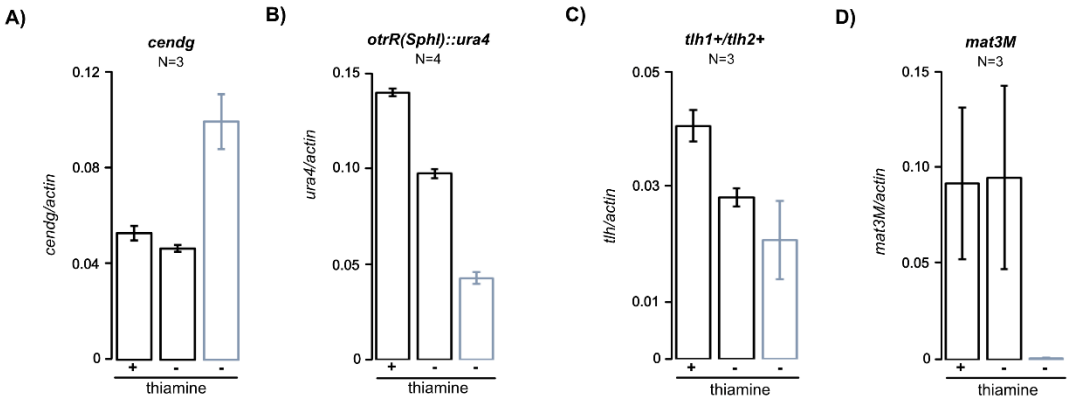

Figure 2.8. Hrp3CDFLAG overexpression strengthens heterochromatin silencing. *Quantification of heterochromatin transcripts by RT-qPCR in pericentromeric reporter strains expressing Hrp3CDFLAG from the strongest, nmt1 promotor (black line). Blue line represents data for strain expressing Hrp3 (nmt1 promotor) copied from Figure 2.7. RNA was isolated before removal of thiamine (+thiamine, Hrp3CDFLAG is not expressed) and then after overnight growth without thiamine (-thiamine, Hrp3CDFLAG is expressed). Plotted is an average of all biological replicates and a standard error of the mean. A) Transcripts from cendg repeat normalized to actin mRNA. N=3. B) Transcripts from ura4 reporter gene inserted in otrR pericentromeric region normalized to actin mRNA. N=4. C) Transcripts from tlh gene in subtelomeric regions normalized to actin mRNA. N=3. D) Transcripts from mat3M in mating type locus normalized to actin mRNA. N=3.*

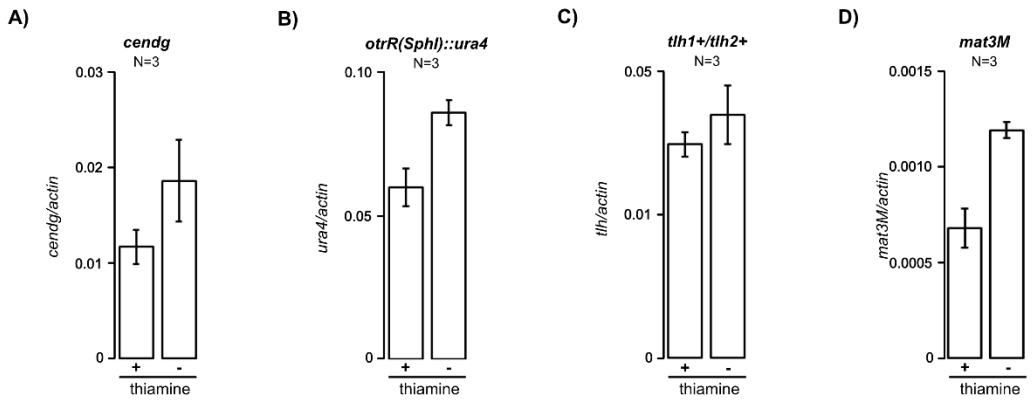

Figure 2.9. CDFLAG overexpression derepresses heterochromatin silencing. *Quantification of heterochromatin transcripts by RT-qPCR in pericentromeric reporter strains expressing CDFLAG from the strongest, nmt1 promotor. RNA was isolated before removal of thiamine (+thiamine, CDFLAG is not expressed) and then after overnight growth without thiamine (-thiamine, CDFLAG is expressed). Plotted is an average of all biological replicates and a standard error of the mean. A) Transcripts from cendg repeat normalized to actin mRNA. N=3. B) Transcripts from ura4 reporter gene inserted in otrR pericentromeric region normalized to actin mRNA. N=4. C) Transcripts from tlh gene in subtelomeric regions normalized to actin mRNA. N=3. D) Transcripts from mat3M in mating type locus normalized to actin mRNA. N=3.*

2.1.5 Hrp3 overexpression causes an ATP hydrolysis-independent defect in nucleosome positioning over gene bodies

To check for defects in a nucleosome positioning in strains overexpressing Hrp3 constructs, I utilized MNase-seq. The cells were grown without thiamine for 6 hours. Before harvesting, bromophenol blue staining confirmed that viability exceeded 95% under all conditions. Following limited MNase digestion, mononucleosome DNA fragments were cut out and sequenced (Figure 2.10.A).

Composite plots for a wild type show typically spaced nucleosomes over gene bodies (Figure 2.10.B, left panel). A region of 750 bp contains five nucleosomes, corresponding to NRL of ~150 bp in the agreement with previously reported tight spacing for *S. pombe* (Givens et al., 2012; Lantermann et al., 2010; Moyle-Heyrman et al., 2013). Main features of a composite plot were insensitive to varying MNase digestion degrees.

I next assessed the effect of Hrp3 overexpression. It seems like Hrp3 moves +1 nucleosome upstream (Figure 2.10.B, middle panel), an effect not reported before. Both Hrp3 and Hrp3K406A mutant overexpression decreased nucleosome array regularity (Figure 2.10.B, middle panel). Similarly, overexpression of Hrp3CDFLAG and Hrp3K406ACDFLAG decreased nucleosome array regularity (Figure 2.10.C; right panel). The data however should not be overinterpreted given different digestion levels of chromatin of compared strains, likely overdigestion (Figure 2.10.A) and absence of biological replicates.

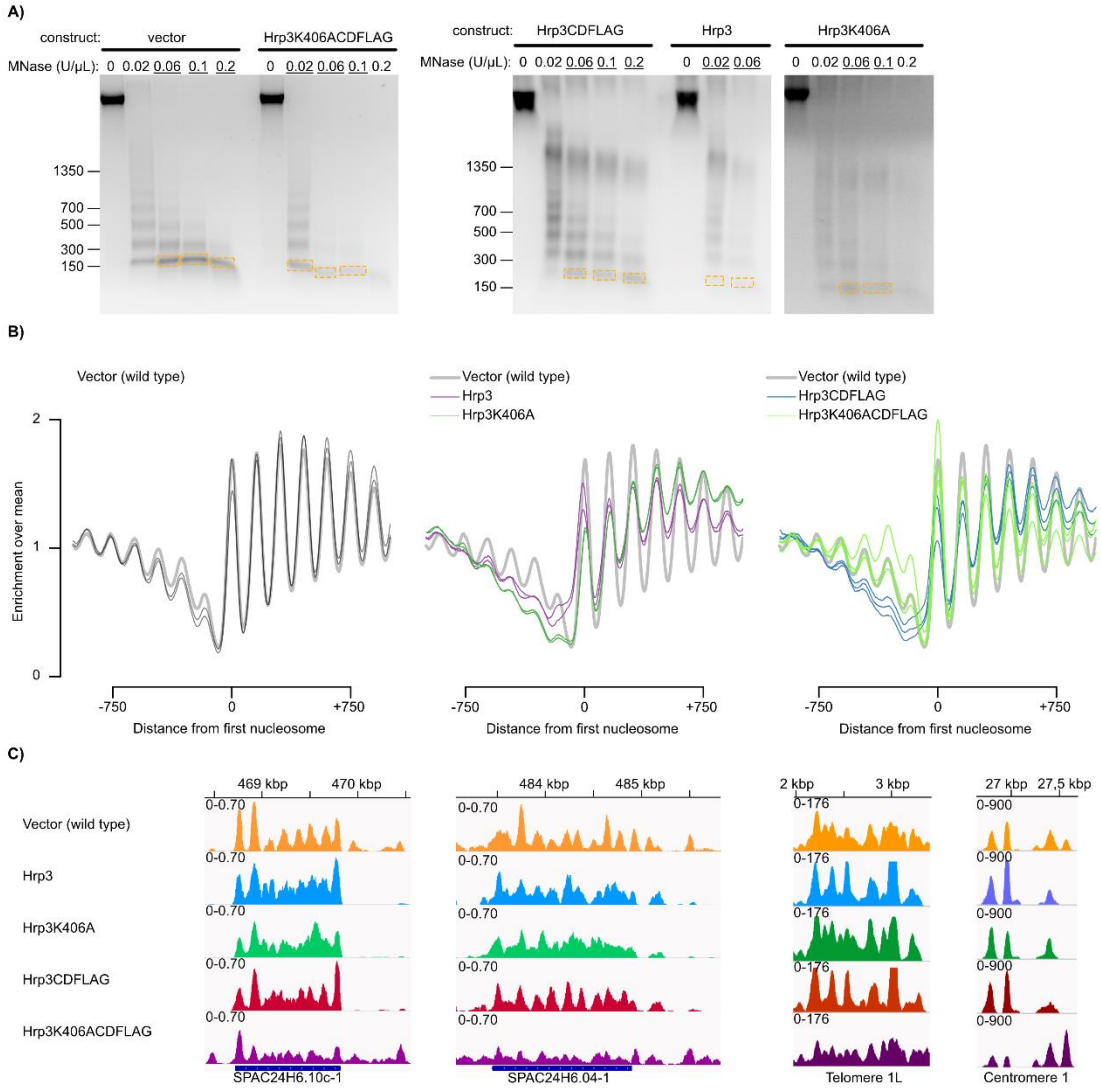

Figure 2.10. MNase-seq experiment of cells overexpressing Hrp3 constructs. *A) Agarose gel of purified DNA after nuclei digestion with varying concentrations of MNase. Labeled sizes are in base pairs. A DNA corresponding to a mononucleosome (~150 bp, orange square) was cut out of the gel, purified and prepared for a paired-end sequencing. For each sample, two or three MNase digestion degrees were sequenced as indicated (underlined). N=1. B) Composite plots of a dyad position aligned to the first nucleosome. See method section 3.2.18.3 for particulars of the analysis. Multiple lines correspond to different MNase digestion degrees. C) Genome browser screenshots of read coverage over two genes (two left panels) and two heterochromatin regions (two right panels). Bigwig files were visualized in Integrative Genomics Viewer (Robinson et al., 2011).*

Decreased regularity of genic chromatin arrays can also be seen in read coverage over single genes (Figure 2.10. D; left). Further, overexpression of Hrp3CDFLAG caused a significant increase of a nucleosome occupancy in intergenic regions. Due to a highly repetitive DNA sequence, information obtained for a heterochromatin region was sparse. An example shows an ATP-dependent increase in a regularity over subtelomeric region (Figure 2.10.D; right).

Together, these preliminary data suggest that overexpression of Hrp3 constructs causes genome-wide changes in nucleosome positioning.

2.1.6 Hrp1/3 and Mit1 decrease nucleosome repeat length in euchromatin

The activities of chromatin remodelers in fission yeast were so far assessed only with composite plots derived from nucleosome positions originating from MNase-seq. This approach has confirmed the defect in a nucleosome positioning in remodeler deficient strains.

To analyze the level of phased regular arrays and NRL on gene-by-gene basis, we performed MNase-seq on wild type fission yeast strains, strains lacking remodelers implicated in a heterochromatin function and *clr4*. We then analyzed nucleosome regularity and spacing in genic regions by applying a bioinformatic algorithm developed in Clark lab (Ocampo et al., 2016; Singh et al., 2021) (Figure 2.11.). In this analysis, an NRL and an array regularity are determined by cross-correlating MNase-seq signal in each gene with an ideal Gaussian pattern.

The analysis was successfully applied to fission yeast data. Regularity score for wild type shows two overlapping peaks that probably correspond to the two main groups of genes of distinct regularities. NRL peaks at 150 base pairs, even shorter than previous estimates (Moyle-Heyrman et al., 2013). As expected, deletion of *clr4* did not influence nucleosome positioning and NRL in genes.

Strain lacking *mit1* has modestly decreased regularity score and slight shift in a distribution towards longer NRLs. Therefore, Mit1 might be a globally acting remodeler that does not strongly influence NRL. Deletion of *hrp1* and *hrp3* drastically decreased regularity score. NRL distribution has flattened and shifted towards longer values. Hrp1/3 data confirm previous suggestions based on composite plots.

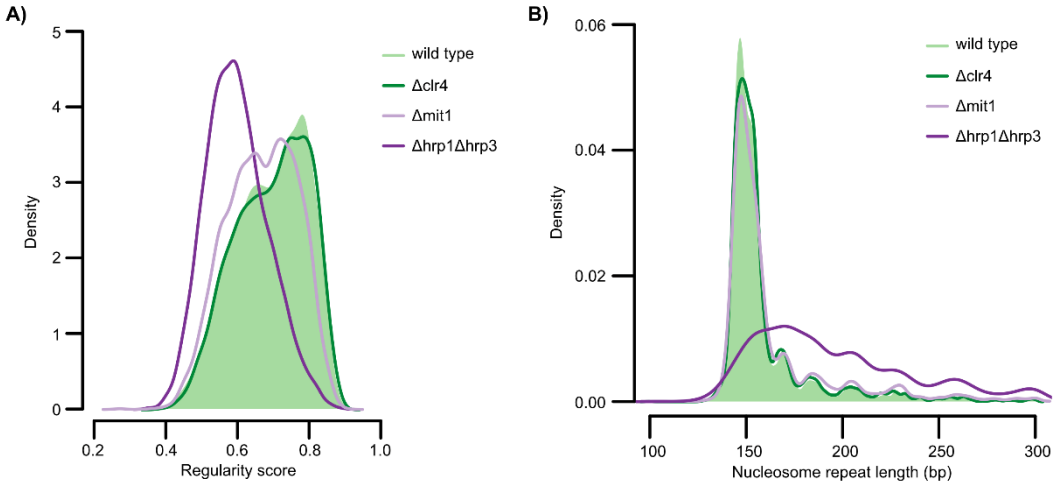

Figure 2.11. Spacing remodelers in fission yeast. *Number of analysed genes was always 5239. N=1. A) Regularity score distributions of nucleosome positions obtained from MNase-seq of strains lacking remodelers. B) NRL distributions obtained from MNase-seq of strains lacking remodelers.*

2.1.7 Towards establishing *ex vivo* remodeling assay

To measure nucleosome sliding on a native substrate, we have isolated nuclei from fission yeast strains lacking *hrp1* and *hrp3.* We then added *D. melanogaster* ISWI and ATP and performed MNase-seq followed by Ocampo analysis described above. The regularity score was minimally changed by addition of both ISWI and ATP (Figure 2.12.A). NRL distribution shifted towards lower values upon ISWI addition in an ATP-independent manner (Figure 2.12.B). The results do not provide conclusive evidence for a spacing activity for ISWI. To ascertain if this approach might be utilized as an *ex vivo* nucleosome remodeling assay, more replicates under varying remodeler,

ATP and salt concentration will be needed. Chromatin remodeling complexes containing auxiliary subunits should also be tested.

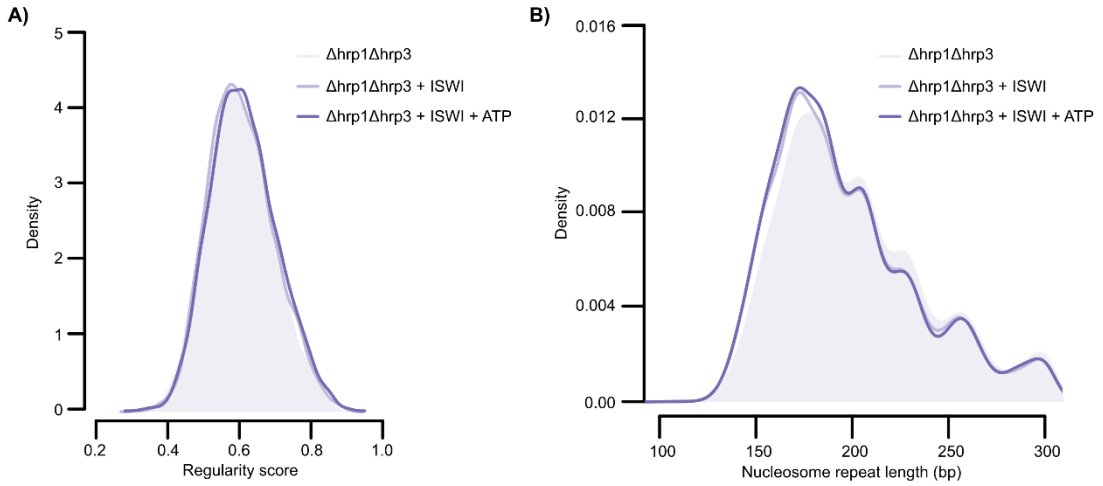

Figure 2.12. *Ex vivo* nucleosome spacing assay. *The nuclei were isolated from 200 mL fission yeast culture of OD=0.4 and divided into three parts. Remodeling reaction was performed with 1/3 of isolated nuclei containing 230 nM ISWI and 2 mM Mg-ATP in MND buffer at 26°C for 30 min. The reaction was stopped with EDTA. Chromatin was digested with MNase, DNA purified and fragments <400 bp sequenced in a pair-end manner. Number of analysed genes was always 5239 A) Regularity score distributions of nucleosome positions obtained from MNase-seq of chromatin isolated strains lacking hrp1 and hrp3 and supplemented with ISWI and ATP. B) NRL distributions of nucleosome positions obtained from MNase-seq of chromatin isolated strains lacking hrp1 and hrp3 and supplemented with ISWI and ATP.*

2.1.8 Discussion and outlook

Heterochromatin is a compact form of chromatin, but it has to be replicated, repaired, regulated and even transcribed. In this chapter, we have established *Schizosaccharomyces pombe* as a model organism in our group and performed the first steps to try and establish the methods to study how much does heterochromatin affect kinetics of chromatin remodeling.

We have used overexpression of chromatin remodelers involved in heterochromatin and checked if there are changes in nucleosome positioning by indirect and direct methods. In addition, the remodeler fusion with a chromodomain was used with a hope to target remodelers more effectively onto heterochromatin.

Overexpression of chromatin remodelers inhibited yeast growth, Hrp3 severely. As the growth is slowed down but the cells are not dying, this suggests that the remodeler overexpression might cause a cell cycle arrest. Absence or overexpression of chromatin remodelers have been reported before to negatively affect the cell growth. In an absence of Fft3 there were severe chromosome segregation defects (Strålfors et al., 2011). Hrp1 overexpression has already been shown to cause a reduction in a growth rate (Jin et al., 1998) and to disrupt a mitotic chromosome segregation (Jae Yoo et al., 2004). This growth defect limited interpretation of silencing assays based on a growth of reporter strains.

To test the effect of the remodeler overexpression on heterochromatin silencing, we determined the amount of heterochromatin transcripts by RT-qPCR. Hrp3 overexpression derepressed heterochromatin silencing in an ATP-independent manner. Contrary to the overexpression of Hrp3, overexpression of Hrp3CDFLAG further repressed transcription from heterochromatin. Preliminary data show that this effect was also ATP-independent. It is possible that Hrp3CD-containing

fusion proteins strongly bind to H3K9me2 and block access to chromatin, inhibiting genomic processes. However, RT-qPCR analysis is complicated by the fact that remodeler overexpression might change transcription of a reference gene to which data are normalized (Pointner et al., 2012; Walfridsson et al., 2005).

Nucleosome mapping by MNase-seq similarly revealed an ATP-independent defect in nucleosome positioning over gene bodies. Strong transcription might cause irregular nucleosome arrays (Singh et al., 2021). Curiously, overexpression of Hrp3K406CDFLAG had the mildest defect in a nucleosome array formation and a significant increase in a nucleosome occupancy in intergenic regions. Although the information obtained for heterochromatin region was sparse, we have identified an ATP-dependent (but chromodomain independent) increase in a regularity over a subtelomeric region. We have confirmed an extremely short NRL reported previously for *S. pombe* both in composite and Ocampo plots (Givens et al., 2012; Lantermann et al., 2010; Moyle-Heyrman et al., 2013).

In this preliminary study, the overexpression had to be induced by washing the cells from thiamine present in a full media and inducing them in a synthetic media. Because yeast has an intracellular reserve of thiamine, induction time and strength might vary between experiments. Alternative to thiamine-repressed promotors would be recently published *S. pombe* vectors that can be induced by addition of a chemical (Kjærulff & Nielsen, 2015; Ohira et al., 2017).

Lastly, we have started to develop a novel nucleosome spacing assay. We have isolated nuclei from strains lacking *hrp1/3* and added to it a purified chromatin remodeler *D. melanogaster* ISWI together with ATP. MNase-seq followed by Ocampo analysis showed a very small increase in a nucleosome regularity score upon addition of both ISWI and ATP. Interestingly, the nucleosome repeat length decreased with the addition of ISWI in an ATP-independent fashion. As an ATPase, ISWI has no strong spacing activity on its own (Varga-Weisz et al., 1997; Corona et al., 1999; Längst et al., 1999; Brehm et al., 2000; Mueller-Planitz et al., 2013). Therefore, the assay should be repeated with a complete remodeler complex with *bona fide* spacing activity, for example ACF (Baldi et al., 2018; Ito et al., 1997; Lusser et al., 2005).

A development of this project in the future will require a utilization of methods that can map nucleosome positions in heterochromatin regions or at least determine its regularity and spacing, for example a single molecule long read sequencing following methylation footprinting (Abdulhay et al., 2020; Lay et al., 2018; Lee et al., 2020; Oberbeckmann et al., 2019; Shipony et al., 2020; Stergachis et al., 2020; Wang et al., 2019). Then a strain with a defect in a nucleosome positioning can be used to follow kinetics of a nucleosome array recovery by inducing remodeler expression or *ex vivo*. *Clr4* can be deleted to compare remodeling of the same region without heterochromatin present.

Additionally, further technique development will enable us to answer additional exciting questions about a nucleosome positioning in fission yeast. Does *hrp1hrp3mit1*Δ strain have residual spacing? We have confirmed that all three remodelers space nucleosomes, but an attempt to make a triple deletion did not give any viable offspring (Pointner et al., 2012). This problem may be circumvented by an anchor-away technique (Haruki et al., 2008; Singh et al., 2021). This rapid, chemical-induced depletion of the target protein from the nucleus was recently adapted to fission yeast (Ding et al., 2014). Other questions to be answered include: what happens to the spacing in a histone depleted fission yeast? What is the role of INO80, transcription and statistical positioning in biogenesis of nucleosome arrays and are these mechanisms evolutionary conserved (Singh et al., 2021)? Does nucleosome organization of heterochromatin underly its silencing function? Which chromatin remodelers, if any, are required for a heterochromatin establishment,

spreading and maintenance? I envision that methodological improvements, including long read nucleosome mapping approaches (Abdulhay et al., 2020), will play a pivotal role in answering these fundamental questions in the future.

2.2 Chapter 2: Nucleosome sliding in a condensed chromatin

2.2.1 Contributions and Acknowledgments

I thank my collaborators who have contributed to this chapter as follows:

Experiments showed in Figure 2.13.A)-D) were performed by Dr. Nicola Hepp.

Data presented in Figure 2.14.C)-E) (analytical ultracentrifugation) were collected and analyzed by Dr. Michaela Smolle from the BMC Biophysics facility.

Amelie Lentz purified GST-GFP and cloned ISWI-GFP.

Dr. Alessandro Scacchetti performed FRAP experiments.

Dieter Kamp performed optical tweezers data collection and analysis.

Mariano Gonzales Pisfil performed confocal imaging and FLIM in BMC Bioimaging facility and analyzed FLIM data.

Dr. Johannes Stigler and Dieter Kamp helped to build a final model.

2.2.2 Background

Reconstituted nucleosome arrays fold into various structures (Routh et al., 2008) and undergo phase separation (Gibson et al., 2019). Biomolecular condensates can harbor distinct chemical environments that can modulate enzymatic reactions. As such, certain enzymes and cofactors might be excluded from condensates, providing intriguing avenues for cellular regulation.

If and how folding impacts enzymatic processes and nucleosome remodeling enzymes has not been systematically investigated. In fact, most studies employ mononucleosome substrates to study nucleosome remodeling, a model substrate that does not fold into chromatin fibers (Clapier et al., 2017).

Chromatin condensate formation and folding poses two challenges to enzymes that are acting on it. First, there is an accessibility problem, i.e., enzyme may be unable to reach buried nucleosomes. Second, important epitopes may be involved in intramolecular and intermolecular chromatin interactions.

ISWI is an ATP-dependent chromatin remodeler that can slide nucleosomes along DNA without disrupting the histone octamer (Hamiche et al., 1999; Längst et al., 1999). Its activity is enhanced by interaction with nucleosome epitopes - linker DNA flanking the nucleosome (Kagalwala et al., 2004; Yang et al., 2006), H4 N-terminal tail (Clapier et al., 2001) and an acidic patch (Dann et al., 2017; Gamarra et al., 2018).

In this chapter we are addressing how chromatin intramolecular folding and phase separation influence activity of chromatin modifying enzymes on the example of chromatin remodeler ISWI. Further, we are asking how ISWI and its ATPase activity influence biophysical properties of chromatin condensates.

2.2.3 Intramolecular chromatin folding does not impede remodeling

A previous student in our group, Dr. Nicola Hepp, designed a DNA containing 25 repeats of a strong nucleosome 601 positioning sequence. 13 of these sequences encoded a unique

restriction enzyme site. A restriction enzyme accessibility assay can therefore be used to detect sliding of each one of these barcoded nucleosomes (Figure 2.13.A) (Ludwigsen et al., 2018). The restriction sites are occluded by nucleosomes and upon nucleosome sliding become exposed for a cleavage.

Using restriction enzymes, Dr. Nicola Hepp concluded that the nucleosome sliding is minimally affected by intramolecular folding. Dr. Hepp derived this conclusion from a comparison of remodeling rates obtained in unfolded and intramolecularly folded arrays (Figure 2.13.B). Unfolded arrays were prepared in 0.2 mM Mg^{2+} and folding was then induced by addition of 1.7 mM $MgCl_2$. She measured the sliding rates of both internal and external nucleosome in both Mg^{2+} conditions. Even though internal nucleosomes in folded nucleosome fibers are less accessible and more stable than external nucleosomes (Hagerman et al., 2009; Poirier et al., 2008, 2009; Schram et al., 2015) (Figure 2.13.C-D), ISWI remodeled internal and more external nucleosomes with identical rate constants regardless ($0.18 \pm 0.02\ s^{-1}$ and $0.18 \pm 0.01\ s^{-1}$, respectively) in loosely folded nucleosome arrays (0.2 mM Mg^{2+}). Induction of fiber folding by supplementing Mg^{2+} to 1.7 mM reduced remodeling rate coefficient by ~two-fold to $0.07 \pm 0.02\ s^{-1}$ for internal and $0.08 \pm 0.02\ s^{-1}$ for external nucleosome. The latter results suggested at most a two- to three-fold contribution of folding on remodeling rates.

To check if the reduced rate is in part due to reduced ATP hydrolysis under these conditions, I performed mononucleosome stimulated ATPase assay (Figure 2.13.E). Indeed, ATPase activity of ISWI stimulated by mononucleosomes that cannot undergo folding was ~two-fold lower in 1.7 mM $MgCl_2$ compared to 0.2 mM $MgCl_2$.

After an *in vitro* nucleosome reconstitution, three independent quality controls confirmed saturation of array DNA with nucleosomes (Figure 2.14.A-B). I confirmed that 25mer array is more folded in 1.7 mM Mg^{2+} than it is in 0.2 mM Mg^{2+}. Analytical ultracentrifugation sedimentation velocity analysis showed that the higher Mg^{2+} concentration led to an increased sedimentation coefficient and lower frictional ratio (Figure 2.14.C-E), consistent with more spherical shape of nucleosome arrays as a result of intramolecular folding. Only around 10% of arrays have oligomerized in presence of 1.7 mM Mg^{2+}. In a negative stain electron microscopy, single particles exhibited heterogenous structures in both conditions (Figure 2.14.F). However, their Feret´s diameter decreased (Figure 2.14.G) and their circularity (Figure 2.14.H) increased with increasing Mg^{2+} concentration, consistent with Mg^{2+}-induced intramolecular folding.

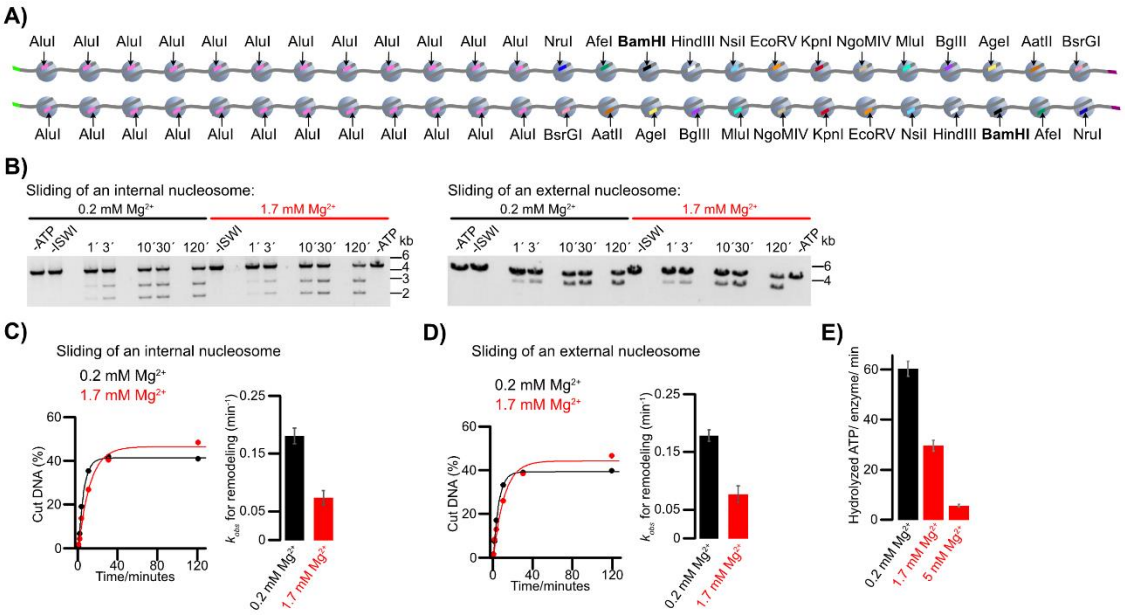

Figure 2.13. Intramolecular chromatin folding does not impede nucleosome sliding. ***A)*** *An array containing 25 repeats of 197 bp long DNA, obtained by ligating 12x197 array with 13x197 array in two different orientations. The repeat has 601 nucleosome positioning sequence and 50 bp long linker DNA. 13mer DNA is bar-coded with a unique restriction enzyme site in every nucleosome positioning sequence. The arrays were cut out from the plasmid with the help of HincII (left, light green) and EcoRI (right, magenta) sites. In these two arrays, BamHI site was utilized to measure sliding of an internal and an external nucleosome, respectively.* ***B)*** *BamHI accessibility nucleosome sliding assay for differently positioned BamHI sites – internal (left) and external (right). Each sliding reaction contained 4 nM respective 25mer and 5 μM ATP and it was started with 200 nM ISWI. One out of two consistent independent replicates is shown.* ***C), D)****, Quantification of gels in B). Bar plots are derived rate coefficients for the respective plots. For each condition, average of two independent replicates is represented and error bars are their minimal and maximal value.* ***E)*** *Mononucleosome stimulated ATPase assay. Mononucleosome-stimulated ATP turnover. ATPase rates were measured in the presence of saturating mononucleosome concentration (using three times less mononucleosomes lead to the same results). Bars are mean values of two independent experiments, error bars their minimal and maximal values. Increasing Mg-concentrations reduce mononucleosome-stimulated ATP hydrolysis rates at saturating concentrations of ATP (1 mM) and mononucleosomes (1.33 μM).*

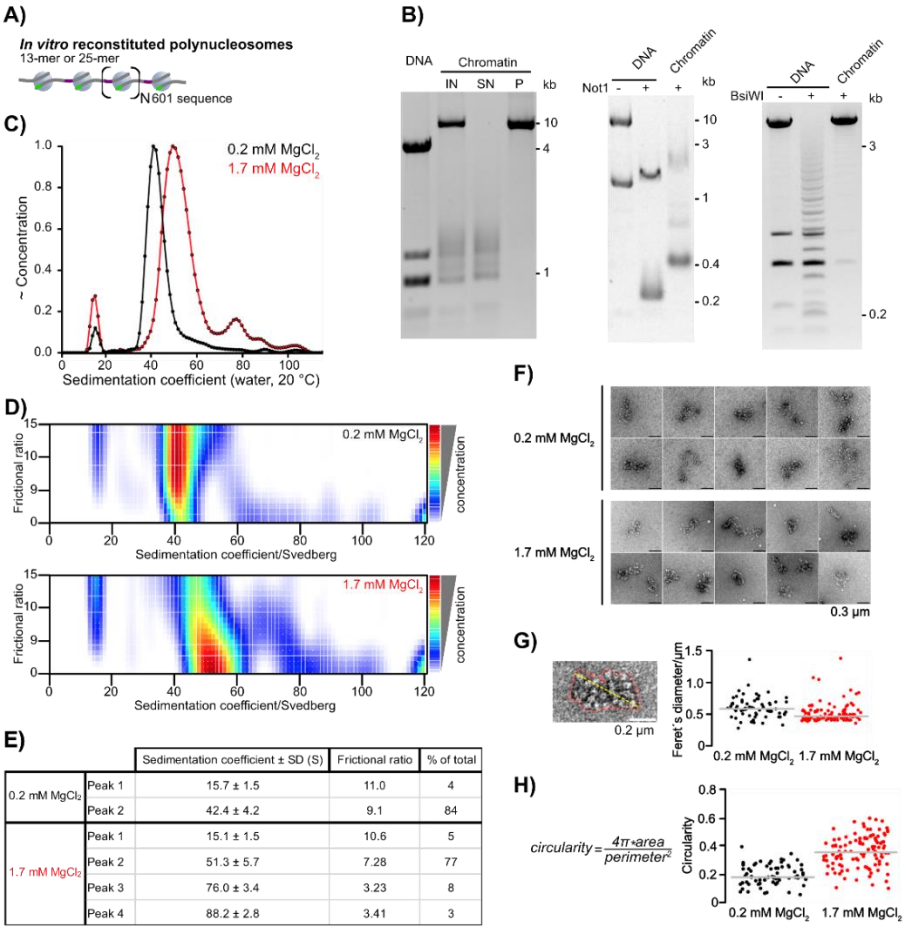

		Sedimentation coefficient ± SD (S)	Frictional ratio	% of total
0.2 mM $MgCl_2$	Peak 1	15.7 ± 1.5	11.0	4
	Peak 2	42.4 ± 4.2	9.1	84
1.7 mM $MgCl_2$	Peak 1	15.1 ± 1.5	10.6	5
	Peak 2	51.3 ± 5.7	7.28	77
	Peak 3	76.0 ± 3.4	3.23	8
	Peak 4	88.2 ± 2.8	3.41	3

Figure 2.14. Structural characterization of folded nucleosome arrays. ***A****) Chromatin arrays used in this study contain BsiWI restriction site in each nucleosome positioning sequence and NotI restriction site in each linker DNA. Digestion with these two enzymes served as a quality control for octamer binding on every 601 site. Octamer binding will render nucleosome inaccessible for BsiWI digestion. Following NotI digest, free DNA-containing 601-site runs around 200 bp, while the one with bound octamer runs around 400 bp. Absence of the ~200 bp band confirms saturation of each 601 site with octamer.* ***B)*** *Quality controls for assembled chromatin 25mer array. From left to the right: agarose gel after magnesium precipitation and resolubilization (IN=unput, SN=supernatant, P=pellet. Only saturated arrays precipitated completely out of the assembly. Overassembly can be detected by smearing of competitor DNA and its coprecipitation.); Not1 digestion, BsiWI digestion.* ***C)*** *Sedimentation velocity analysis of 25mer in remodeling buffer without glycerol supplemented with 0.2 (black) or 1.7 mM $MgCl_2$ (red). At the higher $MgCl_2$ concentration, the arrays have a higher sedimentation coefficient (51.3 ± 5.7 Svedberg (S)), indicating that arrays are more compact and therefore sediment faster. At the lower $MgCl_2$ concentration, they are much more extended, therefore render a lower sedimentation coefficient (42.4 ± 4.2 S). The structures with the slowest sedimentation are probably residual free competitor DNA, whereas structures with the highest sedimentation coefficients (76.0 ± 3.4 S and 88.2 ± 2.8 S) are array oligomers. Presence of oligomers confirms that the higher $MgCl_2$ concentration also causes intermolecular folding.* ***D)*** *Frictional ratio (ratio of the experimental sedimentation coefficient and the maximal sedimentation coefficient calculated for a sphere of the same molecular weight under the same solution conditions) plotted against sedimentation coefficient.* ***E)*** *Peak table from analysis in C).* ***F)*** *Representative micrographs of 25mer from negative stain electron microscopy (EM). Arrays were diluted in remodeling buffer supplemented with 0.2/1.7 mM $MgCl_2$ until single particles could be distinguished in micrographs.* ***G, H),*** *Single-particle analysis of negative stain EM micrographs of 25mer. N (0.2 mM $MgCl_2$) = 67, N (1.7 mM $MgCl_2$) = 107. Outline of a single particle (red line) was determined with the help of trainable Weka segmentation in ImageJ. Feret´s diameter (the maximum distance between two parallel tangential lines, yellow line) and circularity were calculated for this outline. Middle line is a median.*

We conclude that ISWI is not strongly affected by intramolecular nucleosome array folding. It also shows no preference for external nucleosomes as both nucleosomes are similarly accessible to ISWI and readily available for remodeling, consistent with conclusions derived before from modeling (Schram et al., 2015).

2.2.4 Establishing chromatin condensates as a substrate for studying chromatin remodeling

Spherical condensates formed upon addition of a salt in a concentration dependent manner, indicative of a surface tension driven phase separation (Figure 2.15.A). We investigated the effects of a physiologically relevant mixed ionic environment of Na^+/K^+ and Na^+/Mg^{2+}, which are the main cations of the cell cytoplasm (Allahverdi et al., 2015) and constructed a phase diagram by systematically changing nucleosome array and salt concentrations (Figure 2.15.B). The phase separation of chromatin arrays in 50 mM NaCl was induced with both increasing KOAc concentration and increasing $MgCl_2$ concentration. By increasing chromatin concentrations, condensates grew in number or/and size (Figure 2.15.B). Under the same total nucleosome concentration, 25mer was more prone to phase separation as expected due to its higher multivalency. Confocal microscopy imaging of condensates containing 5% of Cy3-labeled array revealed that under certain conditions, chromatin condensates had an outer rim of a higher material density (2.15.C). Chromatin arrays might be accumulating at the rim due to slower diffusion coefficient close to the phase boundary (Hubatsch et al., 2021; Zhang et al., 2022). Comparing intensities from confocal images of condensates of similar sizes (Figure 2.15.D) revealed that under every condition, condensates exhibited similar chromatin density.

Using holotomography, we determined the nucleosome concentration in the condensates formed by 25mer arrays to be 225 ± 59 µM, equivalent to ~45 g/l (Figure 2.15.E). Holotomography is a type of a label-free, quantitative phase microscopy, and the concentration is obtainable from the measured refractive index. Our measurement is in an agreement with concentration estimates in condensates formed by tetra- and 12mer nucleosome arrays, determined by cryogenic electron tomography and fluorescence microscopy, respectively (195 to 550 µM) (Gibson et al., 2019; Zhang et al., 2022). A wide range of conditions thus leads to surprisingly static nucleosome concentrations. *In vivo* nucleosome concentrations fall into the same range. In *Indian Muntjac* cells, the nucleosome concentration varies between 0.1 mM and 0.5 mM (Hihara et al., 2012; Weidemann et al., 2003). *In vitro* reconstituted chromatin condensates are therefore useful model substrates to study challenges encountered by remodelers in a crowded chromatin environment.

Given the high nucleosome concentration, chromatin condensates may act as a barrier for the diffusion of big molecules. To determine the size exclusion limit of chromatin condensates, we used a series of fluorophore-labeled dextrans of different sizes and determined their partition coefficients (Figure 2.15.F). With increasing molecular mass, dextrans were progressively excluded from chromatin, but even large, 500 kD dextrans were able to enter. There was no enrichment of any dextran in the condensates, arguing against artifacts that may arise from the interactions between the probe and condensate components. The data suggest that the chromatin condensates are porous or pliable enough to accommodate even large complexes. Whereas condensates showed a distinct ultrastructure, dextran distribution patterns were homogeneous (Figure 2.15.F, left). In contrast, dextran distribution *in vivo* tended to be more granular, particularly for larger dextrans (Görisch et al., 2003), suggesting that components absent in our reconstituted system create chromatin subcompartments *in vivo*.

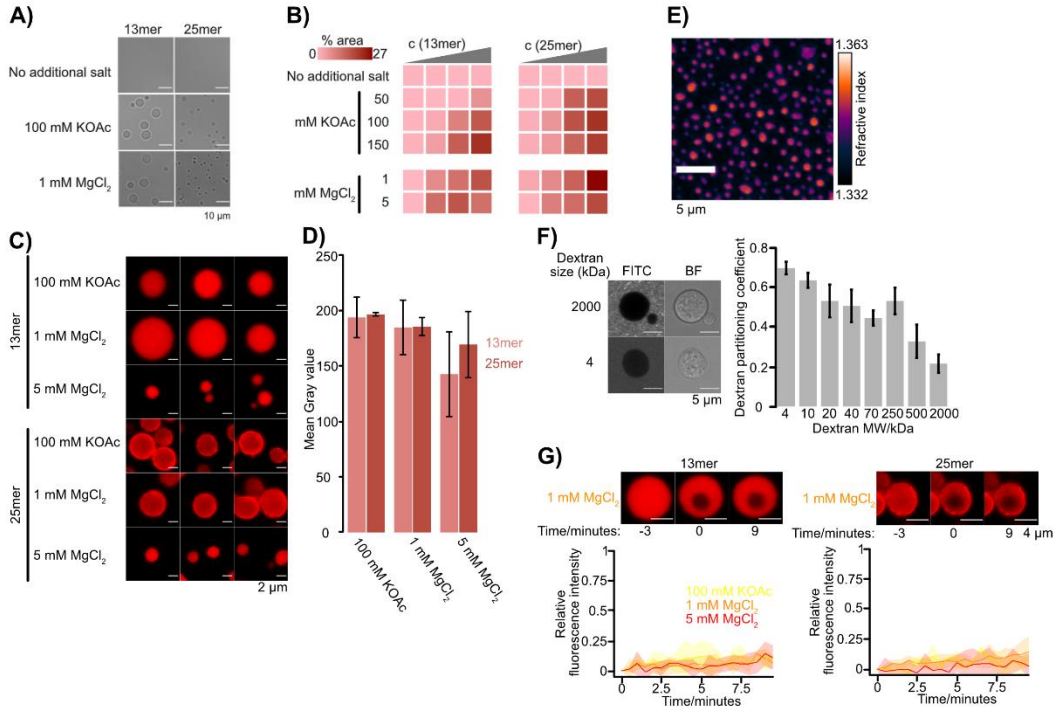

Figure 2.15. Establishing chromatin condensates as a substrate for studying chromatin remodeling. ***A)*** *Phase separation of 13mer and 25mer (1200 nM total nucleosome concentration). The data were collected in 25 mM Hepes-KOH pH 7.6, 0.1 mM EDTA, 50 mM NaCl, 10% glycerol, 1 mM DTT, 0.2 g/L BSA and added salts as noted.* ***B)*** *Representation of an entire phase diagram – area percentage of field of view occupied by condensates. Total nucleosome concentrations were: 25 nM, 100 nM, 400 nM and 1200 nM.* ***C)*** *Confocal images of 13mer and 25mer (90 nM total array concentration, 5% is Cy3-labeled).* ***D)*** *Fluorescence intensity of Cy3-labeled chromatin inside chromatin condensates across different conditions. Data were collected for 90 nM 13mer/25mer with 5% label and added salts as noted. In the same order as on the image, the number of analyzed condensates is: 11, 4, 8, 6, 28 and 13. Average Gray value and standard deviation of two independent replicates are plotted.* ***E)*** *Holotomogram of chromatin condensates in 5 mM $MgCl_2$. Average nucleosome concentration was determined from linear relation of concentration and refractive index. One out of two consistent replicates is shown.* ***F)*** *Partition coefficient of FITC-labeled dextrans of various sizes. Data were collected in 90 nM 13mer with 0.1 mg/mL FITC-labeled dextran. Dextran partitioning coefficient was calculated for 18 condensates for each sample on average. Their average and standard deviations are plotted.* ***G)*** *Limited internal dynamics of Cy3-labeled chromatin array as measured by FRAP. The data were collected with added salts as noted. Scale bar 4 µm. N=3-5 for each condition. One out of many consistent independent replicates is shown.*

In interphase, chromatin moves across micron-scale regions for a few seconds (Nozaki et al., 2017; Shaban et al., 2018; Xiang et al., 2018; Zidovska et al., 2013b). We probed the dynamics of chromatin inside the condensates by fluorescence recovery after photobleaching (FRAP) and measured little to no recovery over eight minutes (Figure 2.15.G), in contrast to previously published study (Gibson et al., 2019). This might be due to interdigitating of chromatin fibres in a probable structure of the condensate and/or strong intermolecular nucleosome interactions. It is consistent with the most recent data for both *in vitro* chromatin condensates and chromatin in live cells (Strickfaden et al., 2020a). However, interaction with the glass surface can lead to changes in material properties of condensates and therefore it is recommended to compare behavior on glass slides with a variety of coatings (Alberti et al., 2019). Additionally, gelation effects could be induced during imaging acquisition (Gibson et al., 2021). Apart of experimental artifacts, chromatin movements might occur on a smaller scale and thus be inaccessible by such photobleaching experiments. Prolonged incubation of the condensates did not influence the dynamics

significantly, although the differences might be challenging to detect in a first place, because of the very low percentage of the mobile phase or timescale of molecular rearrangements shorter than 15 minutes.

Enzymatic reactions depend on physical characteristics of a milieu in which they are taking place. Therefore, to characterize viscoelastic properties of chromatin condensates, we employed optical tweezers to fuse them in a controlled manner (Figure 2.16.A) (Kaur et al., 2019; Wang et al., 2018). Chromatin condensates fused with different efficiencies in different buffer conditions (Figure 2.16.B). Salts modulated condensate behavior from a liquid-like (fast fusion) to a gel-like or a solid-like (very slow or no fusion). Specifically, binding of Mg^{2+} makes the condensates more solid like. Fusion is accelerated by a surface tension of the condensates and retarded by an interior viscosity (Alshareedah et al., 2019; Ghosh & Zhou, 2020; Kaur et al., 2019). Fitting the force response from optical traps to a stretched logistic fit allowed us to determine fusion velocity at the inflection point (Figure 2.16.C). When normalized to the condensate radius, fusion velocity was not different for 13mer and 25mer condensates under the same salt condition (Figure 2.16.D). Therefore, the initiation of fusion depends on both the array length and the buffer composition (Figure 2.16.B), however once when it starts, its velocity is exclusively salt-dependent (Figure 2.16.D), indicating that the condensate fusion possesses at least two steps, each of the steps differently regulated by the salt and the array length.

Taken together, we have an adequate system to study effects of condensation on remodeling enzymes.

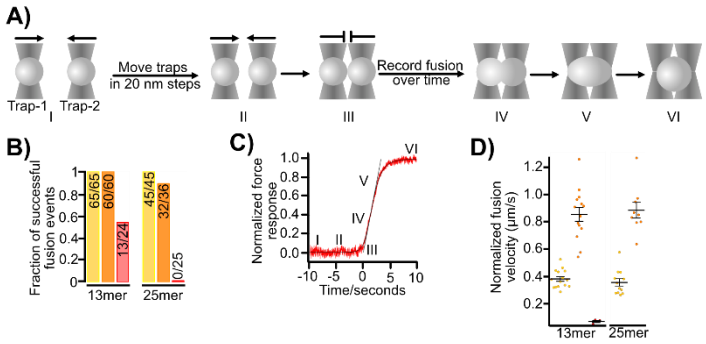

Figure 2.16. Characterization of viscoelastic properties of chromatin condensates. ***A)*** *Controlled condensate fusion with optical tweezers.* ***B)*** *Fraction of successful fusion events for 13mer and 25mer condensates. The data were collected in a buffer supplemented with 100 mM KOAc (yellow), 1 mM $MgCl_2$ (orange) or 5 mM $MgCl_2$ (red). Total nucleosome concentration was 1200 nM. Behaviour of chromatin condensates depends on the chain length and the buffer composition.* ***C)*** *Force readout of optical traps during controlled condensate fusion. Roman numbers correspond to fusion steps as annotated in A).* ***D)*** *Normalized fusion velocity of 13mer and 25mer condensates. The data were collected in a buffer supplemented with 100 mM KOAc (yellow), 1 mM $MgCl_2$ (orange) or 5 mM $MgCl_2$ (red). Total nucleosome concentration was 1200 nM.*

2.2.5 Chromatin remodeler ISWI increases viscosity of chromatin condensates in an ATP-independent manner

I found above that large dextran molecules can be accommodated by chromatin condensates, predicting that remodelers can do so too. I tested this possibility with ISWI, the ATPase subunit of *D. melanogaster* chromatin remodeler ACF and ChRAC (Ito et al., 1997; Varga-Weisz et al., 1997). First, I assessed if ISWI binding is compatible with chromatin phase separation. I premixed ISWI-GFP with nucleosome arrays followed by salt addition to induce phase separation (Figure 2.17.A). Condensates formed and ISW-GFP was enriched in these condensates six to 40-fold (Figure 2.17.B). Next, I tested if ISWI-GFP can enter preformed condensates. Based on their porosity for dextrans, the expectation was that ISWI will enter chromatin condensates by passive diffusion appropriate to its size. But ISWI-GFP again got quantitively enriched in chromatin condensates (Figure 2.17.A). Further, no nucleotide was necessary for remodeler binding to chromatin as shown before (Tilly et al., 2021) and its recruitment in condensates. Control experiments proved that GFP or ISWI-GFP did not form condensates by themselves and that GFP did not enrich in chromatin condensates (Figure 2.17.A).

Interestingly, the presence of ISWI leads to a slower condensate fusion in a concentration-dependent manner, regardless of ATP´s absence (Figure 2.17.C) or presence (Figure 2.17.D). To identify if this effect is due to an increase in a viscosity or a decrease in a surface tension of chromatin condensates, I varied ISWI concentration and measured fluorescence of a widely utilized molecular rotor thioflavin T (ThT) (Figure 2.17.E). Molecular rotors are a specific class of fluorophores that consist of two moieties, which are connected by a single bond. In a low viscosity medium, the rotor rotates freely, and the energy of excitation is dissipated non-radiatively. However, in a high viscosity medium, rotation through the C-C bond is constrained, and the excitation energy is released as an emission (Ghosh et al., 2020; Kaur et al., 2019; Miao et al., 2019). The increase in a ThT fluorescence in a concentration dependent manner, strongly suggests an increase in a viscosity of chromatin condensates with the addition of ISWI (Figure 2.17.E). It cannot be excluded that the effect is due to increased ISWI concentration or that the surface tension does not change as well. Addition of ISWI to chromatin condensates caused an exclusion of FITC-dextrans (Figure 2.17.F) and increase in size of chromatin condensates (Figure 2.17.G).

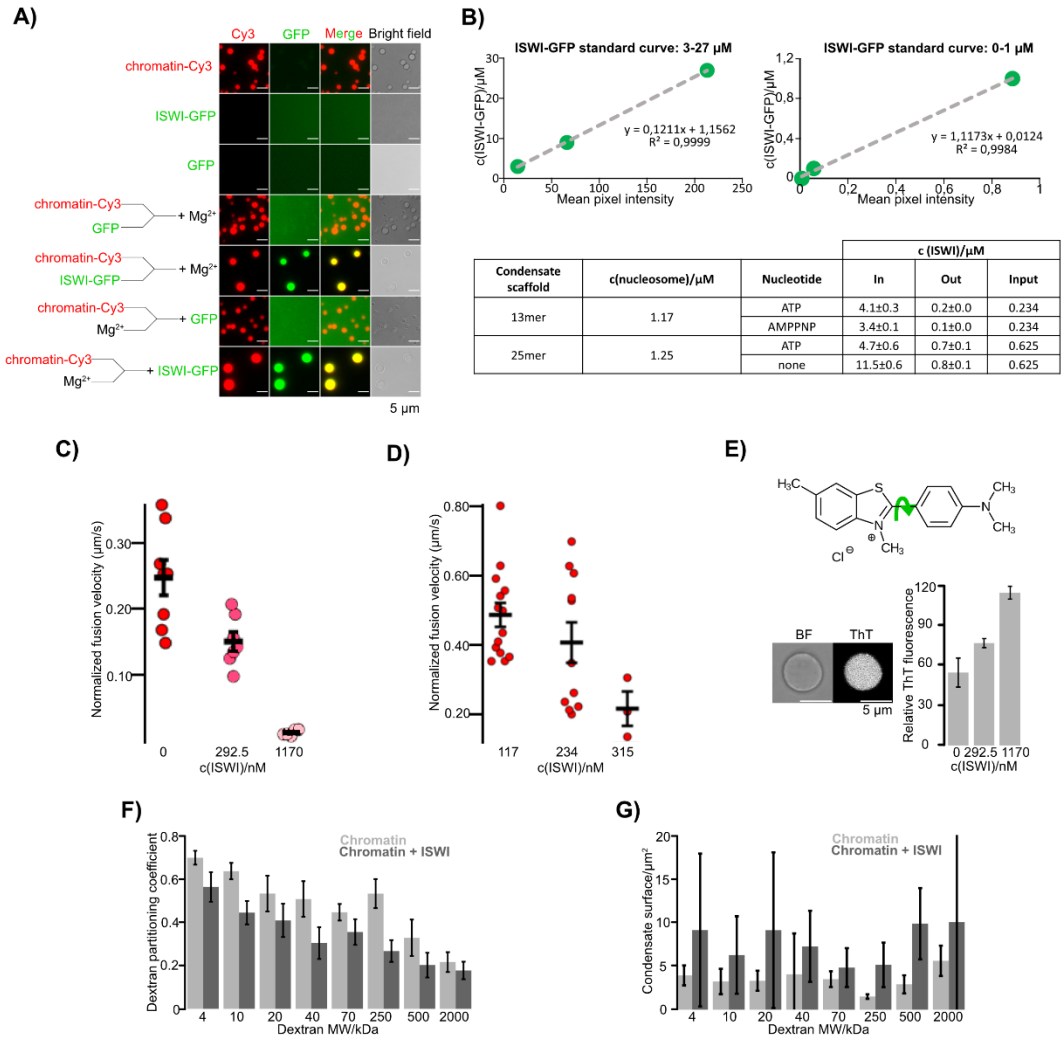

Condensate scaffold	c(nucleosome)/µM	Nucleotide	c (ISWI)/µM		
			In	Out	Input
13mer	1.17	ATP	4.1±0.3	0.2±0.0	0.234
		AMPPNP	3.4±0.1	0.1±0.0	0.234
25mer	1.25	ATP	4.7±0.6	0.7±0.1	0.625
		none	11.5±0.6	0.8±0.1	0.625

Figure 2.17. ***A)*** *Chromatin remodeler ISWI is enriched in chromatin condensates. Chromatin and ISWI colocalization experiment was performed with 40 nM of unlabeled 25mer, 10 nM of 25mer-Cy3 and 1.1 µM ISWI-GFP/GFP-GST. One out of two consistent independent replicates is shown.* ***B)*** *Standard curve for a mean Gray value dependence on ISWI-GFP concentration was obtained from ISWI-GFP dilutions. Different microscope settings were used to image lower and higher dilutions. ISWI-GFP concentration was then determined inside condensates and in a surrounding solution for 90 nM 13mer, 230 nM ISWI-GFP, 1 mM ATP/AMPPNP, ATP-regeneration system and for 45 nM 25mer, 125 nM 0N60 mononucleosomes, 625 nM ISWI-GFP, 1 mM ATP/no nucleotide, ATP-regeneration system. Average and standard deviation of two independent replicates are shown.* ***C)*** *Normalized fusion velocities of condensates containing different ISWI concentrations collected with 90 nM 13mer. One out of two consistent independent replicates is shown.* ***D)*** *Normalized fusion velocities of condensates containing different ISWI concentrations collected with 90 nM 13mer and supplemented with 1 mM ATP. One out of two consistent independent replicates is shown.* ***E)*** *Molecular rotor thioflavin T (ThT) is a reporter of condensate viscosity. Relative ThT fluorescence is the fluorescence inside the condensate normalized to the fluorescence of the surrounding solution. Data were collected for condensates containing different ISWI concentrations with 90 nM 13mer and supplemented with 40 µM Thioflavin T (ThT). Average of relative ThT fluorescence of 5-7 condensates and their standard deviations are plotted for each condition.* ***F, G)*** *Partition coefficient of FITC-labeled dextrans of various sizes. Data were collected in 90 nM 13 mer, 0/60 nM ISWI, 0.1 mg/mL FITC-labeled dextran. Dextran partitioning coefficient in F) and the condensate size in G) were determined. Average of 18/24 condensates and standard deviations are plotted for both quantities.*

2.2.6 ISWI slides nucleosomes inside chromatin condensates.

ISWI sliding might be inhibited in chromatin condensates. To test this, I performed resctriction enzyme accessibility assay (Ludwigsen et al., 2018). I induced phase separation of 25mer nucleosome arrays and then initiated remodeling by addition of ISWI and Mg-ATP. Remodeling was clearly detectable under condensate-inducing conditions (Figure 2.18.A) but slowed down (~seven-fold).

Due to different chemical environments, Mg-ATP binding parameters might differ in solution and inside of condensates. I have determined Michaelis-Menten parameters by measuring initial remodeling velocity in different Mg-ATP concentration (Figure 2.18.B). The maximum observed initial nucleosome sliding rate was ~five-fold lower in condensate-inducing 5 mM Mg^{2+} than in 0.2 mM Mg^{2+}. Michaelis-Menten constant (K_M), a substrate concentration at which velocity equals one half of a maximum velocity, was ~five-fold higher in condensate-inducing 5 mM Mg^{2+} than in 0.2 mM Mg^{2+}. Therefore, in condensates, ISWI binds Mg-ATP with a lower affinity or ATP concentrations do not equilibrate between condensates and the dilute phase.

ISWI´s interaction with its other substrate, the nucleosome, could conceivanly be disrupted by chromatin condensation as well. The H4-tail is a nucleosome epitope needed for ISWI activation. It is also involved in interactions with DNA in chromatin condensates (Gibson et al., 2019). This might make it inaccesible for ISWI to bind and slow down the nucleosome sliding. If that is true, a mutant that has lost the sensitivity to H4-tail, ISWI R458D (Ludwigsen et al., 2017), should not be affected by chromatin condensation. I measured nucleosome sliding by wild type ISWI (wtISWI) and ISWI R458D, in solution (1 mM Mg^{2+}) and condensates (5 mM Mg^{2+}) (Figure 2.18.C). ISWI R458D was even more strongly affected by condensation, disproving the former hypothesis.

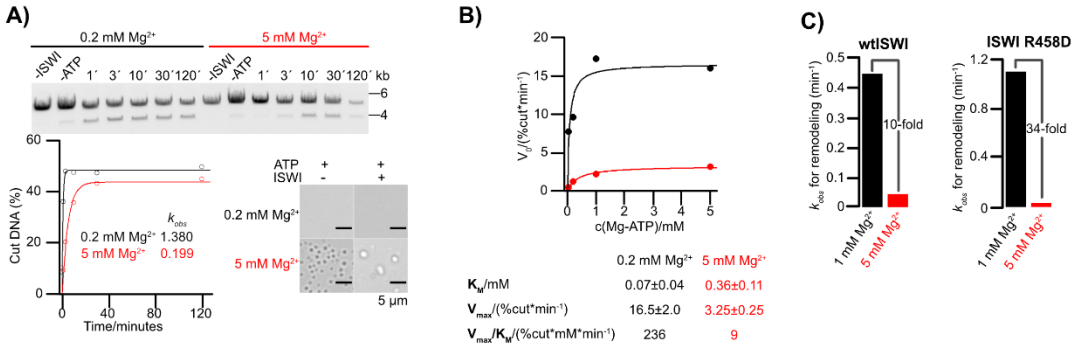

Figure 2.18. Nucleosome sliding in an array under condensate inducing conditions. ***A)*** *KpnI accessibility nucleosome sliding assay adapted to chromatin condensates (15 nM 25mer, 750 nM ISWI, supplemented with 0.2 or 5 mM $MgCl_2$, 1 mM Mg-ATP). Reaction is started with ISWI addition. One of two consistent independent replicates is shown.* ***B)*** *KpnI accessibility assays were performed in solution (0.2 mM Mg^{2+}, black) or under condensate-inducing conditions (5 mM Mg^{2+}, red). Each reaction contained 15 nM 25mer, 750 nM ISWI and it was started by adding different Mg-ATP concentration. Initial nucleosome sliding velocities (V_0) correspond to the slopes of linear fits of %DNA cut versus time in early time points. Above, V_0 was plotted against Mg-ATP concentrations and the curve represents Michaelis-Menten fit. Parameters obtained from the fit for both conditions are in the table under the graph. N=1.* ***C)*** *k_{obs} for KpnI accessibility nucleosome sliding assay performed in 15 nM 25mer, 300 nM wtISWI or ISWI R458D, supplemented with 1 or 5 mM $MgCl_2$ and 1 mM Mg-ATP). Reaction is started with ISWI addition. N=1.*

However, ISWI´s ATPase activity itself, stimulated by mononucleosomes that do not form condensates, was also strongly impaired in 5 mM $MgCl_2$ (~10-fold) (Figure 2.13.E). In conclusion, the ISWI was able to slide nucleosomes inside chromatin condensates although with a reduced

rate. The reduced rate is likely caused by slower ATPase activity in 5 mM Mg^{2+}, that is used to induce condensation.

To see if nucleosome sliding happens inside the chromatin condensates, and not only in the solution or on a surface of condensates, we adapted a FRET-based nucleosome sliding assay (Yang & Narlikar, 2007) on the condensates. We designed and assembled FRET labeleled mononucleosomes, mixed them with chromatin condensates and measured donor lifetime through fluorescence lifetime imaging (FLIM) (Figure 2.19.A). The donor dye atto565 was coupled to H2AK119C and the acceptor dye atto647N was on an octamer proximal end of DNA. FRET-nucleosomes preferentially partitioned into condensates with 17- to 90-fold enrichment (Figure 2.19.B). Whole-condensate FRAP showed little exchange of the FRET nucleosomes between the condensate and the surrounding dilute phase (Figure 2.19.C). Acceptor photobleaching caused donor unquenching and higher donor lifetime, confirming presence of FRET (Figure 2.19.D). Donor lifetime decreased upon adding an acceptor, confirming FRET. The FRET decreased again (lifetime increased) after incubation with ISWI and Mg-ATP. This change corresponds to the drop in FRET efficiency from 22% to 17% upon addition of Mg-ATP. Donor lifetime did not change with addition of Mg-ATP without the presence of the acceptor dye (Figure 2.19.E). For analysis we used a phasor representation where no assumption is made on the number of decay rates present nor on the specific modelling of the decay (exponential, non-exponential) (Digman et al., 2008) (Figure 2.19.F). We thus established FLIM-FRET as a sensitive technology to visualize nucleosome remodeling with spatial resolution.

Having optimized the technical conditions by measuring end-point FLIM-FRET, we used a flow chamber to flow in an 1 mM Mg-ATP solution to chromatin condensates containing FRET-mononucleosomes and then followed nucleosome sliding in real time. Indeed, already in the first minutes of the assay, the donor lifetime increased significantly (FRET decreased). This did not happen when a non-hydrolysable analogue Mg-AMPPNP was used (Figure 2.20.A). To quantitatively compare nucleosome sliding in condensates versus in solution, we determined the initial sliding rate (slope of the linear dependence of early timepoints in a lifetime diagram) in condensates, solution around the condensates and solution only, where arrays were replaced by stochiometric amounts of mononucleosomes thereby removing the possibility of phase separation, but keeping all other condition the same (Figure 2.20.B). Initial velocities are equal in solution only ($(2\pm0)*10^{-4}$ s^{-1}) and solution around the condensates ($(2.3\pm0.6)*10^{-4}$ s^{-1}. The initial velocity for nucleosome sliding inside the condensates ($(0.77\pm0.06)*10^{-4}$ s^{-1}) is only two-fold lower than in solution. Apart from different starting positions, visual comparison of phasor change during course of reaction did not reveal any significant differences that might point to distinct nucleosome sliding outcomes in condensates and in solution. We repeated the experiment with 5 mM Mg-ATP and the results did not change (Figure 2.20.C). When we used four times less enzyme, FRET appeared to increase (i.e., the lifetime decreased) in both condensates and solution around condensates (Figure 2.20.D). We did not explore this phenomenon any further. A possible cause might be conformational change of a nucleosome upon ISWI binding or a presence of an intermediate, observed before for Snf2h in bulk FRET assays in a solution (Yang & Narlikar, 2007). Taken together, ISWI slides nucleosomes inside chromatin condensates and condensates do not pose a strong barrier for sliding.

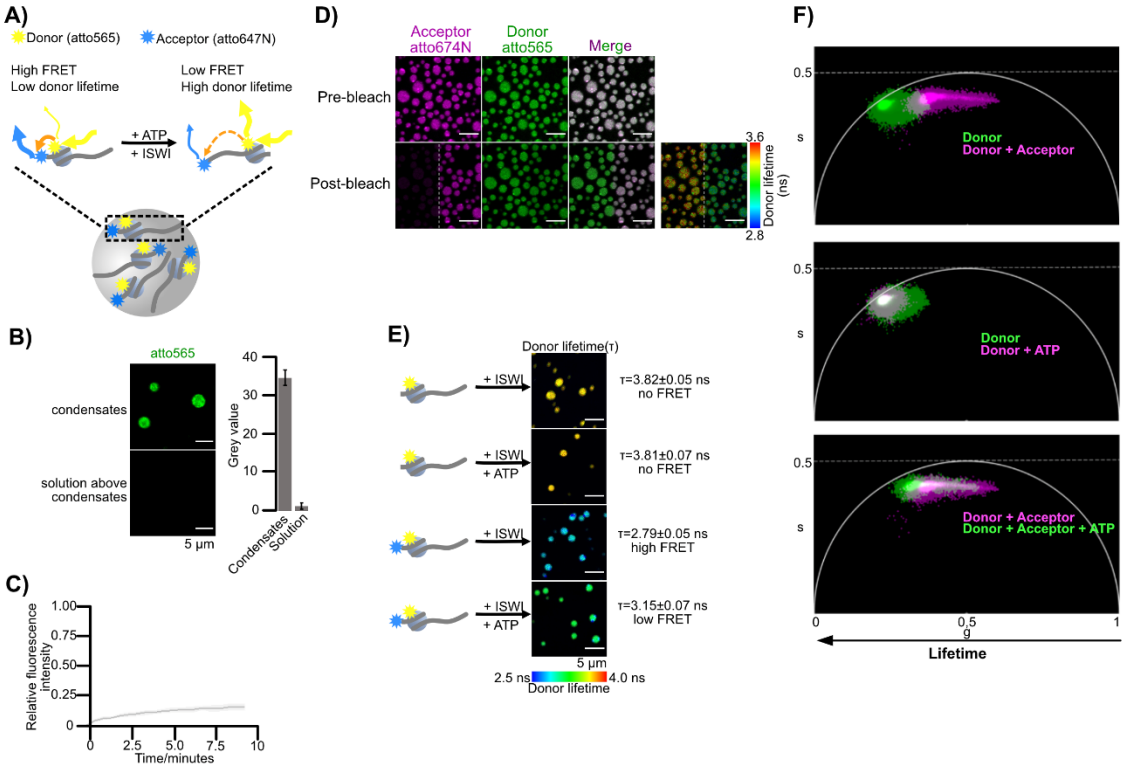

Figure 2.19. Development of imaging-based nucleosome sliding assay with spatial resolution. ***A)*** *End-point imaging-based FRET-sliding assay. Donor dye atto565 was coupled to H2AK119C and acceptor dye atto647N was on an octamer proximal end of DNA.* ***B)*** *Enrichment of FRET-0N60 mononucleosomes in chromatin condensates, N= 3 ± SD.* ***C)*** *Whole condensate FRET-0N60 mononucleosome FRAP to assess their exchange between condensate and solution. One out of two consistent independent replicates is shown.* ***D)*** *Imaging of FRET-0N60 mononucleosomes in chromatin condensates. Acceptor fluorophore was bleached in a left half of a field of view. Subsequently, donor fluorescence was brighter and donor lifetime higher in a left half of a field of view.* ***E)*** *Donor lifetime decreased upon adding an acceptor, confirming FRET. Addition of ISWI and Mg-ATP to condensates containing FRET-nucleosomes, but not donor-only nucleosomes, increased the donor lifetime, indicative of nucleosome sliding. This change corresponds to the drop in FRET efficiency from 22% to 17% upon addition of Mg-ATP. One out of 2 independent replicates is shown. Standard deviations are calculated for lifetimes across ten fields of view of the same sample. Each field of view was imaged 30 times, in total 300 images per condition were collected. Data are collected with 45 nM 25mer, 125 nM FRET-0N60 mononucleosomes and 625 nM ISWI, 5 mM $MgCl_2$, 1 mM Mg-ATP.* ***F)*** *Phasor representation of experiment in E). Upon introduction of the acceptor, donor's lifetime distribution moves away from the universal circle line (single exponential lifetimes). This is consistent with an existence of at least two or even three different populations of donor: high FRET (donor on H2A closer to DNA label), low FRET (donor on H2A further from DNA label) and no FRET.*

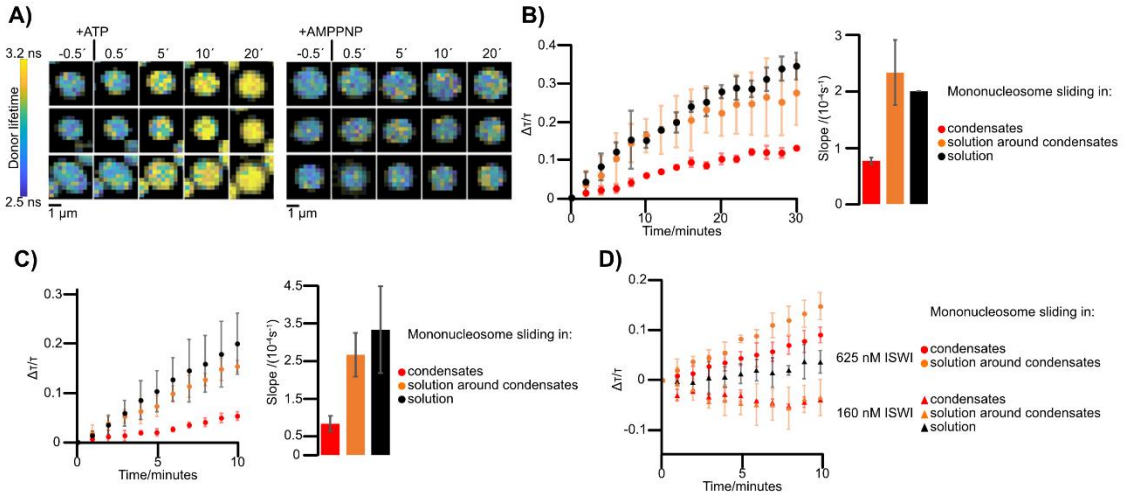

Figure 2.20. ISWI slides nucleosomes inside chromatin condensates. ***A)*** *FLIM time lapse microscopy. Data are collected with 45 nM 25mer, 125 nM FRET-0N60 mononucleosomes and 625 nM ISWI in 5 mM $MgCl_2$, 1 mM Mg-ATP/Mg-AMPPNP. Mg-ATP or Mg-AMPPNP were flown into the imaging chamber at t = 0. Lifetimes for individual condensates are shown. One out of two independent replicates with similar results is shown.* ***B)*** *Nucleosome sliding in condensates (red) and solution surrounding condensates (orange) (45 nM 25mer, 125 nM FRET-0N60 mononucleosomes and 625 nM ISWI in 5 mM $MgCl_2$, 1 mM Mg-ATP flown in), and in solution only (black), where mononucleosomes are stoichiometrically added instead of 25mer (1125 nM unlabeled 0N60 mononucleosomes, 125 nM FRET-0N60 mononucleosomes and 625 nM ISWI in 5 mM $MgCl_2$, 1 mM Mg-ATP flown in). Average of two independent replicates (solution) and three independent replicates (condensates and solution around condensates) is plotted and error bars are their SD. The linear part of a curve was fitted to obtain slopes (initial velocities) and their average values are presented in the bar chart on the right; error bars are their SD.* ***C)*** *Same as B), but with 5 mM ATP. Average of three independent replicates is plotted and error bars are their SD.* ***D)*** *Same as B), but with two ISWI concentrations compered – 160 nM and 625 nM; c(Mg-ATP) = 1 mM. Average of two independent replicates (solution) and three independent replicates (condensates and solution around condensates for each enzyme concentration) is plotted and error bars are their SD.*

2.2.7 The ATPase activity of the chromatin remodeler ISWI enhances liquid-like properties of chromatin condensates

The high activity of ISWI in condensates was intriguing, considering significant immobility of chromatin. We hypothesized that chromatin might have more gel-like properties and act as a stable platform whereas ISWI molecules in condensates are more liquid-like in nature. To test this, we performed FRAP on ISWI-GFP. When we bleached the entire condensate, there was no recovery of ISWI-GFP signal neither with Mg-ATP nor with an equivalent amount of Mg-UTP to control for an ionic strength (Figure 2.21.A). This might indeed be caused by low dynamics of the enzyme or by a low concentration of the enzyme in the surrounding solution. To look exclusively at ISWI´s dynamics inside the condensate, we only bleached the centre. In that case, addition of Mg-ATP sped up ISWI-GFP recovery (Figure 2.21.B). Interestingly, no other nucleotide rendered ISWI dynamic inside chromatin condensates (Figure 2.21.C). In the presence of Mg-ATP, recovery kinetics of ISWI-GFP was dependent on the ratio of ISWI to nucleosomes (Figure 2.21.D). Therefore, stoichiometry is an important aspect when designing future experiments. Higher amounts of ISWI led to a decrease in a contribution from a fast-recovering fraction and to an increase in a contribution from an immobile fraction (Figure 2.21.E). Mg-ATP was not limiting for the ISWI-GFP dynamics, since the use of 1 mM Mg-ATP and 3 mM Mg-ATP produced the same recovery curves

(Figure 2.21.D, compare purple and green line). We conclude that active ATP hydrolysis is required for the remodeler´s dynamics on chromatin.

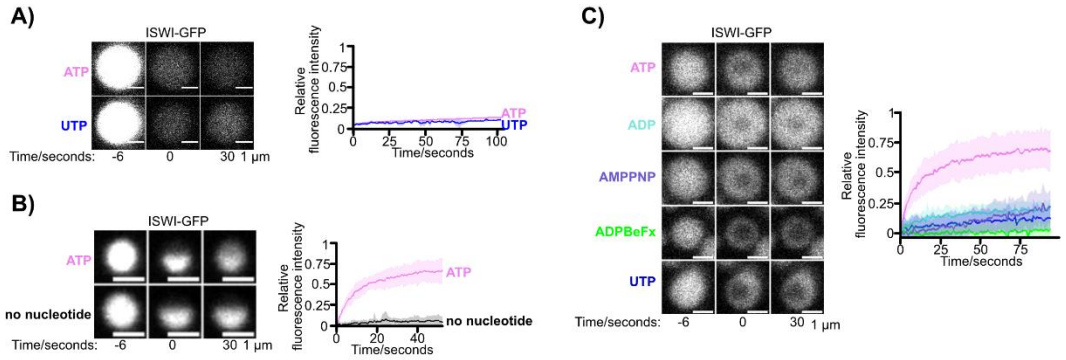

	Fast recovering fraction		Slow recovering fraction		Immobile fraction
ratio	%	$t_{1/2}$/seconds	%	$t_{1/2}$/seconds	%
0,5	32	2,9	40	21,4	28
0,5	52	2,2	19	25,8	29
0,5	42	2,5	29	14,0	29
1	35	3,4	37	18,9	28
2	9	3,4	46	28,0	46
2	6	1,6	43	10,7	52

Figure 2.21. ISWI mobility in chromatin condensates. ***A)*** *ISWI-GFP does not exchange with surrounding solution. Left: Entire condensate was bleached in the presence of Mg-ATP or Mg-UTP. Experimental conditions: 100 nM 25mer, 4.5 nM 25mer-Cy3, 1.3 µM ISWI-GFP, 5 mM $MgCl_2$, 1 mM Mg-ATP/Mg-UTP. Right: Quantification of FRAP time courses. The line is an average and the shaded area represents the SD of all bleached condensates. Five condensates were analysed for Mg-ATP and three for Mg-UTP. N=1.* ***B)*** *Intra-condensate mobility of ISWI-GFP measured by partial-condensate FRAP. Left: Half of a condensate was bleached in presence and absence of Mg-ATP (1 mM). Right: Line is an average and shadow SD of 15 bleached condensates for each condition. One out of four consistent independent replicates is depicted.* ***C)*** *Left: Partial-condensate FRAP of ISWI-GFP in presence of indicated nucleotides (all 0.77 mM). Addition of Mg-ATP, but no other nucleotide, allowed fast FRAP. Right: Quantification of FRAP time courses. The line is an average and the shaded area represents the SD of all bleached condensates; 20 condensates were analysed for Mg-AMPPNP and Mg-UTP, 15 for Mg-ADP, 25 for Mg-ADPBeFx and 30 for Mg-ATP. One out of two independent replicates is shown, in the second replicate ISWI-GFP recovery in Mg-ADP condition was faster, everything else was consistent.* ***D)*** *Quantification of partial-condensate FRAP of ISWI-GFP in presence of Mg-ATP and differing in stoichiometrical n(ISWI):n(nucleosome) ratio. Experimental conditions: 100 nM 25mer, 1.3 µM ISWI-GFP, 5 mM $MgCl_2$, 1 mM Mg-ATP (black line, 5 condensates analysed); 37 nM 25mer, 1.75 nM Cy3-25mer, 500 nM ISWI-GFP, 5 mM $MgCl_2$, 0.77 mM Mg-ATP (blue line, 15 condensates analysed); 76 nM 25mer, 1.75 nM Cy3-25mer, 1 µM ISWI-GFP, 5 mM $MgCl_2$, 0.77 mM Mg-ATP (violet line, 30 condensates analysed); 15 nM 25mer, 375 nM ISWI-GFP, 5 mM $MgCl_2$, 1 mM Mg-ATP (turquoise line, 15 condensates analysed); 15 nM 25mer, 750 nM ISWI-GFP, 5 mM $MgCl_2$, 1 mM Mg-ATP (green line, 12 condensates analysed); 15 nM 25mer, 750 nM ISWI, 5 mM $MgCl_2$, 3 mM Mg-ATP (purple line, 11 condensates analysed). The line is an average of all condensates analysed and the shaded area represents the SD.* ***E)*** *Parameters obtained from fitting recovery curves in D) in double exponential. The double exponential assumes two mobile fractions of ISWI-GFP with different recovery half-times ($t_{1/2}$) and an immobile fraction, ISWI-GFP that does not recover at the end of experiment. The double exponential fitted to the experimental data slightly better than single exponential.*

It has been suggested that ATP-dependent chromatin remodelers might act as molecular stirbars, enhancing the chromatin dynamics (Larson & Narlikar, 2018). However, addition of Mg-ATP in the presence of ISWI did not change chromatin mobility as measured by FRAP, even after 60 minutes (Figure 2.22.A). Given the change in a mobility of the molecular motor upon Mg-ATP addition, we asked whether this affects biophysical properties of chromatin condensates. We

flowed in Mg-ATP or non-hydrolysable analogue into the imaging chamber with chromatin condensates containing ISWI and FITC-dextran and observed real time changes by confocal microscopy (Figure 2.22.B). There was no difference in dextran partitioning coefficient during time between the two conditions, consistent with no drastic changes in accessibility during the time course of remodeling. Further, we flowed in Mg-ATP or non-hydrolysable analog into the imaging chamber with chromatin condensates containing ISWI and ThT and observed real time changes by confocal microscopy (Figure 2.22.C). Similarly, ThT fluorescence intensity stayed the same during the reaction time in both conditions, indicating no drastic changes in viscosity of chromatin condensates during the time course of remodeling. However, dextran and ThT measurements require more careful analysis and might not be sensitive enough to detect changes upon chromatin remodeling.

To further test if biophysical properties of chromatin condensates change upon remodeling, we again made use of our dual trap controlled fusion assay. For these experiments I used 13mer instead of 25mer, low ISWI concentrations and 1 mM Mg^{2+}, to ensure enough dynamic range of measurements; because 25mer decreased the number of efficient fusions (Figure 2.16.B), and high ISWI (Figure 2.17.C, D) and high Mg^{2+} (Figure 2.16.D) concentration slowed down condensate fusion. Addition of Mg-ATP only slightly sped up fusion of ISWI-containing condensates while addition of Mg-ADP or nonhydrolyzable ATP-analogues, Mg-AMPPNP and Mg-ADPBeFx, inhibited fusion completely (Figure 2.22.D). An ATPase dead version of ISWI, which carries the mutation E257Q, can bind Mg-ATP but it cannot hydrolyse it. This mutant slowed down the fusion in the presence of Mg-ATP (Figure 2.22.E). This effect was not observed with wild type ISWI (Figure 2.22.F). We conclude that ISWI that is bound to nucleotides can harden (stiffen) condensates and that active hydrolysis is necessary to prevent ISWI from doing so.

To summarize, Mg-ATP hydrolysis is required for ISWI´s dynamics inside chromatin condensates and it prevents nucleotide-induced condensate hardening. In collaboration with Dr. Johannes Stigler and Dieter Kamp, we derived a model to describe our experimental observations. ISWI can bridge two nucleosomes via its two nucleosome-binding domains, its ATPase domain and the HSS domain (Bhardwaj et al., 2020; Yamada et al., 2011). These domains are flexibly linked (Ludwigsen et al., 2013) and undergo large conformational changes during the ATPase cycle (Harrer et al., 2018; Leonard & Narlikar, 2015). These conformational changes would allow ISWI to dynamically bind and unbind nucleosomes during the ATPase cycle. Therefore, we hypothesised that the affinity of each ISWIs site for a nucleosome is different in different nucleotide states (Figure 2.22.G) and proposed a so-called monkey bar model (Figure 2.22.H) (Rudolph et al., 2018). In the Mg-ATP bound state, both domains form strong interactions with nucleosomes. This corresponds to the experimental condition with non-hydrolysable nucleotides. Upon hydrolysis one of these interactions is significantly weakened, allowing the release of one nucleosome. Subsequent Mg-ADP release switches the strengths of the two interactions, leading to the rebinding of the first domain to a nucleosome, while releasing the second nucleosome interaction. This alternating binding and unbinding of the two domains would enable ISWI to actively move through the chromatin condensate and prevents ISWI from stably crosslinking neighbouring arrays, while interacting tightly with nucleosomes with at least one of its binding domains in any nucleotide state. To test this model, Dr. Johannes Stigler and Dieter Kamp performed molecular dynamics simulations. Simulated FRAP and simulated condensate fusion results were in qualitative agreement with experimental FRAP and fusion data (Vizjak *et al.*, unpublished). In conclusion, the monkey bar model qualitatively explains the experimental data.

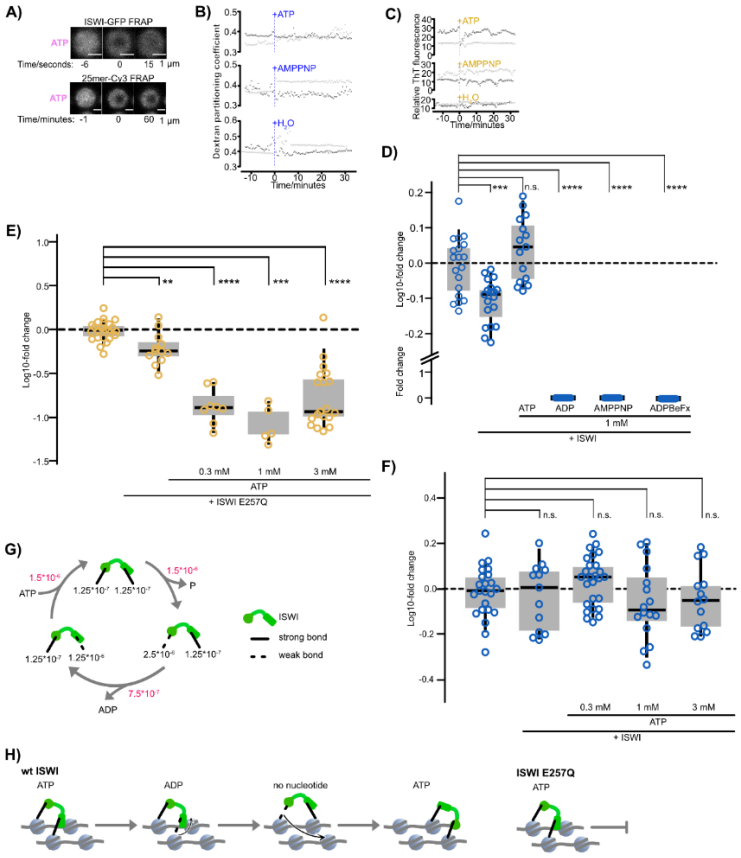

Figure 2.22. ATP hydrolysis powers mobility of ISWI and prevents ISWI-mediated hardening of condensates in the nucleotide bound state. ***A)*** *The mobility of ISWI-GFP exceeds that of chromatin in condensates. Dual FRAP of ISWI-GFP and Cy3-labeled arrays in chromatin condensates. Condensates were formed by 100 nM 25mer arrays and 1.125 µM ISWI-GFP in presence of 1 mM Mg-ATP. One of many independent replicates with similar results is shown.* ***B)*** *Partition coefficient of 20 kDa FITC-labeled dextran, timelapse after flowing 1 mM Mg-ATP, Mg-AMPPNP or buffer into an imaging chamber. Data were collected in 90 nM 13mer and 625 nM ISWI. For each condition, two independent replicates are shown (black and grey).* ***C)*** *Relative ThT fluorescence (fluorescence inside condensate normalized to the surrounding solution), timelapse after flowing 1 mM Mg-ATP, Mg-AMPPNP or buffer into an imaging chamber. Data were collected in 50 nM 25mer and 1.17 µM ISWI. For each condition, two independent replicates are shown (black and grey).* ***D)*** *Fusion velocities of condensates measured by optical trapping. ISWI in presence of non-hydrolysable nucleotides, but not of Mg-ATP, slows down fusion, indicative of hardening condensates. Log10-fold change in velocity relative to the mean of the chromatin only condition (dotted line). Data points came from at least two independent replicates per condition. Statistical significance of the velocity changes was determined by t-test. Data is visualized in boxplots showing the median ± quartiles, with whiskers indicating the 9th and 91st percentile.* ***E)*** *Addition of Mg-ATP to an ATPase dead mutant of ISWI (E257Q) slows down the condensate fusion. Log10-fold change in velocity relative to the mean of the chromatin only condition (dotted line). Data from two independent experiments. Data representation as in D).* ***F)*** *Addition of Mg-ATP to wild type ISWI does not affect condensate fusion. Log10-fold change in velocity relative to the mean of the chromatin only condition (dotted line). Data from two independent experiments. Data representation as in D).* ***G)*** *A model for the independent switching of the strengths of the two nucleosome interaction sites during ISWI´s ATPase cycle. Escape rates (black) and transition rates (red) in timestep^{-1} are indicated.* ***H)*** *ISWI possesses two nucleosome-interacting domains, which can bridge neighboring nucleosomes in dense chromatin. Via large nucleotide-induced conformational changes (not shown), the domains cycle through high and low affinity states towards nucleosomes, allowing ISWI to actively translocate through chromatin. The model predicts that ATPase compromised remodeler mutants will crosslink two nucleosomes upon ATP binding and change mechanical properties of the chromatin.*

In summary, we propose the existence of a novel functionality of ISWI's ATPase activity: Besides nucleosome sliding, ATP hydrolysis is used to break non-productive nucleosome interactions and to actively diffuse through dense nucleosomes. These two novel features are likely shared by other ATPases. Our model further predicts that ATPase compromised remodeler mutants, upon ATP binding, will crosslink two nucleosomes and lead to a stiffening (hardening) of the chromatin (Figure 2.22.H, right). It would be exciting to explore what is the impact of these mutants on chromatin dynamics *in vivo* and pathologies.

2.2.8 Discussion

In this work we have addressed the influence of chromatin intramolecular folding and phase separation on the activity of chromatin remodelers on the example of an ATPase ISWI.

We prepared 25mer nucleosome array (Ludwigsen et al., 2018) and identified conditions under which the intramolecular folding of the array predominates. We hypothesised that the folding would decrease nucleosome accessibility and that the epitopes important for ISWI activation could already be involved in internucleosome interactions. For example, it was suggested that the contacts involve N-terminal tail of H4 and the acidic patch (Luger et al., 1997; Dorigo et al., 2004; Kan, Caterino and Hayes, 2009). However, solid-state NMR studies demonstrated that the N-terminal tail of H4 remains similarly flexible in extended, folded and highly condensed self-associated nucleosome arrays (Gao et al., 2013). According to our results, the rate of nucleosome sliding catalysed by ISWI was not affected by intramolecular nucleosome array folding. Epitopes important for ISWI activation are therefore either not all involved in the intramolecular folding or their mutual interactions are relatively weak.

Under higher salt and nucleosome array concentrations, phase separation was induced and spherical condensates have formed. Total nucleosome concentration in reconstituted condensates was in the same range as in a cell nucleus and their interior was accessible to big molecules. In the nucleus, the entire chromatin network is readily accessible to inert molecules, although differences in apparent pore size do exist (Dross et al., 2009; Görisch et al., 2005). Quantitative analysis found no differences in MNase accessibility for different chromatin regions in *Drosophila* and HeLa cells, not even between euchromatin and heterochromatin (Chereji et al., 2019; Schwartz et al., 2019). We analysed dynamics of the nucleosome arrays in chromatin condensates by FRAP and measured little to no recovery. This is in a disparity with observations made in Rosen group (Gibson et al., 2019) but in an agreement with the data reported by Hansen and Hendzel groups (Strickfaden, Tolsma, et al., 2020). In contrast to this solid-like behaviour, in some buffer conditions, chromatin condensates fused to each other, like liquids. We employed dual trap optical tweezers to fuse them in a controlled manner and measured a velocity of the fusion. The fusion velocity gives valuable information about material properties. Binding of Mg^{2+} makes the condensates more solid-like and slows down the fusion. Free Mg^{2+} increases during mitosis (Maeshima et al., 2018), facilitates sister chromatid condensation and makes chromosomes more rigid (Shimamoto et al., 2017). This is particularly advantageous for chromosome segregation and transmission during anaphase, which are subject to a mechanical shearing stress. In summarry, we found that the reconstituted chromatin condensates are a suitable substrate to study challenges enzymes encountere in dense nucleosome environments in the nucleus.

Different chemical environments inside chromatin condensates might lead to an exclusion of enzymes. Nevertheless, ISWI was readily enriched in preformed chromatin condensates. It is possible that bigger remodeling complexes present in a mammalian nucleus will be excluded,

especially considering a plethora of chromatin modifications that could give rise to variable chemical environments. For example, the remodeler BRM was largely exluded from heterochromatin bands in polyten chromosomes (Tilly et al., 2021), possibly due to proteins present on a chromatin platform and not higher chromatin condensation *per se*. ISWI can fine tune mechanical properties of chromatin. Its titration led to an increase in a viscosity and a slower condensate fusion. ISWI binding might change a fiber persistence length and its mass density. Hardening of condensates might limit the access for redundant remodelers therefore distributing them equally through the nucleus.

We have developed a novel imaging-based nucleosome sliding assay and established FLIM-FRET as a sensitive technology to visualize nucleosome remodeling with spatial resolution. This kind of technologies will be beneficial in future for tracking enzymatic processes inside biomolecular condensates in real time (Lyon et al., 2020). We confirmed that ISWI indeed slides nucleosomes inside chromatin condensates. It does so with a comparable efficiency, only modestly slower than under equivalent conditions in a solution. The rate of sliding might be decreased due to different chemical environment inside biomolecular condensates (e.g., due to different salt concentration, enrichment of molecules). Our system is ideal to study an effect of the chemical environment because we measure sliding on mononucleosomes, avoiding additional complication from a high degree of nucleosome array folding in condensates. Enzymatic reactions inside biological condensates were suggested to benefit from high concentration of components (see section 1.4.3). Macromolecular crowding, an expected environment in the nucleus and biomolecular condensates, was reported to also increase a protein stability. For instance, phosphoglycerate kinase stability was reported to be higher in the nucleus and its folding rate increased, both relative to *in vitro* and to the cytoplasm (Dhar et al., 2011). However, we do not observe an enhancement of nucleosome sliding rate in chromatin condensates.

Chromatin has gel-like properties and acts as a stable platform whereas ISWI is more liquid-like in nature, at least in the presence of ATP. The ATP-hydrolysis was already recognized to increase dynamics of *Drosophila* SWI/SNF remodeleres (Tilly et al., 2021) and budding yeast remodelers (Kim et al., 2021). Further, ATPase mutants ChIP-ed more efficiently, the effect attributed to the tighter binding to chromatin targets (Gelbart et al., 2005; Tilly et al., 2021). Building on that, our approach shows that no other factors or accessory subunits are necessary, the ATPase subunit is solely responsible for a fast remodeler recycling on the chromatin. It has been suggested that remodelers sample the genome through rapid probing (Kim et al., 2021; Tilly et al., 2021). Contrary, lack of the ATPase activity led to a small increase in Snf2H and Snf2L mobility in U2OS and HEK 293T cells (Erdel et al., 2010). Our approach circumvents the complexity of living cells and we showed that the ATP-hydrolysis activity of ISWI is required for its dynamics on chromatin, nucleotide binding is not enough. Lastly, we show that ISWI that is bound to nucleotides can harden (stiffen) condensates and that active hydrolysis is necessary to prevent ISWI from doing so. Changed dynamics of biomolecular condensates can disturb biological functions (Li et al., 2020; Shi et al., 2021). We propose that besides nucleosome sliding, ISWI uses ATP hydrolysis to break non-productive interactions with nucleosomes and to actively diffuse through dense chromatin. This newly described property is likely shared by other ATPases. A half of SMARCA4 mutations in cancer lies in the ATP cleft and these mutants show slower FRAP recovery and loss of superenhancer accessibility (Hodges et al., 2018). Expression of ATPase dead BRM in *Drosophila* caused peripheral nervous system defects, homeotic transformations, and decreased viability (Elfring et al., 1998). All phenotypes were dominant negative (Elfring et al., 1998; Hodges et al., 2018) and might be caused by a change in chromatin dynamics, not exclusively by a disruption of canonical remodeler functions.

Together with Dr. Johannes Stigler and Dieter Kamp, we devised a model for a molecular mechanism to explain these observations. ISWI possesses two flexibly linked, nucleosome binding domains and it can effectively crosslink two nucleosomes on different arrays. The conformational changes the ISWI goes through during the ATPase cycle allow it to dynamically bind and dissociate from nucleosomes and actively move through the chromatin condensate. As one binding side will be always engaged with a nucleosome, we named this model a monkey-bar model. If the ATPase cycle is impaired, ISWI will stably crosslink two nucleosomes and lead to the stiffening of the chromatin.

Going forward, we would like to further test our monkey bar model *in vitro* and *in vivo*. ISWI lacking one out of the two nucleosome binding domains, for example ISWI lacking the HSS domain, should not cause stiffening of chromatin condensates. Similarly, it should be dynamic in the FRAP assay and its recovery not drastically different with different nucleotides. Contrary, ISWI E257Q is predicted to be immobile in every nucleotide state and ATP presence should not render it dynamic. In the nucleus, the ATPase ISWI works as a complex with other auxiliary subunits. It is important to test if chromatin remodeling complexes will behave the same as the ATPase in the fusion and FRAP assays. To corroborate the model further in a more quantitative manner, the rates of dissociation of different ISWI mutants from nucleosome in the presence of different nucleotides can be measured.

Total concentration of all chromatin remodelers in the nucleus was estimated to be in the 10 µM range (Erdel et al., 2010). Given this high concentration, remodelers might influence chromatin dynamics and its mechanical properties, both in inactive manner via binding and active manner via their ATPase activity. Indeed, spontaneous chromatin condensation fluctuations, likely responsible for chromatin accessibility (Hihara et al., 2012), are affected by ATP, and ATP depletion induced chromatin condensation (Audugé et al., 2019). Activity of nuclear enzymes acting on the chromatin fiber is required to generate coherent chromatin motion, as predicted by several models and corroborated by experiments (Saintillan et al., 2018). Chromatin locus mobility was enhanced by targeting INO80 (Neumann et al., 2012). Locus dynamics was diminished upon ATP depletion in both yeast and bacteria (Weber et al., 2012). To test the monkey-bar model, we want to introduce ATPase dead chromatin remodeler in the nucleus and study its influence on chromatin dynamics and its mechanical properties. Atomic force microscopy (AFM) (Liu et al., 2014), microrheology (Feric et al., 2015), nucleus deformation by micropipette aspiration (Rowat et al., 2006) or locus micromanipulation by controlled magnetic forces (Keizer et al., 2022) could be used to infer changes in a mechanoresponse in cells with ATPase compromised remodelers.

2.3 Chapter 3: Interaction of ISWI with acidic patch

2.3.1 Contributions

Laura Mataitė performed experiments under my supervision during an internship.

Dr. Sabrina Pfennig cloned H2AR71C.

I purified histones and octamers with a crosslinker and interpreted the data.

2.3.2 Background

Many chromatin binding proteins engage a nucleosome through an acidic patch (reviewed in McGinty and Tan, 2015). The acidic patch is a negatively charged surface formed by a cluster of H2A (E56, E61, E64, D90, E91 and E92) and H2B (E102 and E110) residues (Figure 2.23.). There are two acidic patches, one on each face of the nucleosome. The chromatin enzymes and factors use a common structural motif named arginine-anchor that binds to a cavity formed by residues in the acidic patch (McGinty & Tan, 2015).

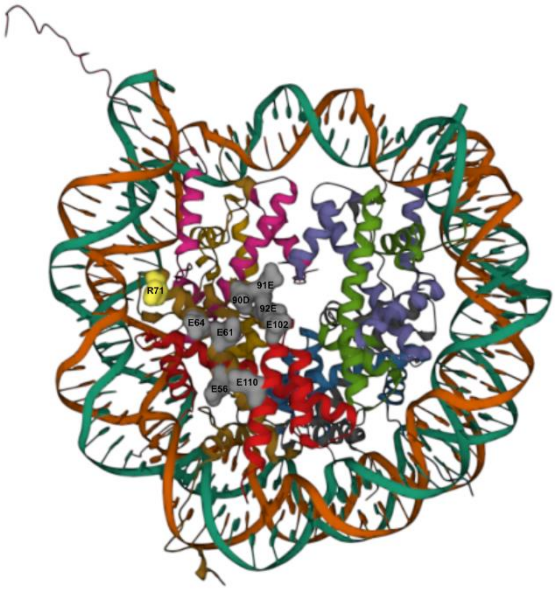

Figure 2.23. Acidic patch on a nucleosome core particle *(H2A brown and grey, H2B red and blue, H3 purple and magenta, H4 green and ochre, 146 bp DNA strands are in orange and dark blue). Residues of one acidic patch are highlighted with molecular surface representations in grey. Residues belong to H2A (E56, E61, E64, D90, E91 and E92) and H2B (E102 and E110). H2A R71 residue (highlighted with a molecular surface representation in yellow) was mutated in cysteine and covalently bound to the 4-MBP cross-linker. PDB ID: 1AOI (Luger et al., 1997). The image is created with Mol*Viewer (Berman et al., 2000; Sehnal et al., 2021).*

The acidic patch was recently proven to be necessary for a maximum nucleosome sliding activity of multiple remodeling families: ISWI, SWI/SNF, CHD and INO80 (Dann et al., 2017; Gamarra et al., 2018; Levendosky et al., 2016; Levendosky & Bowman, 2019). The activity could also be tuned by modifications of amino acids in the vicinity of the acidic patch (Dann et al., 2017). These results were consistent with prior studies that found that H2A.Z- containing nucleosomes, which possess a larger acidic patch, enhances ISWI (Goldman et al., 2010) and INO80 remodeling activity (Brahma et al., 2017).

Interesting observations were made when only one acidic patch was mutated: the rate of nucleosome sliding by ISWI strongly depended on entry-side acidic patch, while Chd1 was equally affected by entry- and exit- side mutations (Levendosky & Bowman, 2019). Chd1 still exhibited nucleosome centering activity, but instead of centering, ISWI slid these asymmetric nucleosomes towards the side possessing wild type acidic patch. Regardless of flanking DNA length, ISWI slid nucleosome all the way to the DNA end eventually destabilizing the nucleosome and producing hexasomes and free DNA (Levendosky & Bowman, 2019). Therefore, asymmetry in two acidic patches can override ISWI´s normal preference to shift nucleosome toward longer flanking DNA (Levendosky & Bowman, 2019). Similar observations were made for human ISWI enzyme, Snf2h. Nucleosomes with both acidic patches mutated or the one on the same side as a longer flanking DNA were completely immobile (Dao et al., 2020). A nucleosome with a mutated acidic patch on the opposite side as a longer flanking DNA was slid with a similar rate as a wild type nucleosome, but instead of being centered, it was end-positioned (Dao et al., 2020). In addition, experiments on dinucleosomes showed that asymmetry leads to aberrant nucleosome spacing by Snf2h (Dao et al., 2020). For ISWI, the acidic patch is likely a more important epitope than linker DNA. However, different remodelers seem to respond to the acidic patch through different mechanisms.

The recognition mechanism of the acidic patch by ISWI remodelers is mediated by the ATPase subunit (Dann et al., 2017; Gamarra et al., 2018). Crosslinking coupled with mass spectrometry was utilized in a search for a region that binds acidic patch (Dao et al., 2020; Gamarra et al., 2018). ADP-bound state and ADPBeF$_x$-bound state enriched in different crosslinks supporting different conformations in resting and translocating state; different SNF2h domains contact the acidic patch in different steps of the remodeling reaction (Gamarra et al., 2018). Namely, experiments place AutoN and NegC near the acidic patch in activated state. Data suggest that the acidic patch recognition relieves autoinhibition imposed by NegC and AutoN (Gamarra et al., 2018). Single molecule FRET traces revealed that sliding of acidic patch mutant nucleosomes proceeds with noticeably longer pauses before translocation steps and smaller translocation step size (decreased distance travelled per translocation event) (Gamarra et al., 2018). These deleterious effects were rescued by 2RA mutation of Snf2h AutoN and the NegC mutant where 32 residues were replaced with a flexible linker. In the absence of ATP, site specific crosslinking of acidic patch with Snf2h identified a conserved basic motif (KRERK) located at the boundary of the NegC-HSS linker region and HSS (Dao et al., 2020) and closely resembling known arginine anchors. Mutation of basic residues within the motif diminished the sliding activity (Dao et al., 2020). The motif is probably functionally connected to the HSS domain, as inserting a linker between these two regions decreased sliding activity (Dao et al., 2020).

However, the remodeler engages a nucleosome at SHL2 and somehow it interacts with acidic patch that is located at SHL6. Snf2h functions most optimally as a dimer (Racki et al., 2009). The most recent cryoEM structure (Armache et al., 2019) reports a disordered acidic patch distal to the active Snf2h protomer, that might allosterically inhibit the second Snf2h protomer and prevent a tug-of-war. However, high resolution structures of regulatory domains (HSS, AutoN, NegC) when ISWI is bound to a nucleosome, are missing due to their high conformational flexibility (Armache et al., 2019; Chittori et al., 2019; Yan & Wu, 2019). Regulatory domains on ISWI are conformationally flexible and interaction with the acidic patch very likely changes through the ATPase cycle.

Therefore, to obtain more complete insights in which part of ISWI is contacting acidic patch, our approach was to stabilize the conformation and reduce flexibility by site specific crosslinking. If this were possible, the crosslinked complex may be amenable to structural studies using cryoEM.

The aim of this preliminary work was to explore conditions for efficient crosslinking by varying flanking DNA length, nucleotide analogues, concentration of reactants and cofactors.

2.3.3 Crosslinking efficiency of ISWI to acidic patch is influenced by linker length and nucleotide state

We reconstituted and purified nucleosomes on 601 positioning sequence with variable flanking DNA lengths (Figure 2.24.A). The histone octamer contained H2AR71C that was labeled with 4-(*N*-maleinimido)-benzophenon (4-MBP) via a thioether bond (see Methods). Upon ultraviolet (UV) irradiation (wavelength = 250 nm), 4-MBP will bind to nearby molecules via a diradical excited state mostly followed by C-H insertion. We then incubated nucleosomes containing H2AR71C-4-MBP and different flanking DNA lengths with ATPase ISWI and exposed the mixture to the UV. The crosslinked protein, H2AR71C-4-MBP-ISWI, was detected with SDS-PAGE as an upshifted band above ISWI. Without any nucleotide present, weak crosslinking was observed for 0N20 and 0N60 nucleosomes and no crosslinking was detected for 0N0 nucleosomes (Figure 2.24.B). Faint bands were detected at ~25 kDa and they likely correspond to H2AR71C-4-MBP crosslinked to other histones. When the same experiment was repeated with higher ISWI and nucleosome concentration and with Mg-ADPBeF$_x$ present, crosslinking was more efficient. Quantification revealed that up to 15% of ISWI could be crosslinked to H2AR71C-4-MBP (Figure 2.24.C). The longer the DNA flanking the nucleosome, the crosslinking was more efficient. Further, crosslinking was also more efficient in the presence of Mg-ADPBeF$_x$ and Mg-ADPAlF$_4$ and less efficient with Mg-ADP, Mg-AMPPMP and without a nucleotide (Figure 2.24.D). A similar tendency was observed when we used three times higher amounts of the nucleotides, although crosslinking efficiency seems to be generally decreased (Figure 2.24.E). This result suggests that we are working with saturating amounts of the nucleotides. Lastly, we used substoichiometric concentration of ISWI and the trends in the dependence of crosslinking efficiency on a nucleotide present did not change (Figure 2.24.F). Interestingly, crosslinking was usually the worst with the Mg-AMPPNP present (Figure 2.24. D-F). However, in every experiment performed in the presence of nucleotides, big part of the crosslinked complex precipitates after crosslinking, as observed from SDS-PAGE of a supernatant after crosslinking followed by a centrifugation.

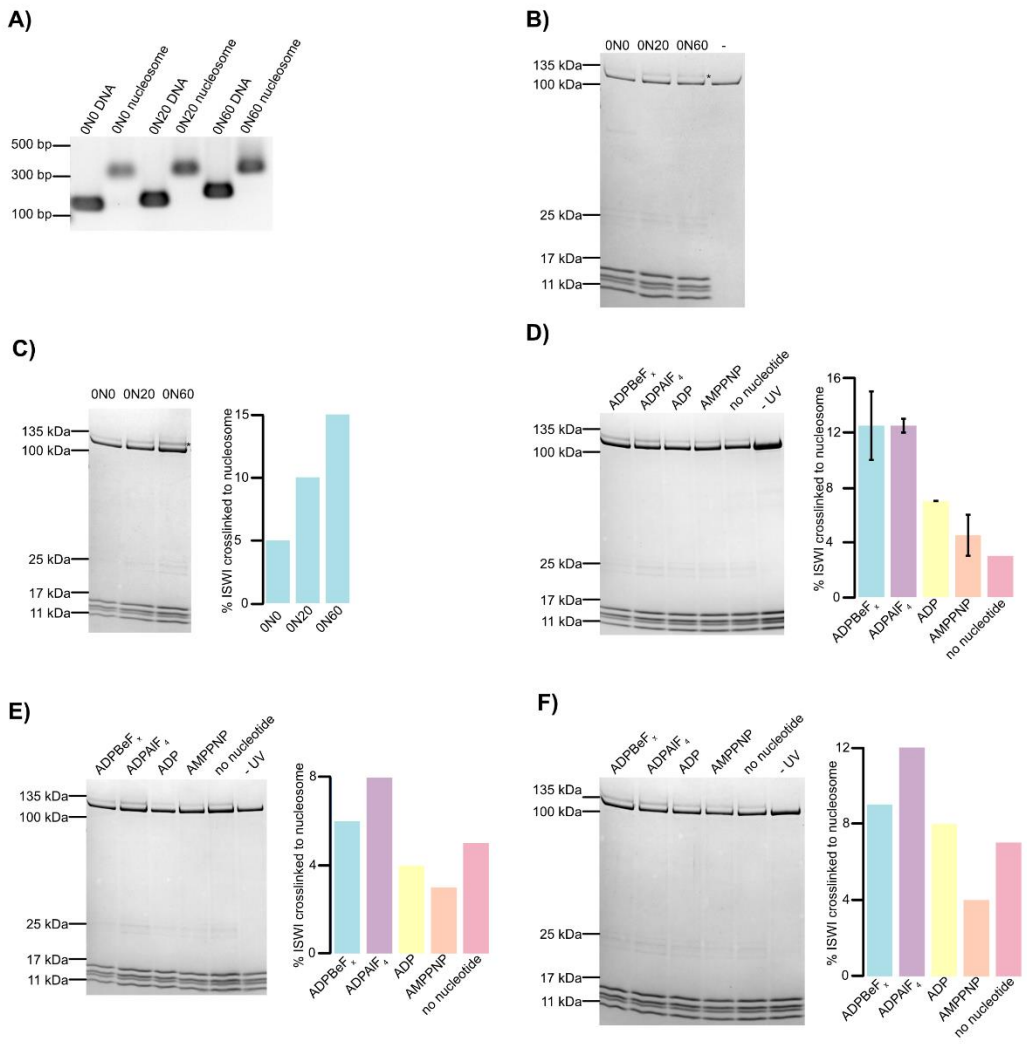

Figure 2.24. Results of a preliminary experiment suggest that the crosslinking efficiency between ISWI and H2AR71C-4-MBP is influenced by the flanking DNA length and the nucleotide state. ***A)*** *An EtBr-stained agarose gel showing mononucleosomes assembled on a 601-positioning sequence with variable flanking DNA lengths used in this study. Mononucleosomes were reconstituted and purified via glycerol gradient ultracentrifugation. Naked DNA was loaded for each corresponding mononucleosome. Nucleosome formation is confirmed by upshifted DNA band upon octamer binding.* ***B)*** *ISWI (0.3 µM) was crosslinked to the mononucleosomes (0.7 µM) with varying flanking DNA lengths and products were analyzed on SDS-PAGE. Upshifted band corresponding to H2AR71C-4-MBP-ISWI is marked with an asterisk. N=1.* ***C)*** *Left: SDS-PAGE after crosslinking ISWI (1 µM) to the mononucleosomes (1 µM) with varying flanking DNA lengths in the presence of Mg-ADPBeF$_x$ (0.5 mM). Upshifted band corresponding to H2AR71C-4-MBP-ISWI is marked with an asterisk. Right: quantification of the gel on the left. N=1.* ***D)*** *Left: SDS-PAGE after crosslinking ISWI (1 µM) to the 0N60 mononucleosomes (1 µM) in the presence of different Mg-nucleotides (0.5 mM). -UV control was done in the presence of Mg-ADPBeF$_x$ (0.5 mM). Right: quantification of the gel on the left. Bars represent an average value of two independent replicates and error bars are their minimal and maximal values.* ***E)*** *Nucleotide saturation control. Left: SDS-PAGE after crosslinking ISWI (1 µM) to the 0N60 mononucleosomes (1 µM) in the presence of different Mg-nucleotides (1.5 mM). -UV control was done in the presence of Mg-ADPBeF$_x$ (1.5 mM). Right: quantification of the gel on the left. N=1.* ***F)*** *Substoichiometric concentrations of ISWI. Left: SDS-PAGE after crosslinking ISWI (0.5 µM) to the 0N60 mononucleosomes (1 µM) in the presence of different Mg-nucleotides (0.5 mM). -UV control was done in the presence of Mg-ADPBeF$_x$ (0.5 mM). Right: quantification of the gel on the left. N=1.*

2.3.4 Discussion

To summarize, the crosslinking efficiency of ISWI with nucleosomes containing the reactive crosslinker coupled to the H2AR71C, neighboring acidic patch, was influenced by both flanking DNA length and the nucleotide state. The results should be considered preliminary, as they remain unreplicated so far. Crosslinking efficiency increased with the increased length of flanking DNA. This result is in line with literature, where nucleosomes with longer flanking DNA bind to ISWI with higher affinity (Brehm et al., 2000; Whitehouse et al., 2003), arguing stronger interaction with these substrates. Further, the crosslinking was the most efficient in the presence of Mg-ADPBeF_x and Mg-ADPAlF_4, in agreement with previously published higher binding affinity of ISWI to nucleosome with Mg-ADPBeF_x than with Mg-ADP or without a nucleotide (Racki et al., 2009). ADPBeF_x and ADPAlF_4 are analogues of catalytical transition state while AMPPNP is a non- or slowly hydrolysable ATP analogue and it should therefore mimic ATP-bound state (Bagshaw, 2001; Nielsen et al., 2009). Interestingly, Mg-AMPPNP did not phenocopy Mg-ADPBeF_x and Mg-ADPAlF_4 in our experiments. This might indicate that the interaction of ISWI and acidic patch is the strongest and should therefore play the most important role during the catalytical step. It further implies that the enzyme and/or acidic patch undergo conformational change between ATP binding and hydrolysis and back between ATP hydrolysis and phosphate release. However, interpretation is complicated by the report that Mg-AMPPNP supports low levels of remodeling (Racki et al., 2009).

Going forward, it is going to be important to obtain more efficient crosslinking. Degree of labeling H2AR71C with 4-MBP moiety should be determined for example by mass spectrometry and optimized as needed. It should be ascertained that the nucleosomes carrying H2AR71C-4-MBP are still properly recognized by remodeler by performing ATPase and nucleosome sliding assays. Although 4-MBP on H2AR71 position should not disrupt the acidic patch itself, it might be needed to use a different moiety to minimize disturbance of the interface, for example the one that carries positive charge. Further, other crosslinkers and alternative positions for placing them should be tested for efficiency of crosslinking. Acidic patch residues were already tested for crosslinking efficiency with Snf2h (Dao et al., 2020).

Although acidic patch has been shown to be important for all remodeler families, its recognition and regulation may not share the common mechanism across the families. As discussed above, Chd1 and ISWI have different requirements for the acidic patch (Levendosky & Bowman, 2019), and INO80 lacks AutoN and NegC-like motifs (Udugama et al., 2011), that were recently suggested to be important for mediating acidic patch interaction for Snf2h (Gamarra et al., 2018). Therefore, our study should be extended to other remodeler families. Acidic patch was suggested to mediate communication between two remodeler molecules bound on the two sides of the same nucleosome (Armache et al., 2019). Several cancer-associated histone mutations map to the nucleosome acidic patch and depending on their location, they inhibited or activated Snf2h-mediated nucleosome sliding (Dao et al., 2020). As humans have more gene copies for every histone, it is highly probable that the heterotypic nucleosomes will form and influence not only kinetics of nucleosome sliding reaction, but also its outcomes, namely nucleosome positioning and spacing (Dao et al., 2020). It remains to be seen how pathological acidic patch mutants influence these important properties. Our structural study will inform future studies of nucleosome spacing and positioning *in vivo* in remodeler and acidic patch mutants.

3. Material and Methods

3.1 Materials

3.1.1 List of *Schizosaccharomyces pombe* strains

Table 3.1. Schizosaccharomyces pombe strains used and/or created in this thesis.

BenchlingID	LabBookID	Name	Genotype	Source
spFMP001	spFMP001	mating type locus reporter strain	h90 mat3::ura4+ ura4-DS/E leu1-32 ade6-M210	Dr. Mario Halić (176)
spFMP002	spFMP002	Telomeric reporter strain	h90 tel(1L)::his3 tel(2L)::ura4 otr1R::ade6	Dr. Mario Halić (588) (Nimmo et al., 1998)
spFMP003	spFMP003	972h-	h- wild type	Dr. Philipp Korber
spFMP004	spFMP004	pericentromeric reporter strain	h+ otrR(SphI)::ura4 ura4 DS/E leu1-32 ade6-M210	Dr. Mario Halić (63) (Allshire et al., 1995)
spFMP005	spFMP005		h90 mat3::ura4+ ura4-DS/E leu1-32 ade6-M210 pFMP504 [nmt1 Hrp3K406CDFLAG]	This study (transformation of spFMP001)
spFMP006	spFMP006		h+ otrR(SphI)::ura4 ura4 DS/E leu1-32 ade6-M210 pFMP501 [nmt1 Hrp3CDFLAG]	This study (transformation of spFMP004)
spFMP007	spFMP007		h+ otrR(SphI)::ura4 ura4 DS/E leu1-32 ade6-M210 pFMP502 [nmt1 CDFLAG]	This study (transformation of spFMP004)
spFMP008	spFMP008		h+ otrR(SphI)::ura4 ura4 DS/E leu1-32 ade6-M210 pFMP503 [nmt1 Hrp3]	This study (transformation of spFMP004)
spFMP009	spFMP009		h+ otrR(SphI)::ura4 ura4 DS/E leu1-32 ade6-M210 pFMP488 [nmt1 ∅]	This study (transformation of spFMP004)
spFMP010	spFMP010		h+ otrR(SphI)::ura4 ura4 DS/E leu1-32 ade6-M210 pFMP505 [nmt1 Hrp3K406A]	This study (transformation of spFMP004)
spFMP011	spFMP011		h90 mat3::ura4+ ura4-DS/E leu1-32 ade6-M210 pFMP501 [nmt1 Hrp3CDFLAG]	This study (transformation of spFMP001)
spFMP012	spFMP012		h+ otrR(SphI)::ura4 ura4 DS/E leu1-32 ade6-M210 pFMP504 [nmt1 Hrp3K406ACDFLAG]	This study (transformation of spFMP004)
spFMP013	spFMP013		h90 mat3::ura4+ ura4-DS/E leu1-32 ade6-M210 pFMP488 [nmt1 ∅]	This study (transformation of spFMP001)
spFMP014	spFMP014		h90 mat3::ura4+ ura4-DS/E leu1-32 ade6-M210 pFMP502 [nmt1 CDFLAG]	This study (transformation of spFMP001)

spFMP015	spFMP015	h90 mat3::ura4+ ura4-DS/E leu1-32 ade6-M210 pFMP791 [nmt1 Fft3CDFLAG]	This study (transformation of spFMP001)
spFMP016	spFMP016	h90 mat3::ura4+ ura4-DS/E leu1-32 ade6-M210 pFMP792 [nmt1 Fft3]	This study (transformation of spFMP001)
spFMP017	spFMP017	h90 mat3::ura4+ ura4-DS/E leu1-32 ade6-M210 pFMP790 [nmt1 FLAGCDFft3]	This study (transformation of spFMP001)
spFMP018	spFMP018	h+ otrR(SphI)::ura4 ura4 DS/E leu1-32 ade6-M210 pFMP790 [nmt1 FLAGCDFft3]	This study (transformation of spFMP004)
spFMP019	spFMP019	h+ otrR(SphI)::ura4 ura4 DS/E leu1-32 ade6-M210 pFMP792 [nmt1 Fft3]	This study (transformation of spFMP004)
spFMP052	spFMP020	h+ otrR(SphI)::ura4 ura4 DS/E leu1-32 ade6-M210 pFMP791 [nmt1 Fft3CDFLAG]	This study (transformation of spFMP004)
spFMP053	spFMP022	h90 mat3::ura4+ ura4-DS/E leu1-32 ade6-M210 pFMP503 [nmt1 Hrp3]	This study (transformation of spFMP001)
spFMP055	spFMP043	h+ otrR(SphI)::ura4 ura4 DS/E leu1-32 ade6-M210 pFMP795 [nmt41 Hrp3]	This study (transformation of spFMP004)
spFMP056	spFMP044	h+ otrR(SphI)::ura4 ura4 DS/E leu1-32 ade6-M210 pFMP796 [nmt81 Hrp3]	This study (transformation of spFMP004)
spFMP057	spFMP045	h+ otrR(SphI)::ura4 ura4 DS/E leu1-32 ade6-M210 pFMP793 [nmt1 Hrp3FLAG]	This study (transformation of spFMP004)

3.1.2 List of *Escherichia coli* strains

Table 3.2. List of *Escherichia coli* strains used in this study.

Strain name	Use	Genotype	Inherent antibiotic resistance	Manufacturer Catalogue number
DH5α	Cloning	*fhuA2 Δ(argF-lacZ)U169 phoA glnV44 Φ80 Δ(lacZ)M15 gyrA96 recA1 relA1 endA1 thi-1 hsdR17*	None	NEB C2987
BL21DE3 Gold	Protein expression	*E. coli* B F$^-$ *ompT hsdS*(r_B^- m_B^-) *dcm*$^+$ Tet^r *gal* λ(DE3) *endA* Hte	Tetracycline	Agilent (Stratagene) 230132
BL21 Star™ (DE3) pLysS	Protein expression	F$^-$ *ompT hsdSB* (r_B^-, m_B^-) *galdcmrne*131 (DE3) pLysS (Cam^R)	Chloramphenicol	Invitrogen C602003
BL21-Codon-Plus (DE3)-RIL	Protein expression	*E. coli* B F$^-$ *ompT hsdS*(r_B^- m_B^-) *dcm*$^+$ Tet^r *gal* λ(DE3) *endA* Hte [*argU ileY leuW* Cam^r]	Chloramphenicol, Tetracycline	Agilent 230245

Rosetta™ (DE3)	2	Protein expression	F⁻ *omp*T *hsdSB*(r_B^- m_B^-) *gal dcm* (DE3) pRARE2 (Cam^R)	Chloramphenicol	Merck 71400-3

3.1.3 Oligonucleotide list

Table 3.3. List of PCR primers used for cloning.

Name	Sequence (5'->3')	Use
oFMP714	aggttctggatcaggcagtgactataaggaccacgacgga	3xFLAG amplification from pAc-sgRNA-Cas9 with 5´ $(GS)_3$ overlap for Gibson assembly of pFM502, fwd
oFMP715	cggggatcctgcggccgcattacttatcgtcatcgtctttgtaatc	3xFLAG amplification from pAc-sgRNA-Cas9 with pJR overlap for Gibson assembly of pFM502, rev
oFMP716	ttgttaaattggcctcgaggtctggtagcggttcaggtgagacagacgcgga	Chp1CD amplification from genomic DNA with 5´ $(GS)_{2.5}$ and pJR overlap for Gibson assembly of pFM502, fwd
oFMP717	ctgcctgatccagaacctaacttttccgtttttccatttttaag	Chp1CD amplification from genomic DNA with added $(GS)_3$ for Gibson assembly of pFM502, rev
oFMP748	cctcgaggccaatttaacaaag	To open pFMP502 by inverse PCR for Gibson assembly of pFMP501, rev
oFMP749	ggatcaggttctggctctggtagcggttcaggtg	To open pFMP502 by inverse PCR with (GS)2.5 overlap for Gibson assembly of pFMP501, fwd
oFMP753	agagccagaacctgatcccttcatcttttcatacatgctgatc	Hrp3 amplification from genomic DNA with added $(GS)_{2.5}$ and pJR overlap for Gibson assembly of pFMP501, rev
oFMP755	agagccagaacctgatccatcatcgtcatcttcagcctcc	Fft3 amplification from genomic DNA with added $(GS)_{2.5}$ and pJR overlap for Gibson assembly of pFMP791, rev
oFMP777	ttgttaaattggcctcgaggatggatggaaaaagaaaaatagagcatacc	Fft3 amplification from genomic DNA with added pJR overlap for Gibson assembly of pFMP791, fwd
oFMP784	ttgttaaattggcctcgaggatgagtacaagtgctatagcacttgct	Hrp3 amplification from genomic DNA with added pJR overlap for Gibson assembly of pFMP501, fwd
oFMP797	taatgcggccgcaggatc	Deletes C-terminal cassette (CDFLAG) by inverse PCR from pFMP501 and after religation pFMP503 forms
oFMP798	tgttaaattggcctcgaggatggactataaggaccacgacggag	3xFLAG amplification from pFMP501 with added start codon and pJR overlap for Gibson assembly of pFM790, fwd
oFMP799	acctgaaccgctaccagacttatcgtcatcgtctttgtaatcaatatc	3xFLAG amplification from pFMP501 with added $(SG)_3$ overlap for Gibson assembly of pFM790, rev
oFMP800	ctctatttttctttttccatcggagccgctaccactgcctgatccagaacctaacttttttc	CD$(GS)_{2.5}$ amplification from pFMP502 with added $(SG)_{2.5}$ and Fft3 overlap for Gibson assembly of pFM790, rev

oFMP802	tcgtggtccttatagtccatcctcgaggccaatttaacaaag	Amplification of pFMP792 by inverse PCR with added start codon and FLAG overlap for Gibson assembly of pFMP790, rev
oFMP803	cagtggtagcggctccgatggaaaaagaaaaatagagcatac	Amplification of pFMP792 with added $(SG)_{2.5}$ overlap for Gibson assembly of pFMP790, fwd
oFMP804	cttcatcttttcatacatgctgatcaag	Deletes C-terminal cassette (CDFLAG) by inverse PCR from pFMP501 and after religation pFMP503 forms
oFMP812	ggagccgctaccactg	pFMP790 correction, anneals at linker region
oFMP813	atggatggaaaaagaaaaatagagcatac	pFMP790 correction, anneals at Fft3, adds 5´ ATG
oFMP822	cgatgaaatgggtctcggtgcgacagtccaaactgtggc	Amplification of pFMP501, pFMP503 and pFMP793 by inverse PCR with added K406A mutation, after religation pFMP504, pFMP505 and pFMP794 form
oFMP823	gccacagtttggactgtcgcaccgagacccatttcatcg	Amplification of pFMP501, pFMP503 and pFMP793 by inverse PCR with added K406A mutation, after religation pFMP504, pFMP505 and pFMP794 form
oFMP1028	ggttctggatcaggcagtgactataag	Anneals to $(GS)_3$3xFLAG, inverse PCR of pFMP501, religation forms pFMP793
oFMP1029	ccttcatcttttcatacatgctgatc	Anneals to Hrp3, inverse PCR of pFMP501, religation forms pFMP793
oFMP1080	tcgtcatctttataatccatcgagtcgacctcgaggt	Amplification of pFMP488 by inverse PCR, adds 5´ FLAG overlap for a Gibson assembly of pFMP790
oFMP1090	ctcgaggtcgacatgggttctggatcaggcagtgactataag	Amplification of 3xFLAG from pAc-sgRNA-Cas9 with added start codon and pJR overlap for a Gibson assembly of pFMP790

Table 3.4. List of primers used for Sanger sequencing.

Name	Sequence (5'->3')	Use
oFMP705	tttcaatctcattctcactttctga	Anneals to *nmt* promoter
oFMP706	gcttgaatgggcttccatag	Anneals to pJR vector sequence after multiple cloning site (MCS)
oFMP707	aaaggaagaggaatcctggc	Anneals to *nmt* promoter
oFMP708	taatatgcagcttgaatgggc	Anneals to *nmt* terminator
oFMP787	actcctcttggaccacgt	Anneals to *fft3* sequence (binds at base position 898)
oFMP788	ctactagtaaggctgatcg	Anneals to *fft3* sequence (binds at base position 1493)
oFMP793	aacgtgcacgtcgtaaaatg	Anneal to *hrp3* sequence
oFMP794	tttatgatgctatgccaacg	
oFMP795	caatgatacaccctccgaag	
oFMP801	atttctatgatcagaggatc	
oFMP816	gagcctgaacattcga	Anneal to *hrp1* sequence

oFMP817	agcggatgcacaagac
oFMP818	tcgtaccgctttccac
oFMP819	gtcagctatccttactc
oFMP820	ggtgcttctaatatgttcaag
oFMP821	actcacctgcatcgtg

Table 3.5. List of primers used for RT-qPCR in this thesis.

Name	Sequence (5'->3')	Transcript
oFMP972	gattctcatggagcgtggtt	act1
oFMP973	cgctcgtttccgatagtgat	
oFMP974	cagcaatatcgtactcctgaa	ura4
oFMP975	atgctgagaaagtctttgctg	
oFMP976	tgaatcgtgtcactcaaccc	cen-dh
oFMP977	tgctctgacttggcttgtctt	
oFMP978	ccctaacttggaaaggcaca	
oFMP979	cgagacccctaatgctttt	mat3M
oFMP980	ccagggtacattttctgatgttg	
oFMP981	atggtcgtcgcttcagaaattgc	tlh1/thl2
oFMP982	ctccttggaagaattgcaagcctc	
oFMP985	ccaagcctaccaactacga	tdh1
oFMP986	agagacgagcttgacgaa	
oFMP987	aacgtcaagttcgaggaagtcc	adh1
oFMP988	agagcgtgtaaatcggtgtgg	
oFMP983	acttttggccgaaggaggag	hrp3
oFMP984	acgcgatccgccagaatatc	

Table 3.6. List of primers used and/or designed for mononucleosome DNA synthesis by large scale PCR in this thesis.

Fragment	Primer 1 [sequence (5'->3')]	Primer 2 [sequence (5'->3')]
Cy3- 0/60	oFMP838 [Cy3-CTGGA-GAATCCCGGTGCCG]	oFMP839 [GCTTGCATGCCTGCAGGTCG]
0/60	oFMP864 [CTGGAGAATCCCGGTGCCG]	oFMP839 [GCTTGCATGCCTGCAGGTCG]
0/0	oFMP864 [CTGGAGAATCCCGGTGCCG]	oFMP886 [ACAGGATGTATATATCTGACAC-GTGCCTGG]

0/40	oFMP864 [CTGGAGAATCCCGGTGCCG]	oFMP887 [ACTCTAGAGATATCCCGAGAGGTCGC]
0/20	oFMP864 [CTGGAGAATCCCGGTGCCG]	oFMP889 [GGTCGCTGTTCAATACATGCACAGG]
20/20	oFMP888 [GGACCCTATACGCGGCCG]	oFMP889 [GGTCGCTGTTCAATACATGCACAGG]
[atto647N]-0/60-EcoRI	oFMP1261 [atto647N-CTGGA-GAATCCCGGTGCCG]	oFMP1260 [TAAGCAGAATTCGCTTGCATGCCTG-CAGGTCG]
EcoRI-0/60-[atto647N]	oFMP1262 [TAAGCAGAATTCCTGGA-GAATCCCGGTGCCG]	oFMP1264 [atto647N-GCTTGCATGCCTGCAGGTCG]
EcoRI-20/60[-atto647N]	oFMP1263 [TAAGCAGAATTCG-GACCCTATACGCGGCCG]	oFMP1264 [atto647N-GCTTGCATGCCTGCAGGTCG]
0/60-EcoRI	oFMP864 [CTGGAGAATCCCGGTGCCG]	oFMP1261 [atto647N-CTGGAGAATCCCGGTGCCG]

3.1.4 Plasmid list

Table 3.7. List of plasmids used and/or created in this thesis. Vector maps of all plasmids created as part of this thesis are available in the Appendix A.

Plasmid	Common name	Description	Source
pFMP488	pJR1-3xL	(Moreno et al., 2000)	Dr. Mario Halić
pFMP489	pJR41-3xL	(Moreno et al., 2000)	Dr. Mario Halić
pFMP490	pJR81-3xL	(Moreno et al., 2000)	Dr. Mario Halić
pFMP501	pJR1-3xL Hrp3CDFLAG	Hrp3 (*S. pombe*) C-terminally fused with Chp1 (*S. pombe*) chromodomain (residues 15-76) and 3xFLAG under nmt1 promoter	This study
pFMP502	pJR1-3xL CDFLAG	Chp1 (*S. pombe*) chromodomain (residues 15-76) 3xFLAG on its C-terminus under nmt1 promoter	This study
pFMP503	pJR1-3xL Hrp3	Hrp3 (*S. pombe*) under nmt1 promoter	This study
pFMP504	pJR1-3xL Hrp3K406ACDFLAG	Hrp3 (*S. pombe*) K406A (ATPase dead mutant) C-terminally fused with Chp1 (*S. pombe*) chromodomain (residues 15-76) and 3xFLAG under nmt1 promoter	This study
pFMP505	pJR1-3xL Hrp3K406A	Hrp3 (*S. pombe*) K406A (ATPase dead mutant) under nmt1 promoter	This study
pFMP790	pJR1-3xL FLAGCDFft3	Fft3 (*S. pombe*) N-terminally fused with Chp1 (*S. pombe*) chromodomain (residues 15-76) and 3xFLAG under nmt1 promoter	This study

pFMP791	pJR1-3xL Fft3CDFLAG	Fft3 (*S. pombe*) C-terminally fused with Chp1 (*S. pombe*) chromodomain (residues 15-76) and 3xFLAG under nmt1 promoter	This study
pFMP792	pJR1-3xL Fft3	Fft3 (*S. pombe*) under nmt1 promoter	This study
pFMP793	pJR1-3xL Hrp3FLAG	Hrp3 (*S. pombe*) C-terminally fused with 3xFLAG under nmt1 promoter	This study
pFMP794	pJR1-3xL Hrp3K406FLAG	Hrp3 (*S. pombe*) K406A (ATPase dead mutant) C-terminally fused with 3xFLAG under nmt1 promoter	This study
pFMP795	pJR41-3xL Hrp3	Hrp3 (*S. pombe*) under nmt41 promoter	This study
pFMP796	pJR81-3xL Hrp3	Hrp3 (*S. pombe*) under nmt81 promoter	This study
pFMP210	ISWI expression	6xHis-TEV-*dm*ISWI in pProExHT	
pFMP244	ISWIGFP expression	6xHis-TEV-*dm*ISWI-3C-STREP- sfGFP in pProExHT	Dr. Ameli Lentz
pFMP248	GFP expression	GST-sfGFP	Dr. Zeynep Ökten
pFMP110	ISWIE257Q expression	6xHis-TEV-*dm*ISWIE257Q in pProEX-Htb	
pFMP128	H2A expression	Codon optimized *dm*H2A in pET15b	
pFMP129	H2B expression	Codon optimized *dm*H2B in pET15b	
pFMP186	H3 expression	*dm*H3 in pET3c	
pFMP187	H4 expression	*dm*H4 in pET3c	
pFMP269	H2AK119C expression	*dm*H2AK119C in pET15b	Dr. Johanna Ludwigsen
pFMP270	H3C111A expression	*dm*H3C111A in pET3c	Dr. Johanna Ludwigsen
pFMP268	H4T1C expression	*dm*H4T1C in pET3c	Dr. Johanna Ludwigsen
pFMP213	Mononucleosome DNA	1x197 bp 601 in pUC18, Amplification of mononucleosome DNA	Dr. Nicola Hepp
pFMP232	25mer	25 consecutive copies of 197 bp with modified 601 sequence in pUC18	Dr. Nicola Hepp
pFMP233	25mer	25 consecutive copies of 197 bp with modified 601 sequence in pUC18	Dr. Nicola Hepp
pFMP226	13mer	13 consecutive copies of 197 bp with modified 601 sequence in pUC57	Dr. Nicola Hepp

3.1.5 Enzymes and kits

Table 3.8. List of enzymes used for experiments presented in this thesis (alphabetically).

Enzyme	Manufacturer (catalogue number)
Apyrase	New England BioLabs (M0398S)
AseI	New England BioLabs (R0526M)
BamHI-HF	New England BioLabs (R3136S)
Benzonase	Merck Millipore (1016540001 100000)
BsiWI-HF	New England BioLabs (R3553S)
DpnI	New England BioLabs (R0176S)
EcoRI-HF	New England BioLabs (R3101M)

HincII	New England BioLabs (R0103L)
KpnI	New England BioLabs (R3142L)
MNase	Sigma (N5386-500UN)
NotI-HF	New England BioLabs (R0189S, R3189S)
Phusion High-Fidelity DNA Polymerase	New England BioLabs (M0530S, M0530L)
Proteinase K	Bioline (BIO-37039)
Pyruvate kinase/lactate dehydrogenase	Sigma (P0294)
RNase A	Sigma (R4875)
SalI	New England BioLabs (R0138S)
SpeI	New England BioLabs (R0133L)
T5 exonuclease	New England BioLabs (M0363S)
Taq ligase	New England BioLabs (M0208S)
XhoI	New England BioLabs (R0146S)
Zymolyase 100T	Gerbu Biotechnik (07665)

Table 3.9. List of kits used for experiments presented in this thesis (alphabetically):

Kit	Manufacturer (catalogue number)
Freeze 'N-Squeeze DNA Gel Extraction	Biorad (7326166)
NEBNext Ultra II DNA Library Prep kit for Illumina	New England BioLabs (E7645L)
NucleoSpin Gel and PCR Cleanup	Macherey-Nagel (740609.250)
NucleoSpin Plasmid EasyPure	Macherey-Nagel (740727.250)
Plasmid DNA purification kit Nucleobond® PC 10000	Macherey-Nagel (740593)
Superscript III kit	Thermo Fisher (18080093)
Fast SYBR Green Master Mix	Life technologies (4385612)
TURBO DNA-free Treatment and Removal kit	Ambion (M1907)
Qubit dsDNA HS Assay Kit	Thermo Fisher Scientific (Q32854)

3.1.6 Antibodies

Table 3.10. Antibodies used for experiments presented in this thesis.

Antibody	Dilution used	Type	Manufacturer (catalogue number)
α FLAG (mouse IgG M2)	1:1000	monoclonal	Sigma (F3165)
α Mouse (goat IgG)	1:10000	IRDye 680	Li-Cor (926-68070)

3.1.7 Chemicals and consumables

Table 3.11. The list of chemicals used for experiments presented in this thesis (alphabetically).

Chemical	Manufacturer (catalogue number)
1 kb DNA Ladder	New England BioLabs (N3232S)

5-fluoroorotic acid monohydrate (5-FOA)	Biozol (F59500)
100 bp DNA Ladder	New England BioLabs (N3231S)
Acrylamide/bisacrylamide solution	Rotiphorese Gel 30 (37.5:1) Carl Roth GmbH & Co
Adenine	Sigma (A8626)
Agarose universal	Bio&SELL (BS20.46.500)
Agencourt AMPure XP beads	Beckmann Coulter (A63882)
Ampicillin	Roth (K029.2)
AMP-PNP	Sigma (A2647)
Aprotinin	Genaxxon (M6361.0100)
ATP	Sigma (A2754)
Atto-565 maleimide	Atto-tec (AD 565-41)
Bactoagar	BD Biosciences (214010)
Bromophenol Blue	Sigma (B0126-25G)
BSA	New England BioLabs (B9000)
Calcium Chloride	Sigma (C3306)
Chloroform	VWR Chemicals (22711.324)
cOmplete™, EDTA-free protease inhibitor tablets	Roche (04693132001)
DMSO	Roth (A994.2)
dNTPs	New England BioLabs (N0447S)
EMM-glucose	Formedium (PMD0405)
EDTA	Pan Reac Appli Chem (131669.1210)
EGTA	Roth (3054.3)
EtOH 96% - low quality	CLN GmbH (N-1196.9025)
EtOH 100% - high quality	Sigma (32205-2.5L-M)
FITC-dextrans	Sigma (FD4, FD10S, FD20S, FD40S, FD70S, FD250S, FD500S, FD2000S)
Formaldehyde	Sigma (47608)
Gel Loading Dye, Purple (6X)	New England BioLabs (B7024S)
Gel Loading Dye, Purple (6X), no SDS	New England Biolabs (B7025S)
Glucose monohydrat	VWR (1.08342.1000)
Glycerol	VWR (1.04092.2500)
Glycogen	Sigma (10901393001)
HEPES	VWR Chemicals (1.10110.1000)
Imidazole	Carl Roth GmbH & Co
IPTG	Carl Roth GmbH & Co
Isopropanol (propan-2-ol)	Sigma (34863-2.5L-M)
Histidine	VWR (1.04351.0100)
K_2HPO_4*$3H_2O$	VWR (1.05099.1000)
KCl	Sigma (P9541)

KH_2PO_4	VWR (1.04873.1000)
Leucine	Sigma (L8000)
Leupeptin	Genaxxon (M6100.0100)
Low-melt agarose	Biozym (850070)
Lysine hydrochloride	Sigma (L5626)
Methylenblau	Roth (A514.1)
$MgCl_2$	VWR (25108.295)
Milk Powder (Bio Magermilchpulver)	ReformKontor (3030)
NaCl	Serva (30183.01)
NaOH	Neolab (LC-4994.2)
Orange G	Sigma (O-1625)
PEG 8000	Promega (V3011)
Pepstatin	Genaxxon (M6359.0100)
Phenol:Chloroform:Isoamyl alcohol (25:24:1)	Roth (A156.1)
PMSF (Phenylmethanesulfonylfluoride)	Sigma (P7626)
Potassium acetate	VWR (1.04820.1000)
Sodium deoxycholate	Sigma (D6750)
Sodium dodecyl sulfate (SDS)	Serva Electrophoresis (20765.03)
SP-supplements	Formedium (PSU0210)
TBE, 5x liquid concentrate	VWR (J885-4L)
TCA (Trichloroacetic acid)	Sigma (T0699)
Thioflavin T (ThT))	Sigma (T3516)
Triple Color Protein Standard II	Serva (39257.01)
Triple Color Protein Standard III	Serva (39258.01)
Tris ultrapure	Diagonal (A1086.1000)
TRIsure	Bioline/Meridian bioscience (BIO-38033)
Triton X-100	Sigma (T8787)
Tween-20	Sigma (P9416)
Uracil	Sigma (U0750)
Urea	Life technologies (15505027)
UTP	Sigma (U6750)
Yeast extract	BD Biosciences (212750)
β-Mercaptoethanol	Sigma (M6250)

Table 3.12. The list of consumables used for experiments presented in this thesis (alphabetically):

Consumable	Manufacturer (catalogue number)
384 well plate	Greiner (781101)

384 Well Lightcycler Plate, white	Sarstedt (72.1985.202)
Amicon Ultra-4 centrifugal filter units, 10 and 30 kDa MWCO	Merck Millipore
Bottle Top Filter 500 ml	VWR (734-5067)
Coverslips	Paul Marienfeld GmbH (0107242)
Dialysis membranes MWCO: 4000-6000	Roth (E658.1)
Double-sided tape	Willy Heckmann (420.014)
Glass slides	Carl Roth (H879.1)
Haemocytometer	Fischer Scientific (11314052)
HisTrap HP column, 5 mL	GE Healthcare (Cytiva)
HiTrap SP column, 5 mL	GE Healthcare (Cytiva)
HiTrap Q column, 5 mL	GE Healthcare (Cytiva)
Magnetic Rack	GE Healthcare (28948964)
Mono S 5/50 GL column, 1 mL	GE Healthcare (Cytiva)
Nitrocellulose filter	Roth (A014.1)
SDS-PAGE gel, NuPAGE Bis-Tris Protein Gel, 10%, 12%, and 8-16%	Serva (0043266.01, 0043280.01, 0043263.01)
Slide-A-Lyzer Mini7K, 0,1 ml	Life technologies (69562)
Spectra/Por dialysis tubing, 3500, 7000, 6000–8000 and 12000-14000 Da MWCO	Spectrum
Superdex 200 HiLoad 16/60 column	GE Healthcare (Cytiva)
µ-Slide VI$^{0.5}$ Glass Bottom	Ibidi (80607)
qPCR foil	Sarstedt (95.1994)
Zirconia beads 0.5mm diameter	Biospec (11079105z)

3.1.8 Buffers and solutions

Table 3.13. The list of buffers and solutions used for experiments presented in this thesis (alphabetically):

Description	Components
6xOrange G gel loading buffer	0.1% Orange G, 60% (v/v) glycerol in TE buffer
1xTBE buffer	89 mM Tris-HCl, 89 mM boric acid, 0.2 mM EDTA; pH 8.3
1.33X Gibson Reagent Mix	117 mM Tris-HCl pH 7.5, 6.5% (v/v) polyethylene glycol (PEG) 8000, 13 mM $MgCl_2$, 13 mM DTT, 0.26 mM dNTPs, 1.3 mM nicotinamide adenine dinucleotide (NAD), 0.005 U/µL T5 exonuclease, 0.033 U/µL Phusion polymerase, and 5.3 U/µL Taq ligase
ATP regeneration system	6 mM phosphoenolpyruvate, 15.5 U/mL pyruvate kinase/lactate dehydrogenase, 1 mM DTT
CES buffer	50 mM citrate phosphate buffer pH 5.6, 40 mM EDTA pH 8.0 1.2 M sorbitol, 10 mM β-mercaptoethanol
EX50	10 mM Hepes–KOH pH 7.6, 50 mM KCl, 1.5 mM $MgCl_2$, 0.5 mM EGTA
GF buffer	50 mM Hepes KOH pH 7.6, 0.2 mM EDTA pH 8.0, 200 mM KOAc, 10 mM DTT

High salt buffer	2 M NaCl, 10 mM Tris-HCl pH 7.6, 1 mM EDTA pH 8.0, 1 mM DTT
HisA	50 mM Tris-HCl pH 7.4, 300 mM NaCl, 0.5 mM DTT supplemented with 20 mM imidazole pH 7.4, 1 tablet complete-EDTA free protease inhibitors (Roche), as well as leupeptin (1 mg/L), pepstatin (0.7 mg/L) and aprotinin (1 mg/L)
HisB	50 mM Tris-HCl pH 7.4, 300 mM NaCl, 400 mM imidazole
HU buffer	200 mM phosphate buffer pH 6.8, 8 M urea, 5% w/v SDS, 1 mM EDTA pH 8.0, 100 mM DTT, bromophenol blue
Low salt buffer	50 mM NaCl, 10 mM Tris-HCl pH 7.6, 1 mM EDTA pH 8.0, 1 mM DTT
MND buffer	1.2 M sorbitol, 10 mM $CaCl_2$, 100 mM NaCl, 1 mM EDTA pH 8.0, 50 mM Tris–HCl pH 8.0, 0.075% NP-40, 14 mM β-mercaptoethanol, 5 mM spermidine, 1 mM PMS
Mono2000	2 M KCl, 20 mM Tris-HCl pH 7.7, 0.1 mM EDTA pH 8.0, 1 mM DTT
Mono0	20 mM Tris-HCl pH 7.7, 0.1 mM EDTA pH 8.0, 1 mM DTT
MonoS A	15 mM Tris-HCl pH 7.4, 1 mM DTT
MonoS B	15 mM Tris-HCl pH 7.4, 2 M NaCl, 1 mM DTT
Phase separation buffer (PSB)	25 mM Hepes-KOH pH 7.6, 0.1 mM EDTA, 50 mM NaCl, 10% glycerol, 1 mM DTT, 0.2 g/L BSA) supplemented with 1 mM $MgCl_2$ (PSB1) or 5 mM $MgCl_2$ (PSB5).
Refolding buffer	10 mM Tris-HCl pH 7.5, 2 M NaCl, 1 mM EDTA pH 8.0, 5 mM β-mercaptoethanol
Remodeling buffer (RB)	25 mM Hepes pH 7.6, 0.1 mM EDTA pH 8.0, 50 mM NaCl, 10% (v/v) glycerol, 0.2 mg/mL BSA
SA buffer	40 mM NaOAc pH 5.2, 1 mM EDTA pH 8.0, 10 mM lysine
SDS loading buffer	50 mM Tris-HCl pH 6.8, 2% (w/v) SDS, 0.02% (w/v) bromophenol blue, 10% (v/v) glycerol, 0.1 M DTT
TE buffer	10 mM Tris–HCl pH 8.0, 0.1 mM EDTA pH 8.0
Unfolding buffer	20 mM Tris-HCl pH 7.5, 7 mM guanidinium-HCl, 20 mM DTT

3.1.9 Growth media

Table 3.14. The list of growth media used for experiments presented in this thesis.

Description	Components
YES	5 g/L yeast extract, 30 g/L glucose, 225 mg/L adenine, 225 mg/L histidine, 225 mg/L leucine, 225 mg/L uridine, 225 mg/L lysine
EMM	1 g/L EMM-Gluc, 1 g/L SP Supplements, 20 g/L glucose hexahydrate Added as needed: 225 mg/L leucine, 225 mg/L uridine, 1 g/L 5-FOA (plates)
LB	10 g/L trypton, 5 g/L yeast extract, 10 g/L NaCl

3.1.10 Machines and equipment

Table 3.15. The list of machines and devices used for experiments presented in this thesis.

Description	Manufacturer
FPLC systems ÄKTA FPLC, ÄKTApurifier, and ÄKTA Pure	GE Healthcare Life Sciences (Cytiva)

Peristaltic pump, MINIPULS Evolution	Gilson
Sonicator, Sonifier S-250 D digital	Branson Ultrasonics
Lyophilizer Alpha 1–2 and connected pump RZ 2.5	Christ, Vacuubrand
Gradient Master	BioComp
Plate reader	Biotek PowerWave HT
Microfluidizer LM10	Microfluidics
Lightcycler	Roche
Precyllis24	Peqlab
3D Cell Explorer-fluo equipped with dry objective (60x magnification, 0.8 numerical aperture) and low power laser (λ = 520 nm, sample exposure 0.2 mW/mm2)	Nanolive
Sp5 confocal microscope equipped with Argon 488 nm and DPSS 561 nm lasers	Leica
dual-trap C-Trap	Lumicks, Amsterdam
TCS SP8 X FALCON confocal head mounted on an DMi8 confocal microscope	Leica Microsystems
UV-Crosslinker	Bio-Link 365

3.2 Methods

Experiments described in sections 3.2.19 to 3.2.40 were performed as described in a manuscript under review Vizjak *et al.* The text is marked in italic font.

3.2.1 Polymerase chain reaction (PCR)

Unless otherwise stated, PCR reaction contained as follows: 1x Phusion HF buffer, 200 µM dNTPs, 0.5 µM forward primer, 0.5 µM reverse primer, 1 ng template DNA, 20 U/mL Phusion DNA polymerase. The mastermix was aliquoted into 20 or 50 µL aliquots in PCR tubes and reaction was ran in thermocycle with initial denaturation at 98°C for 30 s; 35 cycles of denaturation at 98°C for 10 s, primer annealing for 30 s and DNA synthesis at 72°C for 30 s per kb; final extension at 72°C for 5 min; hold at 10°C. Annealing temperature was determined with NEB Tm calculator (https://tmcalculator.neb.com). PCR product was analyzed on agarose gel electrophoresis and unless otherwise stated, purified with PCR purification kit. DNA concentration was calculated from measured absorbance at 260 nm and extinction coefficient 50 $(\mu g/mL)^{-1}cm^{-1}$. If needed, digestion of a parental plasmid was performed by addition of 1 µL of DpnI (stock concentration 10 U/µL) followed by incubation at 37°C for 1 h. The enzyme was then inactivated by incubation at 80°C for 20 min.

3.2.2 Agarose gel electrophoresis

Agarose (0.49-0.77 g for 0.7-1.1% gel) was dissolved in 70 mL or 120 mL of 1xTBE buffer by heating in microwave with occasional swirling. EtBr solution was added to final concentration 0.1 µg/mL and poured into a casting chamber. Samples were mixed with 1/5 volume of 6x gel loading dye. After the agarose gel polymerized, it was transferred into gel running chamber and covered with 1xTBE, or other buffer identical to buffer with which the gel was prepared. Samples were

loaded into the wells alongside a DNA ladder and the gel was run at ~120 V for 40-120 minutes. DNA bands were visualized with Peqlab Vilber Gel Documentation imaging system with the help of UV light.

3.2.3 Cloning

S. pombe genes were amplified from its genomic DNA (kept at 4°C) obtained from Korber group. Plasmids were linearized by digestion with two different restriction enzymes (SalI and SpeI; XhoI and NotI). DpnI digest was performed as described above and the digestion products were separated on agarose gel and the band corresponding to linearized plasmid was cut out from the gel and DNA purified with NucleoSpin GeI and PCR Cleanup gel extraction kit. Inserts were subcloned into opened vectors by Gibson assembly cloning method (Gibson et al., 2009). PCR was used to amplify inserts by using primers that contained homology region to insert site in a vector sequence. Molarity of inserts and vector were calculated and they were mixed in molar ratio 1:2/1:3 (vector:insert) in a volume of 10 µL (volume was made up with water). In negative controls, insert was omitted and equivalent volume of water was added instead. 10 µL of Gibson master mix was added and the mixture was incubated in PCR machine at 50°C for 30-60 minutes and transformed into chemically competent DH5α *E. coli* cells (see 3.2.5). Plasmid was isolated (see 3.2.6) and the sequence verified by DNA sequencing (see 3.2.7).

3.2.4 Growing *E. coli*

All liquid LB media and media for agar plates was autoclaved (121°C, 15 minutes). Solid media had the same composition as liquid media except bactoagar (final concentration 1.5% (w/v)) was added. After autoclaving and before agar polymerization, media was supplemented with antibiotic (100 µg/mL ampicillin and/or 34 µg/mL chloramphenicol) and poured in plates.

3.2.5 *E. coli* transformation

Aliquot of competent cells (stored at -80°C) was thawed on ice for 20-30 minutes. Agar plates, containing LB and an appropriate antibiotic, were removed from +4°C and left to warm up to room temperature or preincubated at 37°C in incubator. One µL of DNA solution was added to 50 µL of competent cells in an Eppendorf tube and gently mixed by flicking the bottom of the tube with finger a few times. The mixture was incubated on ice for 20-30 minutes (this step was omitted when transforming small, closed plasmids from stocks). Mixtures were then heat shocked in thermoblock at 42°C for 45 seconds and immediately put back on ice for two minutes. 250 µL of LB media without antibiotic was added to the bacteria and put in 37°C shaking incubator for 30-45 minutes (this step was performed only following the cloning, it was omitted while transforming a closed plasmid). With the help of inoculation loop bacteria were spread onto a 10 cm LB agar plate containing the appropriate antibiotic. Plates were incubated overnight at 37°C or at room temperature for two days.

3.2.6 Plasmid purification

Single colony was inoculated into 15 mL Falcon tube containing 5 mL LB media with appropriate antibiotic and incubated at 37°C with shaking overnight or alternatively for eight hours. The plasmid was isolated with NucleoSpin Plasmid EasyPure kit. Plasmid concentration was calculated from measured absorbance at 260 nm and extinction coefficient 50 $(\mu g/mL)^{-1}cm^{-1}$.

3.2.7 Sanger sequencing

Purified plasmids and linear DNA fragments were sequenced by using TubeSeq service provided by Eurofins Genomics. For each primer used for sequencing, 15 µL of plasmid diluted to 50-100 ng/µL was mixed with 2 µL of 10 µM primer. The samples were bar coded and submitted for sequencing. Obtained sequencing results were compared with a reference sequence of interest with NCBI Blast (https://blast.ncbi.nlm.nih.gov) and Expasy translate tool (https://web.expasy.org/translate/).

3.2.8 Growing fission yeast

All liquid media and buffers were filter sterilized while for agar plates the media was autoclaved (121°C, 15 minutes). After autoclaving, 50% glucose sterile solution in water was added. Glycerol stocks were made by mixing equal volumes of liquid culture and 50% glycerol in cryotube. Stocks were flash frozen in liquid N_2.

3.2.9 Plasmid transformation into fission yeast

Ten mL of liquid culture was grown ideally to $OD_{600} \leq 1$. Cells were pelleted at room temperature for three minutes at 3000 rpm and resuspended and washed once with autoclaved water. Pellet was then resuspended in five mL of LiAc-TE. Suspension was spun down (3000 rpm, three minutes, room temperature) and supernatant removed. Pellet was resuspended in residual liquid and cells were divided equally into two Eppendorf tubes. A carrier DNA (2 mg/mL salmon sperm DNA) was heated in thermoblock for five minutes at 95°C and immediately put on ice. Ten µL of carrier DNA was added to fission yeast cells in each Eppendorf tube. In one tube 1 µg of plasmid was added and into another one equal amount of water, to serve as a negative control. Tubes were flicked with finger to mix and left on room temperature for ten minutes, followed by addition of 260 µL of LiAc-TE-PEG. Cells were gently mixed with a pipette and incubated at 30°C 30-60 minutes. DMSO was preheated to 30°C and 43 µL was added to cells and flicked with finger to mix. Yeast was heat-shocked at 42°C for five minutes, pelleted (five minutes, room temperature), washed with one mL of autoclaved water (resuspension followed by pelleting), resuspended in 250 µL of autoclaved water and plated on EMM-Leu plates. Plates were incubated at 30°C for three days.

3.2.10 Spot assays

Precultures were grown as described above. Cells were pelleted (room temperature), washed twice in EMM without supplements and resuspended in 500 µL. To measure OD_{600}, cells were diluted 100x in water (10 µL of cell suspension + 990 µL of water) and the measurements were blanked with water. Cells were diluted to $OD_{600}=2$ in EMM in total volume 1000 µL. 10x dilution in water was prepared (100 µL of cell suspension + 900 µL of water) and OD_{600} was measured again. Serial dilutions of $OD_{600}=2$ cell suspension were prepared in 96-well plate and transferred to different plates with the help of a frogger. Plates were left to dry next to an open flame followed by incubation at 30°C or 32°C for three to four days and imaged.

3.2.11 Methylene blue staining

10 µL of each fission yeast culture was mixed with 10 µL of 0.1% methylene blue solution (w/v in water). The mixture was loaded after 5 five minutes into Neubauer counting chamber

(hemocytometer) and total and dead cells were counted under the microscope. Dead cells were distinguished by blue color.

3.2.12 Protein isolation under denaturating conditions

Equivalent of 1 OD_{600} fission yeast culture was transferred into a 1.5 mL Eppendorf tube and harvested by centrifuging (3000 rpm, 5 min, 4°C). Supernatant was removed, pellet frozen in liquid N_2 and stored at -80°C. The pellet was resuspended in 1 mL ice-cold water and 138.75 µL 2 N NaOH and 11.25 µL β-mercaptoethanol were added to each sample. The mixture was incubated on ice for 15 minutes with occasional vortexing. 150 µL TCA (trichloroacetic acid, 55% w/v in H_2O) was added to each sample and the mixture was incubated on ice for 15 minutes with occasional vortexing. The samples were centrifuged (maximal speed, 20 min, 4°C) and the supernatant was discarded. The pellet was centrifuged again briefly (maximal speed, 1 min, 4°C) and the remaining supernatant was carefully removed. Pellet was resuspended in 50 µL HU buffer. In case the color turned yellow due to some residual TCA in the solubilized protein pellet, 10-20 µL 1 M Tris pH 6.8 were added. The protein samples were heated in thermoblock at 65°C for 10-15 minutes, spun briefly and 5-10 µL (corresponding to 0.1-0.2 OD_{600} of yeast cells) were analyzed on SDS-PAGE.

3.2.13 Protein isolation under native conditions

The culture containing $2x10^8$ *S. pombe* cells was harvested by centrifuging (3000 rpm, 5 min, 4°C). Supernatant was removed and pellet resuspended in ice-cold lysis buffer (25 mM MOPS pH 7.2, 15 mM $MgCl_2$, 10 mM EDTA, 1% Triton, 1 mM DTT, 1 mM PMSF, 20 µg/mL leupeptin, 10 µg/mL pepstatin A) and transferred into a screw-cap microcentrifuge tube. Cells were pelleted by centrifugation (16000g, 15 sec, 4°C), supernatant was removed and the pellet frozen in liquid N_2. The pellet was resuspended in 200 µL and 500 µL of dry volume of glass beads were added. The cells were disrupted by three 30 seconds blasts of vigorous vortexing, interspersed with 5 minutes rest on ice. The bottom of the screw-cap tube was then pierced with a hot needle and the perforated screw-cap tube was inserted into 1.5 mL Eppendorf tube. The supernatant was collected by centrifugation (400g, 2 min, 4°C). The collected supernatant was spun again to get rid of carry-over beads and precipitates (16000g, 15 min, 4°C). The cleared supernatant was transferred into a fresh 1.5 mL Eppendorf tube and further analyzed by SDS-PAGE and Western Blot. Supernatant was frozen in liquid N_2 and stored at -80°C.

3.2.14 Western Blot analysis

Concentration of proteins was measured using NanoDrop and required quantity of protein extract was mixed with SDS loading buffer, denaturated for 3 minutes at 95°C, vortexed and loaded on 8% polyacrylamide gel to run at 180 V until completion. Then, samples were transferred onto a nitrocellulose membrane using semi-dry blotting system for 1 hour at 250 mA. After 1 hour of membrane incubation in blocking solution (5% milk in PBS) the membrane was incubated with anti-Flag M2 antibodies diluted 1:1000 in 5% milk-PBST overnight at 4°C. Then, the membrane was washed three times with 5% milk in PBST and incubated with secondary infrared antibodies (dilution 1:10 000 in 5% milk-PBST) for 1 hour. After three washes with 5% milk-PBST, a signal from the membrane was detected with Odyssey imaging system.

3.2.15 RNA extraction

Strains were streaked out from glycerol stocks on EMM - Leu + thiamine plates and incubated for two to three days at 30°C. Colonies were scooped from the plate with an inoculation loop and resuspended in a sterile Eppendorf tube in 1 mL EMM-Leu by pipetting up and down. To determine OD_{600}, aliquot of 20 µL was diluted 50 times. Suspension was inoculated into 50 mL of EMM-Leu to reach OD_{600}=0.5 and supplemented with 300 µL of 10 mM thiamine (final concentration 60 µM). OD_{600} was checked and the culture incubated overnight at 30°C with shaking. Most of the culture was harvested for RNA and protein isolation (+thiamine sample) as described later. To induce the promoter, two aliquots of 2 mL culture were transferred into two 2 mL sterile Eppendorf tubes, centrifuged (3000 rpm, 5 min, room temperature), pellets were washed twice with 1 mL EMM-Leu each and pooled together. Final suspension volume was 2 mL. 1 mL was used to measure OD_{600}. Suspension was then inoculated in 50 mL of EMM-Leu media. OD_{600} was checked and the culture incubated overnight at 30°C with shaking. The culture was harvested for RNA and protein isolation (-thiamine sample) as described later.

The culture was transferred into a 50 mL Falcon tube and harvested between OD_{600}=0.4-0.8 (3000 rpm, 5 min, 4°C). A cell pellet was resuspended in cold miliQ water by gentle shaking, centrifuged and the supernatant was decanted. The pellet was resuspended in a residual water by pipetting up and down and transferred into 1.5 mL screw cap tubes. Tubes were labeled both on the lid and on the side and centrifuged (2000 rpm, 5 min, 4°C). Supernatant was removed, pellet frozen in liquid N_2 and stored at -80°C.

During RNA extraction and all other work involving RNA, only filter tips were used. Pellets were thawed on ice and resuspended in 1 mL TRIsure. Two scoops (i.e., a small PCR tube ~250 µL volume equivalent) of zirconia beads were added to each sample. Screw cap tubes were tightly sealed and cells disrupted in Precyllis24 three times for 30 seconds (program 1: 6800) with 5 min rest on ice in between. Tubes were spun (12000g, 4°C, 10 min) and the cleared lysate was transferred to 1.5 mL Eppendorf tube to which 200 µL of chloroform was added before. The samples were immediately vortexed for 15 seconds each, incubated at RT for 10 min and spun (12000g, 4°C, 10 min). The aqueous phase was transferred to 1.5 mL Eppendorf tube to which 500 µL of chloroform was added before. The samples were briefly vortexed and immediately spun (12000g, 4°C, 10 min). The aqueous phase was transferred to 1.5 mL Eppendorf tube to which 500 µL of isopropanol was added before. The samples were briefly vortexed, incubated on ice for 15 min and spun (12000g, 4°C, 10 min). Supernatant was removed and pellets were washed twice with 1 mL 75% ethanol (prepared with RNase-free water). Samples were vortexed so the pellet detaches from a wall of an Eppendorf tube and spun at 9600 rpm for 5 min. The supernatant was removed and the pellets dried in speed vac briefly and without heat for 5-10 min and resuspended in 100 µL RNase-free water. To make sure that the RNA is totally dissolved, the samples were incubated at 55°C for 30-45 min with occasional flicking or pipetting. RNA was stored at -80°C and thawed on ice before the next step. The RNA concentration was determined using the Nanodrop and 20 µg RNA was diluted in RNase-free water to total volume of 36 µL (final RNA concentration 0.2-0.5 µg/µL). Each sample was supplemented with 4 µL TURBO DNA-free 10x buffer and 0.5 µL TURBO DNA-free DNase I and incubated at 37°C for 30 min when 0.5 µL more of DNase I was added and the samples were incubated at 37°C for another 30 min. TURBO DNase inactivation reagent was thoroughly resuspended and 6 µL was added to each sample. Samples and the inactivation reagent were mixed well and incubated at RT with occasional mixing for 2 min, followed by centrifugation (10000g, 1.5 min) and transferring of 20-30 µL of supernatant into a fresh Eppendorf tube.

3.2.16 cDNA synthesis (reverse transcription)

In a PCR-strip, for each sample was mixed 11 µL TURBO DNase treated RNA (~5 µg), 1 µL of oligo-$(dT)_{20}$ primers (50 µM stock concentration) and 1 µL of 10 mM dNTP mix. To denature RNA, tubes were incubated at 70°C for 10 min and then incubated on ice for another 10 min. To each sample, 7 µL of enzyme mix (all components are included in Superscript III kit; 4 µL 5x First-Strand buffer, 1 µL 0.1 M DTT, 1 µL RNAseOUT, 0.75 µL RNAse-free H_2O and 0.25 µL SuperScript III or 0.25 µL RNAse-free H_2O for no enzyme (-RT) control) was added. Tubes were incubated at 50°C for 30-60 min followed by heat inactivation of reverse transcriptase at 70°C for 15 min. For degrading RNA:DNA hybrids, 0.5 µL RNase H was added to each sample and incubated at 37°C for 30 min (this step is optional and it can be omitted). Samples were stored at -20°C.

3.2.17 Quantitative PCR (qPCR)

Different cDNA dilutions were prepared for different genomic regions analysed: 1:1000 or 1:2000 cDNA dilutions were used for analysing euchromatic genes, 1:25 cDNA dilutions for heterochromatic single-copy genes (reporters), 1:50 cDNA dilutions for heterochromatic repeats (dg/dh) and 1:25 cDNA dilutions were used for -RT control samples irrespective of transcripts. All samples were measured in triplicates in a 384 well plate. One reaction mixture contained: 5 µL of cDNA dilution made in the step above, 2.5 µL of forward/reverse primer mix (1.5 µM) and 7.5 µL 2xSYBR mix. The primers used are listed in Table 3.6. The 384 plate was sealed with a folium and the analysis was run in Lightcycler machine with a program: polymerase was activated at 94°C for 3 min and the following cycle was repeated 35 times: 94°C for 20 s, 50°C for 20 s, 72°C for 40 s, 73°C 1 s to obtain reading. After qPCR was finished a melting curve was recorded from 70°C to 90°C. A serially diluted RNA sample (1:20, 1:200 and 1:2000) untreated with DNAse was used for constructing standard curves for each primer pair and determining efficiency of amplification. The C_t (concentration threshold) values were exported as .txt file and data were further analysed in Excel. C_t values of technical triplicates were averaged and the relative quantification of a genome region of interest against a housekeeping gene was determined using Livak method (Livak & Schmittgen, 2001).

3.2.18 MNase-seq

3.2.18.1 Spheroplast preparation and chromatin digestion with MNase

Strains were streaked out from glycerol stocks on EMM - Leu + thiamine plates and incubated for two days at 30°C. Cells were then scraped from the plate with inoculation loop and resuspended in one mL EMM – Leu media, pelleted (3000 g, five min, RT), washed one more time with one mL EMM – Leu, finally resuspended in one mL EMM – Leu and OD_{600} was measured. Suspension was inoculated into 150 mL EMM – Leu to OD_{600}=0.02 and grew with gentle shaking at 30°C for 16 h or until OD_{600}=0.75 was reached. 50 mL of culture was taken into a preweighted Falcon tube and ten µL of culture was stained with methylene blue. The experiment was further performed as published previously (Cam and Whitehall, 2016). To the rest of the culture (100 mL) 2.7 mL of 36.5% formaldehyde was added and incubated in shaker for 30 min. Crosslinking reaction was quenched by adding five mL of 2.5 M glycine and incubating for five minutes at 30°C in shaker. Cells were harvested into a preweighted Falcon tube by centrifugation for two min at 1000 g in a benchtop centrifuge and the supernatant was discarded. The procedure was repeated second time to pool pellet from the entire 100 mL culture into the same Falcon tube. Falcon tube with the

pellet was weighted and the mass of the pellet calculated. Pellet was washed in 10 mL CES buffer followed by centrifugation for two min at 1000 g in a benchtop centrifuge. Supernatant was discarded, pellet resuspended in 0.5 mL CES buffer, transferred into an Eppendorf tube and supplemented with 50 µL freshly prepared 10 mg/mL Zymolyase 100T suspension followed by incubation up to one hour at 30°C with gentle shaking on a rotating platform. To test if spheroplasting was complete, five µL aliquots were sampled at 20 min intervals, mixed with 5 µL of 2% SDS on a microscope slide and observed under a microscope. Spheroplasted cells lose refractivity and appear as "ghosts" when examined under a microscope (they do not have well defined rim). When 80-90% of cells were spheroplasted, they were pelleted (800 g, 2 min, 4°C) and supernatant discarded. One mL of ice cold 1.2 M sorbitol was added on the pellet. The pellet was not resuspended but the position of the spine of the tube in the centrifuge was rotated by 180°, centrifuged (800 g, two min, 4°C) and the supernatant discarded. Quickly but gently spheroplasts were resuspended by pipetting up and down in 1 mL of MND buffer. In five 1.5 mL Eppendorf tubes, 300 µL MND buffer was added containing the following amounts of MNase (stock concentration 5 units/µL in EX50 buffer): 0, 2 µL (final concentration during digestion will be 0.02 U/µL), 6 µL (0.06 U/µL), 10 µL (0.1 U/µL) and 20 µL (0.2 U/µL). Tubes were incubated in a thermoblock at 37°C, 200 µL of the spheroplasts were added to each tube and incubated for ten min at 37°C. The MNase digestion was stopped by adding 55 µL of 0.5 M EDTA and 11 µL of 10% SDS. Samples were supplemented with proteinase K (stock concentration 10 mg/mL, 22 µL) and RNase A (stock concentration 10 mg/mL, 1 µL) and incubated overnight at 65°C.

3.2.18.2 DNA purification and library preparation

Next day, tubes were allowed to cool down to room temperature. Samples were extracted twice with an equal volume of phenol:chloroform. DNA was precipitated with 0.1 volume of 3 M sodium acetate and 2 volumes of 100% ethanol, incubating at -20°C for at least 1 h and centrifuging for 15 min at 16000 g at 4°C. Supernatant was discarded and pellet washed with cold 70% ethanol. Speedvac was used to dry the pellet (settings for alcoholic solution concentrator temperature 60°C) and it was then dissolved in 40 µL of miliQ water. One µL of RNase A was added and incubated for 30 min at 37°C. DNA was then mixed with orange G dye and resolved on 1.5% low melting agarose gel for 3-4 hours in TBE buffer. Mononucleosome band was cut out from the gel and extracted with the help of freeze and squeeze tubes. DNA was precipitated with 0.1 volume of 3 M sodium acetate and 2 volumes of 100% ethanol in a presence of glycogen, incubating at -20°C for at least 1 h and centrifuging for 15 min at 16000 g at 4°C. Supernatant was discarded and pellet washed with 1 mL cold 70% ethanol. Speedvac was used to dry the pellet (settings for alcoholic solution concentrator temperature 60°C) and it was then dissolved in 30 µL of miliQ water. Concentration was measured with Qubit and 50 ng of DNA was used to prepare sequencing libraries by using a kit and following instructions provided by manufacturer. Final libraries were visualized using the Agilent 2100 Bioanalyzer on a High Sensitivity DNA chip, purified from agarose gel as described above and submitted for sequencing.

3.2.18.3 Sequencing and data analysis

The libraries were sequenced at the Laboratory for Functional Genome Analysis (LAFUGA), Gene Center, LMU on Illumina HiSeq 1500 for 50 bp in the paired-end mode. Paired-end sequencing reads were aligned to the reference genome Schizosaccharomyces pombe (ASM294v2) using bowtie2 (version 2.2.9). Reads were filtered by mapping quality using samtools (version 1.9) with the parameter -q 2. Fragment coordinates were extracted by sorting the reads by name using samtools and converting bam to bed format using bedtools2 bamtobed

command (version 2.28.0) with the parameter -bedpe. Subsequent analysis was performed in R (version 3.6.1). Fragments were filtered for chromosomes I, II and III and a fragment size less than 500 bp. Fragments were converted to dyad coverages using the bed2dyad function with parameters type = ”PAIRED” and width = 50 from the tsTools package (version 0.1.2; source: https://github.com/musikutiv/tsTools). Dyad coverages were normalized by the total coverage and multiplied by a million. Array regularity was computed by cross-correlation analysis (Ocampo et al., 2016; Singh et al., 2021) using the ocampo3 function from the tsTools package. Parameters were set to beforeRef = 100, afterRef = 1000, smoothingWindow = 100, spacing.low = 100, spacing.high = 300, shift.low = -75, shift.high = 75, sigma_scaled = TRUE, lowess_f = 0.15. For this analysis, TSS +1 nucleosome positions served as reference, which were determined by the nucleR package (version 2.16.0) and the gene annotation ASM294v2.37. Plots were generated by R base graphics. Code is available upon request. Bigwig files were visualized in Integrative Genomics Viewer (IGV, Broad Institute).

3.2.19 Expression and purification of ISWI, ISWI-GFP and ISWI E257Q

As mentioned in the introduction to the methods in section 3.2., experiments here and further below (sections 3.2.19 to 3.2.40) were performed as described in a manuscript that is currently under review (Vizjak *et al.*). The text is cited here and is recognizable by the use of quotation marks and italic font.

“Corresponding plasmids containing D. melanogaster ISWI (pFMP210 for 6xHis-TEV-ISWI, pFMP244 for 6xHis-TEV-ISWI-3C-STREP- sfGFP, pFMP110 for 6xHis-TEV-ISWI E257Q) were freshly transformed into BL21 Star E. coli and plates were incubated at 37°C overnight. The bacterial lawn from one plate was harvested and used to inoculate two litres of LB media. Cultures were grown (37°C, 130 rpm) until OD_{600} 0.5-0.6 when they were induced with 1 mM IPTG. The expression went overnight at 18°C with shaking. The bacterial cultures were harvested (6000xg, 10 min, 4°C). Pellets were gently rinsed with cold water and stored at -80°C. Cells were thawed in a palm of a hand with occasional vortexing and resuspended in HisA buffer supplemented with 20 mM imidazole pH 7.4, 1 tablet complete-EDTA free protease inhibitors, as well as leupeptin (1 mg/L), pepstatin (0.7 mg/L) and aprotinin (1 mg/L). Benzonase (5 µl per litre of culture) and lysozyme (tip of a spatula) were added and suspension was sonicated on ice (6x10 seconds on, 10 seconds off, amplitude 25%). The homogenized bacteria were then cracked with six runs on Microfluidizer LM10 at 1200 bar. Lysates were centrifuged (19000 rpm, JA25.50 rotor, 4°C, 30 min), supernatants filtered through 0.45 µm syringe filter and loaded onto His Trap equilibrated with 5% HisB buffer. The column was washed with 10 column volumes (CV) 5% HisB, then with 6 CV 10% HisB and 1 CV 20% HisB. ISWI was then eluted with 20-100% HisB gradient over 10 CV. ISWI containing fractions were pooled, TEV protease added (0.1 mg for every 8 mg of ISWI) and the mixture was dialyzed (Spectra/Por dialysis membrane, cutoff 12000-14000 kDa) overnight against dialysis buffer (15 mM Tris-HCl pH 7.4, 150 mM NaCl, 1 mM DTT). To remove His-tagged TEV protease, cleaved-off 6xHis-tag and uncleaved 6xHis-TEV-ISWI, a second nickel-affinity chromatography was performed (His Trap, equilibrated in 10% HisB buffer). Sample was loaded and unbound protein further washed out with 10% HisB. The flowthrough was pooled and its conductivity reduced by slow dilution with two volumes of 2% MonoS B buffer, which was diluted with MonoS A and filtered through 0.2 µm syringe filter. A MonoS column was equilibrated with 2% MonoS B. After loading, the protein was eluted with 2-30% MonoS B (10 CV) and 30-100% MonoS B (4 CV). Fractions containing ISWI were pooled together, concentrated and loaded onto the HiLoad Superdex200 size exclusion column equilibrated with GF buffer. ISWI-containing

fractions were pooled and protein was concentrated to ~5 mg/mL. Molar concentration was determined by using calculated extinction coefficient (Expasy Protparam tool). Proteins were aliquoted, frozen in liquid nitrogen and stored at -80°C."

3.2.20 Expression and purification of histones

"Codon-optimized D. melanogaster histones were expressed and purified as previously described (Klinker et al., 2014)*. Corresponding plasmids (pFMP128 for H2A, pFMP129 for H2B, pFMP186 for H3, pFMP187 for H4, pFMP269 for H2AK119C, pFMP270 for H3C111A, pFMP268 for H4T1C) were freshly transformed into BL21 Star E. coli and incubated at 37°C overnight. Bacterial lawns from one plate were then used to inoculate two litres of LB media. Cultures were grown (37°C, 130 rpm) until OD reached 0.5-0.6 when they were induced with 1 mM IPTG. The expression went for three hours at 37°C with shaking. The bacterial cultures were spun down (6000xg, 10 min, 4°C). Pellets were gently resuspended in cold water and transferred to a 15 ml Falcon tube. Samples were centrifuged and the pellets stored at -80°C. Cells were thawed in a palm of a hand with occasional vortexing and resuspended in SA buffer supplemented with 6 M urea, 200 mM NaCl, 1 mg/mL aprotinin, 1 mg/mL leupeptin, 1 mg/mL pepstatin, 1 mM PMSF and 5 mM β-mercaptoethanol. Benzonase (5 µl per liter of culture) and lysozyme (tip of a spatula) were added and suspension was sonicated on ice (15 seconds on, 30 seconds off, amplitude 30%, effective sonication time 20 minutes). The homogenized bacteria were then cracked with six runs on Microfluidizer LM10 with 1200 bar. Lysates were centrifuged (19000 rpm, JA25.50 rotor, 4°C, 30 min), supernatant filtered through 0.45 µm syringe filter and loaded onto a HiTrap Q HP column that was stacked on top of a SP column equilibrated with 20% buffer B (buffer A: 40 mM NaOAc pH 5.2, 1 mM EDTA pH 8.0, 10 mM lysine, 7.5 M urea, 5 mM DTT; buffer B: 40 mM NaOAc pH 5.2, 1 mM EDTA pH 8.0, 10 mM lysine, 7.5 M urea, 5 mM DTT, 1000 mM NaCl). Samples were applied to the stacked columns. The columns were washed with 20% buffer B (1 CV). The Q column was removed and SP column further washed with 25% buffer B (3 CV) and 30% buffer B (3 CV). Histone was eluted with 30-40% buffer B gradient (5 CV), 40-80% buffer B gradient (7 CV), 100% buffer B (3 CV). Pooled fractions were dialyzed (SpectraPor MWCO 3,500 kD) three times against 5 L of miliQ water. Purity was analysed on SDS-PAGE and concentration determined from A_{280} absorption. Histones were aliquoted (1 mg per aliquot), flash frozen in liquid nitrogen and stored at -80°C or -70°C. Histones were lyophilized before use. Lyophilized histones were stored at -20°C."*

3.2.21 Assembly and purification of octamers

"Lyophilized histone aliquots were dissolved in unfolding buffer to 4 mg/ml for 10 minutes in a thermoblock (24°C, 600 rpm). Solutions were spun down in a table top centrifuge (10 minutes, full speed, 4°C), and supernatants transferred to fresh tubes and kept on ice until dialysis. Histone concentrations were remeasured in unfolding buffer by measuring OD_{280} and corrected for purity as assessed from SDS-PAGE gel. Histones were mixed in molar ratio H2A:H2B:H3:H4=1.4:1.4:1:1. The histone mixture was transferred into dialysis membranes (Roth E658.1 MWCO: 4000-6000) which were soaked in water for one hour and rinsed with refolding buffer. The mixture was then dialyzed three times against 1 L of refolding buffer, with the second dialysis step being overnight. Lastly, octamers were purified by size exclusion chromatography (HiLoad 16/60 Superdex 200 prep grade), concentrated to 4 mg/mL (Amicon 15 mL 30 kDa), aliquoted, flash frozen in liquid nitrogen and stored at -80°C or -70°C."

3.2.22 Histone labeling (H2AK119C-atto565, H4T1C-cy3, H2AR71C-4-MBP)

"Lyophilized histone aliquots were dissolved in a labeling buffer (7 M guanidinium-HCl, 20 mM Tris-HCl pH 7.5, 5 mM EDTA pH 8.0, 0.7 mM TCEP) to a final concentration 0.2 mM and incubated two hours to reduce all cysteines. Cyanin-3-maleimide (Lumiprobe) was dissolved in DMSO to final concentration 100 mM and added to the solution in a 5.7-fold excess. 4-(N-maleinimido)-benzophenon (4-MBP) was dissolved in DMF to final concentration 100 mM and added to solution in 57-fold excess. Atto-565 maleimide (Atto-tec) was dissolved in DMF to final concentration 100 mM and added to solution in 13.2-fold excess. Histones were incubated with the dye for 14 hours (3 hours for cy3 and 4-MBP labeling) on rotating wheel at room temperature covered with aluminium folium. To stop the labeling reaction, β-mercaptoethanol was added to final concentration 340 mM. For cy3 labeling, reaction was stopped by adding DTT to final concentration 20 mM. Unreacted dye was partially removed by several rounds of ultrafiltration (15 mL 10K Amicon, Millipore) and successive dilutions with labeling buffer (this step was omitted for Cy3 and 4-MBP labeling). The labeling efficiency was assessed with SDS-PAGE and fluorescence imaging. The labeled histones were assembled into octamers as described in section 3.22.2, but H3C111A was used instead of H3."

3.2.23 Preparation of DNA for nucleosome arrays

"25mer and 13mer nucleosome arrays were prepared as published previously (Ludwigsen et al., 2018)*. Briefly, plasmids carrying 25 (pFMP232, pFMP233) or 13 (pFMP226) consecutive copies of 197 bp with modified 601 sequence were transformed into DH5α E. coli strain and purified from four litres of culture by using plasmid DNA purification kit. Three mg of the plasmid were digested with EcoRI HF (0.25 U/µg DNA) and HincII (0.6 U/µg DNA) in CutSmart Buffer at 37°C for 3 h. When the digest was complete, restriction enzymes were heat-inactivated by incubation at 65°C for 20 min. Tubes were put on ice before AseI was added (0.5 U/ µg DNA) and then incubated at 37°C for four h. After digest was complete, DNA was purified via phenol/chloroform extraction and ethanol precipitated in presence of NaOAc. Finally, it was resuspended in TE buffer and stored at -20°C."*

3.2.24 Preparation of DNA for mononucleosomes

"DNA fragments containing the 601 sequences were amplified by large-scale PCR (Yang & Narlikar, 2007)*. Primers were obtained from Sigma. For primer sequences, see Table 3.6. The PCR was cleaned up by precipitating the plasmid template by addition of ½ of volume 30% PEG 8000 (w/w) in 30 mM $MgCl_2$. The PCR product was then precipitated by adding the same volume of propan-2-ol. The pellet was washed with 70% (v/v) cold ethanol, resuspended in TE buffer and stored at -20°C."*

3.2.25 Chromatin assembly and purification

3.2.25.1 Assembly of 25- and 13mer arrays

"The optimal molar octamer:601 ratio was identified by performing small scale test assemblies, where purified octamers were titrated to 7.5 µg digested plasmid (Ludwigsen et al., 2018)*. Preparative assembly contained 100-500 µg digested plasmid (100 ng/µL of 601-array DNA, which corresponds to 150 or 200 ng/µL of total digested plasmid containing 25mer or 13mer,*

respectively). It also contained corresponding amounts of purified octamers, 2 M NaCl, 10 mM Tris-HCl pH 7.6, 1 mM EDTA pH 8.0, 1 mM DTT. Reactions were transferred into dialysis membrane and underwent salt gradient dialysis: 3 L of low salt buffer were pumped into 1 L of high salt buffer containing the dialysis bag over a period of 24 hours. To maintain the constant volume, buffer was simultaneously pumped out with the same speed. Assemblies were then dialyzed against 1 L of low salt buffer before they were precipitated by addition of equal volume of precipitation buffer (10 mM Tris–HCl pH 7.6, 7 mM or 10 mM $MgCl_2$ for 25mer or 13mer, respectively). Pellets were resuspended in TE buffer (10 mM Tris-HCl pH 7.6, 1 mM EDTA pH 8.0) and quality controls of chromatin array were performed as described (Ludwigsen et al., 2018) *(Fig. 2.14.B). Chromatin concentrations were approximated by UV assuming that 1 OD at 260 nm equals 50 ng/µL of DNA."*

3.2.25.2 Mononucleosomes

"The optimal molar octamer:DNA ratio was first identified by titrating octamers to DNA. Preparative assemblies contained DNA (200 ng/µL), purified octamers, 2 M KCl, 20 mM Tris-HCl pH 7.7, 10 mM DTT. Reactions were transferred into Slide-A-lyzer 7k Mini and underwent salt gradient dialysis in 200 mL of Mono2000 buffer to which 1 L of Mono0 buffer was pumped over 24 hours. To maintain constant volume, buffer was simultaneously pumped out with the same speed. Assemblies were dialysed against Mono0 buffer and purified over 10-30% (w/w) glycerol gradient. Concentrations were determined as above for arrays."

3.2.26 Quality controls of assembled nucleosome arrays

3.2.26.1 Agarose gel of nucleosome arrays

"200 ng of arrays before and after Mg-precipitation was analysed by agarose gel electrophoresis (0.7%)."

3.2.26.2 NotI digestion of nucleosome array

"200 ng of arrays was digested in EX50 buffer with Not1 (20 U/µL) in total volume of 15 µL for three hours at 26°C. Digestion was analysed on 1.1% agarose."

3.2.26.3 BsiWI digestion of nucleosome array

"250 ng of an arrays was digested in buffer (25 mM Hepes–KOH pH 7.6, 0.1 mM EDTA, 50 mM NaCl, 10% glycerol, 2 mM $MgCl_2$) with BsiWI (10 U/µL) for 1 hour at 26°C in total volume of 20 µL. The digestion was stopped with addition of SDS (final concentration 0.4%) and EDTA (final concentration 20 mM) followed by Proteinase K (1 mg/mL) treatment in total volume of 30 µL for three hours at 65°C or overnight at 37°C. DNA was ethanol precipitated and analysed on 1% gel."

3.2.27 Analytical ultracentrifugation

"Sedimentation velocity (SV) experiments of purified, reconstituted arrays were conducted at 20°C in a Beckman Coulter Optima XL-I analytical ultracentrifuge (Palo Alto, CA) using an An-50 Ti rotor. Samples contained 21.6 ng/µL (6.9 nM) of 25mer and were dissolved in buffer (1 mM Tris-HCl pH 8.0, 0.01 mM EDTA pH 8.0, 0.01 mM DTT, 50 mM NaCl, 0.2 mM or 1.7 mM $MgCl_2$). Samples (360 µl) were loaded into 12 mm charcoal-filled epon double sector centerpieces. A rotor speed of 22,000 rpm was selected and absorbance optics scans at a wavelength of 258 nm were

collected every second until sedimentation was complete. Data were analysed using the c(s) model in SEDFIT which directly models the sedimentation boundary as a continuous distribution of discrete, non-interacting species (Schuck, 2000)*. Buffer density and viscosity as well as sample partial specific volumes were calculated using UltraScan III* (Demeler & Gorbet, 2016)*."*

3.2.28 Negative stain electron microscopy

"Quantifoil R2/1 Cu200 C2 grids were plasma cleaned for 20 s at 20 mA (GloCube, Quorum). 3.5 µL of sample containing 1-4 ng/µL (0.3-1.3 nM) of 25mer in buffer (3 mM Tris-HCl pH 8.0, 0.03 mM EDTA pH 8.0, 0.03 mM DTT, 50 mM NaCl, 0.2/1.7 $MgCl_2$) was applied, incubated 30 s, then hand blotted. Grids were negative stained with 2x 3.5 µL of 2% uranyl acetate, and hand blotted after 30 s for each stain application. Images were collected using an FEI Morgagni 100 keV TEM with a SIS Megaview III 1k CCD, at a nominal magnification of 56,000x."

3.2.28.1 Analysis of electron micrographs

"Outlines of single particles were determined with a trainable Weka segmentation in ImageJ (Fiji). Feret´s diameter (the maximum distance between two parallel tangential lines), and circularity were calculated for this outline using equation 1."

$$circularity = \frac{4\pi * area}{perimeter^2} \quad (Eq.\ 1)$$

3.2.29 Restriction based nucleosome sliding assay

"Remodeling assays contained 4 nM 25mer arrays (100 nM total nucleosome concentration), 200 nM ISWI, ATP regeneration system, indicated magnesium concentration and 5 µM Mg-ATP in remodeling buffer RB. Beforehand, chromatin arrays were dialyzed overnight into 10 mM Tris pH 7.6 at 4°C. The reaction was started with addition of ISWI and incubated at 26°C. At different time points, 20 µL aliquots were taken and remodeling was quenched with apyrase (50 mU, 1 min, 26°C). The Mg^{2+} concentration was supplemented to a final concentration of 1.7 mM $MgCl_2$ for all samples. Samples were digested with 10 U/125 ng array of BamHI for 90 min at 26°C. The digestion was stopped with addition of 20 mM EDTA and 0.5% SDS, followed by Proteinase K (final concentration 0.5 mg/mL) treatment for three hours at 37°C. Samples were ethanol precipitated and separated on an agarose gel (0.7% to 0.9% in 0.5xTBE, 20 cm). Gels and running buffers contained 0.5 µg/mL EtBr. The bands were analysed with AIDA Image Analyzer Software and the percentage of Cut-DNA calculated. The dependence of percentage of Cut-DNA versus time was fitted in R into to a single exponential function (Eq.2):"

$$\%cut = \%cut_{max} * (1 - e^{-kobs * t}) \quad (Eq.\ 2)$$

3.2.30 ATPase assay

"An NADH-oxidation coupled ATPase assay was performed as described (Mueller-Planitz et al., 2013)*. Briefly, 30 µL reactions were assembled on a 384-well plate, containing 100 nM ISWI and 0.1/0.5/1.33 µM mononucleosomes (0N60) in remodeling buffer supplemented with ATP-regeneration system and 0.6 mM NADH. Each sample was measured in technical triplicates. Reactions were started by addition of 1 mM Mg-ATP and NADH absorbance was monitored at 340 nm in a plate reader (Biotek PowerWave HT) at 26°C. Absorbance readings between ten and 20 minutes were fit to a linear function."*

3.2.31 Phase separation of nucleosome arrays and imaging of formed chromatin condensates

"All phase separation experiments were performed in phase separation buffer (PSB) supplemented with 1 mM $MgCl_2$ (PSB1) or 5 mM $MgCl_2$ (PSB5). Phase separation was induced by mixing equal volumes of nucleosome arrays diluted in TE buffer pH 7.6 with 2xPSB. The formed chromatin condensates (4-10 µL of sample) were incubated at room temperature for a minute and then loaded onto the imaging chamber made of double-sided tape. Double-sided tape was pierced with a hole puncher beforehand, and sample was deposited into the hole. Cover slips were pre-treated with 20 µL of BSA solution (25 mM Hepes-KOH pH 7.6, 0.1 mM EDTA, 50 mM NaCl, 10% glycerol, 1 mM DTT, 100 mg/mL BSA) for one minute. The imaging chamber was sealed with nail polish, and unless stated otherwise, spun onto the cover slip (1 min, 1000g, room temperature). Samples were then imaged on a widefield microscope (Zeiss Axiovert)."

3.2.31.1 Analysis of phase diagram

"Condensates were detected by Trainable Weka segmentation in ImageJ, their surface was calculated as a percentage of a total field of view surface and plotted in form of a heatmap in R."

3.2.32 Confocal imaging

"Confocal and FLIM images were performed with a TCS SP8 X FALCON confocal head (Leica Microsystems, Wetzlar, Germany) mounted on an inverted microscope (DMi8; Leica Microsystems). For confocal imaging, a white light laser was used as excitation source (561 nm or 633 nm as necessary). Single photons were collected through a 40×/1.3 NA oil-immersion objective and detected on Hybrid Detectors (HyD) (Leica Microsystems) with a 570 – 610 nm, and 650 – 707 nm spectral detection window as necessary. Sequential excitation was performed to avoid potential crosstalk between the fluorophores."

3.2.33 FITC-dextran partitioning in chromatin condensates

"Condensates were formed in a solution containing 100 nM 13mer (final concentration 90 nM), PSB2 supplemented with 2.5 mM DTT and incubated for five minutes at room temperature when the FITC-dextrans diluted in water were added to final concentration of 0.1 mg/mL. Samples were prepared as described above and imaged on Leica laser scanning confocal microscope after 1 h incubation at room temperature.

Images were analyzed in ImageJ, where the dextran partitioning coefficient was determined for individual condensates as a ratio of fluorescence inside the condensate and background fluorescence. Molecular weights of dextrans were converted into Stokes radii with an online tool (https://www.fluidic.com/toolkit/hydrodynamic-radius-converter/)."

3.2.34 ISWI colocalization experiment

"Chromatin and ISWI colocalization experiment was performed with 40 nM of unlabeled 25mer, 10 nM of 25mer-Cy3 and 1.125 µM ISWI-GFP/GFP-GST in PSB5. Condensates were induced by adding Mg^{2+} (5 mM) either after or before addition of GFP-GST or ISWI-GFP.

A standard curve for mean Gray value dependence on ISWI-GFP concentration was obtained from ISWI-GFP dilutions in PSB5. Different microscope settings were used to image lower and

higher dilutions. ISWI-GFP concentration was then determined inside condensates and in a surrounding solution for 90 nM 13mer, 234 nM ISWI-GFP, 1 mM Mg-ATP, ATP-regeneration system, PSB1 and for 45 nM 25mer, 125 nM 0N60 mononucleosomes, 625 nM ISWI-GFP, 1 mM Mg-ATP, ATP-regeneration system, PSB5."

3.2.35 Restriction enzyme accessibility nucleosome sliding assay adapted to chromatin condensates

"A KpnI site was used to compare nucleosome sliding in 25mer arrays fully dissolved or after condensate separation. A remodeling assay contained 15 nM 25mer, 750 nM ISWI, ATP regeneration system and 1 mM Mg-ATP in PSB0.2/5, in total reaction volume of 20 µL. Reaction was started with 2 µL of ISWI or ATP and incubated at 26°C. Before the reaction was started, 6 µL of the reaction mixture were checked under the microscope for chromatin condensates. At different time points, 1 µL of reaction was quenched with 45 µL of quenching solution (10 mU/µL apyrase in apyrase reactions buffer, containing 1.8 µL 2 mM $MgCl_2$ for low magnesium reactions), incubated at 26°C for 15 min and after that kept on ice. After all time points were quenched, the reaction mixture was again checked under the microscope for the presence of condensates. To each tube, 2.5 µL of KpnI was added and incubated at 26°C for 30 min. Cleavage was detected as above for the restriction-based nucleosome sliding assay, except that ImageJ was used for quantification."

3.2.36 FLIM-FRET

3.2.36.1 Slide preparation

"For end point assays (Fig. 2.19.E), 45 nM 25mer (1125 nM nucleosome concentration), 125 nM labeled mononucleosomes, 625 nM ISWI, ATP regeneration system and 1 mM Mg-ATP were mixed in PSB5 in total volume of 10 µL. Samples were incubated at room temperature for 15 minutes, 6 µL was transferred on a slide (see above for slide preparation), spun as above, and imaged after four hours. For time lapse assays (Fig. 2.20.A), 40 µL of the reaction mixture was loaded into the channel of imaging chamber (Ibidi µ-Slide VI$^{0.5}$ Glass Bottom 80607). The imaging chamber was spun down and mounted on the microscope. Lifetimes were measured for two min before addition of nucleotides. Then, 120 µL of 1 mM Mg-ATP or 1 mM Mg-AMPPNP solution, dissolved in identical buffer and supplemented with ATP regeneration system, was filled into one of the reservoirs without removing the chamber from the microscope or stopping the imaging. Nucleotide solution then replaced solution above the condensates by gravity flow. Time lapses were recorded for two h. Finally, time lapses in Fig. 2.20.B-D contained 1125 nM unlabeled mononucleosomes or 45 nM 25mer, 125 nM FRET mononucleosomes and ATP regeneration system in PSB5 in total volume of 18 µL. Two µL of 10x Mg-ATP solution were added to a final concentration 1 or 5 mM, the mixture was loaded into a channel of the imaging chamber and imaged two to four min after ATP addition."

3.2.36.2 Image acquisition

"For FLIM, the same system described in "Confocal Imaging" was used. The white light laser delivered 80 MHz repetition rate at 561 nm. Arrival time of single photons was measured with the included FALCON module. The FLIM acceptor photobleaching image kept the same parameters as the confocal one with 12 frames accumulations instead. The other FLIM images and movies

size was set to 256 × 256 pixels. A 3-fold zoom factor was applied, giving a pixel size of 0.380 µm and an image size of 97 × 97 µm. Pixels number was decreased to favor imaging speed in the time-lapses. Because the statistical determination of the distribution of single photon arrival times requires a minimum number of photons, 60 frames were acquired at 2.34 Hz for each TCSPC recording, for a total time of around 26 s. Corresponding to a scanning speed of 600 Hz. Time-lapses were recorded for at least 15 min with a time point every 2 min."

3.2.36.3 Analysis

"FLIM image analyses were performed in the LAS X software and with a home-made MatLab code (available on request). Lifetime calculations were based on the Phasor approach (Digman et al., 2008)*. Phase and modulation lifetimes were calculated using the Fourier sine and cosine transforms of the lifetime images. The FRET efficiency (E_{FRET}) was calculated according to Eq. 3:*

$$E_{FRET} = 1 - \frac{\tau_{DA}}{\tau_D} \quad \textit{(Eq. 3)}$$

where τ_{DA} is the lifetime of the donor-acceptor sample, and τ_D is the lifetime of the donor alone. Results were expressed as mean ± SD. Lifetimes images shown were done using the phasor approach to maximize the number of photons while keeping a good image resolution. For the time lapse, the linear part of lifetime changes was fitted to a linear function to obtain initial velocity."

3.2.37 Holotomography

"Slide with 25mer condensates containing ISWI in PSB5 buffer was prepared as described above. Refractive index images were collected on 3D Cell Explorer-fluo (Nanolive) equipped with dry objective (60x magnification, 0.8 numerical aperture) and low power laser (λ = 520 nm, sample exposure 0.2 mW/mm^2). 96 slices were collected for a field depth of 30 µm. Software Steve v.1.6.3496 (Nanolive) was used to collect, view and export images. Data were exported as tiff files (floating values of RI) and further processed in ImageJ (Fiji). Eq. 4 was used to calculate chromatin mass concentration in condensates, where n = refractive index, c = mass concentration and dn/dc is a refractive index increment. We assumed $c_{condensate} >> c_{solution}$ and dn/dc to be 0.185 mL/g."

$$n_{condensate} - n_{solution} = \frac{dn}{dc} * (c_{condensate} - c_{solution}) \textit{(Eq. 4)}$$

3.2.38 ISWI-GFP and 25mer-Cy3 FRAP

"Four µL of 2.5x mixture of unlabelled chromatin, labelled chromatin and ISWI-GFP were mixed with six µL 1.7xPSB5 containing 1.7xnucleotide. Final experimental conditions were: 76 nM 25mer, 1.75 nM Cy3-25mer, 1 µM ISWI-GFP, 0.77 mM Mg-nucleotide, PSB5, ATP regeneration system (Fig. 2.21.C); 15 nM 25mer-Cy3, 375 nM ISWI-GFP, PSB5, 1 mM Mg-ATP/no nucleotide (Fig. 2.21.B); 100 nM 25mer, 4.5 nM 25mer-Cy3, 1.3 µM ISWI-GFP, PSB5, ATP regeneration system, 1 mM Mg-ATP (Fig. 2.21.A). The sample was incubated for 1 min and then loaded onto the slide, spun, sealed as above and imaged within 30 minutes of preparation.

Images were acquired at 26°C with a 63X glycerol immersion objective on a Leica Sp5 confocal microscope equipped with Argon 488 nm and DPSS 561 nm lasers. For ISWI-GFP FRAP, 10 frames (512x512 pixel) at 1.2 s intervals were taken as a pre-bleach reference, followed by a single 1.2 s bleaching pulse targeted to a circular region within ≥ 3 droplets at once. After bleaching, 89 frames were taken at 1.2 s intervals to measure fluorescence recovery. For H4-Cy3 FRAP,

10 frames (512x512 pixel) at 1.2 s intervals were taken as pre-bleach reference, followed by four 1.2 s bleaching pulses targeted to a circular region within ≥ 3 droplets at once. After bleaching, 20 frames were taken at 30 s intervals to measure fluorescence recovery. For both cases, bright-field images were also collected in parallel.

All images were processed using Fiji (Schindelin et al., 2012)*. First, drift was corrected using MultiStackReg package (https://biii.eu/multistackreg) by calculating transformation matrices from brightfield images (code available on request). Bleach, control (within droplet but outside the bleached region) and background Region Of Interest (ROIs) were manually defined, and average fluorescence intensity was measured. Intensities were normalized using the easyFRAP web tool* (Koulouras et al., 2018) *to generate FRAP curves with full scale normalization. Normalized FRAP curves from different droplets within the same experiment were considered as technical replicates. FRAP curves from different experiments were averaged and reported together with standard error of the mean (SEM). Plots were generated using R – version 4.2.1 (https://www.R-project.org/)* (R Core Team, 2022)*."*

3.2.39 Controlled condensate fusion with optical tweezers

"Four µL of chromatin ISWI mixture (225 nM 13mer, 585 nM ISWI, volume was made up with TE pH 7.6) was gently mixed with 6 µL 1.7xPSB1 containing 1.7xnucleotide. Final experimental conditions were: 90 nM 13mer, 234 nM ISWI, 1 mM Mg-nucleotide and ATP regeneration system in 1xPSB1. Data on fusion velocity with different ISWI concentrations were collected in 1xPSB1 supplemented with 5 mM DTT. Of note, with an ATP-regeneration system present, slow fusion was detected with AMPPNP and ADPBeFx, presumably due to ADP contamination present in nucleotide preparations. Samples were incubated for 1 min and then loaded onto prepared slides. Optical tweezer experiments were carried out on a dual-trap C-Trap (Lumicks, Amsterdam). For controlled fusion of condensates, a single condensate was trapped in each of the optical traps at minimal laser power. The traps were approached in 20 nm steps until the condensates touched and fusion started which was determined by observation of the force signal. During fusion, the trap distance was then held constant. Fusion was further monitored by brightfield microscopy.

Analysis was performed using custom written code for the IGOR Pro 8 software (WaveMetrics, USA). Fusion velocity was determined by fitting a generalized logistic function (Eq. 5) to the differential force data along the x-axis. With F(start) and F(finish) the differential forces before fusion onset and after finished fusion, respectively.

$$F(x) = F(finish) + \frac{F(start) - F(finish)}{1 + e^{\left(\frac{t - t_0}{\tau}\right)^{\gamma}}} \quad \textit{(Eq. 5)}$$

The force was then normalized so that F(start)=0 and F(finish)=1. The fusion velocity was determined as the slope of the tangent fitted to the normalized force data at the inflection point of the fitted function. As the fusion velocity is inversely proportional to the size of the condensates, the obtained velocity was normalized using the mean size of the two fused condensates which was obtained using radial profiling of the brightfield videos pre-fusion. For comparison between conditions velocities were transformed into the log10-fold change relative to the mean of the chromatin only condition. Statistical significance of the velocity changes was determined by t-test. Data is visualized in boxplots showing the median ± quartiles, with whiskers indicating the 9th and 91st percentile."

3.2.40 ThT fluorescence measurement

"ThT fluorescence intensity was measured with increasing ISWI concentrations with 90 nM 13mer in modified PSB (supplemented with 2 mM $MgCl_2$, 2.5 mM DTT and 40 µM ThT)."

3.2.41 Side-specific Crosslinking

ISWI and nucleosomes were mixed in 20 mM Tris-HCl pH 7.7, 0.1 mM EDTA pH 8.0, 0.5 mM $MgCl_2$ (added only if the nucleotide was used), 140 mM KCl, 3 mM DTT with or without nucleotide. At first the enzyme was thawed, mixed well, spun (15 min, 13200 rpm, 4°C) and transferred in a new tube. 30 µL of crosslinking reaction was prepared for each type of nucleosome. Components are pipetted in the following order: Mono0, Mono2000 (to set KCl concentration), DTT, $MgCl_2$, ISWI, nucleosomes and Mg-ADP or Mg-AMPPNP. For Mg-ADPBeF_x or Mg-ADPAlF_4, ADP was added first (final concentration 0.5 mM). Then after short incubation, $BeSO_4$ (final concentration 0.6 mM) or $Al_2(SO_4)_3$ (final concentration 0.3 mM) were added, respectively. Few minutes was allowed for ions to bind to nucleotide and then NaF was added (final concentration 2.5 mM). For the experiment where 1.5 mM of ADP was used, triple final concentrations of $BeSO_4$ (1.8 mM), $Al_2(SO_4)_3$ (0.9 mM) and NaF (7.5 mM) were added. The mixture was mixed well and 15 µL was pipetted in wells of a 384 plate, crosslinked on ice for 120 min in the UV crosslinker (wavelength: 365 nm). After crosslinking, acidic protein precipitation was performed as follows to remove nucleotides. Samples (15 µL) were transferred into Eppendorf tubes and to each sample were added: 185 µL Mono0 buffer, 20 µL of 1% sodium deoxycholate and 40 µL of 50% TCA. Samples were mixed and incubated at room temperature for 15 min followed by centrifugation (15 min, 13200 rpm, 4°C). Supernatant was discarded and 200 µL acetone was added to the pellet, incubated 15 min at -20°C followed by centrifugation (15 min, 13200 rpm, 4°C). Supernatant was removed and the pellet was dissolved in 10 µL Mono0 and 15 µL 5xSDS loading buffer. Samples were boiled and analyzed by SDS-PAGE.

3.2.42 Data visualization

Affinity Illustrator was used to prepare figures presented in this thesis.

References

Abdulhay, J., Hsieh, L. J., McNally, C. P., Ketavarapu, M., Kasinathan, S., Nanda, A. S., Ostrowski, M. S., Wu, K., Moore, C. M., Goodarzi, H., Narlikar, G. J. & Ramani, V. (2021). Single-fiber nucleosome density shapes the regulatory output of a mammalian chromatin remodeling enzyme. *BioRxiv*. https://doi.org/10.1101/2021.12.10.472156

Abdulhay, N. J., McNally, C. P., Hsieh, L. J., Kasinathan, S., Keith, A., Estes, L. S., Karimzadeh, M., Underwood, J. G., Goodarzi, H., Narlikar, G. J. & Ramani, V. (2020). Massively multiplex single-molecule oligonucleosome footprinting. *ELife*, *9*, 1–23. https://doi.org/10.7554/ELIFE.59404

Ahmed, K., Dehghani, H., Rugg-Gunn, P., Fussner, E., Rossant, J. & Bazett-Jones, D. P. (2010). Global chromatin architecture reflects pluripotency and lineage commitment in the early mouse embryo. *PLoS ONE*, *5*(5). https://doi.org/10.1371/journal.pone.0010531

Ahn, J. H., Davis, E. S., Daugird, T. A., Zhao, S., Quiroga, I. Y., Uryu, H., Li, J., Storey, A. J., Tsai, Y. H., Keeley, D. P., Mackintosh, S. G., Edmondson, R. D., Byrum, S. D., Cai, L., Tackett, A. J., Zheng, D., Legant, W. R., Phanstiel, D. H. & Wang, G. G. (2021). Phase separation drives aberrant chromatin looping and cancer development. *Nature*, *595*(7868), 591–595. https://doi.org/10.1038/S41586-021-03662-5

Alberti, S. & Carra, S. (2018). Quality Control of Membraneless Organelles. *Journal of Molecular Biology*, *430*(23), 4711–4729. https://doi.org/10.1016/J.JMB.2018.05.013

Alberti, S., Gladfelter, A. & Mittag, T. (2019). Considerations and Challenges in Studying Liquid-Liquid Phase Separation and Biomolecular Condensates. *Cell*, *176*(3), 419–434. https://doi.org/10.1016/j.cell.2018.12.035

Alén, C., Kent, N. A., Jones, H. S., O'Sullivan, J., Aranda, A. & Proudfoot, N. J. (2002). A role for chromatin remodeling in transcriptional termination by RNA polymerase II. *Molecular Cell*, *10*(6), 1441–1452. https://doi.org/10.1016/S1097-2765(02)00778-5

Allahverdi, A., Chen, Q., Korolev, N. & Nordenskiöld, L. (2015). Chromatin compaction under mixed salt conditions: Opposite effects of sodium and potassium ions on nucleosome array folding. *Scientific Reports*, *5*. https://doi.org/10.1038/srep08512

Allshire, R. C. & Ekwall, K. (2015). Epigenetic Regulation of Chromatin States in Schizosaccharomyces pombe. *Cold Spring Harb Perspect Biol*, *7*. https://doi.org/10.1101/cshperspect.a018770

Allshire, R. C., Javerzat, J. P., Redhead, N. J. & Cranston, G. (1994). Position effect variegation at fission yeast centromeres. *Cell*, *76*(1), 157–169. https://doi.org/10.1016/0092-8674(94)90180-5

Allshire, R. C. & Madhani, H. D. (2017). Ten principles of heterochromatin formation and function. *Nature Publishing Group*, *19*. https://doi.org/10.1038/nrm.2017.119

Allshire, R. C., Nimmo, E. R., Ekwall, K., Javerzat, J. P. & Cranston, G. (1995). Mutations derepressing silent centromeric domains in fission yeast disrupt chromosome segregation. In *Genes and Development* (Vol. 9, Issue 2). https://doi.org/10.1101/gad.9.2.218

Al-Sady, B., Madhani, H. D. & Narlikar, G. J. (2013). Division of labor between the chromodomains of HP1 and Suv39 methylase enables coordination of heterochromatin spread. *Molecular Cell*, *51*(1), 80–91. https://doi.org/10.1016/J.MOLCEL.2013.06.013

Alshareedah, I., Kaur, T., Ngo, J., Seppala, H., Kounatse, L. A. D., Wang, W., Moosa, M. M. & Banerjee, P. R. (2019). Interplay between Short-Range Attraction and Long-Range Repulsion Controls Reentrant Liquid Condensation of Ribonucleoprotein-RNA Complexes [Research-article]. *Journal of the American Chemical Society*, *141*(37), 14593–14602. https://doi.org/10.1021/jacs.9b03689

Altmeyer, M., Neelsen, K. J., Teloni, F., Pozdnyakova, I., Pellegrino, S., Grøfte, M., Rask, M. B. D., Streicher, W., Jungmichel, S., Nielsen, M. L. & Lukas, J. (2015). Liquid demixing of intrinsically disordered proteins is seeded by poly(ADP-ribose). *Nature Communications 2015 6:1*, *6*(1), 1–12. https://doi.org/10.1038/ncomms9088

Aoyagi, S. & Hayes, J. J. (2002). hSWI/SNF-Catalyzed Nucleosome Sliding Does Not Occur Solely via a Twist-Diffusion Mechanism. *Molecular and Cellular Biology*, *22*(21), 7484–7490. https://doi.org/10.1128/MCB.22.21.7484-7490.2002

Armache, J. P., Gamarra, N., Johnson, S. L., Leonard, J. D., Wu, S., Narlikar, G. J. & Cheng, Y. (2019). Cryo-EM structures of remodeler-nucleosome intermediates suggest allosteric control through the nucleosome. *ELife*, *8*. https://doi.org/10.7554/ELIFE.46057

Armstrong, J. A., Papoulas, O., Daubresse, G., Sperling, A. S., Lis, J. T., Scott, M. P. & Tamkun, J. W. (2002). The Drosophila BRM complex facilitates global transcription by RNA polymerase II. *EMBO Journal*, *21*(19), 5245–5254. https://doi.org/10.1093/EMBOJ/CDF517

Asturias, F. J., Chung, W. H., Kornberg, R. D. & Lorch, Y. (2002). Structural analysis of the RSC chromatin-remodeling complex. *Proceedings of the National Academy of Sciences of the United States of America*, *99*(21), 13477–13480. https://doi.org/10.1073/PNAS.162504299/ASSET/66F0CB20-A21B-4ED9-86EE-F8DDCFE0015C/ASSETS/GRAPHIC/PQ2125042004.JPEG

Audergon, P. N. C. B., Catania, S., Kagansky, A., Tong, P., Shukla, M., Pidoux, A. L. & Allshire, R. C. (2015). Epigenetics. Restricted epigenetic inheritance of H3K9 methylation. *Science (New York, N.Y.)*, *348*(6230), 132–135. https://doi.org/10.1126/SCIENCE.1260638

Audugé, N., Audugé, A., Padilla-Parra, S., Tramier, M., Borghi, N., Ma¨ıt´, M. M. & Coppey-Moisan, M. (2019). Chromatin condensation fluctuations rather than steady-state predict chromatin accessibility. *Nucleic Acids Research*, *47*(12), 6184–6194. https://doi.org/10.1093/nar/gkz373

Bagshaw, C. R. (2001). ATP analogues at a glance. *Journal of Cell Science*, *114*(3), 459–460. https://doi.org/10.1242/JCS.114.3.459

Baldi, S., Korber, P. & Becker, P. B. (2020). Beads on a string—nucleosome array arrangements and folding of the chromatin fiber. *Nature Structural and Molecular Biology*, *27*(2), 109–118. https://doi.org/10.1038/S41594-019-0368-X

Baldi, S., Krebs, S., Blum, H. & Becker, P. B. (2018). Genome-wide measurement of local nucleosome array regularity and spacing by nanopore sequencing. *Nature Structural and Molecular Biology*, *25*(9), 894–901. https://doi.org/10.1038/s41594-018-0110-0

Banani, S. F., Lee, H. O., Hyman, A. A. & Rosen, M. K. (2017). Biomolecular condensates: Organizers of cellular biochemistry. *Nature Reviews Molecular Cell Biology*, *18*(5), 285–298. https://doi.org/10.1038/nrm.2017.7

Banani, S. F., Rice, A. M., Peeples, W. B., Lin, Y., Jain, S., Parker, R. & Rosen, M. K. (2016). Compositional Control of Phase-Separated Cellular Bodies. *Cell*, *166*(3), 651–663. https://doi.org/10.1016/j.cell.2016.06.010

Banjade, S. & Rosen, M. K. (2014). Phase transitions of multivalent proteins can promote clustering of membrane receptors. *ELife*, *3*, 1–24. https://doi.org/10.7554/eLife.04123

Barisic, D., Stadler, M. B., Iurlaro, M. & Schübeler, D. (2019). Mammalian ISWI and SWI/SNF selectively mediate binding of distinct transcription factors. *Nature*, *569*(7754), 136. https://doi.org/10.1038/S41586-019-1115-5

Bascom, G. D., Sanbonmatsu, K. Y. & Schlick, T. (2016). Mesoscale Modeling Reveals Hierarchical Looping of Chromatin Fibers Near Gene Regulatory Elements. *J. Phys. Chem. B*, *120*, 43. https://doi.org/10.1021/acs.jpcb.6b03197

Bascom, G. D. & Schlick, T. (2018). Chromatin Fiber Folding Directed by Cooperative Histone Tail Acetylation and Linker Histone Binding. *Biophysical Journal*, *114*(10), 2376–2385. https://doi.org/10.1016/J.BPJ.2018.03.008

Bazett-Jones, D. P., Coˆté, J., Coˆté, C., Landel, C. C., Peterson, C. L. & Workman, J. L. (1999). The SWI/SNF Complex Creates Loop Domains in DNA and Polynucleosome Arrays and Can Disrupt DNA-Histone Contacts within These Domains. *Molecular and Cellular Biology*, *19*(2), 1470–1478. https://doi.org/10.1128/MCB.19.2.1470

Belmont, A. S., Sedat, J. W. & Agard, D. A. (1987). A three-dimensional approach to mitotic chromosome structure: evidence for a complex hierarchical organization. *Journal of Cell Biology*, *105*(1), 77–92. https://doi.org/10.1083/JCB.105.1.77

Belmont, Andrew S, Braunfeld, M. B., Sedat, J. W. & Agard, D. A. (1989). Large-scale chromatin structural domains within mitotic and interphase chromosomes in vivo and in vitro. *Chromosoma*, *98*(2), 129–143. https://doi.org/10.1007/BF00291049

Belmont, Andrew S & Bruce, K. (1994). Visualization of G1 chromosomes: A folded, twisted, supercoiled chromonema model of interphase chromatid structure. *Journal of Cell Biology*, *127*(2), 287–302. https://doi.org/10.1083/jcb.127.2.287

Berman, H. M., Westbrook, J., Feng, Z., Gilliland, G., Bhat, T. N., Weissig, H., Shindyalov, I. N. & Bourne, P. E. (2000). The Protein Data Bank. *Nucleic Acids Research*, *28*(1), 235–242. https://doi.org/10.1093/NAR/28.1.235

Bernard, P., Maure, J. F., Partridge, J. F., Genier, S., Javerzat, J. P. & Allshire, R. C. (2001). Requirement of heterochromatin for cohesion at centromeres. *Science (New York, N.Y.)*, *294*(5551), 2539–2542. https://doi.org/10.1126/SCIENCE.1064027

Berry, J., Weber, S. C., Vaidya, N., Haataja, M., Brangwynne, C. P. & Weitz, D. A. (2015). RNA transcription modulates phase transition-driven nuclear body assembly. *Proceedings of the National Academy of Sciences of the United States of America*, *112*(38), E5237–E5245. https://doi.org/10.1073/PNAS.1509317112/SUPPL_FILE/PNAS.201509317SI.PDF

Beseda, T., Cápal, P., Kubalová, I., Schubert, V., Doležel, J. & Šimková, H. (2020). Mitotic chromosome organization: General rules meet species-specific variability. In *Computational and Structural Biotechnology Journal* (Vol. 18, pp. 1311–1319). https://doi.org/10.1016/j.csbj.2020.01.006

Bhardwaj, S. K., Hailu, S. G., Olufemi, L., Brahma, S., Kundu, S., Hota, S. K., Persinger, J. & Bartholomew, B. (2020). Dinucleosome specificity and allosteric switch of the ISW1a ATP-dependent chromatin remodeler in transcription regulation. *Nature Communications*. https://doi.org/10.1038/s41467-020-19700-1

Bi, X. (2012). Functions of chromatin remodeling factors in heterochromatin formation and maintenance. *Science China. Life Sciences*, *55*(1), 89–96. https://doi.org/10.1007/S11427-012-4267-1

Bintu, B., Mateo, L. J., Su, J. H., Sinnott-Armstrong, N. A., Parker, M., Kinrot, S., Yamaya, K., Boettiger, A. N. & Zhuang, X. (2018). Super-resolution chromatin tracing reveals domains and cooperative interactions in single cells. *Science*, *362*(6413). https://doi.org/10.1126/SCIENCE.AAU1783/SUPPL_FILE/AAU1783_TABLE_S2.XLSX

Bisht, K. K., Arora, S., Ahmed, S. & Singh, J. (2008). Role of heterochromatin in suppressing subtelomeric recombination in fission yeast. *Yeast (Chichester, England)*, *25*(8), 537–548. https://doi.org/10.1002/YEA.1603

Biswas, D., Takahata, S., Xin, H., Dutta-Biswas, R., Yu, Y., Formosa, T. & Stillman, D. J. (2008). A role for Chd1 and Set2 in negatively regulating DNA replication in Saccharomyces cerevisiae. *Genetics*, *178*(2), 649–659. https://doi.org/10.1534/genetics.107.084202

Bjerling, P., Silverstein, R. A., Thon, G., Caudy, A., Grewal, S. & Ekwall, K. (2002). Functional Divergence between Histone Deacetylases in Fission Yeast by Distinct Cellular Localization and In Vivo Specificity. *MOLECULAR AND CELLULAR BIOLOGY*, *22*(7), 2170–2181. https://doi.org/10.1128/MCB.22.7.2170-2181.2002

Bloomfield, V. A. (1991). Condensation of DNA by multivalent cations: Considerations on mechanism. *Biopolymers*, *31*(13), 1471–1481. https://doi.org/10.1002/bip.360311305

Blosser, T. R., Yang, J. G., Stone, M. D., Narlikar, G. J. & Zhuang, X. (2009). Dynamics of nucleosome remodelling by individual ACF complexes. *Nature*, *462*, 1022–1027. https://doi.org/10.1038/nature08627

Boettiger, A. N., Bintu, B., Moffitt, J. R., Wang, S., Beliveau, B. J., Fudenberg, G., Imakaev, M., Mirny, L. A., Wu, C. T. & Zhuang, X. (2016). Super-resolution imaging reveals distinct chromatin folding for different epigenetic states. *Nature*, *529*(7586), 418–422. https://doi.org/10.1038/NATURE16496

Boija, A., Klein, I. A., Sabari, B. R., Dall'Agnese, A., Coffey, E. L., Zamudio, A. v., Li, C. H., Shrinivas, K., Manteiga, J. C., Hannett, N. M., Abraham, B. J., Afeyan, L. K., Guo, Y. E., Rimel, J. K., Fant, C. B., Schuijers, J., Lee, T. I., Taatjes, D. J. & Young, R. A. (2018). Transcription factors activate genes through the phase separation capacity of their activation domains. *Cell*, *175*(7), 1842. https://doi.org/10.1016/J.CELL.2018.10.042

Bourgo, R. J., Siddiqui, H., Fox, S., Solomon, D., Sansam, C. G., Yaniv, M., Muchardt, C., Metzger, D., Chambon, P., Roberts, C. W. M. & Knudsen, E. S. (2009). SWI/SNF deficiency results in aberrant chromatin organization, mitotic failure, and diminished proliferative capacity. *Molecular Biology of the Cell*, *20*(14), 3192–3199. https://doi.org/10.1091/MBC.E08-12-1224

Bowman, G. D. & Deindl, S. (2019). Remodeling the genome with DNA twists. In *Science* (Vol. 366, Issue 6461, pp. 35–36). American Association for the Advancement of Science. https://doi.org/10.1126/science.aay4317

Bowman, G. D. & Jenkins, T. C. (2010). Mechanisms of ATP-Dependent Nucleosome Sliding. *Curr Opin Struct Biol.* https://doi.org/10.1016/j.sbi.2009.12.002

Bozhenok, L., Wade, P. A. & Varga-Weisz, P. (2002). WSTF-ISWI chromatin remodeling complex targets heterochromatic replication foci. *EMBO Journal*, *21*(9), 2231–2241. https://doi.org/10.1093/EMBOJ/21.9.2231

Brady, J. P., Farber, P. J., Sekhar, A., Lin, Y. H., Huang, R., Bah, A., Nott, T. J., Chan, H. S., Baldwin, A. J., Forman-Kay, J. D. & Kay, L. E. (2017). Structural and hydrodynamic properties of an intrinsically disordered region of a germ cell-specific protein on phase separation. *Proceedings of the National Academy of Sciences of the United States of America*, *114*(39), E8194–E8203. https://doi.org/10.1073/PNAS.1706197114/SUPPL_FILE/PNAS.201706197SI.PDF

Brahma, S., Udugama, M. I., Kim, J., Hada, A., Bhardwaj, S. K., Hailu, S. G., Lee, T. H. & Bartholomew, B. (2017). INO80 exchanges H2A.Z for H2A by translocating on DNA proximal to histone dimers. *Nature Communications*, *8*. https://doi.org/10.1038/NCOMMS15616

Brandani, G. B., Niina, T., Tan, C. & Takada, S. (2018). DNA sliding in nucleosomes via twist defect propagation revealed by molecular simulations. *Nucleic Acids Research*, *46*(6), 2788–2801. https://doi.org/10.1093/nar/gky158

Brangwynne, Clifford P., Eckmann, C. R., Courson, D. S., Rybarska, A., Hoege, C., Gharakhani, J., Jülicher, F. & Hyman, A. A. (2009). Germline P granules are liquid droplets that localize by controlled dissolution/condensation. *Science*, *324*(5935), 1729–1732. https://doi.org/10.1126/SCIENCE.1172046/SUPPL_FILE/BRANGWYNNE.SOM.PDF

Brangwynne, Clifford P., Mitchison, T. J. & Hyman, A. A. (2011). Active liquid-like behavior of nucleoli determines their size and shape in Xenopus laevis oocytes. *Proceedings of the National Academy of Sciences of the United States of America*, *108*(11), 4334–4339. https://doi.org/10.1073/pnas.1017150108

Brangwynne, Cliiord P, Tompa, P., Pappu, R. v, St Louis, in & Louis, S. (2015). Polymer physics of intracellular phase transitions. *Nature Physics*. https://doi.org/10.1038/NPHYS3532

Brehm, A., Längst, G., Kehle, J., Clapier, C. R., Imhof, A., Eberharter, A., Müller, J. & Becker, P. B. (2000). DMi-2 and ISWI chromatin remodelling factors have distinct nucleosome binding and mobilization properties. *EMBO Journal*, *19*(16), 4332–4341. https://doi.org/10.1093/EMBOJ/19.16.4332

Brown, S. A., Imbalzano, A. N. & Kingston, R. E. (1996). Activator-dependent regulation of transcriptional pausing on nucleosomal templates. *Genes and Development*, *10*(12), 1479–1490. https://doi.org/10.1101/gad.10.12.1479

Bühler, M., Verdel, A. & Moazed, D. (2006). Tethering RITS to a Nascent Transcript Initiates RNAi- and Heterochromatin-Dependent Gene Silencing. *Cell*, *125*(5), 873–886. https://doi.org/10.1016/J.CELL.2006.04.025

Buker, S. M., Iida, T., Bühler, M., Villén, J., Gygi, S. P., Nakayama, J. I. & Moazed, D. (2007). Two different Argonaute complexes are required for siRNA generation and heterochromatin assembly in fission yeast. *Nature Structural & Molecular Biology*, *14*(3), 200–207. https://doi.org/10.1038/NSMB1211

Cam, H. P., Sugiyama, T., Chen, E. S., Chen, X., FitzGerald, P. C. & Grewal, S. I. S. (2005). Comprehensive analysis of heterochromatin- and RNAi-mediated epigenetic control of the fission yeast genome. *Nature Genetics*, *37*(8), 809–819. https://doi.org/10.1038/NG1602

Cam, H. P. & Whitehall, S. (2016). Reporter gene silencing assays in fission yeast. *Cold Spring Harbor Protocols*, *2016*(10), 847–849. https://doi.org/10.1101/pdb.prot091512

Caragine, C. M., Haley, S. C. & Zidovska, A. (2018). Surface Fluctuations and Coalescence of Nucleolar Droplets in the Human Cell Nucleus. *Physical Review Letters*, *121*(14). https://doi.org/10.1103/PHYSREVLETT.121.148101

Carmen Morán, M., Graça Miguel, M. & Lindman, B. (2007). *DNA Gel Particles: Particle Preparation and Release Characteristics*. https://doi.org/10.1021/la700672e

Castellana, M., Wilson, M. Z., Xu, Y., Joshi, P., Cristea, I. M., Rabinowitz, J. D., Gitai, Z. & Wingreen, N. S. (2014). Enzyme clustering accelerates processing of intermediates through metabolic channeling. *Nature Biotechnology*, *32*(10), 1011–1018. https://doi.org/10.1038/NBT.3018

Chaban, Y., Ezeokonkwo, C., Chung, W. H., Zhang, F., Kornberg, R. D., Maier-Davis, B., Lorch, Y. & Asturias, F. J. (2008). Structure of a RSC–nucleosome complex and insights into chromatin remodeling. *Nature Structural & Molecular Biology*, *15*(12), 1272. https://doi.org/10.1038/NSMB.1524

Chereji, R. v., Bryson, T. D. & Henikoff, S. (2019). Quantitative MNase-seq accurately maps nucleosome occupancy levels. *Genome Biology*, *20*(1), 198. https://doi.org/10.1186/S13059-019-1815-Z/FIGURES/10

Chittori, S., Hong, J., Bai, Y. & Subramaniam, S. (2019). Structure of the primed state of the ATPase domain of chromatin remodeling factor ISWI bound to the nucleosome. *Nucleic Acids Research*, *47*(17), 9400–9409. https://doi.org/10.1093/nar/gkz670

Cho, W. K., Spille, J. H., Hecht, M., Lee, C., Li, C., Grube, V. & Cisse, I. I. (2018). Mediator and RNA polymerase II clusters associate in transcription-dependent condensates. *Science*, *361*(6400), 412–415. https://doi.org/10.1126/science.aar4199

Chung, I., Leonhardt, H. & Rippe, K. (2011). De novo assembly of a PML nuclear subcompartment occurs through multiple pathways and induces telomere elongation. *Journal of Cell Science*, *124*(21), 3603–3618. https://doi.org/10.1242/JCS.084681

Clapier, C. R. & Cairns, B. R. (2009). The biology of chromatin remodeling complexes. *Annual Review of Biochemistry*, *78*, 273–304. https://doi.org/10.1146/annurev.biochem.77.062706.153223

Clapier, C. R. & Cairns, B. R. (2012). Regulation of ISWI involves inhibitory modules antagonized by nucleosomal epitopes. *Nature*, *492*. https://doi.org/10.1038/nature11625

Clapier, C. R., Iwasa, J., Cairns, B. R. & Peterson, C. L. (2017). Mechanisms of action and regulation of ATP-dependent chromatin-remodelling complexes. *Nature Publishing Group*, *18*. https://doi.org/10.1038/nrm.2017.26

Clapier, C. R., Nightingale, K. P. & Becker, P. B. (2002). A critical epitope for substrate recognition by the nucleosome remodeling ATPase ISWI. In *Nucleic Acids Research* (Vol. 30, Issue 3).

Clapier, C. R., v Corona, D. F., Becker, P. B., Nightingale, K. P. & Programme, I. (2001). Critical Role for the Histone H4 N Terminus in Nucleosome Remodeling by ISWI. *MOLECULAR AND CELLULAR BIOLOGY*, *21*(3), 875–883. https://doi.org/10.1128/MCB.21.3.875-883.2001

Clausell, J., Happel, N., Hale, T. K., Doenecke, D. & Beato, M. (2009). Histone H1 Subtypes Differentially Modulate Chromatin Condensation without Preventing ATP-Dependent Remodeling by SWI/SNF or NURF. *PLOS ONE*, *4*(10), e0007243. https://doi.org/10.1371/JOURNAL.PONE.0007243

Collins, N., Poot, R. A., Kukimoto, I., García-Jiménez, C., Dellaire, G. & Varga-Weisz, P. D. (2002). An ACF1-ISWI chromatin-remodeling complex is required for DNA replication through heterochromatin. *Nature Genetics*, *32*(4), 627–632. https://doi.org/10.1038/NG1046

Colmenares, S. U., Buker, S. M., Buhler, M., Dlakić, M. & Moazed, D. (2007). Coupling of Double-Stranded RNA Synthesis and siRNA Generation in Fission Yeast RNAi. *Molecular Cell*, *27*(3), 449–461. https://doi.org/10.1016/J.MOLCEL.2007.07.007

Corona, D. F. V., Längst, G., Clapier, C. R., Bonte, E. J., Ferrari, S., Tamkun, J. W. & Becker, P. B. (1999). ISWI is an ATP-dependent nucleosome remodeling factor. *Molecular Cell*, *3*(2), 239–245. https://doi.org/10.1016/S1097-2765(00)80314-7

Corona, D. F. V., Siriaco, G., Armstrong, J. A., Snarskaya, N., McClymont, S. A., Scott, M. P. & Tamkun, J. W. (2007). ISWI Regulates Higher-Order Chromatin Structure and Histone H1 Assembly In Vivo. *PLoS Biology*, *5*(9), 2011–2021. https://doi.org/10.1371/JOURNAL.PBIO.0050232

Creamer, K. M., Job, G., Shanker, S., Neale, G. A., Lin, Y., Bartholomew, B. & Partridge, J. F. (2014). The Mi-2 homolog Mit1 actively positions nucleosomes within heterochromatin to suppress transcription. *Molecular and Cellular Biology*, *34*(11), 2046–2061. https://doi.org/10.1128/MCB.01609-13

Dang, W. & Bartholomew, B. (2007). Domain Architecture of the Catalytic Subunit in the ISW2-Nucleosome Complex. *Molecular and Cellular Biology*, *27*(23), 8306–8317. https://doi.org/10.1128/MCB.01351-07

Dang, W., Kagalwala, M. N. & Bartholomew, B. (2006). Regulation of ISW2 by Concerted Action of Histone H4 Tail and Extranucleosomal DNA. *Molecular and Cellular Biology*, *26*(20), 7388–7396. https://doi.org/10.1128/MCB.01159-06/ASSET/4704FBD3-0CF1-4456-BE62-66DCECCEBB25/ASSETS/GRAPHIC/ZMB0200662910008.JPEG

Dann, geoffrey P., Liszczak, glen P., Bagert, J. D., Müller, M. M., Nguyen, uyen, Wojcik, F., Brown, Z. Z., Bos, J., Panchenko, tatyana, Pihl, R., Pollock, samuel B., Diehl, K. L., David allis, C. & Muir, tom W. (2017). *ISWI chromatin remodellers sense nucleosome modifications to determine substrate preference*. https://doi.org/10.1038/nature23671

Dao, H. T., Dul, B. E., Dann, G. P., Liszczak, G. P. & Muir, T. W. (2020). A basic motif anchoring ISWI to nucleosome acidic patch regulates nucleosome spacing. *Nature Chemical Biology*, *16*(2), 134–142. https://doi.org/10.1038/S41589-019-0413-4

Das, R. K., Huang, Y., Phillips, A. H., Kriwacki, R. W. & Pappu, R. v. (2016). Cryptic sequence features within the disordered protein p27Kip1 regulate cell cycle signaling. *Proceedings of the National Academy of Sciences of the United States of America*, *113*(20), 5616–5621. https://doi.org/10.1073/PNAS.1516277113

Davis, B. W., Aumiller, W. M., Hashemian, N., An, S., Armaou, A. & Keating, C. D. (2015). Colocalization and Sequential Enzyme Activity in Aqueous Biphasic Systems: Experiments and Modeling. *Biophysical Journal*, *109*(10), 2182–2194. https://doi.org/10.1016/J.BPJ.2015.09.020

De La Fuente, R., Viveiros, M. M., Wigglesworth, K. & Eppig, J. J. (2004). ATRX, a member of the SNF2 family of helicase/ATPases, is required for chromosome alignment and meiotic spindle organization in metaphase II stage mouse oocytes. *Developmental Biology*, *272*(1), 1–14. https://doi.org/10.1016/J.YDBIO.2003.12.012

Dechassa, M. L., Sabri, A., Pondugula, S., Kassabov, S. R., Chatterjee, N., Kladde, M. P. & Bartholomew, B. (2010). SWI/SNF Has Intrinsic Nucleosome Disassembly Activity that Is Dependent on Adjacent Nucleosomes. *Molecular Cell*, *38*(4), 590–602. https://doi.org/10.1016/J.MOLCEL.2010.02.040

Deindl, S., Hwang, W. L., Hota, S. K., Blosser, T. R., Prasad, P., Bartholomew, B. & Zhuang, X. (2013). ISWI Remodelers Slide Nucleosomes with Coordinated Multi-Base-Pair Entry Steps and Single-Base-Pair Exit Steps. *Cell*, *152*(3), 442–452. https://doi.org/10.1016/J.CELL.2012.12.040

Demeler, B. & Gorbet, G. E. (2016). Analytical Ultracentrifugation Data Analysis with UltraScan-III. In S. Uchiyama, F. Arisaka, W. Stafford & T. (eds.) Laue (Eds.), *Analytical Ultracentrifugation* (pp. 119–143). Springer.

Deryusheva, S. & Gall, J. G. (2009). Small Cajal Body–specific RNAs of Drosophila Function in the Absence of Cajal Bodies. *Molecular Biology of the Cell*, *20*(24), 5250. https://doi.org/10.1091/MBC.E09-09-0777

Deuring, R., Fanti, L., Armstrong, J. A., Sarte, M., Papoulas, O., Prestel, M., Daubresse, G., Verardo, M., Moseley, S. L., Berloco, M., Tsukiyama, T., Wu, C., Pimpinelli, S. & Tamkun, J. W. (2000). The ISWI chromatin-remodeling protein is required for gene expression and the maintenance of higher order chromatin structure in vivo. *Molecular Cell*, *5*(2), 355–365. https://doi.org/10.1016/S1097-2765(00)80430-X

Dhar, A., Girdhar, K., Singh, D., Gelman, H., Ebbinghaus, S. & Gruebele, M. (2011). Protein stability and folding kinetics in the nucleus and endoplasmic reticulum of Eucaryotic Cells. *Biophysical Journal*, *101*(2), 421–430. https://doi.org/10.1016/j.bpj.2011.05.071

Dhayalan, A., Tamas, R., Bock, I., Tattermusch, A., Dimitrova, E., Kudithipudi, S., Ragozin, S. & Jeltsch, A. (2011). The ATRX-ADD domain binds to H3 tail peptides and reads the combined methylation state of K4 and K9. *Human Molecular Genetics*, *20*(11), 2195–2203. https://doi.org/10.1093/HMG/DDR107

Digman, M. A., Caiolfa, V. R., Zamai, M. & Gratton, E. (2008). The phasor approach to fluorescence lifetime imaging analysis. *Biophysical Journal*, *94*(2), 14–16. https://doi.org/10.1529/biophysj.107.120154

Ding, L., Laor, D., Weisman, R. & Forsburg, S. L. (2014). Rapid regulation of nuclear proteins by rapamycin-induced translocation in fission yeast. *Yeast (Chichester, England)*, *31*(7), 253–264. https://doi.org/10.1002/YEA.3014

Dixon, J. R., Selvaraj, S., Yue, F., Kim, A., Li, Y., Shen, Y., Hu, M., Liu, J. S. & Ren, B. (2012). Topological domains in mammalian genomes identified by analysis of chromatin interactions. *Nature*. https://doi.org/10.1038/nature11082

Dorigo, B., Schalch, T., Kulangara, A., Duda, S., Schroeder, R. R. & Richmond, T. J. (2004). Nucleosome arrays reveal the two-start organization of the chromatin fiber. *Science*, *306*(5701), 1571–1573. https://doi.org/10.1126/SCIENCE.1103124/SUPPL_FILE/DORIGO.SOM.PDF

Drobot, B., Iglesias-Artola, J. M., le Vay, K., Mayr, V., Kar, M., Kreysing, M., Mutschler, H. & Tang, T. Y. D. (2018). Compartmentalised RNA catalysis in membrane-free coacervate protocells. *Nature Communications 2018 9:1*, *9*(1), 1–9. https://doi.org/10.1038/s41467-018-06072-w

Dross, N., Spriet, C., Zwerger, M., Müller, G., Waldeck, W. & Langowski, J. (2009). Mapping eGFP Oligomer Mobility in Living Cell Nuclei. *PLOS ONE*, *4*(4), e5041. https://doi.org/10.1371/JOURNAL.PONE.0005041

Dürr, H., Flaus, A., Owen-Hughes, T. & Hopfner, K. P. (2006). Snf2 family ATPases and DExx box helicases: Differences and unifying concepts from high-resolution crystal structures. In *Nucleic Acids Research* (Vol. 34, Issue 15, pp. 4160–4167). https://doi.org/10.1093/nar/gkl540

Ehrensberger, A. H. & Kornberg, R. D. (2011). Isolation of an activator-dependent, promoter-specific chromatin remodeling factor. *Proceedings of the National Academy of Sciences of the United States of America*, *108*(25), 10115–10120. https://doi.org/10.1073/pnas.1101449108

Ekwall, K., Javerzat, J. P., Lorentz, A., Schmidt, H., Cranston, G. & Allshire, R. (1995). The chromodomain protein Swi6: a key component at fission yeast centromeres. *Science (New York, N.Y.)*, *269*(5229), 1429–1431. https://doi.org/10.1126/SCIENCE.7660126

Ekwall, K., Olsson, T., Turner, B. M., Cranston, G. & Allshire, R. C. (1997). Transient inhibition of histone deacetylation alters the structural and functional imprint at fission yeast centromeres. *Cell*, *91*(7), 1021–1032. https://doi.org/10.1016/S0092-8674(00)80492-4

Elfring, L. K., Daniel, C., Papoulas, O., Deuring, R., Sarte, M., Moseley, S., Beek, S. J., Waldrip, W. R., Daubresse, G., DePace, A., Kennison, J. A. & Tamkun, J. W. (1998). Genetic analysis of brahma: The drosophila homolog of the yeast chromatin remodeling factor SWI2/SNF2. *Genetics*, *148*(1), 251–265. https://doi.org/10.1093/genetics/148.1.251

Elgin, S. C. R. & Reuter, G. (2013). Position-Effect Variegation, Heterochromatin Formation, and Gene Silencing in Drosophila. *Cold Spring Harb Perspect Biol* . . https://doi.org/10.1101/cshperspect.a017780

Ellis, R. J. (2001). Macromolecular crowding: an important but neglected aspect of the intracellular environment. *Current Opinion in Structural Biology*, *11*(1), 114–119. https://doi.org/10.1016/S0959-440X(00)00172-X

Eltsov, M., MacLellan, K. M., Maeshima, K., Frangakis, A. S. & Dubochet, J. (2008). Analysis of cryo-electron microscopy images does not support the existence of 30-nm chromatin fibers in mitotic chromosomes in situ. *Proceedings of the National Academy of Sciences of the United States of America*, *105*(50), 19732–19737. https://doi.org/10.1073/PNAS.0810057105/SUPPL_FILE/0810057105SI.PDF

Eltsov, M., Maclellan, K. M., Maeshima, K., Frangakis, A. S. & Dubochet, J. (2008). *Analysis of cryo-electron microscopy images does not support the existence of 30-nm chromatin fibers in mitotic chromosomes in situ*. www.pnas.org/cgi/content/full/

Erdel, F. (2020). Biophysical mechanisms of chromatin patterning. In *Current Opinion in Genetics and Development* (Vol. 61, pp. 62–68). Elsevier Ltd. https://doi.org/10.1016/j.gde.2020.03.006

Erdel, F., Baum, M. & Rippe, K. (2015). The viscoelastic properties of chromatin and the nucleoplasm revealed by scale-dependent protein mobility. *Journal of Physics: Condensed Matter*, *27*(6), 064115. https://doi.org/10.1088/0953-8984/27/6/064115

Erdel, F., Rademacher, A., Vlijm, R., Tünnermann, J., Frank, L., Weinmann, R., Schweigert, E., Yserentant, K., Hummert, J., Bauer, C., Schumacher, S., al Alwash, A., Normand, C., Herten, D. P., Engelhardt, J. & Rippe, K. (2020). Mouse Heterochromatin Adopts Digital Compaction States without Showing Hallmarks of HP1-Driven Liquid-Liquid Phase Separation. *Molecular Cell*, *78*(2), 236-249.e7. https://doi.org/10.1016/j.molcel.2020.02.005

Erdel, F. & Rippe, K. (2018). Formation of Chromatin Subcompartments by Phase Separation. *Biophysical Journal*, *114*(10), 2262–2270. https://doi.org/10.1016/j.bpj.2018.03.011

Erdel, F., Schubert, T., Marth, C., Längst, G. & Rippe, K. (2010). Human ISWI chromatin-remodeling complexes sample nucleosomes via transient binding reactions and become immobilized at active sites. *Proceedings of the National Academy of Sciences of the United States of America*, *107*(46), 19873–19878. https://doi.org/10.1073/pnas.1003438107

Falk, M., Feodorova, Y., Naumova, N., Imakaev, M., Lajoie, B. R., Leonhardt, H., Joffe, B., Dekker, J., Fudenberg, G., Solovei, I. & Mirny, L. A. (2019). Heterochromatin drives compartmentalization of inverted and conventional nuclei. *Nature*, *570*(7761), 395–399. https://doi.org/10.1038/s41586-019-1275-3

Farr, S. E., Woods, E. J., Joseph, J. A., Garaizar, A. & Collepardo-Guevara, R. (2021). Nucleosome plasticity is a critical element of chromatin liquid–liquid phase separation and multivalent nucleosome interactions. *Nature Communications*, *12*(1), 1–17. https://doi.org/10.1038/s41467-021-23090-3

Fasulo, B., Deuring, R., Murawska, M., Gause, M. & Dorighi, K. M. (2012). The Drosophila Mi-2 Chromatin-Remodeling Factor Regulates Higher-Order Chromatin Structure and Cohesin Dynamics In Vivo. *PLoS Genet*, *8*(8), 1002878. https://doi.org/10.1371/journal.pgen.1002878

Feric, M., Broedersz, C. P. & Brangwynne, C. P. (2015). Soft viscoelastic properties of nuclear actin age oocytes due to gravitational creep. *Scientific Reports 2015 5:1*, *5*(1), 1–12. https://doi.org/10.1038/srep16607

Fierz, B. & Poirier, M. G. (2019). *Biophysics of Chromatin Dynamics*. https://doi.org/10.1146/annurev-biophys-070317

Filion, G. J., van Bemmel, J. G., Braunschweig, U., Talhout, W., Kind, J., Ward, L. D., Brugman, W., de Castro, I. J., Kerkhoven, R. M., Bussemaker, H. J. & van Steensel, B. (2010). Systematic Protein Location Mapping Reveals Five Principal Chromatin Types in Drosophila Cells. *Cell*, *143*(2), 212–224. https://doi.org/10.1016/j.cell.2010.09.009

Finch, J. T. & Klug, A. (1976). Solenoidal model for superstructure in chromatin (electron microscopy/packing ratio/supercoil). In *Biochemistry* (Vol. 73, Issue 6).

Flanagan, J. F. & Peterson, C. L. (1999). A role for the yeast SWI/SNF complex in DNA replication. In *Nucleic Acids Research* (Vol. 27, Issue 9).

Flaus, A., Martin, D. M. A., Barton, G. J. & Owen-Hughes, T. (2006). Identification of multiple distinct Snf2 subfamilies with conserved structural motifs. *Nucleic Acids Research*, *34*(10), 2887–2905. https://doi.org/10.1093/nar/gkl295

Flaus, A. & Richmond, T. J. (1998). Positioning and stability of nucleosomes on MMTV 3′LTR sequences. *Journal of Molecular Biology*, *275*(3), 427–441. https://doi.org/10.1006/JMBI.1997.1464

Folco, H. D., Pidoux, A. L., Urano, T. & Allshire, R. C. (2008). Heterochromatin and RNAi Are Required to Establish CENP-A Chromatin at Centromeres. *Science (New York, N.Y.)*, *319*(5859), 94. https://doi.org/10.1126/SCIENCE.1150944

Fowler, D. M., Koulov, A. v., Balch, W. E. & Kelly, J. W. (2007). Functional amyloid--from bacteria to humans. *Trends in Biochemical Sciences*, *32*(5), 217–224. https://doi.org/10.1016/J.TIBS.2007.03.003

Franklin, S. G. & Zweidler, A. (1977). Non-allelic variants of histones 2a, 2b and 3 in mammals [25]. *Nature*, *266*(5599), 273–275. https://doi.org/10.1038/266273a0

Freitag, M. (2017). Histone Methylation by SET Domain Proteins in Fungi. *Annual Review of Microbiology*, *71*, 413–439. https://doi.org/10.1146/ANNUREV-MICRO-102215-095757

Fussner, E., Strauss, M., Djuric, U., Li, R., Ahmed, K., Hart, M., Ellis, J. & Bazett-Jones, D. P. (2012). Open and closed domains in the mouse genome are configured as 10-nm chromatin fibres. *EMBO Reports*, *13*(11), 992–996. https://doi.org/10.1038/embor.2012.139

Fyodorov, D. v., Blower, M. D., Karpen, G. H. & Kadonaga, J. T. (2004). Acf1 confers unique activities to ACF/CHRAC and promotes the formation rather than disruption of chromatin in vivo. *Genes & Development*, *18*(2), 170–183. https://doi.org/10.1101/GAD.1139604

Gallego, L. D., Schneider, M., Mittal, C., Romanauska, A., Gudino Carrillo, R. M., Schubert, T., Pugh, B. F. & Köhler, A. (2020). Phase separation directs ubiquitination of gene-body nucleosomes. *Nature*, *579*(7800), 592–597. https://doi.org/10.1038/s41586-020-2097-z

Gamarra, N., Johnson, S. L., Trnka, M. J., Burlingame, A. L. & Narlikar, G. J. (2018). The nucleosomal acidic patch relieves auto-inhibition by the ISWI remodeler SNF2h. *ELife*, *7*. https://doi.org/10.7554/eLife.35322

Gangaraju, V. K. & Bartholomew, B. (2007). Dependency of ISW1a Chromatin Remodeling on Extranucleosomal DNA. *Molecular and Cellular Biology*, *27*(8), 3217–3225. https://doi.org/10.1128/MCB.01731-06

Gao, M., Nadaud, P. S., Bernier, M. W., North, J. A., Hammel, P. C., Poirier, M. G. & Jaroniec, C. P. (2013). Histone H3 and H4 N-terminal tails in nucleosome arrays at cellular concentrations probed by magic angle spinning NMR spectroscopy. *Journal of the American Chemical Society*, *135*(41), 15278–15281. https://doi.org/10.1021/JA407526S

Garcia, J. F., Dumesic, P. A., Hartley, P. D., El-Samad, H. & Madhani, H. D. (2010). Combinatorial, site-specific requirement for heterochromatic silencing factors in the elimination of nucleosome-free regions. *Genes and Development*, *24*(16), 1758–1771. https://doi.org/10.1101/gad.1946410

García Quiroz, F. & Chilkoti, A. (2015). Sequence heuristics to encode phase behaviour in intrinsically disordered protein polymers. *Nature Materials*. https://doi.org/10.1038/NMAT4418

Garcia-Ramirez, M., Rocchini, C. & Ausio, J. (1995). Modulation of chromatin folding by histone acetylation. *The Journal of Biological Chemistry*, *270*(30), 17923–17928. https://doi.org/10.1074/JBC.270.30.17923

Gavin, I., Horn, P. J. & Peterson, C. L. (2001). SWI/SNF chromatin remodeling requires changes in DNA topology. *Molecular Cell*, *7*(1), 97–104. https://doi.org/10.1016/S1097-2765(01)00158-7

Ge, E., Nora, P., Lajoie, B. R., Schulz, E. G., Giorgetti, L., Okamoto, I., Servant, N., Piolot, T., Van Berkum, N. L., Meisig, J., Sedat, J., Gribnau, J., Barillot, E., Blüthgen, N., Dekker, J. & Heard, & E. (2012). Spatial partitioning of the regulatory landscape of the X-inactivation centre. *Nature*. https://doi.org/10.1038/nature11049

Gelbart, M. E., Bachman, N., Delrow, J., Boeke, J. D. & Tsukiyama, T. (2005). Genome-wide identification of Isw2 chromatin-remodeling targets by localization of a catalytically inactive mutant. *Genes & Development*, *19*(8), 942. https://doi.org/10.1101/GAD.1298905

Ghosh, A., Zhang, X. & Zhou, H. X. (2020). Tug of war between condensate phases in a minimal macromolecular system. *Journal of the American Chemical Society*, *142*(19), 8848–8861. https://doi.org/10.1021/jacs.0c01881

Ghosh, A. & Zhou, H.-X. (2020). *Fusion Speed of Biomolecular Condensates*. *56*, 4–7. https://doi.org/10.1101/2020.06.22.164897

Gibson, B. A., Blaukopf, C., Lou, T., Doolittle, L. K., Narlikar, G. J., Gerlich, D. W. & Rosen, M. K. (2021). *In Diverse Conditions Intrinsic Chromatin Condensates Have Liquid- like Material Properties*.

Gibson, B. A., Doolittle, L. K., Schneider, M. W. G., Jensen, L. E., Gamarra, N., Henry, L., Gerlich, D. W., Redding, S. & Rosen, M. K. (2019). Organization of Chromatin by Intrinsic and Regulated Phase Separation. *Cell*, *179*(2), 470-484.e21. https://doi.org/10.1016/j.cell.2019.08.037

Gibson, D. G., Young, L., Chuang, R.-Y., Craig Venter, J., Hutchison III, C. A. & Smith, H. O. (2009). RECEIVED 5 JANUARY; ACCEPTED 16 MARCH; PUBLISHED ONLINE 12. *NATURE METHODS*, *6*(5). https://doi.org/10.1038/NMETH.1318

Gilbert, N. & Bickmore, W. A. (2006). The relationship between higher-order chromatin structure and transcription. *Biochemical Society Symposium*, *73*(73), 59–66. https://doi.org/10.1042/BSS0730059

Gilbert, N., Boyle, S., Fiegler, H., Woodfine, K., Carter, N. P. & Bickmore, W. A. (2004). Chromatin architecture of the human genome: Gene-rich domains are enriched in open chromatin fibers. *Cell*, *118*(5), 555–566. https://doi.org/10.1016/j.cell.2004.08.011

Givens, R. M., Lai, W. K. M., Rizzo, J. M., Bard, J. E., Mieczkowski, P. A., Leatherwood, J., Huberman, J. A. & Buck, M. J. (2012). Chromatin architectures at fission yeast transcriptional promoters and replication origins. *Nucleic Acids Research*, *40*(15), 7176–7189. https://doi.org/10.1093/nar/gks351

Gkikopoulos, T., Schofield, P., Singh, V., Pinskaya, M., Mellor, J., Smolle, M., Workman, J. L., Barton, G. J. & Owen-Hughes, T. (2011). A role for Snf2-related nucleosome-spacing enzymes in genome-wide nucleosome organization. *Science*, *333*(6050), 1758–1760. https://doi.org/10.1126/SCIENCE.1206097/SUPPL_FILE/GKIKOPOULOS.SOM.PDF

Godiska, R., Mead, D., Dhodda, V., Wu, C., Hochstein, R., Karsi, A., Usdin, K., Entezam, A. & Ravin, N. (2010). Linear plasmid vector for cloning of repetitive or unstable sequences in Escherichia coli. *Nucleic Acids Research*, *38*(6), e88. https://doi.org/10.1093/NAR/GKP1181

Goldman, J. A., Garlick, J. D. & Kingston, R. E. (2010). Chromatin Remodeling by Imitation Switch (ISWI) Class ATP-dependent Remodelers Is Stimulated by Histone Variant H2A.Z. *Journal of Biological Chemistry*, *285*(7), 4645–4651. https://doi.org/10.1074/JBC.M109.072348

Görisch, S. M., Richter, K., Scheuermann, M. O., Herrmann, H. & Lichter, P. (2003). Diffusion-limited compartmentalization of mammalian cell nuclei assessed by microinjected macromolecules. *Experimental Cell Research*, *289*(2), 282–294. https://doi.org/10.1016/S0014-4827(03)00265-9

Görisch, S. M., Wachsmuth, M., Tóth, K. F., Lichter, P. & Rippe, K. (2005). Histone acetylation increases chromatin accessibility. *Journal of Cell Science*, *118*(24), 5825–5834. https://doi.org/10.1242/JCS.02689

Gregan, J., Riedel, C. G., Pidoux, A. L. L., Katou, Y., Rumpf, C., Schleiffer, A., Kearsey, S. E., Shirahige, K., Allshire, R. C. & Nasmyth, K. (2007). The kinetochore proteins Pcs1 and Mde4 and heterochromatin are required to prevent merotelic orientation. *Current Biology : CB*, *17*(14), 1190–1200. https://doi.org/10.1016/J.CUB.2007.06.044

Grewal, S. I. S. & Klar, A. J. S. (1997). A recombinationally repressed region between mat2 and mat3 loci shares homology to centromeric repeats and regulates directionality of mating-type switching in fission yeast. *Genetics*, *146*(4), 1221–1238. https://doi.org/10.1093/GENETICS/146.4.1221

Grüne, T., Brzeski, J., Eberharter, A., Clapier, C. R., Corona, D. F. V., Becker, P. B. & Müller, C. W. (2003). Crystal structure and functional analysis of a nucleosome recognition module of the remodeling factor ISWI. *Molecular Cell*, *12*(2), 449–460. https://doi.org/10.1016/S1097-2765(03)00273-9

Gu, M. & Rice, C. M. (2009). Three conformational snapshots of the hepatitis C virus NS3 helicase reveal a ratchet translocation mechanism. *Proceedings of the National Academy of Sciences of the United States of America*. https://doi.org/10.1073/pnas.0913380107

Hagerman, T. A., Fu, Q., Molinié, B., Denvir, J., Lindsay, S. & Georgel, P. T. (2009). Chromatin stability at low concentration depends on histone octamer saturation levels. *Biophysical Journal*, *96*(5), 1944–1951. https://doi.org/10.1016/j.bpj.2008.10.070

Hamiche, A., Kang, J. G., Dennis, C., Xiao, H. & Wu, C. (2001). Histone tails modulate nucleosome mobility and regulate ATP-dependent nucleosome sliding by NURF. *Proceedings of the National Academy of Sciences of the United States of America*, *98*(25), 14316–14321. https://doi.org/10.1073/PNAS.251421398/SUPPL_FILE/4213FIG8.PDF

Hamiche, A., Sandaltzopoulos, R., Gdula, D. A. & Wu, C. (1999). ATP-dependent histone octamer sliding mediated by the chromatin remodeling complex NURF. *Cell*, *97*(7), 833–842. https://doi.org/10.1016/S0092-8674(00)80796-5

Han, X., Yu, D., Gu, R., Jia, Y., Wang, Q., Jaganathan, A., Yang, X., Yu, M., Babault, N., Zhao, C., Yi, H., Zhang, Q., Zhou, M. M. & Zeng, L. (2020). Roles of the BRD4 short isoform in phase separation and active gene transcription. *Nature Structural and Molecular Biology*, *27*(4), 333–341. https://doi.org/10.1038/s41594-020-0394-8

Hanazawa, M., Yonetani, M. & Sugimoto, A. (2011). PGL proteins self associate and bind RNPs to mediate germ granule assembly in C. elegans. *The Journal of Cell Biology*, *192*(6), 929–937. https://doi.org/10.1083/JCB.201010106

Hansen, A. S., Cattoglio, C., Darzacq, X. & Tjian, R. (2018). Recent evidence that TADs and chromatin loops are dynamic structures. *Nucleus*, *9*(1), 20–32. https://doi.org/10.1080/19491034.2017.1389365

Harrer, N., Schindler, C. E. M., Bruetzel, L. K., Forné, I., Ludwigsen, J., Imhof, A., Zacharias, M., Lipfert, J. & Mueller-Planitz, F. (2018). Structural Architecture of the Nucleosome Remodeler ISWI Determined from Cross-Linking, Mass Spectrometry, SAXS, and Modeling. *Structure*, *26*(2), 282-294.e6. https://doi.org/10.1016/J.STR.2017.12.015

Haruki, H., Nishikawa, J. & Laemmli, U. K. (2008). The Anchor-Away Technique: Rapid, Conditional Establishment of Yeast Mutant Phenotypes. *Molecular Cell*, *31*(6), 925–932. https://doi.org/10.1016/j.molcel.2008.07.020

Hathaway, N. A., Bell, O., Hodges, C., Miller, E. L., Neel, D. S. & Crabtree, G. R. (2012). Dynamics and Memory of Heterochromatin in Living Cells. *Cell*, *149*(7), 1447. https://doi.org/10.1016/J.CELL.2012.03.052

Havas, K., Flaus, A., Phelan, M., Kingston, R., Wade, P. A., Lilley, D. M. J. & Owen-Hughes, T. (2000). Generation of superhelical torsion by ATP-dependent chromatin remodeling activities. *Cell*, *103*(7), 1133–1142. https://doi.org/10.1016/S0092-8674(00)00215-4

Heard, E. & Martienssen, R. A. (2014). Transgenerational Epigenetic Inheritance: Myths and Mechanisms. *Cell*, *157*(1), 95–109. https://doi.org/10.1016/J.CELL.2014.02.045

Heitz, E. (1928). Das Heterochromatin der Moose. *Jahrb.Wiss. Bot.*, *69*, 762–818.

Helbling Chadwick, L., Chadwick, B. P., Jaye, D. L. & Wade, P. A. (2009). The Mi-2/NuRD complex associates with pericentromeric heterochromatin during S phase in rapidly proliferating lymphoid cells. *Chromosoma*, *118*(4), 445–457. https://doi.org/10.1007/S00412-009-0207-7

Hennig, B. P., Bendrin, K., Zhou, Y. & Fischer, T. (2012). Chd1 chromatin remodelers maintain nucleosome organization and repress cryptic transcription. *EMBO Reports*, *13*(11), 997–1003. https://doi.org/10.1038/embor.2012.146

Heun, P., Laroche, T., Shimada, K., Furrer, P. & Gasser, S. M. (2001). Chromosome dynamics in the yeast interphase nucleus. *Science*, *294*(5549), 2181–2186. https://doi.org/10.1126/science.1065366

Hihara, S., Pack, C. G., Kaizu, K., Tani, T., Hanafusa, T., Nozaki, T., Takemoto, S., Yoshimi, T., Yokota, H., Imamoto, N., Sako, Y., Kinjo, M., Takahashi, K., Nagai, T. & Maeshima, K. (2012). Local Nucleosome Dynamics Facilitate Chromatin Accessibility in Living Mammalian Cells. *Cell Reports*, *2*(6), 1645–1656. https://doi.org/10.1016/j.celrep.2012.11.008

Hiriart, E., Vavasseur, A., Touat-Todeschini, L., Yamashita, A., Gilquin, B., Lambert, E., Perot, J., Shichino, Y., Nazaret, N., Boyault, C., Lachuer, J., Perazza, D., Yamamoto, M. & Verdel, A. (2012). Mmi1 RNA surveillance machinery directs RNAi complex RITS to specific meiotic genes in fission yeast. *The EMBO Journal*, *31*(10), 2296. https://doi.org/10.1038/EMBOJ.2012.105

Hodges, H. C., Stanton, B. Z., Cermakova, K., Chang, C. Y., Miller, E. L., Kirkland, J. G., Ku, W. L., Veverka, V., Zhao, K. & Crabtree, G. R. (2018). Dominant-negative SMARCA4 mutants alter the accessibility landscape of tissue-unrestricted enhancers. *Nature Structural and Molecular Biology*, *25*(1), 61–72. https://doi.org/10.1038/s41594-017-0007-3

Holmes, A. M., Kaykov, A. & Arcangioli, B. (2005). Molecular and Cellular Dissection of Mating-Type Switching Steps in Schizosaccharomyces pombe. *Molecular and Cellular Biology*, *25*(1), 303. https://doi.org/10.1128/MCB.25.1.303-311.2005

Hondele, M., Sachdev, R., Heinrich, S., Wang, J., Vallotton, P., Fontoura, B. M. A. & Weis, K. (2019). DEAD-box ATPases are global regulators of phase-separated organelles. *Nature*, *573*(7772), 144–148. https://doi.org/10.1038/S41586-019-1502-Y

Horn, P. J., Carruthers, L. M., Logie, C., Hill, D. A., Solomon, M. J., Wade, P. A., Imbalzano, A. N., Hansen, J. C. & Peterson, C. L. (2002). Phosphorylation of linker histones regulates ATP-dependent chromatin remodeling enzymes. *Nature Structural Biology*, *9*(4), 263–267. https://doi.org/10.1038/NSB776

Horowitz, R. A., Agard, D. A., Sedat, J. W. & Woodcock, C. L. (1994). The three-dimensional architecture of chromatin in situ: Electron tomography reveals fibers composed of a continuously variable zig-zag nucleosomal ribbon. *Journal of Cell Biology*, *125*(1), 1–10. https://doi.org/10.1083/jcb.125.1.1

Hou, F., Sun, L., Zheng, H., Skaug, B., Jiang, Q. X. & Chen, Z. J. (2011). MAVS forms functional prion-like aggregates to activate and propagate antiviral innate immune response. *Cell*, *146*(3), 448–461. https://doi.org/10.1016/J.CELL.2011.06.041

Hu, Y., Kireev, I., Plutz, M., Ashourian, N. & Belmont, A. S. (2009). Large-scale chromatin structure of inducible genes: transcription on a condensed, linear template. *The Journal of Cell Biology*, *185*(1), 87–100. https://doi.org/10.1083/JCB.200809196

Huang, J., Hsu, J. M. & Laurent, B. C. (2004). The RSC nucleosome-remodeling complex is required for cohesin's association with chromosome arms. *Molecular Cell*, *13*(5), 739–750. https://doi.org/10.1016/S1097-2765(04)00103-0

Hubatsch, L., Jawerth, L. M., Love, C., Bauermann, J., Tang, T. Y. D., Bo, S., Hyman, A. A. & Weber, C. A. (2021). Quantitative theory for the diffusive dynamics of liquid condensates. *ELife*, *10*. https://doi.org/10.7554/ELIFE.68620

Hyman, A. A. & Brangwynne, C. P. (2011). Beyond Stereospecificity: Liquids and Mesoscale Organization of Cytoplasm. *Developmental Cell*, *21*(1), 14–16. https://doi.org/10.1016/j.devcel.2011.06.013

Inagaki, H., Ohye, T., Kogo, H., Yamada, K., Kowa, H., Shaikh, T. H., Emanuel, B. S. & Kurahashi, H. (2005). Palindromic AT-rich repeat in the NF1 gene is hypervariable in humans and evolutionarily conserved in primates. *Human Mutation*, *26*(4), 332–342. https://doi.org/10.1002/HUMU.20228

Isaac, R. S., Sanulli, S., Tibble, R., Hornsby, M., Ravalin, M., Craik, C. S., Gross, J. D. & Narlikar, G. J. (2017). Biochemical Basis for Distinct Roles of the Heterochromatin Proteins Swi6 and Chp2. *Journal of Molecular Biology*, *429*(23), 3666–3677. https://doi.org/10.1016/J.JMB.2017.09.012

Ito, T., Bulger, M., Pazin, M. J., Kobayashi, R. & Kadonaga, J. T. (1997). ACF, an ISWI-containing and ATP-utilizing chromatin assembly and remodeling factor. *Cell*, *90*(1), 145–155. https://doi.org/10.1016/S0092-8674(00)80321-9

Itoh, Y., Iida, S., Tamura, S., Nagashima, R., Shiraki, K., Goto, T., Hibino, K., Ide, S. & Maeshima, K. (2021). 1,6-hexanediol rapidly immobilizes and condenses chromatin in living human cells. *Life Science Alliance*, *4*(4). https://doi.org/10.26508/LSA.202001005/VIDEO-2

Jae Yoo, E., Hwan Jin, Y., Kyu Jang, Y., Bjerling, P., Tabish, M., Hwan Hong, S., Ekwall, K. & Dai Park, S. (2004). Fission yeast Hrp1, a chromodomain ATPase, is required for proper chromosome segregation and its overexpression interferes with chromatin condensation. In *Nucleic Acids Research* (Vol. 28, Issue 9).

Jae Yoo, E., Kyu Jang, Y., Ae Lee, M., Bjerling, P., Bum Kim, J., Ekwall, K., Hyun Seong, R. & Dai Park, S. (2002). Hrp3, a chromodomain helicase/ATPase DNA binding protein, is required for heterochromatin silencing in fission yeast. *Biochemical and Biophysical Research Communications*, *295*(4), 970–974. https://doi.org/10.1016/S0006-291X(02)00797-0

Jain, A. & Vale, R. D. (2017). *RNA phase transitions in repeat expansion disorders*. https://doi.org/10.1038/nature22386

Jain, S., Wheeler, J. R., Walters, R. W., Agrawal, A., Barsic, A. & Parker, R. (2016). ATPase-Modulated Stress Granules Contain a Diverse Proteome and Substructure. *Cell*, *164*(3), 487–498. https://doi.org/10.1016/j.cell.2015.12.038

Jeppesen, P. & Turner, B. M. (1993). The inactive X chromosome in female mammals is distinguished by a lack of histone H4 acetylation, a cytogenetic marker for gene expression. *Cell*, *74*(2), 281–289. https://doi.org/10.1016/0092-8674(93)90419-Q

Jia, S., Noma, K. I. & Grewal, S. I. S. (2004). RNAi-independent heterochromatin nucleation by the stress-activated ATF/CREB family proteins. *Science (New York, N.Y.)*, *304*(5679), 1971–1976. https://doi.org/10.1126/SCIENCE.1099035

Jin, Y. H., Yoo, E. J., Jang, Y. K., Kim, S. H., Kim, M. J., Shim, Y. S., Lee, J. S., Choi, I. S., Seong, R. H., Hong, S. H. & Park, S. D. (1998). Isolation and characterization of hrp1+, a new member of the SNF2/SWI2 gene family from the fission yeast Schizosaccharomyces pombe. *Molecular and General Genetics*, *257*(3), 319–329. https://doi.org/10.1007/s004380050653

Job, G., Brugger, C., Xu, T., Lowe, B. R., Pfister, Y., Qu, C., Shanker, S., Baños Sanz, J. I., Partridge, J. F. & Schalch, T. (2016). SHREC Silences Heterochromatin via Distinct Remodeling and Deacetylation Modules. *Molecular Cell*, *62*(2), 207–221. https://doi.org/10.1016/J.MOLCEL.2016.03.016

Johnson, S. L. & Narlikar, G. J. (2022). ATP Hydrolysis Coordinates the Activities of Two Motors in a Dimeric Chromatin Remodeling Enzyme. *Journal of Molecular Biology*, *434*(14). https://doi.org/10.1016/J.JMB.2022.167653

Kagalwala, M. N., Glaus, B. J., Dang, W., Zofall, M. & Bartholomew, B. (2004). Topography of the ISW2-nucleosome complex: Insights into nucleosome spacing and chromatin remodeling. *EMBO Journal*, *23*(10), 2092–2104. https://doi.org/10.1038/sj.emboj.7600220

Kaiser, T. E., Intine, R. v. & Dundr, M. (2008). De novo formation of a subnuclear body. *Science*, *322*(5908), 1713–1717. https://doi.org/10.1126/SCIENCE.1165216/SUPPL_FILE/KAISER.SOM.REVISION1.PDF

Kandasamy, M. K., McKinney, E. C., Deal, R. B., Smith, A. P. & Meagher, R. B. (2009). Arabidopsis actin-related protein ARP5 in multicellular development and DNA repair. *Developmental Biology*, *335*(1), 22–32. https://doi.org/10.1016/J.YDBIO.2009.08.006

Kanoh, J., Sadaie, M., Urano, T. & Ishikawa, F. (2005). Telomere binding protein Taz1 establishes Swi6 heterochromatin independently of RNAi at telomeres. *Current Biology : CB*, *15*(20), 1808–1819. https://doi.org/10.1016/J.CUB.2005.09.041

Kassabov, S. R., Zhang, B., Persinger, J. & Bartholomew, B. (2003). SWI/SNF unwraps, slides, and rewraps the nucleosome. *Molecular Cell*, *11*(2), 391–403. https://doi.org/10.1016/S1097-2765(03)00039-X

Kaur, T., Alshareedah, I., Wang, W., Ngo, J., Moosa, M. M. & Banerjee, P. R. (2019). Molecular crowding tunes material states of ribonucleoprotein condensates. *Biomolecules*, *9*(2), 1–17. https://doi.org/10.3390/biom9020071

Keizer, V. I. P., Grosse-Holz, S., Woringer, M., Zambon, L., Aizel, K., Bongaerts, M., Delille, F., Kolar-Znika, L., Scolari, V. F., Hoffmann, S., Banigan, E. J., Mirny, L. A., Dahan, M., Fachinetti, D. & Coulon, A. (2022). Live-cell micromanipulation of a genomic locus reveals interphase chromatin mechanics. *Science*, *377*(6605), 489–495. https://doi.org/10.1126/SCIENCE.ABI9810/SUPPL_FILE/SCIENCE.ABI9810_MDAR_REPRODUCIBILITY_CHECKLIST.PDF

Kharchenko, P. V, Alekseyenko, A. A., Schwartz, Y. B., Minoda, A., Riddle, N. C., Ernst, J., Sabo, P. J., Larschan, E., Gorchakov, A. A., Gu, T., Linder-Basso, D., Plachetka, A., Shanower, G., Tolstorukov, M. Y., Luquette, L. J., Xi, R., Jung, Y. L., Park, R. W., Bishop, E. P., … Park, P. J. (2011). Comprehensive analysis of the chromatin landscape in Drosophila melanogaster. *Nature*, *471*(7339), 480–486. https://doi.org/10.1038/nature09725

Kim, J. M., Visanpattanasin, P., Jou, V., Liu, S., Tang, X., Zheng, Q., Li, K. Y., Snedeker, J., Lavis, L. D., Lionnet, T. & Wu, C. (2021). Single-molecule imaging of chromatin remodelers reveals role of atpase in promoting fast kinetics of target search and dissociation from chromatin. *ELife*, *10*. https://doi.org/10.7554/eLife.69387

Kireev, I., Lakonishok, M., Liu, W., Joshi, V. N., Powell, R. & Belmont, A. S. (2008). In vivo immunogold labeling confirms large-scale chromatin folding motifs. *Nature Methods 2008 5:4*, *5*(4), 311–313. https://doi.org/10.1038/nmeth.1196

Kireeva, N., Lakonishok, M., Kireev, I., Hirano, T. & Belmont, A. S. (2004). Visualization of early chromosome condensation a hierarchical folding, axial glue model of chromosome structure. *Journal of Cell Biology*, *166*(6), 775–785. https://doi.org/10.1083/JCB.200406049

Kjærulff, S. & Nielsen, O. (2015). An IPTG-inducible derivative of the fission yeast nmt promoter. *Yeast*, *32*(6), 469–478. https://doi.org/10.1002/yea.3073

Klein, I. A., Boija, A., Afeyan, L. K., Hawken, S. W., Fan, M., Dall'Agnese, A., Oksuz, O., Henninger, J. E., Shrinivas, K., Sabari, B. R., Sagi, I., Clark, V. E., Platt, J. M., Kar, M., McCall, P. M., Zamudio, A. v., Manteiga, J. C., Coffey, E. L., Li, C. H., … Young, R. A. (2020). Partitioning of cancer therapeutics in nuclear condensates. *Science*, *368*(6497), 1386–1392. https://doi.org/10.1126/science.aaz4427

Klinker, H., Haas, C., Harrer, N., Becker, P. B. & Mueller-Planitz, F. (2014). Rapid purification of recombinant histones. *PLoS ONE*, *9*(8). https://doi.org/10.1371/JOURNAL.PONE.0104029

Klosin, A., Oltsch, F., Harmon, T., Honigmann, A., Jülicher, F., Hyman, A. A. & Zechner, C. (2020). Phase separation provides a mechanism to reduce noise in cells. *Science*, *367*(6476), 464–468. https://doi.org/10.1126/SCIENCE.AAV6691/SUPPL_FILE/AAV6691S2.MOV

Koulouras, G., Panagopoulos, A., Rapsomaniki, M. A., Giakoumakis, N. N., Taraviras, S. & Lygerou, Z. (2018). EasyFRAP-web: a web-based tool for the analysis of fluorescence recovery after photobleaching data. *Nucleic Acids Research*, *46*, 467–472. https://doi.org/10.1093/nar/gky508

Krietenstein, N., Wal, M., Watanabe, S., Park, B., Peterson, C. L., Pugh, B. F. & Korber, P. (2016). Genomic Nucleosome Organization Reconstituted with Pure Proteins. *Cell*, *167*(3), 709-721.e12. https://doi.org/10.1016/J.CELL.2016.09.045

Kroschwald, S., Maharana, S., Mateju, D., Malinovska, L., Nüske, E., Poser, I., Richter, D. & Alberti, S. (2015). Promiscuous interactions and protein disaggregases determine the material state of stress-inducible RNP granules. *ELife*, *4*(AUGUST2015). https://doi.org/10.7554/ELIFE.06807

Kroschwald, S., Maharana, S. & Simon, A. (2017). Hexanediol: a chemical probe to investigate the material properties of membrane-less compartments. *Matters*. https://doi.org/10.19185/MATTERS.201702000010

Kroschwald, S., Munder, M. C., Maharana, S., Franzmann, T. M., Richter, D., Ruer, M., Hyman, A. A. & Alberti, S. (2018). Different Material States of Pub1 Condensates Define Distinct Modes of Stress Adaptation and Recovery. *Cell Reports*, *23*(11), 3327–3339. https://doi.org/10.1016/J.CELREP.2018.05.041

Kubik, S., Bruzzone, M. J., Challal, D., Dreos, R., Mattarocci, S., Bucher, P., Libri, D. & Shore, D. (2019). Opposing chromatin remodelers control transcription initiation frequency and start site selection. *Nature Structural and Molecular Biology*, *26*(8), 744–754. https://doi.org/10.1038/s41594-019-0273-3

Küffner, A. M., Prodan, M., Zuccarini, R., Palmiero, U. C., Faltova, L. & Arosio, P. (2020). Acceleration of an Enzymatic Reaction in Liquid Phase Separated Compartments Based on Intrinsically Disordered Protein Domains. *ChemSystemsChem*, *2*(4), e2000001. https://doi.org/10.1002/SYST.202000001

Kulić, I. M. & Schiessel, H. (2003). Nucleosome repositioning via loop formation. *Biophysical Journal*, *84*(5), 3197–3211. https://doi.org/10.1016/S0006-3495(03)70044-7

Kuznetsova, I. M., Zaslavsky, B. Y., Breydo, L., Turoverov, K. K. & Uversky, V. N. (2015). Beyond the Excluded Volume Effects: Mechanistic Complexity of the Crowded Milieu. *Molecules*, *20*(1), 1377. https://doi.org/10.3390/MOLECULES20011377

Kwon, S. Y., Xiao, H., Glover, B. P., Tjian, R., Wu, C. & Badenhorst, P. (2008). The nucleosome remodeling factor (NURF) regulates genes involved in Drosophila innate immunity. *Developmental Biology*, *316*(2), 538–547. https://doi.org/10.1016/J.YDBIO.2008.01.033

Lachner, M., O'Carroll, D., Rea, S., Mechtler, K. & Jenuwein, T. (2001). Methylation of histone H3 lysine 9 creates a binding site for HP1 proteins. *Nature*, *410*(6824), 116–120. https://doi.org/10.1038/35065132

Lachner, Monika & Jenuwein, T. (2002). The many faces of histone lysine methylation. *Current Opinion in Cell Biology*, *14*(3), 286–298. https://doi.org/10.1016/S0955-0674(02)00335-6

Lai, B., Gao, W., Cui, K., Xie, W., Tang, Q., Jin, W., Hu, G., Ni, B. & Zhao, K. (2018). Principles of nucleosome organization revealed by single-cell micrococcal nuclease sequencing. *Nature*, *562*(7726), 281–285. https://doi.org/10.1038/S41586-018-0567-3

Längst, G. & Becker, P. B. (2001). ISWI induces nucleosome sliding on nicked DNA. *Molecular Cell*, *8*(5), 1085–1092. https://doi.org/10.1016/S1097-2765(01)00397-5

Längst, G. & Becker, P. B. (2004). Nucleosome remodeling: One mechanism, many phenomena? *Biochimica et Biophysica Acta - Gene Structure and Expression*, *1677*(1–3), 58–63. https://doi.org/10.1016/J.BBAEXP.2003.10.011

Längst, G., Bonte, E. J., Corona, D. F. V. & Becker, P. B. (1999). Nucleosome movement by CHRAC and ISWI without disruption or trans-displacement of the histone octamer. *Cell*, *97*(7), 843–852. https://doi.org/10.1016/S0092-8674(00)80797-7

Lantermann, A. B., Straub, T., Strålfors, A., Yuan, G. C., Ekwall, K. & Korber, P. (2010). Schizosaccharomyces pombe genome-wide nucleosome mapping reveals positioning mechanisms distinct from those of Saccharomyces cerevisiae. *Nature Structural and Molecular Biology*, *17*(2), 251–257. https://doi.org/10.1038/nsmb.1741

Larson, A. G., Elnatan, D., Keenen, M. M., Trnka, M. J., Johnston, J. B., Burlingame, A. L., Agard, D. A., Redding, S. & Narlikar, G. J. (2017). Liquid droplet formation by HP1α suggests a role for phase separation in heterochromatin. In *Nature* (Vol. 547, Issue 7662, pp. 236–240). https://doi.org/10.1038/nature22822

Larson, A. G. & Narlikar, G. J. (2018). The Role of Phase Separation in Heterochromatin Formation, Function, and Regulation. *Biochemistry*, *57*(17), 2540–2548. https://doi.org/10.1021/acs.biochem.8b00401

Lavigne, M., Eskeland, R., Azebi, S., Saint-André, V., Jang, S. M., Batsché, E., Fan, H. Y., Kingston, R. E., Imhof, A. & Muchardt, C. (2009). Interaction of HP1 and Brg1/Brm with the Globular Domain of Histone H3 Is Required for HP1-Mediated Repression. *PLoS Genetics*, *5*(12). https://doi.org/10.1371/JOURNAL.PGEN.1000769

Lay, F. D., Kelly, T. K. & Jones, P. A. (2018). Nucleosome Occupancy and Methylome Sequencing (NOMe-seq). *Methods in Molecular Biology (Clifton, N.J.)*, *1708*, 267–284. https://doi.org/10.1007/978-1-4939-7481-8_14

Lee, I., Razaghi, R., Gilpatrick, T., Molnar, M., Gershman, A., Sadowski, N., Sedlazeck, F. J., Hansen, K. D., Simpson, J. T. & Timp, W. (2020). Simultaneous profiling of chromatin accessibility and methylation on human cell lines with nanopore sequencing. *Nature Methods*, *17*(12), 1191–1199. https://doi.org/10.1038/s41592-020-01000-7

Lee, J. Y. & Yang, W. (2006). UvrD Helicase Unwinds DNA One Base Pair at a Time by a Two-Part Power Stroke. *Cell*, *127*(7), 1349–1360. https://doi.org/10.1016/J.CELL.2006.10.049

Lee, W., Tillo, D., Bray, N., Morse, R. H., Davis, R. W., Hughes, T. R. & Nislow, C. (2007). A high-resolution atlas of nucleosome occupancy in yeast. *Nature Genetics*, *39*(10), 1235–1244. https://doi.org/10.1038/ng2117

Leforestier, A. & Livolant, F. (1997). Liquid crystalline ordering of nucleosome core particles under macromolecular crowding conditions: evidence for a discotic columnar hexagonal phase. *Biophysical Journal*, *73*(4), 1771–1776. https://doi.org/10.1016/S0006-3495(97)78207-9

Leonard, J. D. & Narlikar, G. J. (2015). A Nucleotide-Driven Switch Regulates Flanking DNA Length Sensing by a Dimeric Chromatin Remodeler. *Molecular Cell*, *57*(5), 850–859. https://doi.org/10.1016/J.MOLCEL.2015.01.008

Levendosky, R. F. & Bowman, G. D. (2019). Asymmetry between the two acidic patches dictates the direction of nucleosome sliding by the ISWI chromatin remodeler. *ELife*, *8*. https://doi.org/10.7554/ELIFE.45472

Levendosky, R. F., Sabantsev, A., Deindl, S. & Bowman, G. D. (2016). The Chd1 chromatin remodeler shifts hexasomes unidirectionally. *ELife*, *5*. https://doi.org/10.7554/ELIFE.21356

Li, C. H., Coffey, E. L., Dall'Agnese, A., Hannett, N. M., Tang, X., Henninger, J. E., Platt, J. M., Oksuz, O., Zamudio, A. v., Afeyan, L. K., Schuijers, J., Liu, X. S., Markoulaki, S., Lungjangwa, T., LeRoy, G., Svoboda, D. S., Wogram, E., Lee, T. I., Jaenisch, R. & Young, R. A. (2020). MeCP2 links heterochromatin condensates and neurodevelopmental disease. *Nature*, *586*(7829), 440–444. https://doi.org/10.1038/S41586-020-2574-4

Li, J., Santoro, R., Koberna, K. & Grummt, I. (2005). The chromatin remodeling complex NoRC controls replication timing of rRNA genes. *EMBO Journal*, *24*(1), 120–127. https://doi.org/10.1038/SJ.EMBOJ.7600492

Li, P., Banjade, S., Cheng, H.-C., Kim, S., Chen, B., Guo, L., Llaguno, M., Hollingsworth, J. v, King, D. S., Banani, S. F., Russo, P. S., Jiang, Q.-X., Nixon, B. T. & Rosen, M. K. (2012). *Phase transitions in the assembly of multivalent signalling proteins*. https://doi.org/10.1038/nature10879

Li, W., Hu, J., Shi, B., Palomba, F., Digman, M. A., Gratton, E. & Jiang, H. (2020). Biophysical properties of AKAP95 protein condensates regulate splicing and tumorigenesis. *Nature Cell Biology*, *22*(8), 960–972. https://doi.org/10.1038/s41556-020-0550-8

Lia, G., Praly, E., Ferreira, H., Stockdale, C., Tse-Dinh, Y. C., Dunlap, D., Croquette, V., Bensimon, D. & Owen-Hughes, T. (2006). Direct observation of DNA distortion by the RSC complex. *Molecular Cell*, *21*(3), 417–425. https://doi.org/10.1016/J.MOLCEL.2005.12.013

Lima de Faria, A. (1949). GENETICS, ORIGIN AND EVOLUTION OF KINETOCHORES. *Hereditas*, *35*(4), 422–444. https://doi.org/10.1111/J.1601-5223.1949.TB02883.X

Lin, Y., Protter, D. S. W., Rosen, M. K. & Parker, R. (2015). Formation and Maturation of Phase-Separated Liquid Droplets by RNA-Binding Proteins. *Molecular Cell*, *60*(2), 208–219. https://doi.org/10.1016/j.molcel.2015.08.018

Lis, J. T. & Schleif, R. (1975). Size fractionation of double-stranded DNA by precipitation with polyethylene glycol. *Nucleic Acids Research*, *2*(3), 383. https://doi.org/10.1093/NAR/2.3.383

Liu, H., Wen, J., Xiao, Y., Liu, J., Hopyan, S., Radisic, M., Simmons, C. A. & Sun, Y. (2014). In situ mechanical characterization of the cell nucleus by atomic force microscopy. *ACS Nano*, *8*(4), 3821–3828. https://doi.org/10.1021/NN500553Z

Liu, M., He, S., Cheng, L., Qu, J. & Xia, J. (2020). Phase-Separated Multienzyme Biosynthesis. *Biomacromolecules*, *21*(6), 2391–2399. https://doi.org/10.1021/ACS.BIOMAC.0C00321

Liu, X., Jiang, S., Ma, L., Qu, J., Zhao, L., Zhu, X. & Ding, J. (2021). Time-dependent effect of 1,6-hexanediol on biomolecular condensates and 3D chromatin organization. *Genome Biology*. https://doi.org/10.1186/s13059-021-02455-3

Livak, K. J. & Schmittgen, T. D. (2001). Analysis of relative gene expression data using real-time quantitative PCR and the 2-ΔΔCT method. *Methods*, *25*(4), 402–408. https://doi.org/10.1006/METH.2001.1262

Logie, C. & Peterson, C. L. (1997). Catalytic activity of the yeast SWI/SNF complex on reconstituted nucleosome arrays. *EMBO Journal*, *16*(22), 6772–6782. https://doi.org/10.1093/EMBOJ/16.22.6772

Lohr, D. & van Holde, K. E. (1979). Organization of spacer DNA in chromatin. *Proceedings of the National Academy of Sciences*, *76*(12), 6326–6330. https://doi.org/10.1073/PNAS.76.12.6326

Long, M., Sun, X., Shi, W., Yanru, A., Leung, S. T. C., Ding, D., Cheema, M. S., MacPherson, N., Nelson, C. J., Ausio, J., Yan, Y. & Ishibashi, T. (2019). A novel histone H4 variant H4G regulates rDNA transcription in breast cancer. *Nucleic Acids Research*, *47*(16), 8399–8409. https://doi.org/10.1093/nar/gkz547

Lorch, Y., Maier-Davis, B. & Kornberg, R. D. (2006). Chromatin remodeling by nucleosome disassembly in vitro. *Proceedings of the National Academy of Sciences of the United States of America*, *103*(9), 3090–3093. https://doi.org/10.1073/PNAS.0511050103/ASSET/ABFBEDC7-E7F8-42FA-AF5D-3778E1E54E2E/ASSETS/GRAPHIC/ZPQ0070613240005.JPEG

Lorch, Y., Maier-Davis, B. & Kornberg, R. D. (2010). Mechanism of chromatin remodeling. *Proceedings of the National Academy of Sciences of the United States of America*, *107*(8), 3458–3462. https://doi.org/10.1073/PNAS.1000398107/SUPPL_FILE/PNAS.1000398107_SI.PDF

Lu, A., Magupalli, V. G., Ruan, J., Yin, Q., Atianand, M. K., Vos, M. R., Schröder, G. F., Fitzgerald, K. A., Wu, H. & Egelman, E. H. (2014). Unified Polymerization Mechanism for the Assembly of ASC-dependent Inflammasomes. *Cell*, *156*(6), 1193. https://doi.org/10.1016/J.CELL.2014.02.008

Ludwigsen, J., Hepp, N., Klinker, H., Pfennig, S. & Mueller-Planitz, F. (2018). Remodeling and repositioning of nucleosomes in nucleosomal arrays. In *Methods in Molecular Biology*. https://doi.org/10.1007/978-1-4939-8556-2_18

Ludwigsen, J., Klinker, H. & Mueller-Planitz, F. (2013). No need for a power stroke in ISWI-mediated nucleosome sliding. *EMBO Reports*, *14*(12), 1092–1097. https://doi.org/10.1038/EMBOR.2013.160

Ludwigsen, J., Pfennig, S., Singh, A. K., Schindler, C., Harrer, N., Forné, I., Zacharias, M. & Mueller-Planitz, F. (2017). Concerted regulation of ISWI by an autoinhibitory domain and the H4 N-terminal tail. *ELife*. https://doi.org/10.7554/eLife.21477

Luger, K., Mäder, A. W., Richmond, R. K., Sargent, D. F. & Richmond, T. J. (1997). Crystal structure of the nucleosome core particle at 2.8 Å resolution. *Nature 1997 389:6648*, *389*(6648), 251–260. https://doi.org/10.1038/38444

Lusser, A., Urwin, D. L. & Kadonaga, J. T. (2005). Distinct activities of CHD1 and ACF in ATP-dependent chromatin assembly. *NATURE STRUCTURAL & MOLECULAR BIOLOGY*, *12*. https://doi.org/10.1038/nsmb884

Lyon, A. S., Peeples, W. B. & Rosen, M. K. (2020). A framework for understanding the functions of biomolecular condensates across scales. *Nature Reviews Molecular Cell Biology*. https://doi.org/10.1038/s41580-020-00303-z

Ma, L., Gao, Z., Wu, J., Zhong, B., Xie, Y., Huang, W. & Lin, Y. (2021). Co-condensation between transcription factor and coactivator p300 modulates transcriptional bursting kinetics. *Molecular Cell*, *81*(8), 1682-1697.e7. https://doi.org/10.1016/J.MOLCEL.2021.01.031

Maeshima, K., Matsuda, T., Shindo, Y., Imamura, H., Tamura, S., Imai, R., Kawakami, S., Nagashima, R., Soga, T., Noji, H., Oka, K. & Nagai, T. (2018). A Transient Rise in Free Mg2+ Ions Released from ATP-Mg Hydrolysis Contributes to Mitotic Chromosome Condensation. *Current Biology*, *28*(3), 444-451.e6. https://doi.org/10.1016/j.cub.2017.12.035

Maeshima, K., Rogge, R., Tamura, S., Joti, Y., Hikima, T., Szerlong, H., Krause, C., Herman, J., Seidel, E., DeLuca, J., Ishikawa, T. & Hansen, J. C. (2016). Nucleosomal arrays self-assemble into supramolecular globular structures lacking 30-nm fibers. *The EMBO Journal*, *35*(10), 1115–1132. https://doi.org/10.15252/EMBJ.201592660

Maier, V. K., Chioda, M., Rhodes, D. & Becker, P. B. (2008). ACF catalyses chromatosome movements in chromatin fibres. *The EMBO Journal*, *27*(6), 817–826. https://doi.org/10.1038/SJ.EMBOJ.7601902

Mao, Y. S., Sunwoo, H., Zhang, B. & Spector, D. L. (2010). Direct visualization of the co-transcriptional assembly of a nuclear body by noncoding RNAs. *Nature Cell Biology 2010 13:1*, *13*(1), 95–101. https://doi.org/10.1038/ncb2140

Martienssen, R. & Moazed, D. (2015). RNAi and Heterochromatin Assembly. *Cold Spring Harb Perspect Biol.*, *7*(8). https://doi.org/10.1101/cshperspect.a019323

Martin, E. W., Holehouse, A. S., Peran, I., Farag, M., Incicco, J. J., Bremer, A., Grace, C. R., Soranno, A., Pappu, R. v & Mittag, T. (2020). Valence and patterning of aromatic residues determine the phase behavior of prion-like domains. *Science*. https://doi.org/10.1126/science.aaw8653

Martin, N., Tian, L., Spencer, D., Coutable-Pennarun, A., Anderson, J. L. R., Mann, S., Martin, N., Tian, L., Spencer, D., Mann, R. S., Outable-Pennarun, A. C., Nderson, J. L. R. A. & Mann, S. (2019). Photoswitchable Phase Separation and Oligonucleotide Trafficking in DNA Coacervate Microdroplets. *Angew. Chem. Int. Ed. Engl.*, *58*, 4594–14598. https://doi.org/10.1002/ange.201909228

McDowall, A. W., Smith, J. M. & Dubochet, J. (1986). Cryo-electron microscopy of vitrified chromosomes in situ. *The EMBO Journal*, *5*(6), 1395–1402. https://doi.org/10.1002/J.1460-2075.1986.TB04373.X

McDowell, T. L., Gibbons, R. J., Sutherland, H., O'Rourke, D. M., Bickmore, W. A., Pombo, A., Turley, H., Gatter, K., Picketts, D. J., Buckle, V. J., Chapman, L., Rhodes, D. & Higgs, D. R. (1999). Localization of a putative

transcriptional regulator (ATRX) at pericentromeric heterochromatin and the short arms of acrocentric chromosomes. *Proceedings of the National Academy of Sciences of the United States of America*, *96*(24), 13983–13988. https://doi.org/10.1073/PNAS.96.24.13983

McGinty, R. K. & Tan, S. (2014). Histone, Nucleosome, and Chromatin Structure. In J. L. Workman & S. M. Abmayr (Eds.), *Fundamentals of Chromatin* (pp. 1–23). Springer. https://doi.org/10.1007/978-1-4614-8624-4

McGinty, R. K. & Tan, S. (2015). Nucleosome structure and function. *Chemical Reviews*, *115*(6), 2255–2273. https://doi.org/10.1021/CR500373H/ASSET/IMAGES/LARGE/CR-2014-00373H_0014.JPEG

McKnight, J. N., Jenkins, K. R., Nodelman, I. M., Escobar, T. & Bowman, G. D. (2011). Extranucleosomal DNA Binding Directs Nucleosome Sliding by Chd1. *Molecular and Cellular Biology*, *31*(23), 4746–4759. https://doi.org/10.1128/MCB.05735-11

McSwiggen, D. T., Hansen, A. S., Teves, S. S., Marie-Nelly, H., Hao, Y., Heckert, A. B., Umemoto, K. K., Dugast-Darzacq, C., Tjian, R. & Darzacq, X. (2019). Evidence for DNA-mediated nuclear compartmentalization distinct from phase separation. *ELife*, *8*, 1–31. https://doi.org/10.7554/eLife.47098

Meersseman, G., Pennings, S. & Bradbury, E. M. (1992). Mobile nucleosomes--a general behavior. *The EMBO Journal*, *11*(8), 2951–2959. https://doi.org/10.1002/J.1460-2075.1992.TB05365.X

Miao, W., Yu, C., Hao, E. & Jiao, L. (2019). Functionalized BODIPYs as Fluorescent Molecular Rotors for Viscosity Detection. *Frontiers in Chemistry*, *7*(November), 1–6. https://doi.org/10.3389/fchem.2019.00825

Mitrea, D. M., Mittasch, M., Gomes, B. F., Klein, I. A. & Murcko, M. A. (2022). Modulating biomolecular condensates: a novel approach to drug discovery. *Nature Reviews. Drug Discovery*. https://doi.org/10.1038/S41573-022-00505-4

Mizuguchi, G., Shen, X., Landry, J., Wu, W. H., Sen, S. & Wu, C. (2004). ATP-driven exchange of histone H2AZ variant catalyzed by SWR1 chromatin remodeling complex. *Science (New York, N.Y.)*, *303*(5656), 343–348. https://doi.org/10.1126/SCIENCE.1090701

Mizuguchi, T., Barrowman, J. & Grewal, S. I. S. (2015). *Chromosome domain architecture and dynamic organization of the fission yeast genome*. https://doi.org/10.1016/j.febslet.2015.06.008

Moazed, D. (2009). Small RNAs in transcriptional gene silencing and genome defence. *Nature 2009 457:7228*, *457*(7228), 413–420. https://doi.org/10.1038/nature07756

Moraru, M. & Schalch, T. (2019). Chromatin fiber structural motifs as regulatory hubs of genome function? *Essays in Biochemistry*, *63*, 123–132. https://doi.org/10.1042/EBC20180065

Moreno, B. M., Duran, A. & Ribas, J. C. (2000). *A family of multifunctional thiamine-repressible expression vectors for fission yeast*.

Motamedi, M. R., Hong, E. J. E., Li, X., Gerber, S., Denison, C., Gygi, S. & Moazed, D. (2008). HP1 Proteins Form Distinct Complexes and Mediate Heterochromatic Gene Silencing by Non-Overlapping Mechanisms. *Molecular Cell*, *32*(6), 778. https://doi.org/10.1016/J.MOLCEL.2008.10.026

Motamedi, M. R., Verdel, A., Colmenares, S. U., Gerber, S. A., Gygi, S. P. & Moazed, D. (2004). Two RNAi Complexes, RITS and RDRC, Physically Interact and Localize to Noncoding Centromeric RNAs. *Cell*, *119*(6), 789–802. https://doi.org/10.1016/J.CELL.2004.11.034

Moyle-Heyrman, G., Zaichuk, T., Xi, L., Zhang, Q., Uhlenbeck, O. C., Holmgren, R., Widom, J. & Wang, J. P. (2013). Chemical map of Schizosaccharomyces pombe reveals species-specific features in nucleosome positioning. *Proceedings of the National Academy of Sciences of the United States of America*, *110*(50), 20158–20163. https://doi.org/10.1073/pnas.1315809110

Mueller-Planitz, F., Klinker, H., Ludwigsen, J. & Becker, P. B. (2013). The ATPase domain of ISWI is an autonomous nucleosome remodeling machine. *Nature Structural and Molecular Biology*. https://doi.org/10.1038/nsmb.2457

Mukai, A., Ichiraku, A. & Horikawa, K. (2016). Reliable handling of highly A/T-rich genomic DNA for efficient generation of knockin strains of Dictyostelium discoideum. *BMC Biotechnology*, *16*(1). https://doi.org/10.1186/S12896-016-0267-8

Muller, H. J. (1930). Types of visible variations induced by X-rays in Drosophila. *Journal of Genetics 1930 22:3*, *22*(3), 299–334. https://doi.org/10.1007/BF02984195

Müller, M., Fierz, B., Bittova, L., Liszczak, G. & Muir, T. W. (2016). A two-state activation mechanism controls the histone methyltransferase Suv39h1. *Nature Chemical Biology*. https://doi.org/10.1038/nchembio.2008

Müller, W. G., Rieder, † Dietmar, Kreth, † Gregor, Cremer, C., Trajanoski, Z. & Mcnally, J. G. (2004). Generic Features of Tertiary Chromatin Structure as Detected in Natural Chromosomes. *Molecular and Cellular Biology*, *24*(21), 9359–9370. https://doi.org/10.1128/MCB.24.21.9359-9370.2004

Muzzopappa, F., Hertzog, M. & Erdel, F. (2021). DNA length tunes the fluidity of DNA-based condensates. *Biophysical Journal*, *120*(7), 1288–1300. https://doi.org/10.1016/J.BPJ.2021.02.027

Nakano, M., Cardinale, S., Noskov, V. N., Gassmann, R., Vagnarelli, P., Kandels-Lewis, S., Larionov, V., Earnshaw, W. C. & Masumoto, H. (2008). Inactivation of a Human Kinetochore by Specific Targeting of Chromatin Modifiers. *Developmental Cell*, *14*(4), 507. https://doi.org/10.1016/J.DEVCEL.2008.02.001

Nakayama, J., Rice, J. C., Strahl, B. D., Allis, C. D. & Grewal, S. I. S. (2001). Role of histone H3 lysine 9 methylation in epigenetic control of heterochromatin assembly. *Science (New York, N.Y.)*, *292*(5514), 110–113. https://doi.org/10.1126/SCIENCE.1060118

Neumann, F. R., Dion, V., Gehlen, L. R., Tsai-Pflugfelder, M., Schmid, R., Taddei, A. & Gasser, S. M. (2012). Targeted INO80 enhances subnuclear chromatin movement and ectopic homologous recombination. *Genes and Development*, *26*(4), 369–383. https://doi.org/10.1101/gad.176156.111

Nielsen, K. H., Chamieh, H., Andersen, C. B. F., Fredslund, F., Hamborg, K., le Hir, H. & Andersen, G. R. (2009). Mechanism of ATP turnover inhibition in the EJC. *RNA (New York, N.Y.)*, *15*(1), 67–75. https://doi.org/10.1261/RNA.1283109

Nimmo, E. R., Pidoux, A. L., Perry, P. E. & Allshire, R. C. (1998). *Defective meiosis in telomere-silencing mutants of Schizosaccharomyces pombe*.

Nishino, Y., Eltsov, M., Joti, Y., Ito, K., Takata, H., Takahashi, Y., Hihara, S., Frangakis, A. S., Imamoto, N., Ishikawa, T. & Maeshima, K. (2012). Human mitotic chromosomes consist predominantly of irregularly folded nucleosome fibres without a 30-nm chromatin structure. *EMBO Journal*, *31*(7), 1644–1653. https://doi.org/10.1038/EMBOJ.2012.35

Noma, K. I., Allis, C. D. & Grewal, S. I. S. (2001). Transitions in distinct histone H3 methylation patterns at the heterochromatin domain boundaries. *Science (New York, N.Y.)*, *293*(5532), 1150–1155. https://doi.org/10.1126/SCIENCE.1064150

Nott, T. J., Craggs, T. D. & Baldwin, A. J. (2016). Membraneless organelles can melt nucleic acid duplexes and act as biomolecular filters. *Nature Chemistry*, *8*(6), 569–575. https://doi.org/10.1038/NCHEM.2519

Nott, T. J., Petsalaki, E., Farber, P., Jervis, D., Fussner, E., Plochowietz, A., Craggs, T. D., Bazett-Jones, D. P., Pawson, T., Forman-Kay, J. D. & Baldwin, A. J. (2015). Phase Transition of a Disordered Nuage Protein Generates Environmentally Responsive Membraneless Organelles. *Molecular Cell*, *57*(5), 936–947. https://doi.org/10.1016/j.molcel.2015.01.013

Nozaki, T., Imai, R., Tanbo, M., Nagashima, R., Tamura, S., Tani, T., Joti, Y., Tomita, M., Hibino, K., Kanemaki, M. T., Wendt, K. S., Okada, Y., Nagai, T. & Maeshima, K. (2017). Dynamic Organization of Chromatin Domains Revealed by Super-Resolution Live-Cell Imaging. *Molecular Cell*, *67*(2), 282-293.e7. https://doi.org/10.1016/j.molcel.2017.06.018

Oberbeckmann, E., Wolff, M., Krietenstein, N., Heron, M., Ellins, J. L., Schmid, A., Krebs, S., Blum, H., Gerland, U. & Korber, P. (2019). Absolute nucleosome occupancy map for the Saccharomyces cerevisiae genome. *Genome Research*, *29*(12), 1996–2009. https://doi.org/10.1101/gr.253419.119

Ocampo, J., Azvan, R., Chereji, V., Eriksson, P. R. & Clark, D. J. (2016). The ISW1 and CHD1 ATP-dependent chromatin remodelers compete to set nucleosome spacing in vivo. *Nucleic Acids Research*, *44*(10), 4625–4635. https://doi.org/10.1093/nar/gkw068

Ohira, M. J., Hendrickson, D. G., Scott McIsaac, R. & Rhind, N. (2017). An estradiol-inducible promoter enables fast, graduated control of gene expression in fission yeast. *Yeast*, *34*(8), 323–334. https://doi.org/10.1002/yea.3235

Ohzeki, J. I., Bergmann, J. H., Kouprina, N., Noskov, V. N., Nakano, M., Kimura, H., Earnshaw, W. C., Larionov, V. & Masumoto, H. (2012). Breaking the HAC Barrier: Histone H3K9 acetyl/methyl balance regulates CENP-A assembly. *The EMBO Journal*, *31*(10), 2391. https://doi.org/10.1038/EMBOJ.2012.82

Olins, A. L. & Olins, D. E. (1974). Spheroid chromatin units (v bodies). *Science*, *183*(4122), 330–332. https://doi.org/10.1126/science.183.4122.330

Olins, D. E. & Olins, A. L. (2003). Chromatin history: Our view from the bridge. In *Nature Reviews Molecular Cell Biology* (Vol. 4, Issue 10, pp. 809–814). https://doi.org/10.1038/nrm1225

Oliveira, G. M., Oravecz, A., Kobi, D., Maroquenne, M., Bystricky, K., Sexton, T. & Molina, N. (2021). Precise measurements of chromatin diffusion dynamics by modeling using Gaussian processes. *Nature Communications*, *12*(1), 1–11. https://doi.org/10.1038/s41467-021-26466-7

Ou, H. D., Phan, S., Deerinck, T. J., Thor, A., Ellisman, M. H. & O'Shea, C. C. (2017). ChromEMT: Visualizing 3D chromatin structure and compaction in interphase and mitotic cells. *Science*, *357*(6349). https://doi.org/10.1126/science.aag0025

Papamichos-Chronakis, M. & Peterson, C. L. (2008). *The Ino80 chromatin-remodeling enzyme regulates replisome function and stability*. https://doi.org/10.1038/nsmb.1413

Parnell, T. J., Huff, J. T. & Cairns, B. R. (2008). RSC regulates nucleosome positioning at Pol II genes and density at Pol III genes. *EMBO Journal*, *27*(1), 100–110. https://doi.org/10.1038/SJ.EMBOJ.7601946

Partridge, J. F., Borgstrøm, B. & Allshire, R. C. (2000). Distinct protein interaction domains and protein spreading in a complex centromere. *Genes & Development*, *14*(7), 783. https://doi.org/10.1101/gad.14.7.783

Patel, A., Lee, H. O., Jawerth, L., Maharana, S., Jahnel, M., Hein, M. Y., Stoynov, S., Mahamid, J., Saha, S., Franzmann, T. M., Pozniakovski, A., Poser, I., Maghelli, N., Royer, L. A., Weigert, M., Myers, E. W., Grill, S., Drechsel, D., Hyman, A. A. & Alberti, S. (2015). A Liquid-to-Solid Phase Transition of the ALS Protein FUS Accelerated by Disease Mutation. *Cell*, *162*(5), 1066–1077. https://doi.org/10.1016/j.cell.2015.07.047

Patel, A., Malinovska, L., Saha, S., Wang, J., Alberti, S., Krishnan, Y. & Hyman, A. A. (2017). Biochemistry: ATP as a biological hydrotrope. *Science*, *356*(6339), 753–756. https://doi.org/10.1126/science.aaf6846

Peeples, W. & Rosen, M. K. (2021). Mechanistic dissection of increased enzymatic rate in a phase-separated compartment. *Nature Chemical Biology*. https://doi.org/10.1038/s41589-021-00801-x

Peng, J. C. & Karpen, G. H. (2007). H3K9 methylation and RNA interference regulate nucleolar organization and repeated DNA stability. *NATURE CELL BIOLOGY*, *9*. https://doi.org/10.1038/ncb1514

Pennings, S., Meersseman, G. & Bradbury, E. M. (1991). Mobility of positioned nucleosomes on 5 S rDNA. *Journal of Molecular Biology*, *220*(1), 101–110. https://doi.org/10.1016/0022-2836(91)90384-I

Pennings, S., Meersseman, G. & Bradbury, E. M. (1994). Linker histones H1 and H5 prevent the mobility of positioned nucleosomes. *Proceedings of the National Academy of Sciences of the United States of America*, *91*(22), 10275. https://doi.org/10.1073/PNAS.91.22.10275

Perišić, O., Collepardo-Guevara, R. & Schlick, T. (2010). *Modeling studies of chromatin fiber structure as a function of DNA linker length*. https://doi.org/10.1016/j.jmb.2010.07.057

Peskett, T. R., Rau, F., O'Driscoll, J., Patani, R., Lowe, A. R. & Saibil, H. R. (2018). A Liquid to Solid Phase Transition Underlying Pathological Huntingtin Exon1 Aggregation. *Molecular Cell*, *70*(4), 588-601.e6. https://doi.org/10.1016/J.MOLCEL.2018.04.007

Pfander, C., Anar, B., Schwach, F., Otto, T. D., Brochet, M., Volkmann, K., Quail, M. A., Pain, A., Rosen, B., Skarnes, W., Rayner, J. C. & Billker, O. (2011). A scalable pipeline for highly effective genetic modification of a malaria parasite. *Nature Methods*, *8*(12), 1078. https://doi.org/10.1038/NMETH.1742

Pointner, J., Persson, J., Prasad, P., Norman-Axelsson, U., Strålfors, A., Khorosjutina, O., Krietenstein, N., Peter Svensson, J., Ekwall, K. & Korber, P. (2012). CHD1 remodelers regulate nucleosome spacing in vitro and align nucleosomal arrays over gene coding regions in S. pombe. *EMBO Journal*, *31*(23), 4388–4403. https://doi.org/10.1038/emboj.2012.289

Poirier, M. G., Bussiek, M., Langowski, J. & Widom, J. (2008). Spontaneous Access to DNA Target Sites in Folded Chromatin Fibers. *Journal of Molecular Biology*, *379*(4), 772–786. https://doi.org/10.1016/j.jmb.2008.04.025

Poirier, M. G., Oh, E., Tims, H. S. & Widom, J. (2009). Dynamics and function of compact nucleosome arrays. *Nature Structural and Molecular Biology*, *16*(9), 938–944. https://doi.org/10.1038/nsmb.1650

Poot, R. A., Bozhenok, L., van den Berg, D. L. C., Steffensen, S., Ferreira, F., Grimaldi, M., Gilbert, N., Ferreira, J. & Varga-Weisz, P. D. (2004). The Williams syndrome transcription factor interacts with PCNA to target chromatin remodelling by ISWI to replication foci. *Nature Cell Biology 2004 6:12*, *6*(12), 1236–1244. https://doi.org/10.1038/ncb1196

Post, C. B. & Zimm, B. H. (1982). Theory of DNA condensation: Collapse versus aggregation. *Biopolymers*, *21*(11), 2123–2137. https://doi.org/10.1002/BIP.360211104

Prouteau, M., Desfosses, A., Sieben, C., Bourgoint, C., Mozaffari, N. L., Demurtas, D., Mitra, A. K., Guichard, P., Manley, S. & Loewith, R. (2017). TORC1 Organised in Inhibited Domains (TOROIDs) regulate TORC1 activity. *Nature*, *550*(7675), 265. https://doi.org/10.1038/NATURE24021

Provost, P., Silverstein, R. A., Dishart, D., Walfridsson, J., Djupedal, I., Kniola, B., Wright, A., Samuelsson, B., Rådmark, O. & Ekwall, K. (2002). Dicer is required for chromosome segregation and gene silencing in fission yeast cells. *Proceedings of the National Academy of Sciences of the United States of America*, *99*(26), 16648–16653. https://doi.org/10.1073/PNAS.212633199/SUPPL_FILE/6331FIG5.PDF

R Core Team. (2022). *R: A Language and Environment for Statistical Computing* (4.2.1). R Foundation for Statistical Computing.

Racki, L. R., Yang, J. G., Naber, N., Partensky, P. D., Acevedo, A., Purcell, T. J., Cooke, R., Cheng, Y. & Narlikar, G. J. (2009). *The chromatin remodeller ACF acts as a dimeric motor to space nucleosomes*. https://doi.org/10.1038/nature08621

Ragunathan, K., Jih, G. & Moazed, D. (2015). Epigenetic inheritance uncoupled from sequence-specific recruitment. *Science (New York, N.Y.)*, *348*(6230), 1258699. https://doi.org/10.1126/SCIENCE.1258699

Ramachandran, A., Omar, M., Cheslock, P. & Schnitzler, G. R. (2003). Linker histone H1 modulates nucleosome remodeling by human SWI/SNF. *The Journal of Biological Chemistry*, *278*(49), 48590–48601. https://doi.org/10.1074/JBC.M309033200

Rao, S. S. P., Huang, S. C., Glenn St Hilaire, B., Engreitz, J. M., Perez, E. M., Kieffer-Kwon, K. R., Sanborn, A. L., Johnstone, S. E., Bascom, G. D., Bochkov, I. D., Huang, X., Shamim, M. S., Shin, J., Turner, D., Ye, Z., Omer, A. D., Robinson, J. T., Schlick, T., Bernstein, B. E., … Aiden, E. L. (2017). Cohesin Loss Eliminates All Loop Domains. *Cell*, *171*(2), 305-320.e24. https://doi.org/10.1016/J.CELL.2017.09.026

Rao, S. S. P., Huntley, M. H., Durand, N. C., Stamenova, E. K., Bochkov, I. D., Robinson, J. T., Sanborn, A. L., Machol, I., Omer, A. D., Lander, E. S. & Aiden, E. L. (2014). A 3D map of the human genome at kilobase resolution reveals principles of chromatin looping. *Cell*, *159*(7), 1665–1680. https://doi.org/10.1016/J.CELL.2014.11.021/ATTACHMENT/CB0E9D91-BC65-40C2-ACB4-623802E0869F/MMC3.XLSX

Rattner, J. B. & Lin, C. C. (1985). Radial loops and helical coils coexist in metaphase chromosomes. *Cell*, *42*(1), 291–296. https://doi.org/10.1016/S0092-8674(85)80124-0

Rea, S., Eisenhaber, F., Â nal, D. O., Strahl, B. D., Sun, Z.-W., Schmid, M., Opravil, S., Mechtler, K., Ponting, C. P., David Allis, C. & Jenuwein, T. (2000). Regulation of chromatin structure by site-specific histone H3 methyltransferases. In *NATURE* (Vol. 406). www.nature.com593

Reinhart, B. J. & Bartel, D. P. (2002). Small RNAs correspond to centromere heterochromatic repeats. *Science*, *297*(5588), 1831. https://doi.org/10.1126/SCIENCE.1077183/ASSET/D8976E01-B466-4531-AFD8-7399A6A6446C/ASSETS/SCIENCE.1077183.FP.PNG

Riback, J. A., Katanski, C. D., Kear-Scott, J. L., Pilipenko, E. v., Rojek, A. E., Sosnick, T. R. & Drummond, D. A. (2017). Stress-Triggered Phase Separation Is an Adaptive, Evolutionarily Tuned Response. *Cell*, *168*(6), 1028-1040.e19. https://doi.org/10.1016/j.cell.2017.02.027

Riback, J. A., Zhu, L., Ferrolino, M. C., Tolbert, M., Mitrea, D. M., Sanders, D. W., Wei, M. T., Kriwacki, R. W. & Brangwynne, C. P. (2020). Composition-dependent thermodynamics of intracellular phase separation. *Nature*, *581*(7807), 209–214. https://doi.org/10.1038/s41586-020-2256-2

Ricci, M. A., Manzo, C., García-Parajo, M. F., Lakadamyali, M. & Cosma, M. P. (2015). Chromatin fibers are formed by heterogeneous groups of nucleosomes in vivo. *Cell*, *160*(6), 1145–1158. https://doi.org/10.1016/J.CELL.2015.01.054

Robinson, J. T., Thorvaldsdóttir, H., Winckler, W., Guttman, M., Lander, E. S., Getz, G. & Mesirov, J. P. (2011). Integrative Genomics Viewer. *Nature Biotechnology*, *29*(1), 24. https://doi.org/10.1038/NBT.1754

Robinson, P. J. J., Fairall, L., Huynh, V. A. T. & Rhodes, D. (2006). EM measurements define the dimensions of the “30-nm” chromatin fiber: Evidence for a compact, interdigitated structure. *Proceedings of the National Academy of Sciences of the United States of America*, *103*(17), 6506–6511. https://doi.org/10.1073/PNAS.0601212103/SUPPL_FILE/01212FIG6.JPG

Routh, A., Sandin, S. & Rhodes, D. (2008). *Nucleosome repeat length and linker histone stoichiometry determine chromatin fiber structure*. www.pnas.org/cgi/content/full/

Rowat, A. C., Lammerding, J. & Ipsen, J. H. (2006). Mechanical Properties of the Cell Nucleus and the Effect of Emerin Deficiency. *Biophysical Journal*, *91*(12), 4649. https://doi.org/10.1529/BIOPHYSJ.106.086454

Rowbotham, S. P., Barki, L., Neves-Costa, A., Santos, F., Dean, W., Hawkes, N., Choudhary, P., Will, W. R., Webster, J., Oxley, D., Green, C. M., Varga-Weisz, P. & Mermoud, J. E. (2011). Maintenance of Silent Chromatin through Replication Requires SWI/SNF-like Chromatin Remodeler SMARCAD1. *Molecular Cell*, *42*(3), 285–296. https://doi.org/10.1016/j.molcel.2011.02.036

Rudolph, J., Mahadevan, J., Dyer, P. & Luger, K. (2018). Poly(ADP-ribose) polymerase 1 searches DNA via a 'monkey bar' mechanism. *ELife*, *7*. https://doi.org/10.7554/ELIFE.37818

Sabari, B. R., Dall'agnese, A. & Young, R. A. (2020). Biomolecular Condensates in the Nucleus. *Trends Biochem Sci*, *45*(11), 961–977. https://doi.org/10.1016/j.tibs.2020.06.007

Sachs, P., Ding, D., Bergmaier, P., Lamp, B., Schlagheck, C., Finkernagel, F., Nist, A., Stiewe, T. & Mermoud, J. E. (2019). SMARCAD1 ATPase activity is required to silence endogenous retroviruses in embryonic stem cells. *Nature Communications*, *10*(1). https://doi.org/10.1038/S41467-019-09078-0

Saha, S., Weber, C. A., Nousch, M., Adame-Arana, O., Hoege, C., Hein, M. Y., Osborne-Nishimura, E., Mahamid, J., Jahnel, M., Jawerth, L., Pozniakovski, A., Eckmann, C. R., Jülicher, F. & Hyman, A. A. (2016). Polar Positioning of Phase-Separated Liquid Compartments in Cells Regulated by an mRNA Competition Mechanism. *Cell*, *166*(6), 1572-1584.e16. https://doi.org/10.1016/J.CELL.2016.08.006

Saintillan, D., Shelley, M. J. & Zidovska, A. (2018). Extensile motor activity drives coherent motions in a model of interphase chromatin. *Proceedings of the National Academy of Sciences of the United States of America*, *115*(45), 11442–11447. https://doi.org/10.1073/pnas.1807073115

Sanulli, S., Trnka, M. J., Dharmarajan, V., Tibble, R. W., Pascal, B. D., Burlingame, A. L., Griffin, P. R., Gross, J. D. & Narlikar, G. J. (2019). HP1 reshapes nucleosome core to promote phase separation of heterochromatin. *Nature*, *575*(7782), 390–394. https://doi.org/10.1038/s41586-019-1669-2

Schalch, T., Duda, S., Sargent, D. F. & Richmond, T. J. (2005). *X-ray structure of a tetranucleosome and its implications for the chromatin fibre*. https://doi.org/10.1038/nature03686

Schalch, T., Job, G., Noffsinger, V. J., Shanker, S., Kuscu, C., Joshua-Tor, L. & Partridge, J. F. (2009). High-Affinity Binding of Chp1 Chromodomain to K9 Methylated Histone H3 Is Required to Establish Centromeric Heterochromatin. *Molecular Cell*, *34*(1), 36–46. https://doi.org/10.1016/J.MOLCEL.2009.02.024

Schiessel, H., Widom, J., Bruinsma, R. F. & Gelbart, W. M. (2001). Polymer Reptation and Nucleosome Repositioning. *Physical Review Letters*, *86*(19), 4414. https://doi.org/10.1103/PhysRevLett.86.4414

Schindelin, J., Arganda-Carreras, I., Frise, E., Kaynig, V., Longair, M., Pietzsch, T., Preibisch, S., Rueden, C., Saalfeld, S., Schmid, B., Tinevez, J. Y., White, D. J., Hartenstein, V., Eliceiri, K., Tomancak, P. & Cardona, A. (2012). Fiji: an open-source platform for biological-image analysis. *Nature Methods*, *9*(7), 676–682. https://doi.org/10.1038/NMETH.2019

Schneider, M. W. G., Gibson, B. A., Otsuka, S., Spicer, M. F. D., Petrovic, M., Blaukopf, C., Langer, C. C. H., Batty, P., Nagaraju, T., Doolittle, L. K., Rosen, M. K. & Gerlich, D. W. (2022). A mitotic chromatin phase transition prevents perforation by microtubules. *Nature*, *609*, 183. https://doi.org/10.1038/s41586-022-05027-y

Schoeftner, S. & Blasco, M. A. (2009). A 'higher order'' of telomere regulation: telomere heterochromatin and telomeric RNAs.' *The EMBO Journal*, *28*(16), 2323. https://doi.org/10.1038/EMBOJ.2009.197

Schram, R. D., Klinker, H., Becker, P. B. & Schiessel, H. (2015). Computational study of remodeling in a nucleosomal array. *European Physical Journal E*, *38*(8). https://doi.org/10.1140/epje/i2015-15085-4

Schuck, P. (2000). Size-distribution analysis of macromolecules by sedimentation velocity ultracentrifugation and Lamm equation modeling. *Biophysical Journal*, *78*(3), 1606–1619. https://doi.org/10.1016/S0006-3495(00)76713-0

Schultz, J. & Dobzhansky, T. H. (1934). The Relation of a Dominant Eye Color in Drosophila Melanogaster to the Associated Chromosome Rearrangement. *Genetics*, *19*(4), 344. https://doi.org/10.1093/GENETICS/19.4.344

Schwanbeck, R., Xiao, H. & Wu, C. (2004). Spatial contacts and nucleosome step movements induced by the NURF chromatin remodeling complex. *The Journal of Biological Chemistry*, *279*(38), 39933–39941. https://doi.org/10.1074/JBC.M406060200

Schwartz, U., Németh, A., Diermeier, S., Exler, J. H., Hansch, S., Maldonado, R., Heizinger, L., Merkl, R. & Längst, G. (2019). Characterizing the nuclease accessibility of DNA in human cells to map higher order structures of chromatin. *Nucleic Acids Research*, *47*(3), 1239–1254. https://doi.org/10.1093/NAR/GKY1203

Sehnal, D., Bittrich, S., Deshpande, M., Svobodová, R., Berka, K., Bazgier, V., Velankar, S., Burley, S. K., Koča, J. & Rose, A. S. (2021). Mol* Viewer: modern web app for 3D visualization and analysis of large biomolecular structures. *Nucleic Acids Research*, *49*(W1), W431–W437. https://doi.org/10.1093/NAR/GKAB314

Sexton, T., Yaffe, E., Kenigsberg, E., Bantignies, F., Leblanc, B., Hoichman, M., Parrinello, H., Tanay, A. & Cavalli, G. (2012). Three-Dimensional Folding and Functional Organization Principles of the Drosophila Genome. *Cell*, *148*(3), 458–472. https://doi.org/10.1016/J.CELL.2012.01.010

Shaban, H. A., Barth, R. & Bystricky, K. (2018). Formation of correlated chromatin domains at nanoscale dynamic resolution during transcription. *Nucleic Acids Research*, *46*(13), e77. https://doi.org/10.1093/nar/gky269

Shakya, A. & King, J. T. (2018). DNA Local-Flexibility-Dependent Assembly of Phase-Separated Liquid Droplets. *Biophysical Journal*, *115*(10), 1840–1847. https://doi.org/10.1016/J.BPJ.2018.09.022

Shevtsov, S. P. & Dundr, M. (2011). Nucleation of nuclear bodies by RNA. *Nature Cell Biology 2011 13:2*, *13*(2), 167–173. https://doi.org/10.1038/ncb2157

Shi, B., Li, W., Song, Y., Wang, Z., Ju, R., Ulman, A., Hu, J., Palomba, F., Zhao, Y., Le, J. P., Jarrard, W., Dimoff, D., Digman, M. A., Gratton, E., Zang, C. & Jiang, H. (2021). UTX condensation underlies its tumour-suppressive activity. *Nature*, *597*(7878), 726–731. https://doi.org/10.1038/s41586-021-03903-7

Shi, M., You, K., Chen, T., Hou, C., Liang, Z., Liu, M., Wang, J., Wei, T., Qin, J., Chen, Y., Zhang, M. Q. & Li, T. (2021). Quantifying the phase separation property of chromatin-associated proteins under physiological conditions using an anti-1,6-hexanediol index. *Genome Biology*. https://doi.org/10.1186/s13059-021-02456-2

Shim, Y. S., Choi, Y., Kang, K., Cho, K., Oh, S., Lee, J., Grewal, S. I. S. & Lee, D. (2012). Hrp3 controls nucleosome positioning to suppress non-coding transcription in eu-and heterochromatin. *EMBO Journal*, *31*(23), 4375–4387. https://doi.org/10.1038/emboj.2012.267

Shimada, K., Oma, Y., Schleker, T., Kugou, K., Ohta, K., Harata, M. & Gasser, S. M. (2008). Ino80 Chromatin Remodeling Complex Promotes Recovery of Stalled Replication Forks. *Current Biology*, *18*(8), 566–575. https://doi.org/10.1016/J.CUB.2008.03.049

Shimamoto, Y., Tamura, S., Masumoto, H. & Maeshima, K. (2017). Nucleosome-nucleosome interactions via histone tails and linker DNA regulate nuclear rigidity. *Molecular Biology of the Cell*, *28*(11), 1580–1589. https://doi.org/10.1091/mbc.E16-11-0783

Shin, Y., Chang, Y. C., Lee, D. S. W., Berry, J., Sanders, D. W., Ronceray, P., Wingreen, N. S., Haataja, M. & Brangwynne, C. P. (2018). Liquid Nuclear Condensates Mechanically Sense and Restructure the Genome. *Cell*, *175*(6), 1481-1491.e13. https://doi.org/10.1016/J.CELL.2018.10.057

Shipony, Z., Marinov, G. K., Swaffer, M. P., Sinnott-Armstrong, N. A., Skotheim, J. M., Kundaje, A. & Greenleaf, W. J. (2020). Long-range single-molecule mapping of chromatin accessibility in eukaryotes. *Nature Methods*, *17*(3), 319–327. https://doi.org/10.1038/s41592-019-0730-2

Shrinivas, K., Sabari, B. R., Coffey, E. L., Klein, I. A., Boija, A., Zamudio, A. v., Schuijers, J., Hannett, N. M., Sharp, P. A., Young, R. A. & Chakraborty, A. K. (2019). Enhancer features that drive formation of transcriptional condensates. *Molecular Cell*, *75*(3), 549. https://doi.org/10.1016/J.MOLCEL.2019.07.009

Sikorav, J. L., Pelta, J. & Livolant, F. (1994). A liquid crystalline phase in spermidine-condensed DNA. *Biophysical Journal*, *67*(4), 1387–1392. https://doi.org/10.1016/S0006-3495(94)80640-X

Simic, R., Lindstrom, D. L., Tran, H. G., Roinick, K. L., Costa, P. J., Johnson, A. D., Hartzog, G. A. & Arndt, K. M. (2003). Chromatin remodeling protein Chd1 interacts with transcription elongation factors and localizes to transcribed genes. *EMBO Journal*, *22*(8), 1846–1856. https://doi.org/10.1093/EMBOJ/CDG179

Simpson, R. T., Thoma, F. & Brubaker, J. M. (1985). Chromatin reconstituted from tandemly repeated cloned DNA fragments and core histones: A model system for study of higher order structure. *Cell*, *42*(3), 799–808. https://doi.org/10.1016/0092-8674(85)90276-4

Sims, J. K. & Wade, P. A. (2011). Mi-2/NuRD complex function is required for normal S phase progression and assembly of pericentric heterochromatin. *Molecular Biology of the Cell*, *22*(17), 3094–3102. https://doi.org/10.1091/MBC.E11-03-0258

Singh, A. K. & Mueller-Planitz, F. (2021). Nucleosome Positioning and Spacing: From Mechanism to Function. *Journal of Molecular Biology*, *433*(6), 166847. https://doi.org/10.1016/j.jmb.2021.166847

Singh, A. K., Schauer, T., Pfaller, L., Straub, T. & Mueller-Planitz, F. (2021). The biogenesis and function of nucleosome arrays. *Nature Communications*, *12*(1). https://doi.org/10.1038/s41467-021-27285-6

Sinha, K. K., Gross, J. D. & Narlikar, G. J. (2017). Distortion of histone octamer core promotes nucleosome mobilization by a chromatin remodeler. *Science*, *355*(6322). https://doi.org/10.1126/science.aaa3761

Siriaco, G., Deuring, R., Chioda, M., Becker, P. B. & Tamkun, J. W. (2009). Drosophila ISWI Regulates the Association of Histone H1 With Interphase Chromosomes in Vivo. *Genetics*, *182*(3), 661. https://doi.org/10.1534/GENETICS.109.102053

Snyder, M. W., Kircher, M., Hill, A. J., Daza, R. M. & Shendure, J. (2016). Cell-free DNA Comprises an in Vivo Nucleosome Footprint that Informs Its Tissues-Of-Origin. *Cell*, *164*(1–2), 57–68. https://doi.org/10.1016/j.cell.2015.11.050

Sofueva, S., Yaffe, E., Chan, W. C., Georgopoulou, D., Vietri Rudan, M., Mira-Bontenbal, H., Pollard, S. M., Schroth, G. P., Tanay, A. & Hadjur, S. (2013). Cohesin-mediated interactions organize chromosomal domain architecture. *The EMBO Journal*, *32*(24), 3119. https://doi.org/10.1038/EMBOJ.2013.237

Sokolova, E., Spruijt, E., Hansen, M. M. K., Dubuc, E., Groen, J., Chokkalingam, V., Piruska, A., Heus, H. A. & Huck, W. T. S. (2013). Enhanced transcription rates in membrane-free protocells formed by coacervation of cell lysate. *Proceedings of the National Academy of Sciences of the United States of America*, *110*(29), 11692–11697. https://doi.org/10.1073/PNAS.1222321110/SUPPL_FILE/SM01.AVI

Song, F., Chen, P., Sun, D., Wang, M., Dong, L., Liang, D., Xu, R. M., Zhu, P. & Li, G. (2014). Cryo-EM study of the chromatin fiber reveals a double helix twisted by tetranucleosomal units. *Science*, *344*(6182), 376–380. https://doi.org/10.1126/SCIENCE.1251413/SUPPL_FILE/SONG.SM.PDF

Soufi, A., Donahue, G. & Zaret, K. S. (2012). Facilitators and Impediments of the Pluripotency Reprogramming Factors' Initial Engagement with the Genome. *Cell*, *151*(5), 994. https://doi.org/10.1016/J.CELL.2012.09.045

Spracklin, G. & Pradhan, S. (2020). Protect-seq: genome-wide profiling of nuclease inaccessible domains reveals physical properties of chromatin. *Nucleic Acids Research*, *48*(3), E16. https://doi.org/10.1093/NAR/GKZ1150

Steglich, B., Strålfors, A., Khorosjutina, O., Persson, J., Smialowska, A., Javerzat, J. P. & Ekwall, K. (2015). The Fun30 Chromatin Remodeler Fft3 Controls Nuclear Organization and Chromatin Structure of Insulators and Subtelomeres in Fission Yeast. *PLoS Genetics*, *11*(3), 1005101. https://doi.org/10.1371/JOURNAL.PGEN.1005101

Stergachis, A. B., Debo, B. M., Haugen, E., Churchman, L. S. & Stamatoyannopoulos, J. A. (2020). Single-molecule regulatory architectures captured by chromatin fiber sequencing. *Science*, *368*(6498). https://doi.org/10.1126/SCIENCE.AAZ1646/SUPPL_FILE/AAZ1646_STERGACHIS_SM.PDF

Straka, C. & Horz, W. (1991). A functional role for nucleosomes in the repression of a yeast promoter. *EMBO Journal*, *10*(2), 361–368. https://doi.org/10.1002/j.1460-2075.1991.tb07957.x

Strålfors, A, Walfridsson, J., Bhuiyan, H. & Ekwall, K. (2011). The FUN30 Chromatin Remodeler, Fft3, Protects Centromeric and Subtelomeric Domains from Euchromatin Formation. *PLoS Genet*, *7*(3), 1001334. https://doi.org/10.1371/journal.pgen.1001334

Strålfors, Annelie, Walfridsson, J., Bhuiyan, H. & Ekwall, K. (2011). The FUN30 Chromatin Remodeler, Fft3, Protects Centromeric and Subtelomeric Domains from Euchromatin Formation. *PLoS Genetics*, *7*(3), 1001334. https://doi.org/10.1371/JOURNAL.PGEN.1001334

Strickfaden, H., Tolsma, T. O., Sharma, A., Underhill, D. A., Hansen, J. C. & Hendzel, M. J. (2020a). Condensed Chromatin Behaves like a Solid on the Mesoscale In Vitro and in Living Cells. *Cell*, *183*(7), 1772-1784.e13. https://doi.org/10.1016/J.CELL.2020.11.027

Strickfaden, H., Tolsma, T., Sharma, A., Underhill, D. A., Hansen, J. & Hendzel, M. (2020b). Condensed Chromatin Behaves Like a Solid on the Mesoscale in Vitro and in Living Cells. *SSRN Electronic Journal*. https://doi.org/10.1101/2020.05.06.079905

Strohkendl, I., Saifuddin, F. A., Gibson, B. A., Rosen, M. K., Russell, R. & Finkelstein, I. J. (2021). Inhibition of CRISPR-Cas12a DNA targeting by nucleosomes and chromatin. In *Sci. Adv* (Vol. 7). https://www.science.org

Strohner, R., Wachsmuth, M., Dachauer, K., Mazurkiewicz, J., Hochstatter, J., Rippe, K. & Längst, G. (2005). A "loop recapture" mechanism for ACF-dependent nucleosome remodeling. *NATURE STRUCTURAL & MOLECULAR BIOLOGY*, *12*. https://doi.org/10.1038/nsmb966

Strom, A. R., Emelyanov, A. V, Mir, M., Fyodorov, D. V, Darzacq, X. & Karpen, G. H. (2017). *Phase separation drives heterochromatin domain formation*. https://doi.org/10.1038/nature22989

Struhl, K. & Segal, E. (2013). Determinants of nucleosome positioning. *Nature Structural and Molecular Biology*, *20*(3), 267–273. https://doi.org/10.1038/nsmb.2506

Strulson, C. A., Molden, R. C., Keating, C. D. & Bevilacqua, P. C. (2012). RNA catalysis through compartmentalization. *Nature Chemistry 2012 4:11*, *4*(11), 941–946. https://doi.org/10.1038/nchem.1466

Su, X., Ditlev, J. A., Hui, E., Xing, W., Banjade, S., Okrut, J., King, D. S., Taunton, J., Rosen, M. K. & Vale, R. D. (2016). Phase separation of signaling molecules promotes T cell receptor signal transduction. *Science (New York, N.Y.)*, *352*(6285), 595. https://doi.org/10.1126/SCIENCE.AAD9964

Sugiyama, T., Cam, H. P., Sugiyama, R., Noma, K. ichi, Zofall, M., Kobayashi, R. & Grewal, S. I. S. (2007). SHREC, an Effector Complex for Heterochromatic Transcriptional Silencing. *Cell*, *128*(3), 491–504. https://doi.org/10.1016/j.cell.2006.12.035

Syed, S. H., Goutte-Gattat, D., Becker, N., Meyer, S., Shukla, M. S., Hayes, J. J., Everaers, R., Angelov, D., Bednar, J. & Dimitrov, S. (2010). Single-base resolution mapping of H1-nucleosome interactions and 3D organization of the nucleosome. *Proceedings of the National Academy of Sciences of the United States of America*, *107*(21), 9620–9625. https://doi.org/10.1073/PNAS.1000309107/-/DCSUPPLEMENTAL

Tabata, T. & Iwabuchi, M. (1984). Molecular cloning and nucleotide sequence of a variant wheat histone H4 gene. *Gene*, *31*, 285–289.

Takata, H., Hanafusa, T., Mori, T., Shimura, M. & Iida, Y. (2013). Chromatin Compaction Protects Genomic DNA from Radiation Damage. *PLoS ONE*, *8*(10), 75622. https://doi.org/10.1371/journal.pone.0075622

Taneja, N., Zofall, M., Balachandran, V., Thillainadesan, G., Sugiyama, T., Wheeler, D., Zhou, M. & Grewal, S. I. S. (2017). SNF2 Family Protein Fft3 Suppresses Nucleosome Turnover to Promote Epigenetic Inheritance and Proper Replication. *Molecular Cell*, *66*(1), 50. https://doi.org/10.1016/J.MOLCEL.2017.02.006

Taylor, N. O., Wei, M. T., Stone, H. A. & Brangwynne, C. P. (2019a). Quantifying Dynamics in Phase-Separated Condensates Using Fluorescence Recovery after Photobleaching. *Biophysical Journal*, *117*(7), 1285–1300. https://doi.org/10.1016/J.BPJ.2019.08.030

Taylor, N. O., Wei, M. T., Stone, H. A. & Brangwynne, C. P. (2019b). Quantifying Dynamics in Phase-Separated Condensates Using Fluorescence Recovery after Photobleaching. *Biophysical Journal*, *117*(7), 1285–1300. https://doi.org/10.1016/J.BPJ.2019.08.030

Tilly, B. C., Chalkley, G. E., van der Knaap, J. A., Moshkin, Y. M., Kan, T. W., Dekkers, D. H. W., Demmers, J. A. A. & Peter Verrijzer, C. (2021). In vivo analysis reveals that ATP-hydrolysis couples remodeling to SWI/SNF release from chromatin. *ELife*, *10*. https://doi.org/10.7554/eLife.69424

Torigoe, S. E., Patel, A., Khuong, M. T., Bowman, G. D. & Kadonaga, J. T. (2013). ATP-dependent chromatin assembly is functionally distinct from chromatin remodeling. *ELife*, *2*. https://doi.org/10.7554/ELIFE.00863

Trojanowski, J., Frank, L., Rademacher, A., Grigaitis, P. & Rippe, K. (2021). Transcription activation is enhanced by multivalent interactions independent of liquid-liquid phase separation. *BioRxiv*, *82*(10), 2021.01.27.428421. https://doi.org/10.1016/J.MOLCEL.2022.04.017

Tsukiyama, T., Palmer, J., Landel, C. C., Shiloach, J. & Wu, C. (1999). *Characterization of the Imitation Switch subfamily of ATP-dependent chromatin-remodeling factors in Saccharomyces cerevisiae*. www.genesdev.org

Tumbar, T., Sudlow, G. & Belmont, A. S. (1999). Large-Scale Chromatin Unfolding and Remodeling Induced by VP16 Acidic Activation Domain. *The Journal of Cell Biology*, *145*(7), 1341. https://doi.org/10.1083/JCB.145.7.1341

Udugama, M., Sabri, A. & Bartholomew, B. (2011). The INO80 ATP-Dependent Chromatin Remodeling Complex Is a Nucleosome Spacing Factor. *Molecular and Cellular Biology*, *31*(4), 662–673. https://doi.org/10.1128/MCB.01035-10

Ulianov, S. v, Velichko, A. K., Magnitov, M. D., Luzhin, A. v, Golov, A. K., Ovsyannikova, N., Kireev, I. I., Gavrikov, A. S., Mishin, A. S., Garaev, A. K., Tyakht, A. v, Gavrilov, A. A., Kantidze, O. L. & Razin, S. v. (2021). Suppression of liquid-liquid phase separation by 1,6-hexanediol partially compromises the 3D genome organization in living cells. *Nucleic Acids Research*, *49*(18), 10524–10541. https://doi.org/10.1093/nar/gkab249

Valouev, A., Johnson, S. M., Boyd, S. D., Smith, C. L., Fire, A. Z. & Sidow, A. (2011). Determinants of nucleosome organization in primary human cells. *Nature*. https://doi.org/10.1038/nature10002

Van Attikum, H., Fritsch, O. & Gasser, S. M. (2007). Distinct roles for SWR1 and INO80 chromatin remodeling complexes at chromosomal double-strand breaks. *EMBO Journal*, *26*(18), 4113–4125. https://doi.org/10.1038/SJ.EMBOJ.7601835

Van Attikum, H., Fritsch, O., Hohn, B. & Gasser, S. M. (2004). Recruitment of the INO80 complex by H2A phosphorylation links ATP-dependent chromatin remodeling with DNA double-strand break repair. *Cell*, *119*(6), 777–788. https://doi.org/10.1016/J.CELL.2004.11.033

van Holde, K. E. & Yager, T. D. (1985). Nucleosome Motion: Evidence and Models. *Structure and Function of the Genetic Apparatus*, 35–53. https://doi.org/10.1007/978-1-4684-5024-8_4

van Holde, K. & Yager, T. (2003). Models for chromatin remodeling: A critical comparison. *Biochemistry and Cell Biology*, *81*(3), 169–172. https://doi.org/10.1139/o03-038

Varga-Weisz, P. D., Wilm, M., Bonte, E., Dumas, K., Mann, M. & Becker, P. B. (1997). Chromatin-remodelling factor CHRAC contains the ATPases ISWI and topoisomerase II. *Nature*, *388*(6642), 598–602. https://doi.org/10.1038/41587

Velankar, S. S., Soultanas, P., Dillingham, M. S., Subramanya, H. S. & Wigley, D. B. (1999). Crystal structures of complexes of PcrA DNA helicase with a DNA substrate indicate an inchworm mechanism. *Cell*, *97*(1), 75–84. https://doi.org/10.1016/S0092-8674(00)80716-3

Vendruscolo, M. & Fuxreiter, M. (2022). Protein condensation diseases: therapeutic opportunities. *Nature Communications*. https://doi.org/10.1038/s41467-022-32940-7

Verdel, A., Jia, S., Gerber, S., Sugiyama, T., Gygi, S., Grewal, S. I. S. & Moazed, D. (2004). RNAi-mediated targeting of heterochromatin by the RITS complex. *Science (New York, N.Y.)*, *303*(5658), 672–676. https://doi.org/10.1126/SCIENCE.1093686

Verschure, P. J., van der Kraan, I., de Leeuw, W., van der Vlag, J., Carpenter, A. E., Belmont, A. S. & van Driel, R. (2005). In vivo HP1 targeting causes large-scale chromatin condensation and enhanced histone lysine methylation. *Molecular and Cellular Biology*, *25*(11), 4552–4564. https://doi.org/10.1128/MCB.25.11.4552-4564.2005

Vincent, J. A., Kwong, T. J. & Tsukiyama, T. (2008). ATP-dependent chromatin remodeling shapes the DNA replication landscape. *Nature Structural & Molecular Biology*, *15*(5), 477–484. https://doi.org/10.1038/NSMB.1419

Wakimoto, B. T. & Hearn, M. G. (1990). *The Effects of Chromosome Rearrangements on the Expression of Heterochromatic Genes in Chromosome 2L of Drosophila melanogaster*. https://academic.oup.com/genetics/article/125/1/141/6000728

Walfridsson, J., Bjerling, P., Thalen, M., Yoo, E. J., Park, S. D. & Ekwall, K. (2005). The CHD remodeling factor Hrp1 stimulates CENP-A loading to centromeres. *Nucleic Acids Research*, *33*(9), 2868–2879. https://doi.org/10.1093/nar/gki579

Wang, J., Choi, J. M., Holehouse, A. S., Lee, H. O., Zhang, X., Jahnel, M., Maharana, S., Lemaitre, R., Pozniakovsky, A., Drechsel, D., Poser, I., Pappu, R. v., Alberti, S. & Hyman, A. A. (2018). A Molecular Grammar Governing the Driving Forces for Phase Separation of Prion-like RNA Binding Proteins. *Cell*, *174*(3), 688-699.e16. https://doi.org/10.1016/j.cell.2018.06.006

Wang, Xi, Zhou, X., Yan, Q., Liao, S., Tang, W., Xu, P., Gao, Y., Li, Q., Dou, Z., Yang, W., Huang, B., Li, J. & Zhang, Z. (2022). LLPSDB v2.0: an updated database of proteins undergoing liquid–liquid phase separation in vitro. *Bioinformatics*, *38*(7), 2010. https://doi.org/10.1093/BIOINFORMATICS/BTAC026

Wang, Xiaoyi & Moazed, D. (2017). DNA sequence-dependent epigenetic inheritance of gene silencing and histone H3K9 methylation. *Science (New York, N.Y.)*, *356*(6333), 88–91. https://doi.org/10.1126/SCIENCE.AAJ2114

Wang, Xiaoying, He, C., Moore, S. C. & Ausió, J. (2001). Effects of histone acetylation on the solubility and folding of the chromatin fiber. *The Journal of Biological Chemistry*, *276*(16), 12764–12768. https://doi.org/10.1074/JBC.M100501200

Wang, Y., Wang, A., Liu, Z., Thurman, A. L., Powers, L. S., Zou, M., Zhao, Y., Hefe, A., Li, Y., Zabner, J. & Au, K. F. (2019). Single-molecule long-read sequencing reveals the chromatin basis of gene expression. *Genome Research*, *29*(8), 1329–1342. https://doi.org/10.1101/GR.251116.119

Weber, S. C. (2017). Sequence-encoded material properties dictate the structure and function of nuclear bodies. *Current Opinion in Cell Biology*, *46*, 62–71. https://doi.org/10.1016/J.CEB.2017.03.003

Weber, S. C. & Brangwynne, C. P. (2015). Inverse size scaling of the nucleolus by a concentration-dependent phase transition. *Current Biology*, *25*(5), 641–646. https://doi.org/10.1016/J.CUB.2015.01.012

Weber, S. C., Spakowitz, A. J. & Theriot, J. A. (2012). Nonthermal ATP-dependent fluctuations contribute to the in vivo motion of chromosomal loci. *Proceedings of the National Academy of Sciences of the United States of America*, *109*(19), 7338–7343. https://doi.org/10.1073/pnas.1119505109

Wei, M. T., Elbaum-Garfinkle, S., Holehouse, A. S., Chen, C. C. H., Feric, M., Arnold, C. B., Priestley, R. D., Pappu, R. v. & Brangwynne, C. P. (2017). Phase behaviour of disordered proteins underlying low density and high permeability of liquid organelles. *Nature Chemistry*, *9*(11). https://doi.org/10.1038/NCHEM.2803

Weidemann, T., Wachsmuth, M., Knoch, T. A., Müller, G., Waldeck, W. & Langowski, J. (2003). Counting nucleosomes in living cells with a combination of fluorescence correlation spectroscopy and confocal imaging. *Journal of Molecular Biology*, *334*(2), 229–240. https://doi.org/10.1016/j.jmb.2003.08.063

Whitehouse, I., Rando, O. J., Delrow, J. & Tsukiyama, T. (2007). Chromatin remodelling at promoters suppresses antisense transcription. *Nature*, *450*(7172), 1031–1035. https://doi.org/10.1038/nature06391

Whitehouse, I., Stockdale, C., Flaus, A., Szczelkun, M. D. & Owen-Hughes, T. (2003). Evidence for DNA Translocation by the ISWI Chromatin-Remodeling Enzyme. *Molecular and Cellular Biology*, *23*(6), 1935–1945. https://doi.org/10.1128/MCB.23.6.1935-1945.2003

Wiechens, N., Singh, V., Gkikopoulos, T., Schofield, P., Rocha, S. & Owen-Hughes, T. (2016). The Chromatin Remodelling Enzymes SNF2H and SNF2L Position Nucleosomes adjacent to CTCF and Other Transcription Factors. *PLOS Genetics*, *12*(3), e1005940. https://doi.org/10.1371/JOURNAL.PGEN.1005940

Wilbertz, J. H., Voigt, F., Horvathova, I., Roth, G., Zhan, Y. & Chao, J. A. (2019). Single-Molecule Imaging of mRNA Localization and Regulation during the Integrated Stress Response. *Molecular Cell*, *73*(5), 946-958.e7. https://doi.org/10.1016/J.MOLCEL.2018.12.006

Wilkinson, C. R. M., Bartlett, R., Nurse, P. & Bird, A. P. (1995). The fission yeast gene pmt1 + encodes a DNA methyltransferase homologue. In *Nucleic Acids Research* (Vol. 23, Issue 2).

Wood, V., Gwilliam, R., Rajandream, M. A., Lyne, M., Lyne, R., Stewart, A., Sgouros, J., Peat, N., Hayles, J., Baker, S., Basham, D., Bowman, S., Brooks, K., Brown, D., Brown, S., Chillingworth, T., Churcher, C., Collins, M., Connor, R., … Nurse, P. (2002). The genome sequence of Schizosaccharomyces pombe. *Nature 2002 415:6874*, *415*(6874), 871–880. https://doi.org/10.1038/nature724

Woodcock, C. L. F. (1973). Ultrastructure of inactive chromatin. *Journal of Cell Biology*, *59*, A368.

Woodcock, C. L. F., Frado, L. L. Y. & Rattner, J. B. (1984). The higher-order structure of chromatin: evidence for a helical ribbon arrangement. *The Journal of Cell Biology*, *99*(1 Pt 1), 42. https://doi.org/10.1083/JCB.99.1.42

Woodcock, C. L. & Horowitz, R. A. (1995). Chromatin organization re-viewed. In *Trends in Cell Biology* (Vol. 5, Issue 7, pp. 272–277). https://doi.org/10.1016/S0962-8924(00)89038-8

Wutz, G., Várnai, C., Nagasaka, K., Cisneros, D. A., Stocsits, R. R., Tang, W., Schoenfelder, S., Jessberger, G., Muhar, M., Hossain, M. J., Walther, N., Koch, B., Kueblbeck, M., Ellenberg, J., Zuber, J., Fraser, P. & Peters, J. (2017). Topologically associating domains and chromatin loops depend on cohesin and are regulated by CTCF, WAPL, and PDS5 proteins. *The EMBO Journal*, *36*(24), 3573–3599. https://doi.org/10.15252/EMBJ.201798004

Xiang, W., Roberti, M. J., Hériché, J. K., Huet, S., Alexander, S. & Ellenberg, J. (2018). Correction: Correlative live and super-resolution imaging reveals the dynamic structure of replication domains (Journal of Cell Biology (2018) 217:6 DOI: 10.1083/jcb.201709074). *Journal of Cell Biology*, *217*(9), 3315. https://doi.org/10.1083/JCB.20170907408082018c

Xing, Z., Caciagli, A., Cao, T., Stoev, I., Zupkauskas, M., O'Neill, T., Wenzel, T., Lamboll, R., Liu, D. & Eiser, E. (2018). Microrheology of DNA hydrogels. *Proceedings of the National Academy of Sciences of the United States of America*, *115*(32), 8137–8142. https://doi.org/10.1073/PNAS.1722206115/SUPPL_FILE/PNAS.1722206115.SAPP.PDF

Xu, J., Ma, H., Jin, J., Uttam, S., Fu, R., Huang, Y. & Liu, Y. (2018). Super-Resolution Imaging of Higher-Order Chromatin Structures at Different Epigenomic States in Single Mammalian Cells. *Cell Reports*, *24*(4), 873–882. https://doi.org/10.1016/J.CELREP.2018.06.085

Yadav, T. & Whitehouse, I. (2016). Replication-Coupled Nucleosome Assembly and Positioning by ATP-Dependent Chromatin-Remodeling Enzymes. *Cell Reports*, *15*(4), 715–723. https://doi.org/10.1016/J.CELREP.2016.03.059

Yamada, K., Frouws, T. D., Angst, B., Fitzgerald, D. J., Deluca, C., Schimmele, K., Sargent, D. F. & Richmond, T. J. (2011). Structure and mechanism of the chromatin remodelling factor ISW1a. *Nature*. https://doi.org/10.1038/nature09947

Yamamoto, K. & Sonoda, M. (2003). Self-interaction of heterochromatin protein 1 is required for direct binding to histone methyltransferase, SUV39H1. *Biochemical and Biophysical Research Communications*, *301*(2), 287–292. https://doi.org/10.1016/S0006-291X(02)03021-8

Yan, L., Wang, L., Tian, Y., Xia, X. & Chen, Z. (2016). *Structure and regulation of the chromatin remodeller ISWI*. https://doi.org/10.1038/nature20590

Yan, L. & Wu, H. (2019). Structures of the ISWI–nucleosome complex reveal a conserved mechanism of chromatin remodeling. *Nature Structural & Molecular Biology*. https://doi.org/10.1038/s41594-019-0199-9

Yang, J. G., Madrid, T. S., Sevastopoulos, E. & Narlikar, G. J. (2006). The chromatin-remodeling enzyme ACF is an ATP-dependent DNA length sensor that regulates nucleosome spacing. *Nature Structural and Molecular Biology*, *13*(12), 1078–1083. https://doi.org/10.1038/nsmb1170

Yang, J. G. & Narlikar, G. J. (2007). FRET-based methods to study ATP-dependent changes in chromatin structure. *Methods*, *41*(3), 291–295. https://doi.org/10.1016/j.ymeth.2006.08.015

Yokoyama, H., Rybina, S., Santarella-Mellwig, R., Mattaj, I. W. & Karsenti, E. (2009). ISWI is a RanGTP-dependent MAP required for chromosome segregation. *Journal of Cell Biology*, *187*(6), 813–829. https://doi.org/10.1083/JCB.200906020/VIDEO-3

Yuan, G. C., Liu, Y. J., Dion, M. F., Slack, M. D., Wu, L. F., Altschuler, S. J. & Rando, O. J. (2005). Genome-scale identification of nucleosome positions in S. cerevisiae. *Science*, *309*(5734), 626–630. https://doi.org/10.1126/science.1112178

Zhang, K., Mosch, K., Fischle, W. & Grewal, S. I. S. (2008). Roles of the Clr4 methyltransferase complex in nucleation, spreading and maintenance of heterochromatin. *Nature Structural & Molecular Biology 2008 15:4*, *15*(4), 381–388. https://doi.org/10.1038/nsmb.1406

Zhang, M., Díaz-Celis, C., Onoa, B., Cañari-Chumpitaz, C., Requejo, K. I., Liu, J., Vien, M., Nogales, E., Ren, G. & Bustamante, C. (2022). Molecular Organization of the Early Stages of Nucleosome Phase Separation Visualized by Cryo-Electron Tomography. *Molecular Cell*, *82*(16), 3000. https://doi.org/10.1016/J.MOLCEL.2022.06.032

Zhang, Yaojun, Pyo, A. G. T., Jiang, Y., Brangwynne, P., Stone, H. A. & Wingreen, N. S. (2022). Interface resistance of biomolecular condensates. *BioRxiv*, 1–6. https://doi.org/10.1101/2022.03.16.484641

Zhang, Yi, Bertulat, B., Tencer, A. H., Ren, X., Wright, G. M., Black, J., Cardoso, M. C. & Kutateladze, T. G. (2019). MORC3 Forms Nuclear Condensates through Phase Separation. *IScience*, *17*, 182. https://doi.org/10.1016/J.ISCI.2019.06.030

Zhang, Yi, Brown, K., Yu, Y., Ibrahim, Z., Zandian, M., Xuan, H., Ingersoll, S., Lee, T., Ebmeier, C. C., Liu, J., Panne, D., Shi, X., Ren, X. & Kutateladze, T. G. (2021). Nuclear condensates of p300 formed though the structured catalytic core can act as a storage pool of p300 with reduced HAT activity. *Nature Communications*, *12*(1). https://doi.org/10.1038/s41467-021-24950-8

Zhang, Yi, Narlikar, G. J. & Kutateladze, T. G. (2021). Enzymatic Reactions inside Biological Condensates. *Journal of Molecular Biology*, *433*(12). https://doi.org/10.1016/j.jmb.2020.08.009

Zhang, Yongli, Smith, C. L., Saha, A., Grill, S. W., Mihardja, S., Smith, S. B., Cairns, B. R., Peterson, C. L. & Bustamante, C. (2006). DNA translocation and loop formation mechanism of chromatin remodeling by SWI/SNF and RSC. *Molecular Cell*, *24*(4), 559–568. https://doi.org/10.1016/J.MOLCEL.2006.10.025

Zhao, E. M., Suek, N., Wilson, M. Z., Dine, E., Pannucci, N. L., Gitai, Z., Avalos, J. L. & Toettcher, J. E. (2019). Light-based control of metabolic flux through assembly of synthetic organelles. *Nature Chemical Biology*, *15*(6), 589–597. https://doi.org/10.1038/S41589-019-0284-8

Zhao, H., Chiaro, C. R., Zhang, L., Smith, P. B., Chan, C. Y., Pedley, A. M., Pugh, R. J., French, J. B., Patterson, A. D. & Benkovic, S. J. (2015). Quantitative analysis of purine nucleotides indicates that purinosomes increase de novo purine biosynthesis. *The Journal of Biological Chemistry*, *290*(11), 6705–6713. https://doi.org/10.1074/JBC.M114.628701

Zhou, J., Chau, C. M., Deng, Z., Shiekhattar, R., Spindler, M. P., Schepers, A. & Lieberman, P. M. (2005). Cell cycle regulation of chromatin at an origin of DNA replication. *EMBO Journal*, *24*(7), 1406–1417. https://doi.org/10.1038/sj.emboj.7600609

Zhou, Y. B., Gerchman, S. E., Ramakrishnan, V., Travers, A. & Muyldermans, S. (1998). Position and orientation of the globular domain of linker histone H5 on the nucleosome. *Nature 1998 395:6700*, *395*(6700), 402–405. https://doi.org/10.1038/26521

Zidovska, A. (2020). The self-stirred genome: large-scale chromatin dynamics, its biophysical origins and implications. *Current Opinion in Genetics and Development*, *61*, 83–90. https://doi.org/10.1016/j.gde.2020.03.008

Zidovska, A., Weitz, D. A. & Mitchison, T. J. (2013a). Micron-scale coherence in interphase chromatin dynamics. *Proceedings of the National Academy of Sciences of the United States of America*, *110*(39), 15555–15560. https://doi.org/10.1073/pnas.1220313110

Zidovska, A., Weitz, D. A. & Mitchison, T. J. (2013b). Micron-scale coherence in interphase chromatin dynamics. *Proceedings of the National Academy of Sciences of the United States of America*, *110*(39), 15555–15560. https://doi.org/10.1073/pnas.1220313110

Zofall, M., Persinger, J. & Bartholomew, B. (2004). Functional Role of Extranucleosomal DNA and the Entry Site of the Nucleosome in Chromatin Remodeling by ISW2. *Molecular and Cellular Biology*, *24*(22), 10047–10057. https://doi.org/10.1128/MCB.24.22.10047-10057.2004

Zofall, M., Yamanaka, S., Reyes-Turcu, F. E., Zhang, K., Rubin, C. & Grewal, S. I. S. (2012). RNA elimination machinery targeting meiotic mRNAs promotes facultative heterochromatin formation. *Science (New York, N.Y.)*, *335*(6064), 96–100. https://doi.org/10.1126/SCIENCE.1211651

Zuin, J., Dixon, J. R., Van Der Reijden, M. I. J. A., Ye, Z., Kolovos, P., Brouwer, R. W. W., Van De Corput, M. P. C., Van De Werken, H. J. G., Knoch, T. A., Van Ijcken, W. F. J., Grosveld, F. G., Ren, B. & Wendt, K. S. (2014). Cohesin and CTCF differentially affect chromatin architecture and gene expression in human cells. *Proceedings of the National Academy of Sciences of the United States of America*, *111*(3), 996–1001. https://doi.org/10.1073/PNAS.1317788111/SUPPL_FILE/SAPP.PDF

Appendix A: Vector maps of all plasmids created as part of this thesis

pFMP488 (pJR1-3xL) (8833 bp)

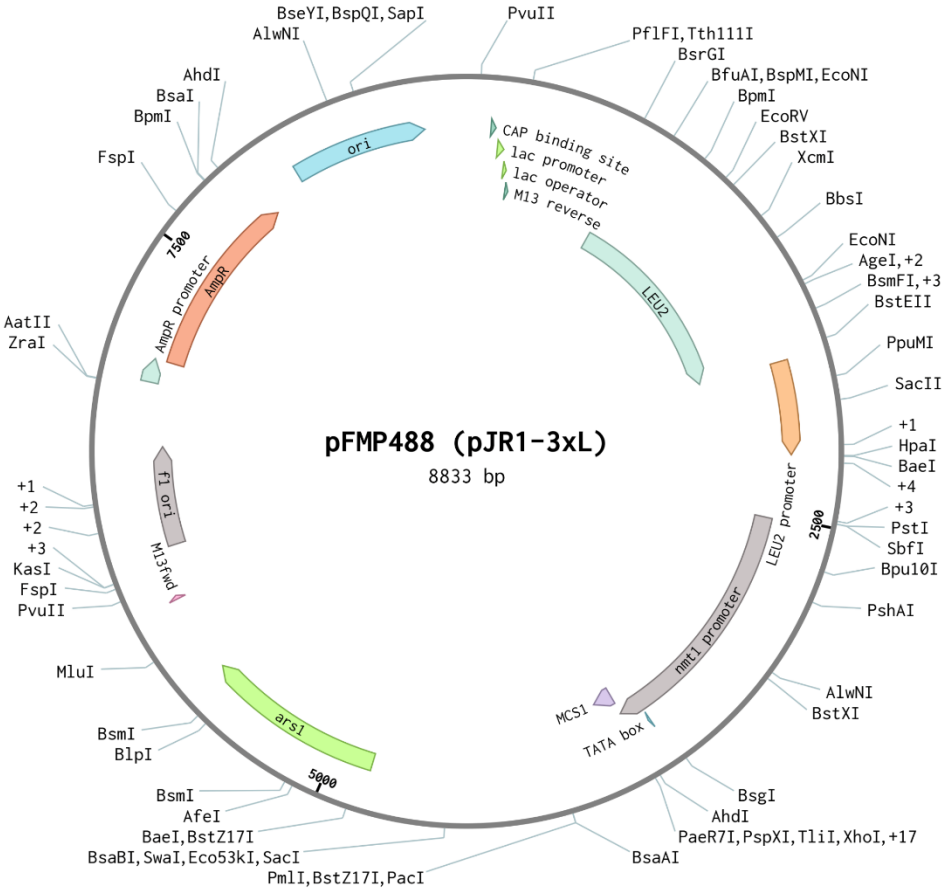

pFMP489 (pJR41-3xL) (8829 bp)

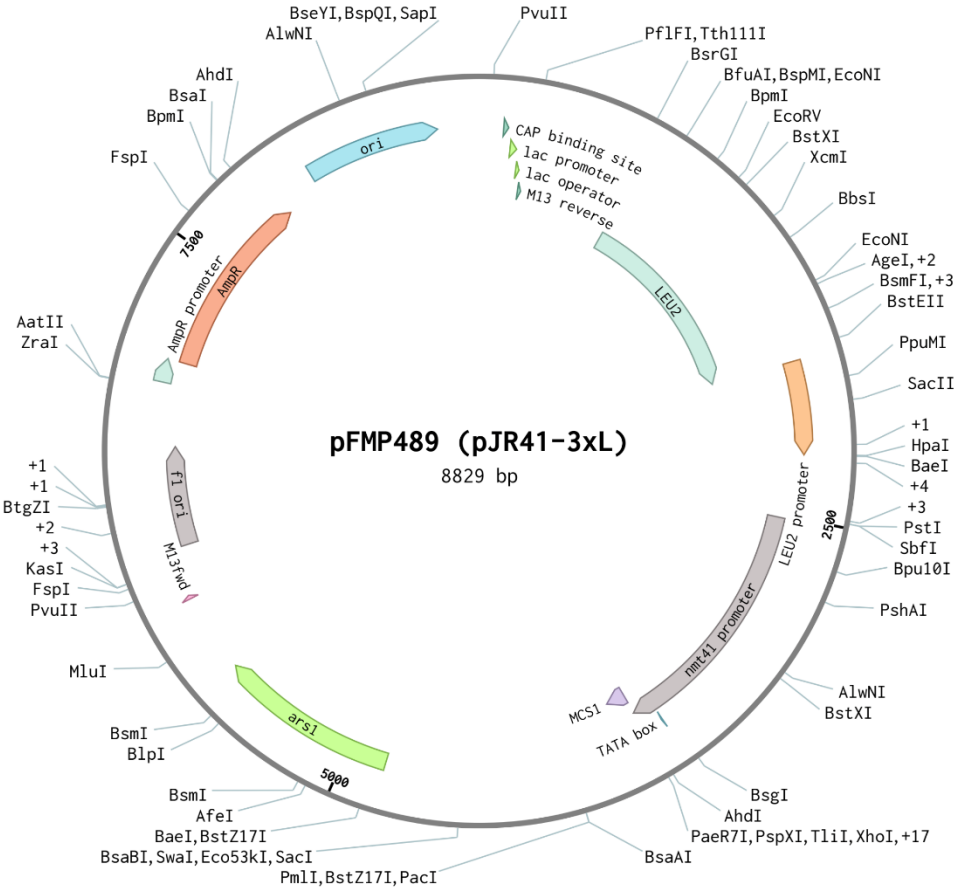

pFMP490 (pJR81-3xL) (8826 bp)

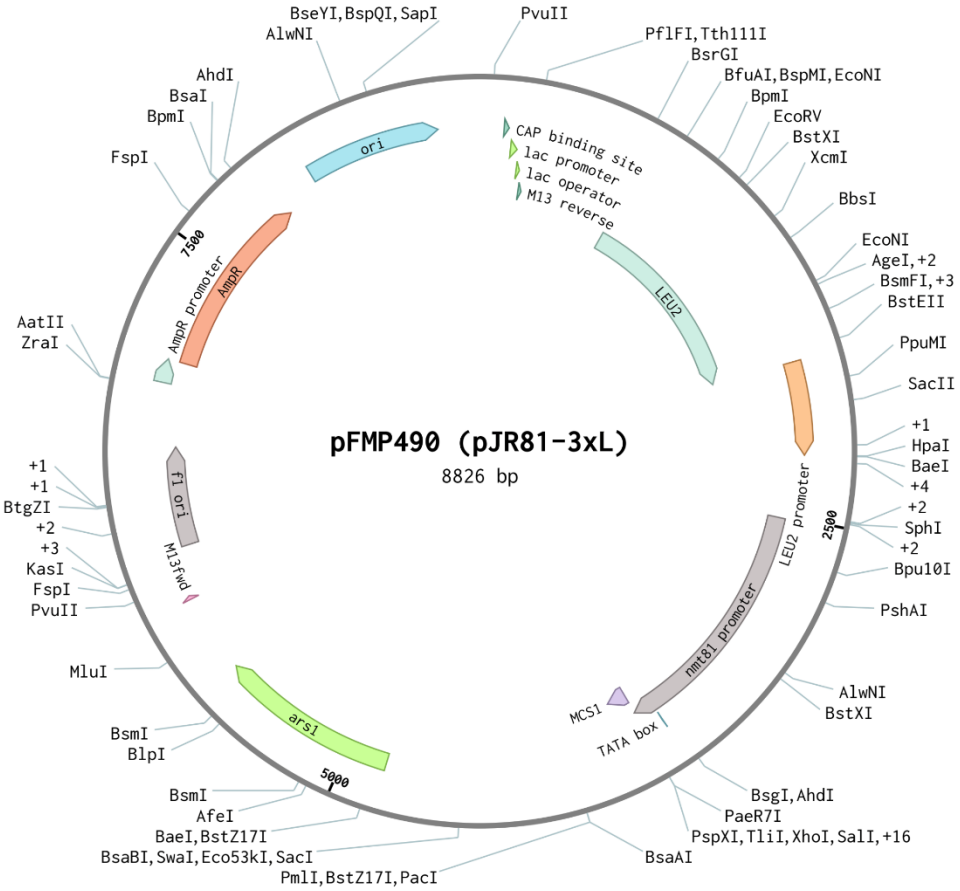

pFMP501 (13256 bp)

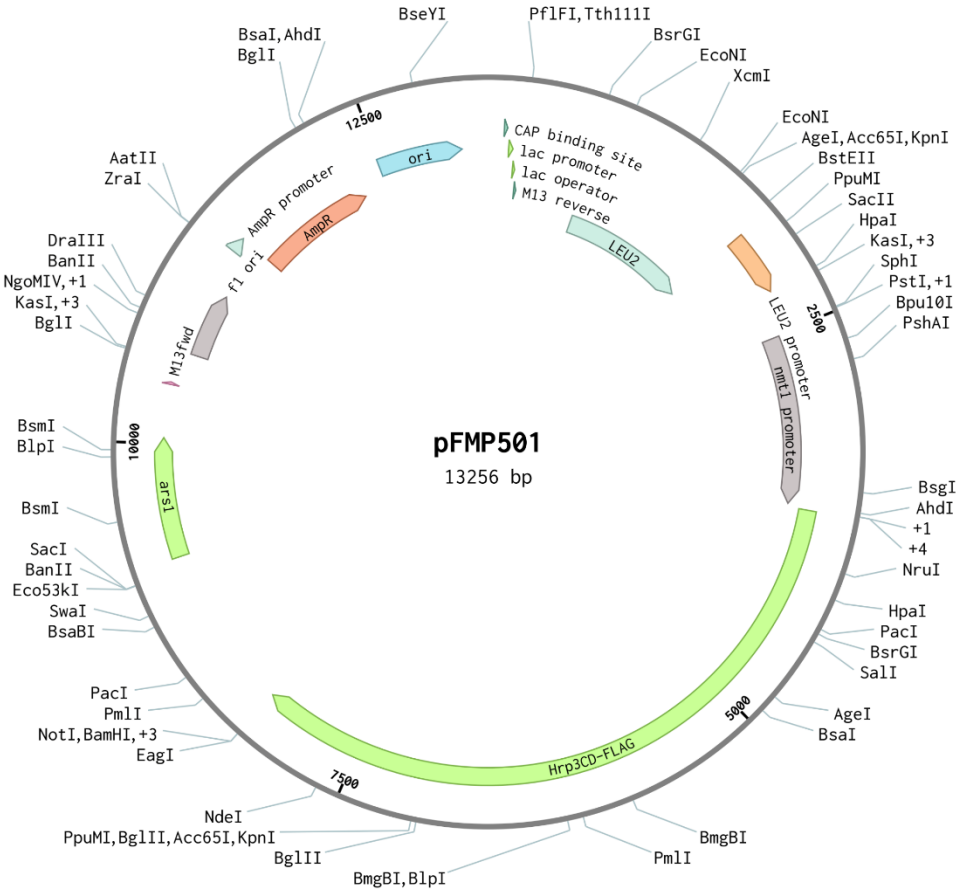

pFMP502 (9072 bp)

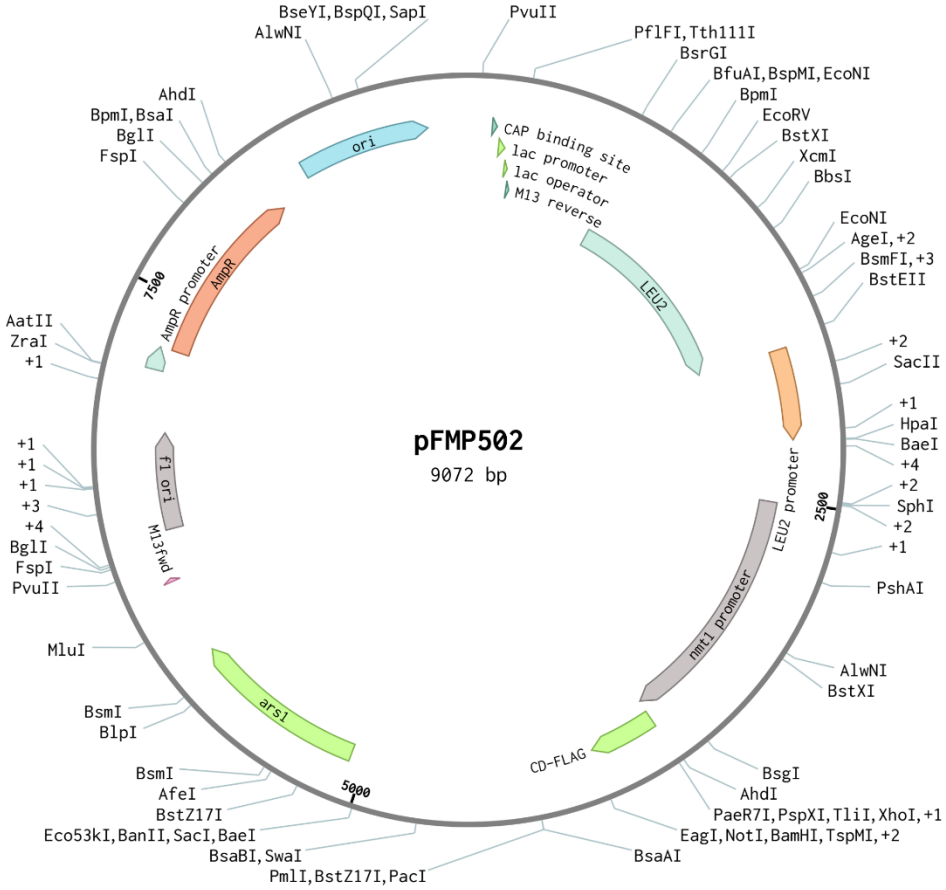

pFMP503 (12959 bp)

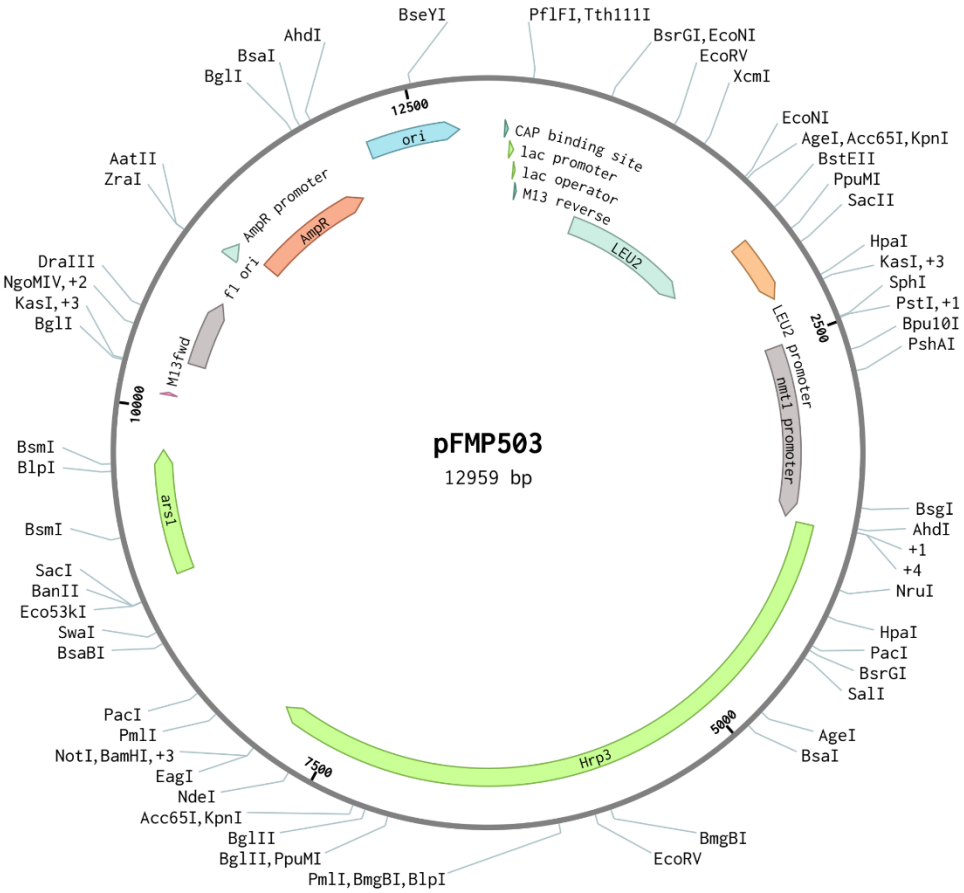

pFMP504 (13256 bp)

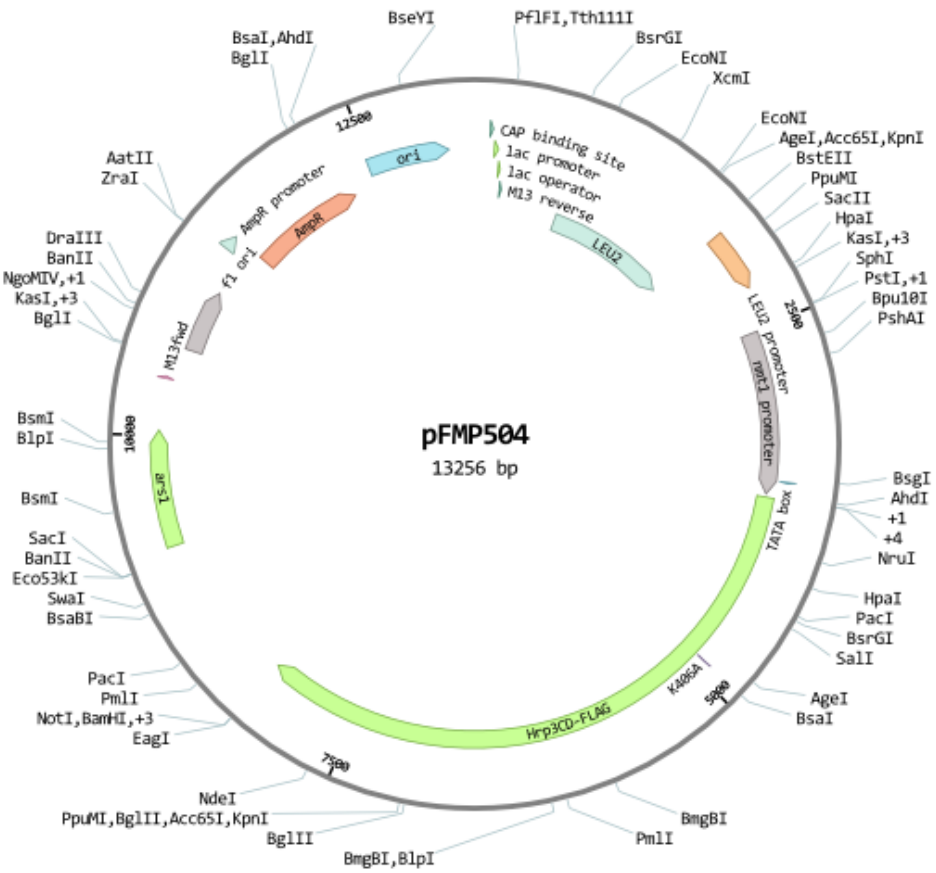

pFMP790 (11902 bp)

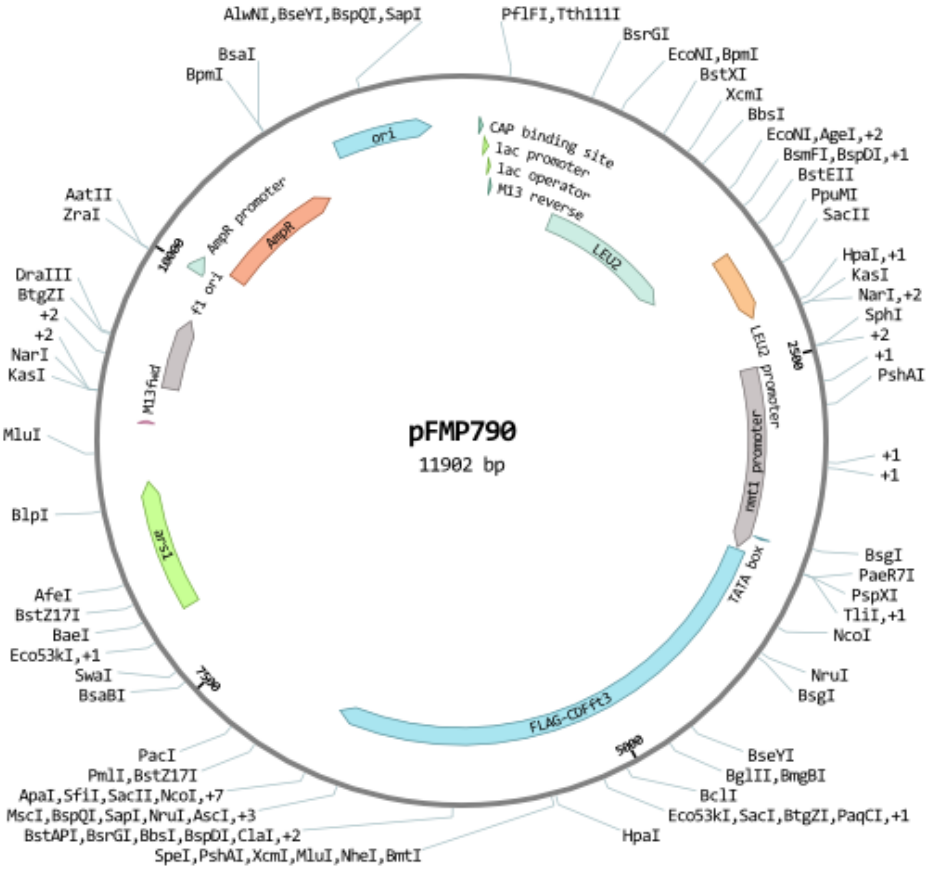

pFMP791 (11893 bp)

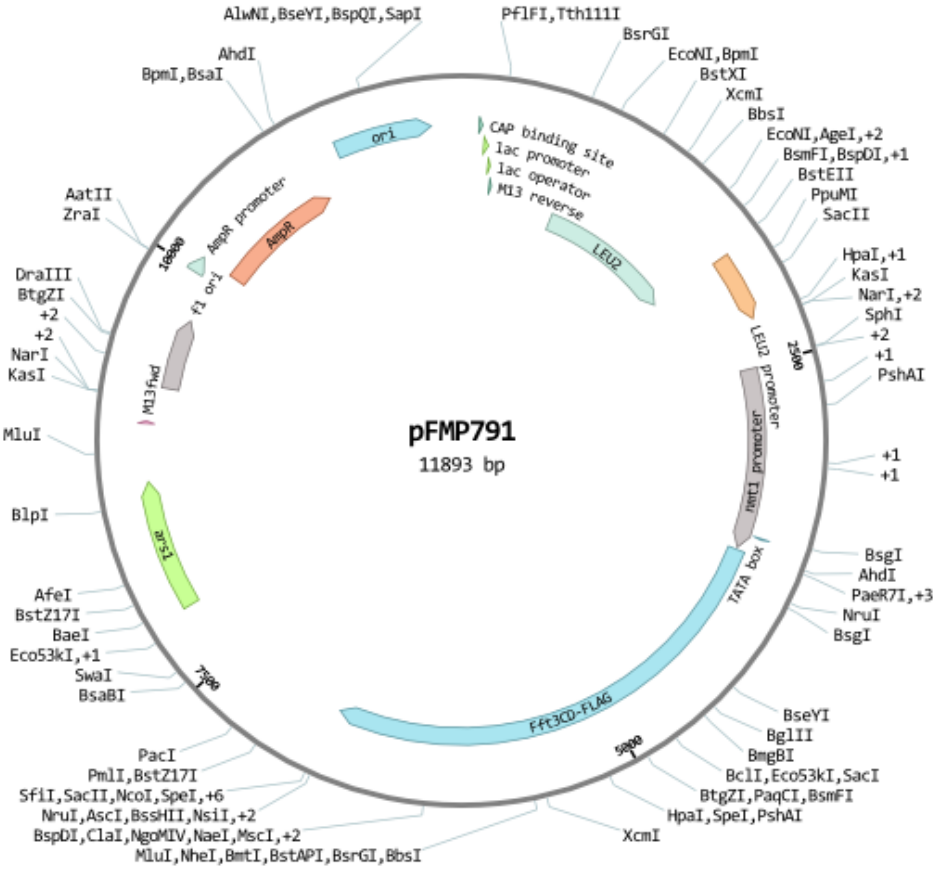

pFMP792(11602 bp)

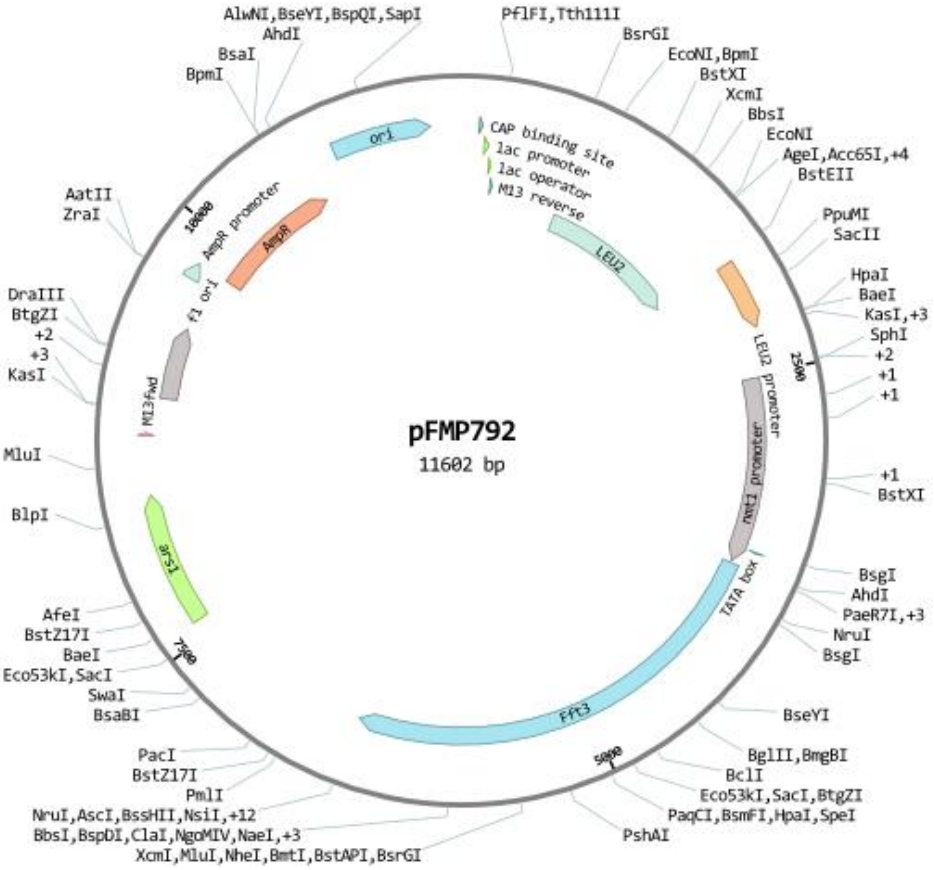

pFMP793 (13046 bp)

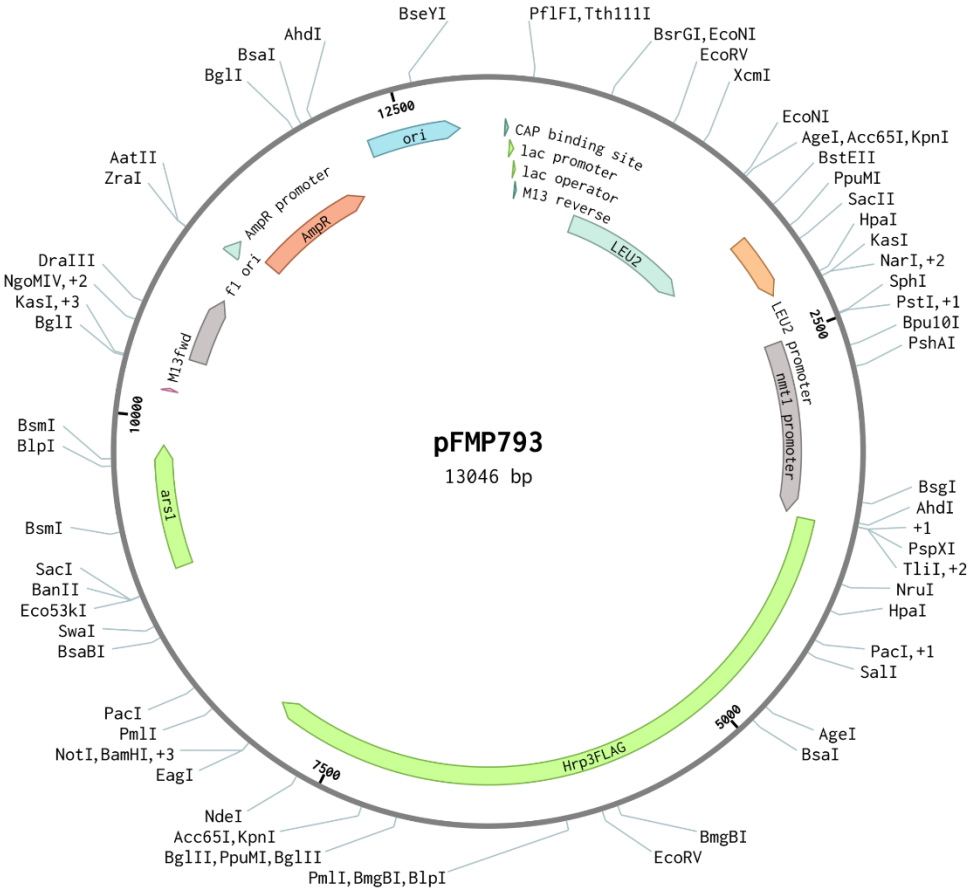

pFMP794 (13046 bp)

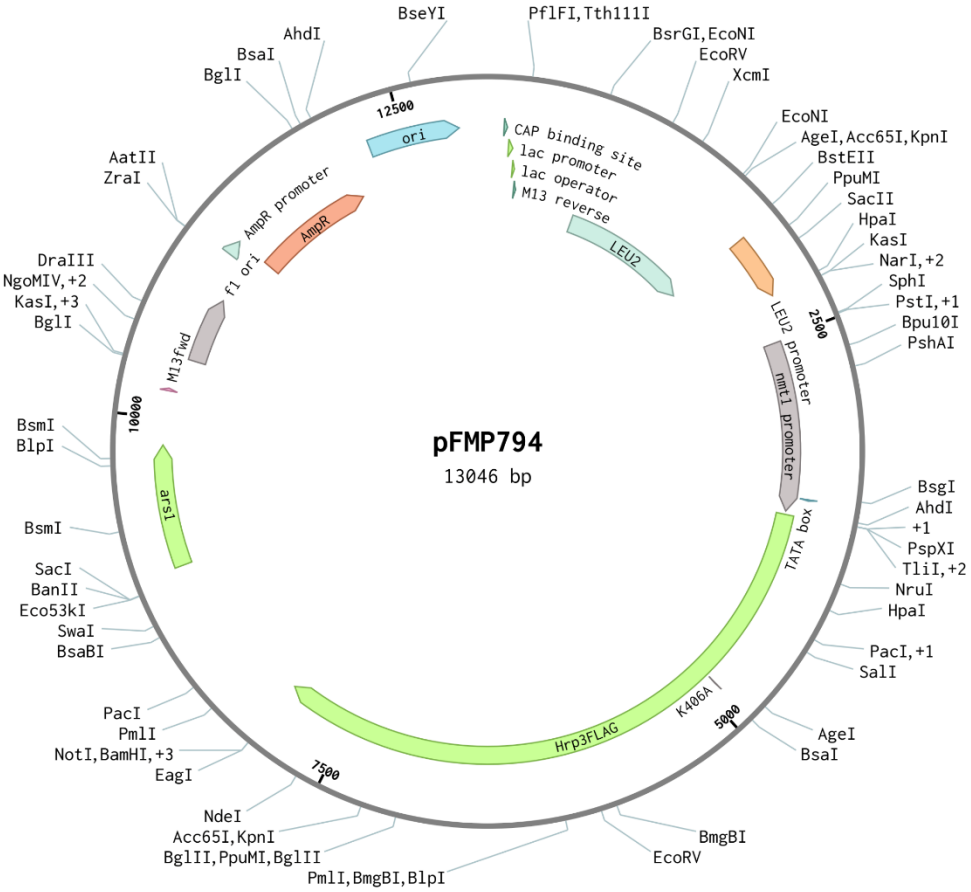

pFMP795 (12955 bp)

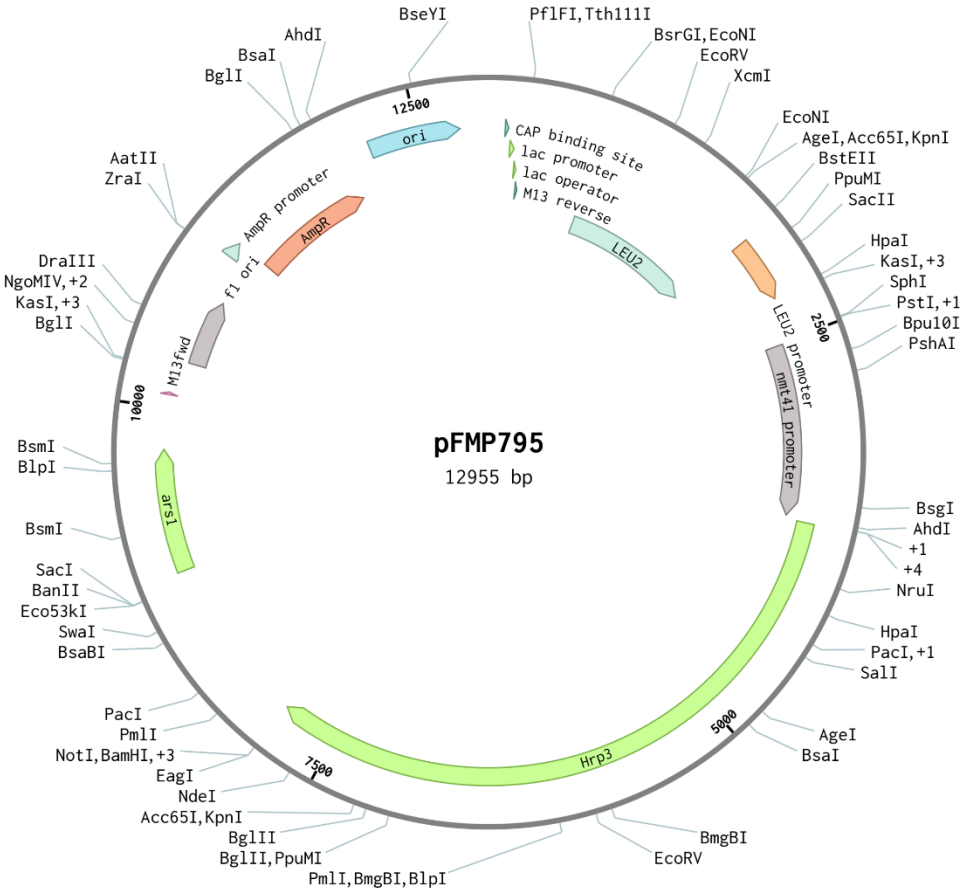

pFMP796 (12952 bp)

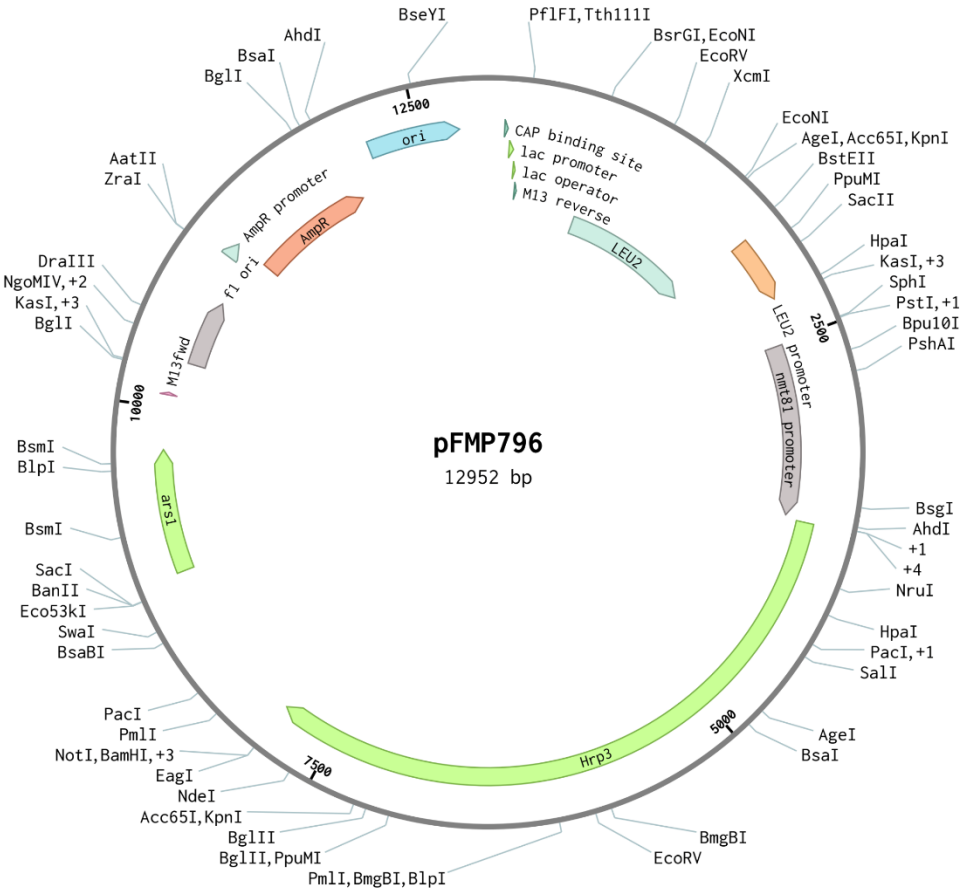

Acknowledgements

First, I want to thank to Prof. Dr. Felix Müller-Planitz for accepting me as his PhD student and for giving me the opportunity to work in his laboratory. Your creativity, passion and commitment to excellence inspired and motivated me during my starting years as a scientist. Thank you for your understanding, advice, constant challenges, patience, opportunities and freedom to drive my own project. I am excited to read about research coming from your group in the future.

Second, I want to thank to Prof. Dr. Peter Becker, my Doktorvater and TAC committee member, for always being available for advice and feedback. I learned a lot from you about leadership. I am very thankful to other TAC committee members: Dr. Magdalena Murawska, Prof. Dr. Dorothee Dormann and Prof. Dr. Mario Halic, for their time, help and feedback on my project.

I feel incredibly privileged to be a part of IRTG Chromatin dynamics graduate school for six years and want to thank to Dr. Elizabeth Schroeder Reiter, a graduate program coordinator, for her dedication to raising a new generation of scientists.

I am largely in debt to all excellent scientists with whom I had a pleasure to collaborate during my PhD. I am thankful to Dr. Alessandro Scacchetti for his time, passion and help to lift off phase separation project. To Mariano Gonzalez Pisfil from BMC Bioimaging facility for his time and expertise given to development of our novel imaging-based nucleosome sliding assay. I would like to express my deepest appreciation to Prof. Dr. Johannes Stigler and Dieter Kamp, your incredible creativity and dedication gave invaluable contribution to this work. Lastly, I am grateful to Prof. Dr. Sigurd Braun and his group for inviting me to join their journal club and sharing their expertise on fission yeast. It was great to work with you all.

Many thanks to all past and present members of our group. Ashish, Daan and Kripi; I tremendously benefited from our constant scientific discussions, creative atmosphere and after-work docu zone beers. Ashish, we were bench neighbours for almost five years and I want to thank you for always helping me out with everything and endless chatting while endlessly pipetting. Special thanks to Dresden part of the lab for giving be a very warm welcome in that beautiful city. I am also grateful to Madhura Khare and Silvia Härtel, two amazing technicians who really helped pushing forward all my projects. Special thanks to students I had a privilege to supervise, for bravely taking on high risk projects and always going an extra mile: Arun, Elodie, Tatiana, Laura and Erik.

Thanks should also go to every member of BMC Molecular biology department for the great atmosphere they have created and cool events they have organized. In particular, I want to thank to Iris and Erika for accepting me into their lunch club and all the great talks we had together.

Finally, I want to thank to my sister, parents and grandmother for always putting my education and my career as their priority. Special thanks to other family members for visiting me in Munich and always asking how science is going. Thanks to my friends for always being there to listen, meet up for a coffee, lunch, a hike or a book club. Naseef, thank you for your endless patience and support.

Affidavit

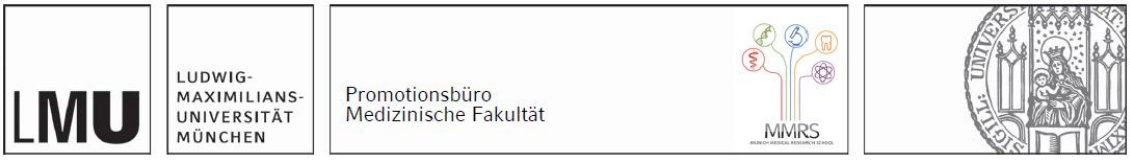

Affidavit

VIZJAK, PETRA

I hereby declare, that the submitted thesis entitled:

Remodeling of higher order chromatin structures

is my own work. I have only used the sources indicated and have not made unauthorized use of services of a third party. Where the work of others has been quoted or reproduced, the source is always given.

I further declare that the submitted thesis or parts thereof have not been presented as part of an examination degree to any other university.

Planegg, 05.02.2024 Petra Vizjak

Place, date Signature doctoral candidate

Confirmation of congruency

LMU LUDWIG-MAXIMILIANS-UNIVERSITÄT MÜNCHEN

Promotionsbüro
Medizinische Fakultät

MMRS

Confirmation of congruency between printed and electronic version of the doctoral thesis

VIZJAK, PETRA

I hereby declare, that the submitted thesis entitled:

Remodeling of higher order chromatin structures

is congruent with the printed version both in content and format.

Planegg, 05.02.2024 Petra Vizjak

Place, date Signature doctoral candidate

List of publications

Vizjak P, Kamp D, Hepp N, Scacchetti A, Gonzalez Pisfil M, Bartho J, Halic M, Becker PB, Smolle M, Stigler J, Mueller-Planitz F. ISWI catalyzes nucleosome sliding in condensed nucleosome arrays. Manuscript under revision

Chacin E, Bansal P, Reusswig KU, Diaz-Santin LM, Ortega P, **Vizjak P**, Gómez-González B, Müller-Planitz F, Aguilera A, Pfander B, Cheung ACM, Kurat CF. A CDK-regulated chromatin segregase promoting chromosome replication. Nat Commun. 2021

Brouwer T, Pham C, Kaczmarczyk A, de Voogd WJ, Botto M, **Vizjak P**, Mueller-Planitz F, van Noort J. A critical role for linker DNA in higher-order folding of chromatin fibers. Nucleic Acids Res. 2021

Rücker-Braun E, Link CS, Schmiedgen M, Tunger A, **Vizjak P**, Teipel R, Wehner R, Kühn D, Fuchs YF, Oelschlägel U, Germeroth L, Schmitz M, Bornhäuser M, Schetelig J, Heidenreich F, Exp. Hematol. 44 (2016) 1024-1033.